AN INVESTIGATION OF THE USE OF ANISOTROPY OF COMPLEX MAGNETIC SUSCEPTIBILITY TO ANALYSE STRAIN IN EXPERIMENTALLY DEFORMED MATERIALS AND MASSIVE SULPHIDES.

Mark Allan Puumala

A thesis submitted in partial
fulfillment for the degree of
Master of Science

Department of Geology
Faculty of Arts and Science
Lakehead University
April, 1991

ABSTRACT

Anisotropy of magnetic susceptibility (AMS) has become a widely accepted method of fabric analysis in rocks, especially those which have been deformed tectonically. The use of anisotropy of complex magnetic susceptibility (ACMS) is a new potential method of fabric analysis in which the imaginary, or out of phase A.C. component of an induction coil used for the measurement of magnetic susceptibility is used to delineate rock fabric. Complex magnetic susceptibility is a function of of electrical conductivity, thus making it potentially useful in the analysis of highly conductive sulphide-rich rocks, some of which are not suitable for AMS analysis.

Preliminary measurements were performed on highly conductive aluminum test specimens of differing shapes to determine the relationship between grain shape anisotropy and ACMS. A relationship was found in which shape anisotropy and resistive ACMS fabrics were of the same sense, but there was no quantitative correlation. Pure and simple shear deformation experiments performed on plasticene containing numerous small aluminum disks exhibited a correlation between ACMS fabric anisotropies and strain in most cases, as the ACMS fabrics were controlled by the distribution of the disks, which became well-aligned as flattening proceeded. Although there was no quantitative relationship between strain and ACMS, they tended to increase together.

Triaxial deformation studies on loose pyrrhotite aggregates and pyrrhotite plus talc mixtures were performed at confining pressures of 150 MPa. The ACMS fabrics developed in these specimens were compared to AMS fabrics and strain analysis data to determine if the ACMS fabrics change as a function of strain. As expected, oblate resistive ACMS fabrics developed during these pure shear deformations. The pyrrhotite aggregates exhibited a complex relationship in which ACMS increased with strain, at least up to a critical strain value, after which ACMS appeared to decrease. The pyrrhotite plus talc mixtures exhibited an unmistakable increase in ACMS with increased strain probably influenced by the presence of the talc matrix. The ACMS fabrics developed in these experiments were undoubtedly the result of grain alignment and distribution within the aggregates, with insignificant contributions from crystallographic resistive anisotropy.

Measurements performed on specimens of massive pyrrhotite revealed ACMS fabrics completely different from those observed in the loose pyrrhotite aggregates, with ambiguous relationships between strain and ACMS. This is because the massive specimens behave electrically as a single grain and anisotropy is almost exclusively crystallographically controlled. Thus the ACMS properties of single minerals must be understood before ACMS fabrics in massive sulphides can be interpreted.

ACKNOWLEDGEMENTS

The research costs for this project were supported by Dr. G. Borradaile's NSERC operating grant # A6861. The author was also the recipient of an NSERC scholarship. Funds covering the cost of the ACMS measurement device were provided by the Bickell Foundation.

A number of people were instrumental in assisting with the completion of this thesis and deserve recognition. Dr. G. Borradaile suggested the topic and provided guidance throughout. Dr. M. Stupavsky provided information on the operation of the ACMS intrument. Dr. S. Kissin assisted in the determination of pyrrhotite compositions, and Dr. M. Hawton performed conductivity measurements on massive sulphide specimens. Technical assistance was provided by Dr. Tom Griffith, Anne Hammond, Elinor Jensen, Allan MacKenzie, and Reino Viitala.

I would also like to thank my fellow geology students and the LU nordic ski team for making the past two years interesting and enjoyable. I would also like to acknowledge my parents for their support and last, but certainly not least, I would like to thank Moira for her moral support over the past year.

TABLE OF CONTENTS

Page

1. ELECTRICAL PROPERTIES OF ROCKS AND MINERALS AND THEIR APPLICATION TO ANISOTROPY OF COMPLEX MAGNETIC SUSCEPTIBILITY

1.1. Introduction

The electrical properties of rocks and minerals have been studied extensively, especially for applications relevant to geophysical prospecting. These properties are summarized in the work of such authors as Keller and Frischnecht (1966), Shankland (1975), Shuey (1975), Keller (1982), and Parkhomenko (1982).

Various types of electrical anisotropy have been studied by Hirihara and Murakami (1958), Brace and Orange (1968), Morrow and Brace (1981), and Krontiras et al. (1984). They studied the anisotropy of individual minerals or sedimentary rocks for application to geophysical exploration and earthquake prediction. Literature utilizing the electrical properties of rocks to analyse strain is quite limited, however, some work has been done by such authors as Hill (1972), Nowina and Strangway (1982), and Hawton and Borradaile (1989). This is the main interest of this study, as electrical anisotropy, using the technique of anisotropy of complex magnetic susceptibility, will be used to attempt analysis of strain in experimentally deformed sulphide aggregates as well as in sulphide-rich, naturally deformed specimens.

The electrical properties of individual minerals within a rock have an important bearing upon the bulk properties of that rock. This is especially important when highly conductive

1.2. How Minerals Conduct Electricity

There are three ways in which minerals can conduct electricity. These are, metallic conduction, electronic semiconduction, and electrolytic conduction (Keller, 1982; Keller and Frischnecht, 1966). Each has a different mechanism and magnitude of conduction.

1.2.1. Metallic conduction

Metallic conduction occurs in the native elements such as gold, silver, platinum, and graphite. It also occurs in a small number of rare minerals such as ulmanite (NiSbS) and breithauptite (NiSb). The table of figure 1.1 gives the zero frequency resistivity of a number of minerals quoted from Keller (1982). Note that conductors have resistivity values in the 10^{-8} Ω-m range.

Conduction in metals is achieved through the free movement of electrons through the crystal lattice upon application of an electric field. If metals had perfect atomic structure, they would have essentially zero resistivity. In nature, no metal is perfect, thus the natural lattice imperfection such as vacancies, impurities, and dislocations impede current somewhat. The resistivity (ρ) of a metal is related to the field applied (E) and current density (j) in the following way:

Conductors	Resistivity (Ω·m)
gold	2.0×10^{-8}
platinum	9.8×10^{-8}
silver	1.5×10^{-8}
graphite	$36\text{–}100 \times 10^{-8}$ parallel cvg.
	$28\text{–}9900 \times 10^{-6}$ perpendicular cvg.
native copper	$1.2\text{–}30 \times 10^{-8}$
aluminum	2.5×10^{-8}
iron	9.0×10^{-8}
lead	19×10^{-8}
Semiconductors	
pyrrhotite	$2\text{–}160 \times 10^{-6}$
chalcopyrite	$150\text{–}9000 \times 10^{-6}$
pyrite	$1.2\text{–}600 \times 10^{-3}$
sphalerite	$2.7 \times 10^{-3} - 1.2 \times 10^{4}$
galena	$6.8 \times 10^{-6} - 9 \times 10^{-2}$
pentlandite	$1\text{–}11 \times 10^{-6}$
arsenopyrite	$20\text{–}300 \times 10^{-6}$
millerite	$2\text{–}4 \times 10^{-7}$
arsenides and tellurides	in 10^{-6} range
magnetite	52×10^{-6}
water	0.24–80

Figure 1.1. Electrical resistivities at zero frequencies for a number of conductors and semiconductors quoted from Keller (1982).

$$E = \rho j$$

Resistivity also is related to resistance:

$$R = \rho\, l/A$$

where l is the length of the conductor and A is its cross-sectional area. The inverse of resistivity is conductivity (σ):

$$\rho = 1/\sigma$$

This is a term which is used frequently and interchangeably with resistivity.

The complex magnetic susceptibility technique used in this study utilizes resistive anisotropy to recognize rock structures. However, resistances obtained using this method may be different from those at zero frequency, as alternating current in an induction coil is used. Resistance of the specimen is related to the complex susceptibility (K"), and will be discussed in a later section of this chapter.

1.2.2. Electronic semiconduction

This method of conduction in minerals also results from the motion of electrons through a material, however, much more energy is required to move electrons from one atom to another than in

metals. The diagram of figure 1.2 from Kip (1969) illustrates the energy band diagrams for crystalline solids derived from the quantum mechanical model. The difference between metallic conduction and semiconduction is the difference in energy between the filled and empty levels. Note that in a metal, there is no energy gap between the filled and empty levels, resulting in greater conductivity.

The electrical properties of semiconductors are a function of impurities and lattice imperfections. These result in the presence of conduction electrons and holes, which are electronic defects, as well as substitutions, which are atomic defects. Schottky and Frenckel defects can also have an effect on conduction (Shuey, 1975).

Minerals can exhibit intrinsic or extrinsic semiconduction. Intrinsic semiconductors contain equal numbers of holes and electrons. Electrons move to higher energy levels, leaving holes behind in the valence band. Impurities or vacancies add electrons or accept electrons, resulting in extrinsic semiconduction, or n- and p-type semiconduction. The band diagram of figure 1.3 illustrates how impurities can change the band structure of semiconductors. The energy gap between the valence and conduction bands in a semiconducting mineral defines its conductivity. As stated previously, this gap is much larger in semiconductors than in conductors.

A stoichiometric compound lacking in impurities would be an intrinsic semiconductor. An example could be troilite (FeS). A

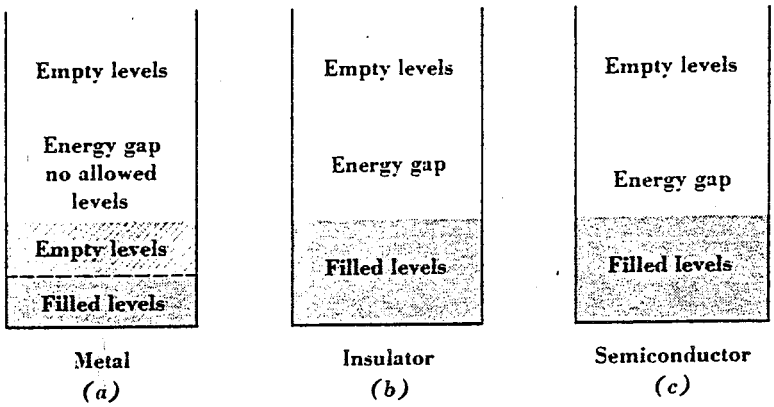

***Fig. 7.11** Energy-band diagrams for crystalline solids. (a) In a metal there are empty allowed states adjacent to filled states; (b) in an insulator the highest filled band is completely filled and other allowed states are separated by a wide forbidden energy gap; (c) in a semiconductor the highest filled band is completely filled but the forbidden gap is narrow enough to allow thermal excitation to bring some electrons into the upper levels above the gap.*

Figure 1.2. These diagrams illustrate the differences in energy required to produce electron flow in (a) conductors, (b) insulators, and (c) semiconductors. Electrolytic conductors referred to in the text are in fact insulators. (Kip, 1969)

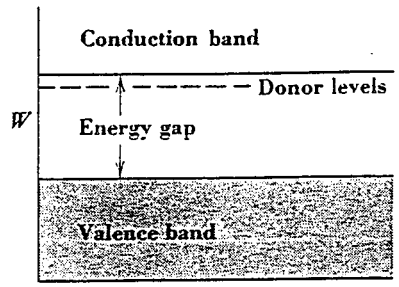

Fig. 7.13 Energy-band diagram of an n-type semiconductor.

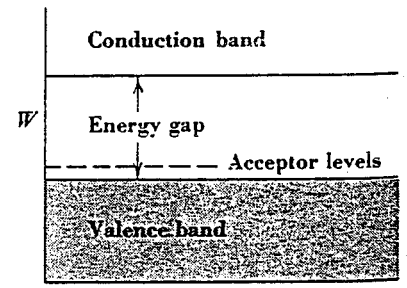

Fig. 7.14 Energy-band diagram of a p-type semiconductor.

Figure 1.3. Extrinsic semiconductors require less energy to conduct due to the presence of acceptor or donor energy levels which are illustrated in the above band diagrams from Kip (1969).

non-stoichiometric compound, such as pyrrhotite ($Fe_{1-x}S$), which has a similar crystal structure to troilite, should be an extrinsic semiconductor since it has a deficiency of iron, resulting in vacancies. Impurity atoms in high enough concentrations could also contribute to extrinsic semiconduction in these and other minerals. Such impurity-band conduction is used by Sakkopolous et al. (1984) to help explain the conductivity properties of a natural pyrrhotite. Impurity band formation occurs in synthetic n- and p- germanium at 10^{16} impurity atoms/cm^3, which they also assume is true for pyrrhotite, which can contain significant amounts of Ni, Co, and Cu. X-ray fluorescence analyses were obtained from pyrrhotite used in this study, and showed that these elements were present.

Semiconduction is a thermally activated process, in which conduction increases as the result of temperature increase. This is the opposite to what occurs in metallic conductors. This temperature dependence is illustrated in the equation:

$$\sigma_t = \sigma_o' \exp(-E_o'/2kT) + \sigma_o'' \exp(-E_o''/2kT)$$

from Parkhomenko (1967), where σ_o' and σ_o'' are the intrinsic and extrinsic conductivities respectively, and E_o is the activation energy, which is different for each mineral. k is Boltzmann's constant and T is absolute temperature.

Electronic semiconduction is the most important means of conduction for the purposes of this study. This is due to the

fact that most sulphide minerals, including pyrrhotite, which are conductive enough to be measured using the anisotropy of complex magnetic susceptibility technique, are semiconducting minerals. Semiconducting minerals have widely varying resistivity values, falling in the range of 10^{3} to 10^{-5} Ω-m (Shuey, 1975). Note that only the lowest resistivity minerals can be detected using the anisotropy of complex magnetic susceptibility technique.

The resistivities of semiconducting minerals are influenced greatly by a number of factors which tend to impede current. Lattice scattering, which is the result of thermally activated processes, is most important at high temperature. At low temperatures, such as room temperature, defect scattering is most prominent. Dislocations, stacking faults, and twin planes can impede current if they are extremely abundant. Note, however, that "tight" grain boundaries have a minimal effect upon resistivity (Shuey, 1975).

Such features as microcracks and mineral replacement zones can have a major effect on conduction, as they can break the continuity of a conducting material. The loose pyrrhotite aggregates used in this study contain many gaps in continuity between and within grains as shown in figure 1.4. This would suggest that these specimens should be much more resistive than massive specimens. This is indeed the case and can be seen in the differences in bulk conductive complex magnetic susceptibility values for the loose aggregates in appendix A, and for the massive specimens in appendix D. For example, the most conductive

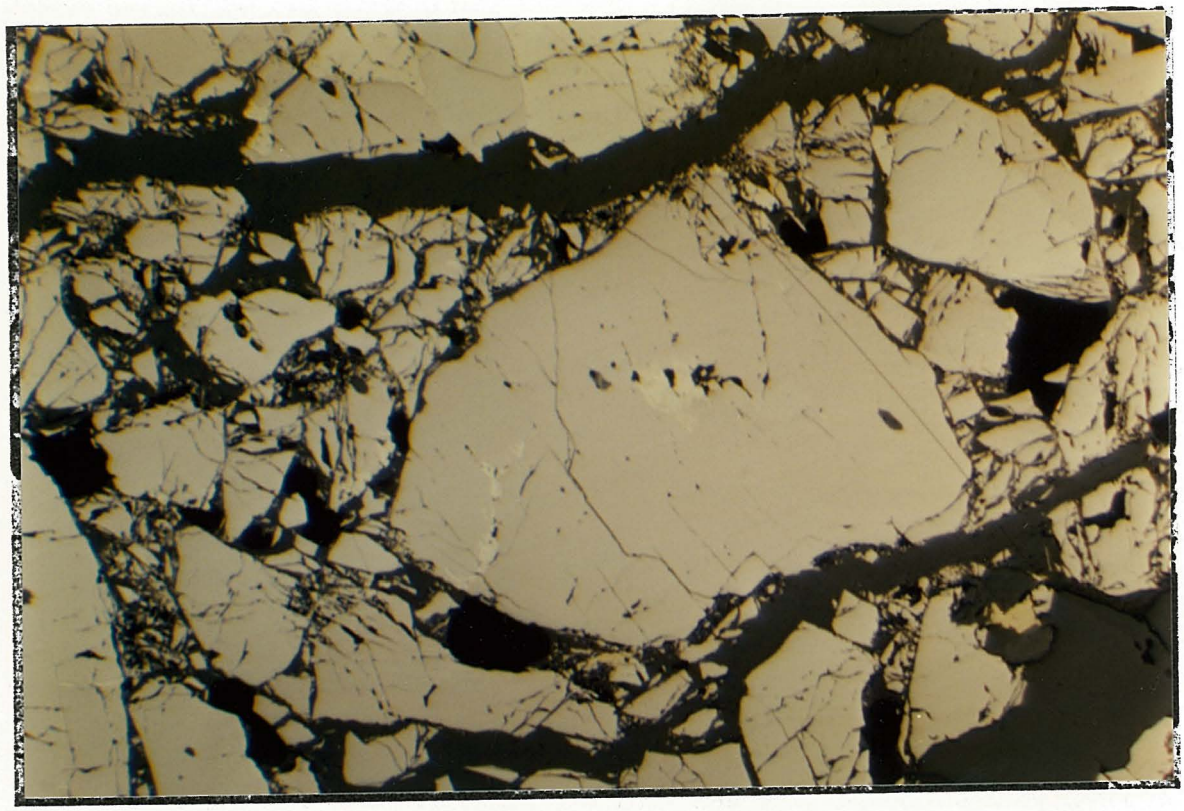

Figure 1.4. Note the gaps between grains as well as the fractures within the grains which reduce electronic conduction.

loose aggregate, P019, has a conductive K" of 7.5606 X 10^{-6} SI/mass while a typical massive specimen such as SB04 has a conductive K" of 0.68734 SI/mass.

1.2.3. Electrolytic conduction

The third and most common geological means of conduction is called electrolytic conduction. This is what occurs in silicates, carbonates, and most other minerals. These are generally ionic materials, in which metal ions give up their valence electrons to complete the outer shells of adjacent anions.

Electric fields are generally not of high enough energy to liberate these electrons, thus effectively making these materials non-conductors. The band diagram for non-conductors is illustrated in figure 1.2 for comparison with metals and semiconductors.

Not surprisingly, electrolytic solids are highly resistive, with values generally higher than 10^{3} Ω-m (Shuey, 1975). Any conduction in these materials is the result of crystal defects, especially Schottky and Frenckel defects. Resistivity is inversely proportional to the mobility of these ions, which in turn is a function of the relative sizes of the moving ions and the interstices of the crystal lattice.

Solid electrolytes exhibit intrinsic and extrinsic behaviour, but it is different from that of semiconductors. Low temperature conduction is extrinsic or structure sensitive, and is due to

weakly bonded impurities and defects. High temperature conduction is intrinsic, resulting from the movement of ions from their regular lattice positions as a result of thermal vibrations. As in semiconductors, conductivity in electrolytes increases with temperature.

Unlike semiconducting and conducting minerals, solid electrolytes exhibit a frequency dependence upon conductivity when AC currents are applied. Figure 1.5 shows that as frequency is increased, resistivity drops (conductivity increases).

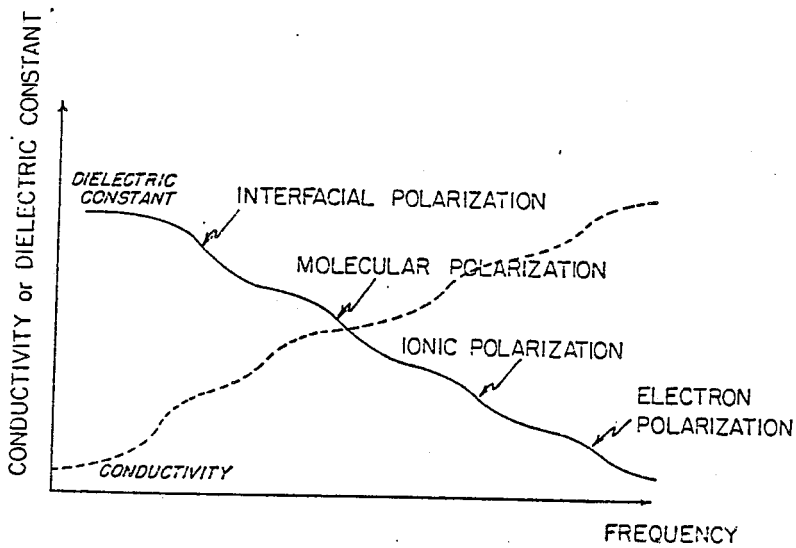

Figure 1.5. This diagram shows how conductivity (dotted line) increases with frequency in a solid electrolyte. (Keller and Frischnecht, 1966)

1.3. Conductivity in Natural Silicate Rocks

Dry silicate rocks generally have extremely low conductivities, as they are dominated by electrolytically conducting minerals, mostly silicates and carbonates. These minerals usually have much lower conductivities than water. As a result, rocks which contain significant quantities of pore water have conductivities governed by pore water content.

Most studies of the electrical properties of rocks have been done on such rocks (eg Brace and Orange, 1968; Drury and Hyndman, 1979; Morrow and Brace, 1981; Worthington, 1981).

1.4. Role of Pore Water

As previously mentioned, most rocks conduct almost solely by pore water conduction (Brace and Orange, 1968). The conductivity of these waters is in turn a function of salinity. Saline solutions have higher conductivities since they conduct by the motion of dissolved ions (electrolytic conduction). Keller (1982) shows that there is a relationship between resistivity and NaCl concentration as shown in figure 1.6. Temperature also affects the conductivity of pore fluids, having a positive correlation.

The theoretical conductivity of a rock containing water can be calculated using Archie's law (Archie, 1942) which states:

$$\rho_t = a\rho_w \emptyset^{-m}$$

where ρ_t is total resistivity, ρ_w is the resistivity of the pore water, a and m are constants, and $\emptyset$ is the porosity fraction. Sedimentary rocks are generally much more porous than igneous and metamorphic rocks, however, all generally have electrical properties which are controlled by water, especially when saturated (Parkhomenko, 1982). Confining pressure is another variable which must be considered to understand pore water conduction in rocks. Fully saturated rocks tend to experience an increase in resistivity as a function of confining pressure, but the opposite is true of partially saturated rocks.

Rocks having significant conductivity on their own are not

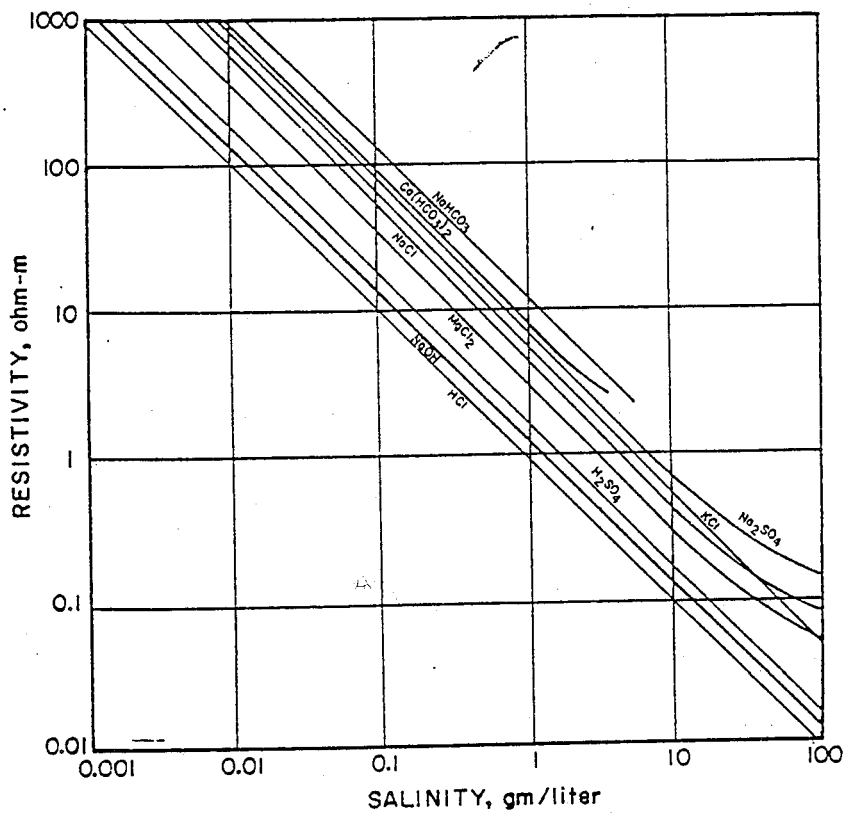

FIGURE 20. Relationship between resistivity and concentration for various salt solutions at a temperature of 18°C.

Figure 1.6. Note how resistivity of saline waters decreases as a function of increased salinity. This is due to the motion of dissolved ions. (Keller, 1982)

affected by pore waters. The Nahant gabbro analysed by Brace and Orange (1968), had abnormally low resistivity of 73-93 Ω-m, with little difference between dry and water-saturated specimens. This specimen was iron-rich and probably derived much of its conductivity from magnetite or a sulphide. The high conductivity of specimens measured during this study ensured that there was no effect due to water. In any case, water is not conductive enough to be detected in the complex magnetic susceptibility measurement unit.

1.5. Electrical Anisotropy

1.5.1. Role of minerals

Many minerals are anisotropic in their electrical response. The electrical anisotropy of a mineral is dependent on crystallography. For example, Krontiras et al. (1984) observed resistivity values parallel to the c-axis of pyrrhotite to be approximately 10% higher than perpendicular to the c-axis. Shuey (1975) suggests that electrical anisotropy may be related to optical anisotropy, however, Parkhomenko (1967) and Nowina and Strangway (1982) state that not enough is known about electrical anisotropy to make such a conclusion. It is clear, however, that minerals which are not of the isometric crystal class are likely to exhibit crystallographically controlled electrical anisotropy. This is similar to what is observed in the study of magnetic anisotropy (eg Borradaile et al., 1987). Anisotropy of resistivity or conductivity is usually quoted parallel and perpendicular to the c-crystallographic axis in uniaxial minerals. The ratio of parallel resistivity to perpendicular resistivity is close to 1.00 for most minerals, but layered structures such as graphite and molybdenite can have anisotropy values in the range of 1000 (Shuey, 1975). Minerals such as hornblende, riebeckite, beryl, and quartz have fairly high anisotropy values, but, since they are not semiconductors, they will not be measurable with the complex magnetic susceptibility

measurement coil.

Isometric minerals such as magnetite are electrically isotropic, thus electrical anisotropy of rocks containing it will be influenced by grain shapes. However, this is also dependent upon the distribution of grains. A specimen of massive magnetite may show very little anisotropy if all grain contacts are tight. In effect, the rock may behave as a single grain of magnetite. Shuey (1975) states that tight grain boundaries generally have a minimal effect on the mobility of charge carriers. This fact may have major implications for the measurement of anisotropy of complex magnetic susceptibility in massive sulphides, as grain shape controlled anisotropy may not exist. Specimens containing disseminated conducting materials will not have this problem, and grain shapes could have a bearing on anisotropy. If the grains have small cross-sectional areas, bulk conductivity might become too small to measure. Stratified sulphides will also show strong anisotropy because of grain contacts in one direction but not another.

1.5.2. Bulk rock anisotropy

Electrical anisotropy of rocks has been studied extensively, with the greatest emphasis having been placed on anisotropy due to pore water and sedimentary fabrics. Since many rocks conduct largely due to the effects of pore water, this influences their anisotropy of resistivity. For example, when current is passed

through sedimentary rocks, resistivity is lowest parallel to the bedding planes (Keller, 1982). This is because pores tend to become joined together in this direction, enhancing conduction. Also, coating of anisotropically shaped grains and filling of fractures by water will produce anisotropies (Tuck and Stacey, 1978; Nowina and Strangway, 1982).

Ignoring pore water, the habit of a mineral is as important as its quantity in determining bulk resistivity. In dielectric-type rocks, the resistivity can be influenced greatly by the nature of boundaries between materials of differing dielectric constant (Nowina and Strangway, (1982). In these rocks, electrical anisotropy is influenced completely by grain shapes when current is passed through them. Lowest resistivity is parallel to lineations and highest resistivity perpendicular to foliation.

The presence of semiconducting minerals will have a profound effect on resistivity and dielectric constants, especially if grains are interconnected. This allows current loops to be set up when conventional resistivity measurement techniques are used, producing minimum resistivity parallel to the direction of interconnectivity. It should now be noted, that when an induction technique of resistance measurement (see Meaden, 1965) such as the complex magnetic susceptibility method is used, that current loops are not set up. Instead, resistance is measured through a cross-section. With this value being proportional to length over cross-sectional area of the conductive medium ($R = \rho l/A$), the

greatest resistances will be measured across sections with less cross-sectional area, for example, the direction of interconnectivity of grains. Thus this method obtains results which are the inverse of conventional resistivity measurements. See figure 1.7.

1.5.3. Electrical anisotropy of tectonically strained rocks

Electrical anisotropy of tectonically strained rocks and metamorphic rocks has not been studied extensively. However, dielectric anisotropy has been used to analyse the fabric of rocks by a number of researchers such as Stacey (1961), Tuck and Stacey (1978), Nowina and Strangway (1982), and Hawton and Borradaile (1989). All found a correlation between rock anisotropy and electrical anisotropy, with the minimum, intermediate, and maximum dielectric responses being parallel to the respective axes of the strain ellipsoid in most cases. One of the most interesting characteristics of dielctric anisotropies is that they tend to be much more anisotropic than magnetic susceptibility anisotropies (Nowina and Strangway, 1982).

Dielectric measurements have some major drawbacks, the most important being the fact that the fabric axes of a rock must be known prior to measurement in order for the dielectric anisotropy to be determined. It is possible that the principal directions of dielectric anisotropy may not coincide with the principal strain directions. Also, water has a major effect on results. Water

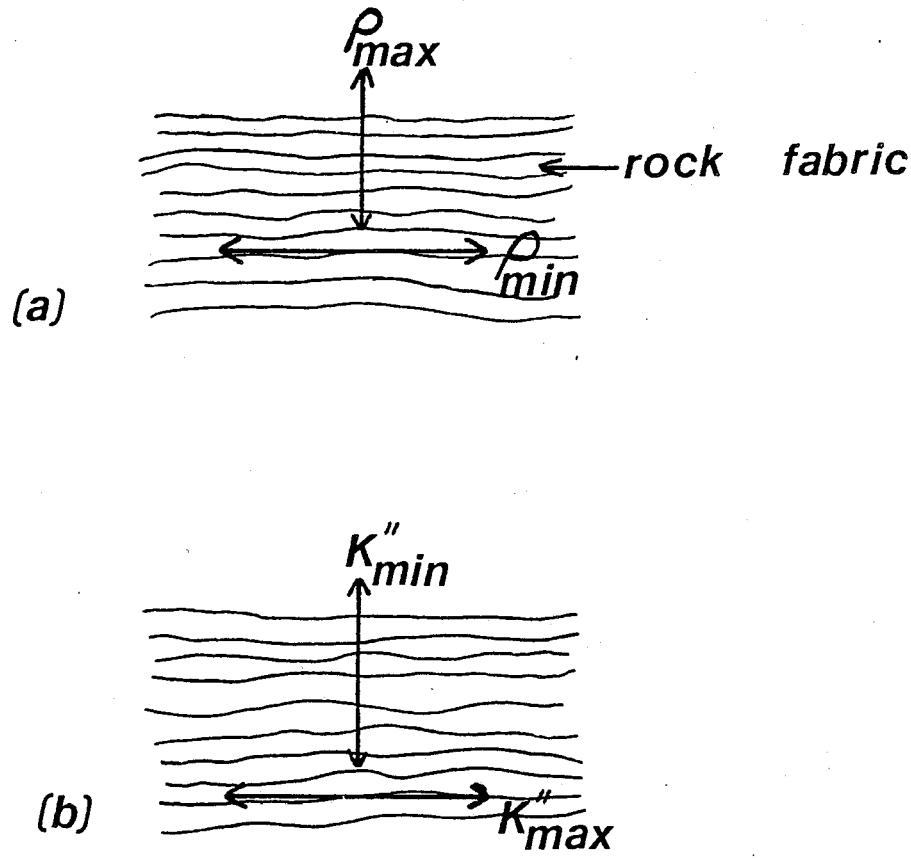

Figure 1.7. (a) Resistivity fabrics versus (b) resistive ACMS fabrics. These are the inverse of each other due to differing measurement techniques.

coatings on grains could enhance dielectric measurements of fabric, but only if there are no water-filled inhomogeneities unrelated to the tectonic fabric, such as fractures.

The anisotropy of complex magnetic susceptibility measurement coil, which will be discussed in the next section, has an advantage over the dielectric method, in that it allows the principal susceptibility axes to be determined independently, much in the same way that the anisotropy of magnetic susceptibility axes are calculated. There is one major drawback to the complex susceptibility technique of fabric analysis relative to the dielectric method. The problem is that its low sensitivity restricts its use to rocks containing significant amounts of highly conductive minerals such as sulphides.

1.6. Anisotropy of Complex Magnetic Susceptibility (ACMS)

Anisotropy of complex magnetic susceptibility (ACMS) can be defined as the out of phase, or imaginary, component of magnetic susceptibility as measured by a magnetic susceptibility measurment coil.

Magnetic susceptibility (K) is made up of the real (dispersive) part (K'), and the imaginary (absorptive) part (K"). They are related as follows:

$$K = K' + iK''$$

K" is the complex magnetic susceptibility.

The ACMS measurement unit consists of an induction coil linked to the serial port of an IBM personal computer which calculates and displays the K" values. The coil is similar to that used in the Sapphire Instruments SI-2 anisotropy of magnetic susceptibility (AMS) measurement unit. Operation of each of these coils is outlined below, since each was utilized in this study.

1.6.1. AMS measurement

In conventional magnetic susceptibility measurement, the following relationships are used (Kittel, 1966):

$$L = (1 + 4\pi K')L_o$$

This equation can be rewritten to determine K':

$$K' = CF\ (L/L_o - 1)$$

where L_o is the inductance of the empty coil, and L is the inductance when a sample is present within the coil. CF is a calibration factor which takes into account the fraction of volume of the coil occupied by the sample and the position of the sample in the coil. The position of the sample is calibrated by using a MnO_2 sample of the same volume, which has a known magnetic susceptibility of 3.29×10^{-4} SI/volume. Calibration can also be done in mass units for cases when volume can not be determined. This is also done using a MnO_2 standard.

The method of measurement involves taking three empty coil measurements alternating with two measurements of the specimen in the coil. The most practical measurement time, incorporating a minimum of electrical "noise" or electrical interference, has been found to be 2.8 seconds in most cases. Sarvas (1988) gives an account of the parameters which affect the accuracy and precision of AMS measurement. The above procedure is repeated in twelve different orientations in order to determine the AMS tensor. Since all AMS measurements in this study were performed on pyrrhotite, which has a relatively high magnetic susceptibility of approximately 1.5 SI/volume (Carmichael, 1982), the precision of ellipsoid determination was generally very high as the data of appendix B illustrates. Standard deviations were generally less

than 1% of the values calculated for the principal axes of the AMS ellipsoid.

1.6.2. ACMS measurement

The calculation of complex magnetic susceptibility is somewhat different from magnetic susceptibility calculation. Coil resistances rather than inductances are utilized to calculate ACMS. The relationship (Kittel, 1966):

$$R = 4\pi\omega K'' L_o + R_o$$

is used. In terms of K" it can be rewritten as:

$$K'' = CF(R - R_o)/4\pi\omega L_o$$

where R_o is the effective coil resistance with only air in the coil, R is the effective coil resistance with the sample in the coil, ω is frequency, and L_o is the inductance of air within the empty coil. The term K" is dimensionless, as ωL_o is inductive impedance in ohms, cancelling out resistance, which is also in ohms. The concept of the calibration factor is the same as for AMS measurement, except that it is not yet known how to calibrate a standard specimen. The units of ACMS used in this study are SI/volume and SI/mass, the same units used in AMS measurement.

The method of measurement is similar to that for AMS, with

two exceptions. First, only two empty coil measurements are taken per reading, and second, the specimens are only measured in six different orientations to define the ACMS ellipsoid.

It can be seen from the equations used to calculate complex magnetic susceptibility (CMS) that K" is a function of coil resistance. Specimen resistance and coil resistance are much different from one another, as coil resistances are modified by eddy currents generated in the specimen being measured, and specimen resistances are intrinsic to the specimen material. Thus the highest coil resistances and therefore highest K" values are produced when the most highly conductive materials are present within the coil. Thus specimen resistance is inversely proportional to K", as the most conductive materials have the lowest resistances (Mike Stupavsky, personal communication).

The K" values, since they are proportional to <u>conductivity,</u> tended to produce ACMS tensors which were of inverse symmetry to the strain and specimen shape tensors calculated in experiments performed to test the viability of ACMS measurement. In the following chapters, which outline the results of these experiments, ACMS tensor data was inverted so that all fabrics could be of the same symmetry sense. This was possible since resistivity is the reciprocal of conductivity and the inverted fabrics can be termed <u>resistive</u> ACMS fabrics. Figure 1.8 illustrates raw conductive ACMS data and how it is converted to resistive ACMS. Note that the data found in the appendices has not been converted, as it is the raw data.

This is the raw conductive ACMS data for PL43:

$$K''_{min} = 1.1130 \times 10^{-3}$$

$$K''_{int} = 2.4576 \times 10^{-3}$$

$$K''_{max} = 6.5389 \times 10^{-3}$$

This obtains the following values for anisotropy data:

$$P' = 5.8943$$

$$T = -0.1053$$

When this data is inverted to obtain resistive ACMS, P' remains unchanged, but T becomes inverted to obtain:

$$T = 0.1053$$

Figure 1.8. This is an illustration of how resistive ACMS data was obtained.

2. INITIAL TESTING OF THE ACMS COIL

2.1. Aluminum Test Specimens

2.1.1. Materials, procedure, and theory of experiment

A number of aluminum test specimens of varying shape were machined for the initial testing of the ACMS coil. The specimens used included four aluminum disks of equal diameter and differing thickness, three rods of differing diameter and equal length, and a 1 cm diameter sphere. The dimensions and masses of each specimen are listed in the table of figure 2.1. The ACMS for each specimen was measured using the procedure outlined in chapter 1. Aluminum was chosen for this test, as it is a highly conductive metal which is electrically isotropic because of its face-centered cubic structure. These specimens were used to test the theory that the shape of a crystallographically isotropic conductor is related to the anisotropy of complex magnetic susceptibility. Theoretically, oblate-shaped conductors should exhibit oblate resistive ACMS and prolate-shaped conductors should exhibit prolate resistive ACMS.

The electrical resistance of an electrically isotropic conductor is inversely proportional to its cross-sectional area from the equation:

$$R = \rho\, 1/A$$

Disks

	Diameter (cm)	Thickness (cm)	Mass (g)
A.	1.96	1.49	10.86
B.	1.96	0.80	5.85
C.	1.96	0.505	3.67
D.	1.96	0.21	1.49

Sphere

	Diameter (cm)	Mass (g)
E.	1.01	1.48

Rods

	Diameter (cm)	Length (cm)	Mass (g)
F.	0.325	2.98	0.63
G.	0.235	3.05	0.37
H.	0.16	3.07	0.16

Figure 2.1. The dimensions and masses of the aluminum test specimens are listed above. The dimensions were used to calculate the anisotropy data for figure 2.4a.

previously introduced in chapter 1. As a result, the direction of lowest resistance will pass through the cross-section of greatest area. This means that in disks, R_{min} is perpendicular to the diameter, and for rods, R_{min} should be perpendicular to length. Also, for disks, R_{max} and R_{int} should be about equal, while for rods, R_{int} and R_{min} should be about equal. These relationships correspond to oblate and prolate uniaxial symmetry respectively.

The numbers obtained in ACMS measurements are not true resistances as noted in chapter one, but complex magnetic susceptibilities (K"). Since K" and R are proportional for any single specimen, the same relationships apply to resistive complex magnetic susceptibilities as to resistances.

2.1.2. Test results

In order to compare ACMS test data to specimen shapes, data was plotted on two Jelinek-Hrouda diagrams. These diagrams are very useful for illustrating the shape (T) and degree of anisotropy (P') of fabric ellipsoids in rocks, whether they are for strain or magnetic susceptibility anisotropy. They are especially useful when anisotropies are low, as is often the case for magnetic fabrics.

The Jelinek-Hrouda diagram is an alternative to the widely used Flinn diagram (Flinn, 1965). Each is illustrated in figure 2.2. The Jelinek-Hrouda diagram has the advantage of illustrating the degree of eccentricity of an ellipsoid versus its sense of

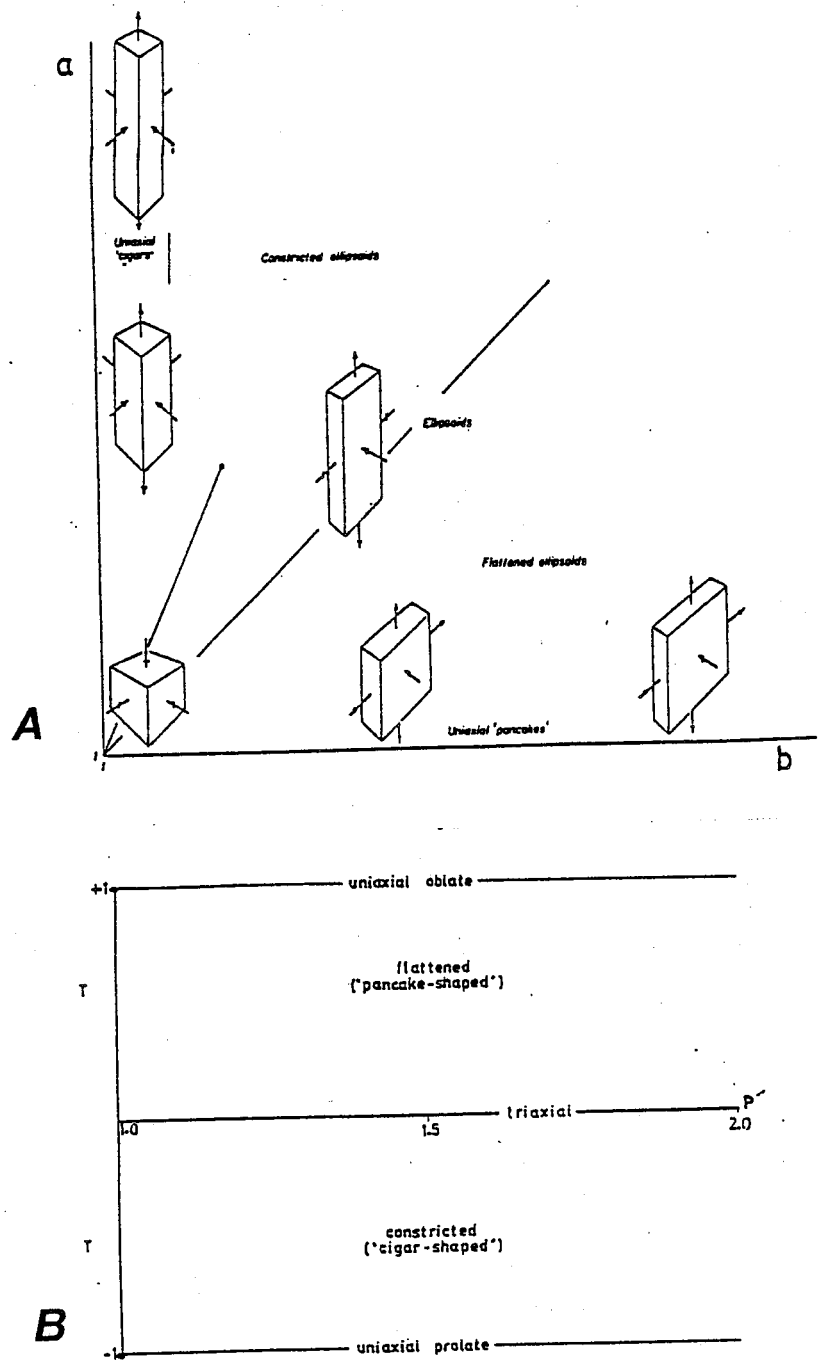

Figure 2.2. This diagram shows (a) a Flinn diagram and (b) a Jelinek-Hrouda diagram for comparison. The fields of constriction and flattening for each diagram are illustrated. Note that the shape (T) and degree of anisotropy (P') are independent of each other in the Jelinek-Hrouda plot. This is its main advantage. (Diagrams from Ramsay and Huber (1983) and Spark (1990).)

symmetry. These parameters are much more difficult to quantify using the Flinn diagram (see Borradaile, 1988). Jelinek-Hrouda (P'-T) diagrams will be used extensively in data presentation throughout this paper.

The parameters P' and T were defined by Jelinek (1981) as:

$$P' = \exp\left[\sqrt{2((a-k)^2 + (b-k)^2 + (c-k)^2)}\right]$$

$$T = 2[(b-c)/(a-c) - 1]$$

where a, b, and c are the natural logarithms of the maximum, intermediate, and minimum fabric parameters, and k is the natural logarithm of the mean of these fabric parameters.

The P'-T diagram is generally used for magnetic susceptibility data, but can be applied to strain, ACMS, or specimen shape data. Larger P' values represent ellipsoids which are more eccentric in shape. T values greater than 0 indicate that a fabric has a dominantly oblate or S-type (Flinn, 1958) fabric, with T = 1 being a uniaxial S-type fabric. T values less than 0 represent prolate or L-type fabric. When T = -1, a uniaxial L-type fabric exists. Figure 2.2 illustrates how ellipsoids of different symmetry are represented on the Flinn and Jelinek-Hrouda diagrams.

The shape anisotropy data for the aluminum test specimens were calculated and plotted on the P'-T diagram of figure 2.3a. This data can be compared to that calculated for ACMS data for

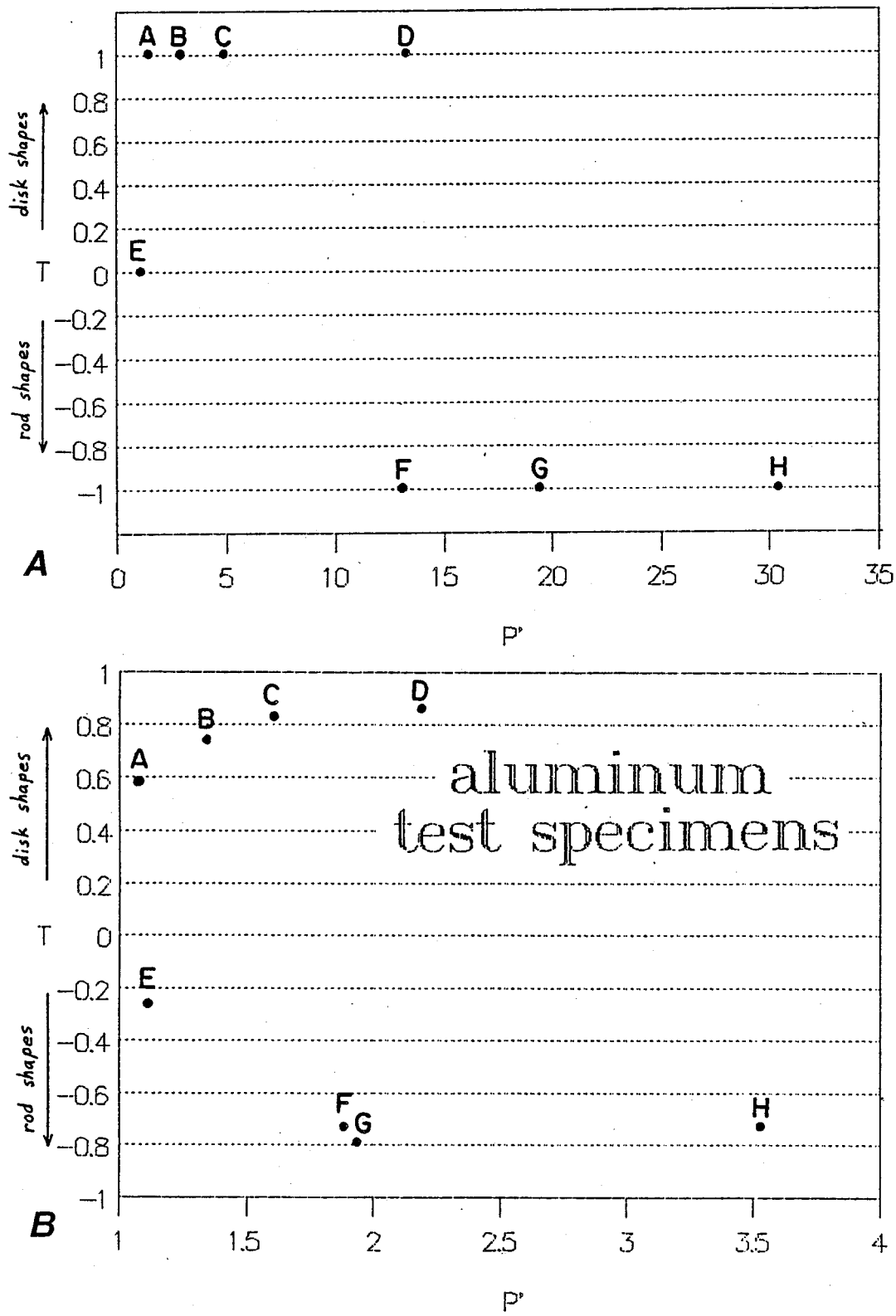

Figure 2.3. The above diagrams illustrate (a) the shape anisotropies of the aluminum test specimens versus (b) their corresponding ACMS anisotropies. Note that there are similar, though non-quantitative distributions in each case.

the same specimens illustrated in figure 2.3b. Note that the disks are perfectly oblate in shape and the rods are perfectly prolate. The diagrams show that the disks A-D show a similar trend in each diagram, as do the rods F-H. The sphere E, produced a nearly isotropic ACMS response, corresponding quite well to its isotropic shape.

The diagrams show clearly that shape P' values are much higher than those for ACMS. However, there is definitely a general, although not quantifiable relationship between specimen shape and resistive ACMS. The imperfect relationship between the shape and ACMS data can be attributed to such factors as impurities and crystal defects within the aluminum, the latter possibly related to the machining process. Rods were composed of welding rod which is somewhat impure. This may account for the less than expected fabric difference between specimens F and G.

The success of this experiment justifies further study to determine if ACMS fabrics have a relationship to progressive deformation and the development of preferred orientations of conductive grains.

2.2. Use of Metal Spheres to Study the Relationship Between Conductive ACMS and Conductivity

Four 1 cm diameter spheres of equal volume (0.524 cm^3) were machined and measured in the ACMS coil to determine if there is a quantifiable relationship between conductivity and raw complex susceptibility. The four metals chosen were iron (low carbon steel), lead, aluminum, and copper. Bulk K" values for each specimen were calculated from numerous ACMS measurements on each specimen. As expected, each specimen had an approximately isotropic response. The table of figure 2.4 lists important data regarding the conduction properties of the specimens. It illustrates that there is obviously no relationship between the theoretical conductivities and the conductive complex susceptibilities. This is not what one might expect, firstly because K" should be a function of the resistance of the specimens, since CMS is calculated from the formula:

$$K'' = CF(R - R_o)/4\pi\omega L_o$$

as ω and L_o are essentially constant for any measurement. Secondly, the resistivity of metallic materials at high frequency should not be a function of resistivity. The frequency at which ACMS measurements are made is in the vicinity of 114 kHz.

Since this is an induction resistance measurement method, the high frequency is the problem. Induction resistance

Table 1

Specimen	Resistivity (ohm m)	Conductivity (mho/m)	Raw ACMS
copper	1.6×10^{-8}	6.25×10^{7}	0.109
aluminum	2.5×10^{-8}	4×10^{7}	0.152
iron	9.0×10^{-8}	1.11×10^{7}	1.26
lead	19×10^{-8}	5.26×10^{6}	0.346

Table 2

Specimen	Calculated density	Theoretical density
aluminum	2.70	2.82
iron	7.86	7.86
copper	8.96	8.84
lead	11.4	11.24

Figure 2.4. Table 1 displays the zero frequency conductivity of the test specimens. Notice that iron has the highest raw ACMS but only the third highest conductivity. Table 2 confirms that the test specimens were very pure, as calculated densities matched theoretical densities.

measurement techniques are discussed by Meaden (1965), revealing that for successful quantitative resistance measurement of metals, audio frequencies, rather than radio frequencies (ie. 114 kHz) are required. When radio frequencies are used, currents only flow through the regions of the conductor near the surface of a specimen ("skin effect"). This is the most likely explanation for the data obtained for the CMS measurements on the metal spheres. For example, the ferrimagnetic character of iron allows deeper penetration, giving it higher K". There is a slim possibility that the differences from expected results were influenced by impurities and defects in the specimens, but in all likelihood the variations would have been less spectacular, especially in the case of iron.

Despite the fact that CMS values can not be related simply to resistivity, the four metal specimens can be used as standard specimens, since their CMS values are consistent for numerous measurements. Thus the coil can be tested for "drift".

Nor does this data mean that there is a problem with anisotropy data, since for a given specimen, bulk CMS is not a factor in anisotropy. The data for experiments in following chapters bear this out. However, the "skin effect" means that not the entire sample is measured in any test. Thus larger specimen size is desirable. The skin effect also may explain why there was no quantitative correlation between ACMS data for the aluminum specimens in the previous section.

2.3. Plasticene Plus Aluminum Progressive Deformation Experiments

2.3.1. Materials and procedure

The first set of deformation experiments were performed on aggregates consisting of Harbutt's plasticene as used by Puumala (1989), mixed with 3.2 mm diameter aluminum disks 0.076 mm thick (aspect ratio = 42) cut from an aluminum pie plate. The ICP analysis data of figure 2.5 show that the pie plate material contained more than 98% aluminum. Manganese and iron were the main impurities. Varying numbers of disks were placed in the plasticene matrix to obtain a strong ACMS signal. In all, seven experiments were run successfully in which pure and simple shear were simulated approximately.

The pure shear experiments were accomplished by using a piston press which produced several quantifiable increments of deformation. After each deformation, ACMS measurements were performed to measure the development of anisotropy within each specimen. In order to facilitate measurement, specimens were trimmed using a utility knife and placed into a sample holder. The specimens were then analysed in six different orientations to determine their ACMS. As a result of the flattening, the specimens became thinner and wider after each successive deformation. However, in these specimens, shape was determined to have a negligible effect on ACMS values. A single thin wedge of plasticene and a cut and "stacked" wedge of the same degree of deformation were analysed and found to have essentially the same

Element	Weight %
Al	98.3
Ba	0.00023
Ca	0.0035
Co	0.00035
Cr	0.010
Cu	0.051
Fe	0.44
Mg	0.050
Mn	0.98
Na	0.018
Ti	0.035
V	0.0082
Zn	0.075
Zr	0.00078

Figure 2.5. These are the results of ICP analysis on a piece of aluminum pie plate. This confirms that the material is relatively pure, with iron and manganese being the only significant impurities.

ACMS. This occurs in these samples since the aluminum disks are not numerous enough to impinge on one another, and the measurement device measures resistance across the same cross-sectional area of disks regardless of their configuration.

Simple shear experiments were performed using a shear box constructed from a pair of door hinges. The walls of the shear box were pushed against a cubic block of plasticene to allow it to shear. ACMS was measured for a number of strain increments in each experiment. After some shear increments, the block was cut, with the cut-off piece replaced on the opposite side of the specimen as illustrated in figure 2.6. This cutting allowed for greater strains to be produced and made measurement easier. It is important to note that the cutting of specimens sometimes led to difficulties in sample measurement, as the aluminum disks were quite large and prone to disturbance when specimens were cut. The cutting process often caused anomalous anisotropy values.

2.3.2. Pure shear data

Four pure shear deformation experiments were run. The data will be presented separately for each experiment.

Experiment #1 (PL08-15)

This was the first successful pure shear deformation experiment. Strain increments of 0, 10, 20, 30, 40, 50, 60, and

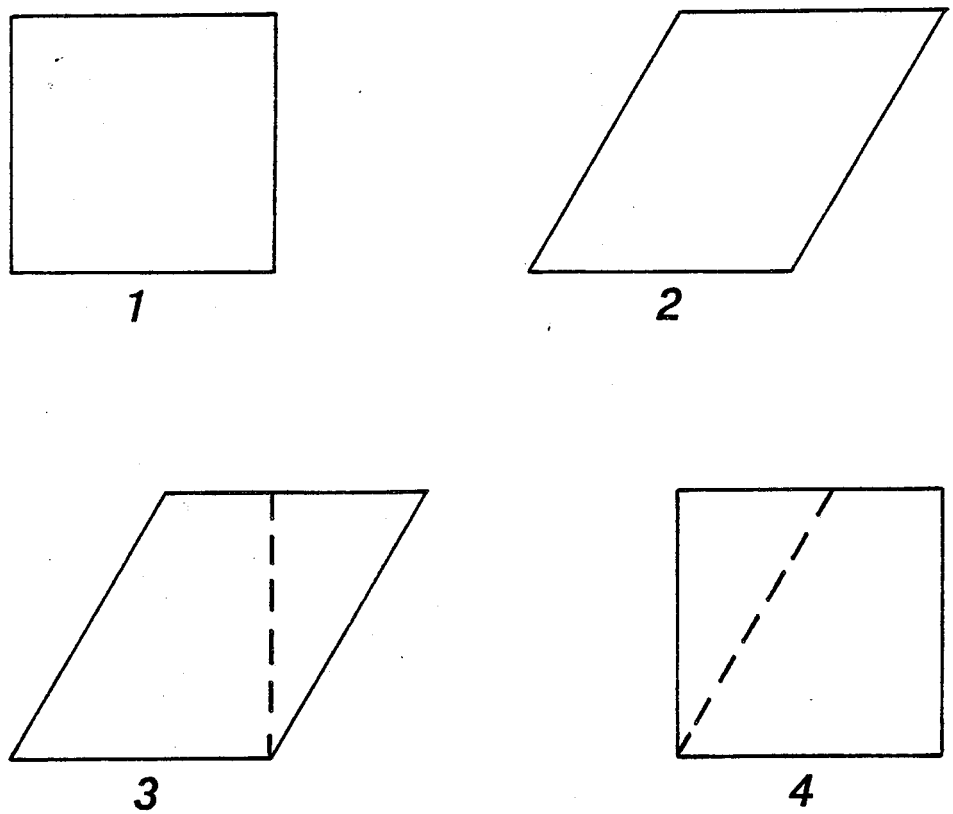

Figure 2.6. This diagram illustrates the progression of a plasticene plus aluminum disks specimen from the (1) undeformed state to the (2) fully sheared state with subsequent (3) cutting and (4) reassembly. This procedure was followed a number of times during each simple shear experiment.

65% shortening were imposed upon a single plasticene + aluminum specimen. The specimen contained 40 aluminum disks within a total volume of roughly 8 cm^3. Before straining, it was shaped into a cube. The results of the experiment are summarized in figure 2.7 by a stereo-net and a Jelinek-Hrouda diagram. The stereo-net illustrates progressive motion of the three principal axes of the ACMS ellipsoid as a result of deformation. The diagram clearly shows that the minimum susceptibility rotates towards the vertical, which is the direction of maximum compressive strain or shortening. The intermediate and maximum susceptibilities rotate to become parallel to the plane of flattening ("foliation"). The P'-T plot shows a general, although erratic increase in the degree of anisotropy (P') of the ACMS ellipsoid as deformation proceeds. The deformation appears to be approximately in the field of plane strain (equal L and S character). However, an increased degree of oblateness is noticed for the strain increments of greater than 40% shortening. Thus the ACMS ellipsoid is behaving in roughly the same way as the strain ellipsoid, obtaining a greater oblateness with deformation.

It is clear from the P'-T diagram that there is not a simple quantitative relationship between the finite strain and the degree of anisotropy of ACMS. It is important to recognize that the ACMS fabric will not mirror that of the strain ellipsoid precisely. This is due to the fact that the specimen had an initial preferred orientation of aluminum disks which had an effect on the ACMS fabric which developed. The diagrams of figure

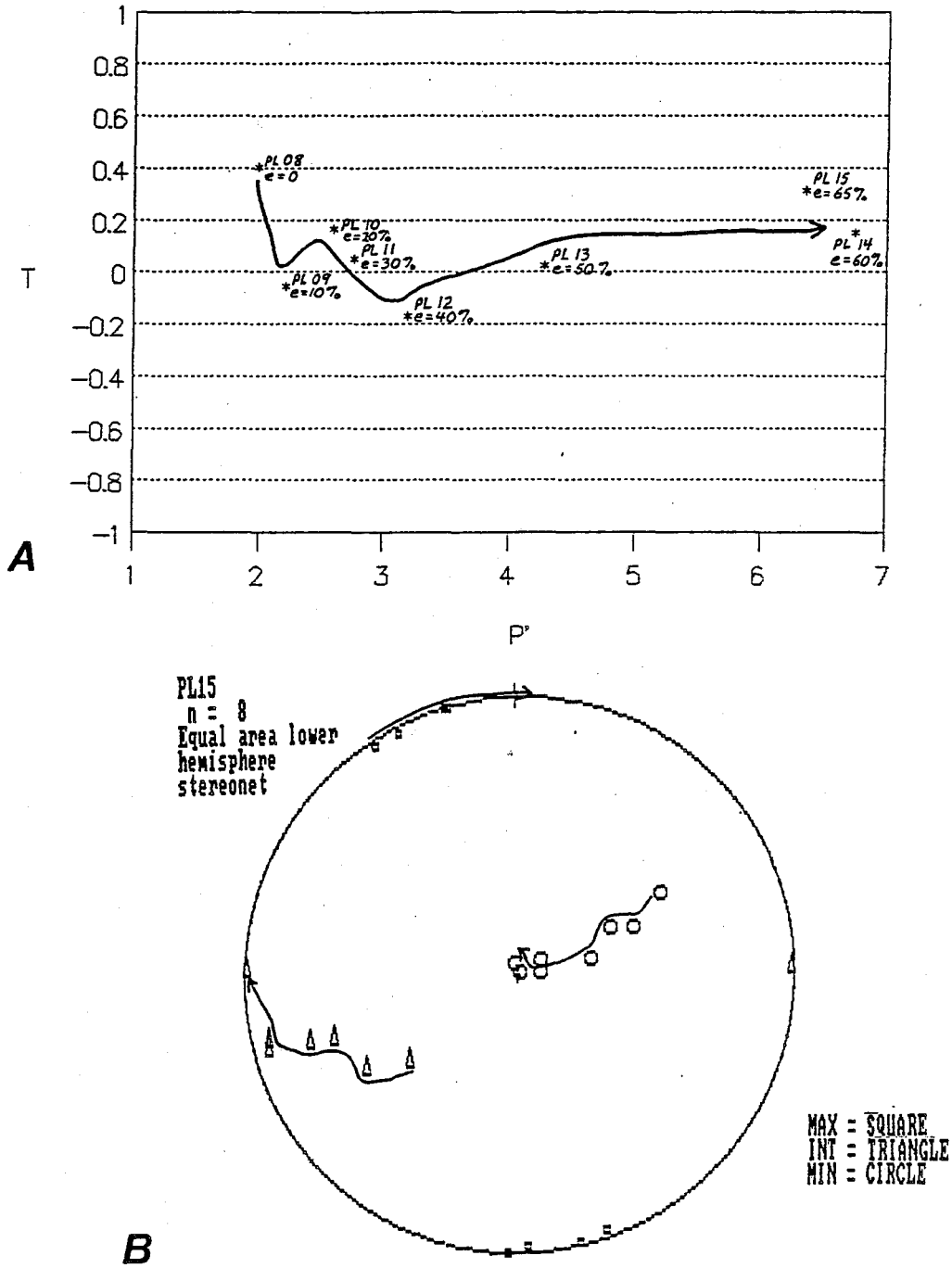

Figure 2.7. (a) P'-T diagram and (b) stereonet illustrating the progression of complex magnetic susceptibility fabrics during the first pure shear experiment performed on plasticene plus aluminum disks. Note that the calculated strains for each deformation increment are shown in the P'-T diagram.

2.8 (Ramsay and Huber, 1983; Borradaile, 1988) show how initial fabrics can be affected by strain. Methods such as the Rf/Ø destraining method discussed by Borradaile (1987) must be used to obtain accurate strain estimates in such cases where random particle orientations were not present. Also, the effects of interaction between the relatively large aluminum disks, their small numbers, and the possibility of "saturation" alignment at high strain contribute to the non-quantitative relationship. This is a similar interpretation to that made by Puumala (1989) for magnetic fabrics in experimentally deformed plasticene.

Experiment # 2 (PL16-23)

This experiment utilized exactly the same materials as the first successful pure shear experiment. The same strain increments were produced, resulting in the data presented in figure 2.9. As before, K''_{min} proceeded to become vertical, while the other principal susceptibilities defined the plane of flattening. In this experiment, a much stronger oblate fabric was generated than in the first experiment. The initial increments produced little increase in anisotropy, however, a rapid change from prolate to oblate anisotropy was observed. The sample reached a maximum degree of oblateness, after which P' increased rapidly. Once again, there was no apparent quantitative relationship between ACMS and strain. This can be attributed to the same possible reasons cited for the first experiment.

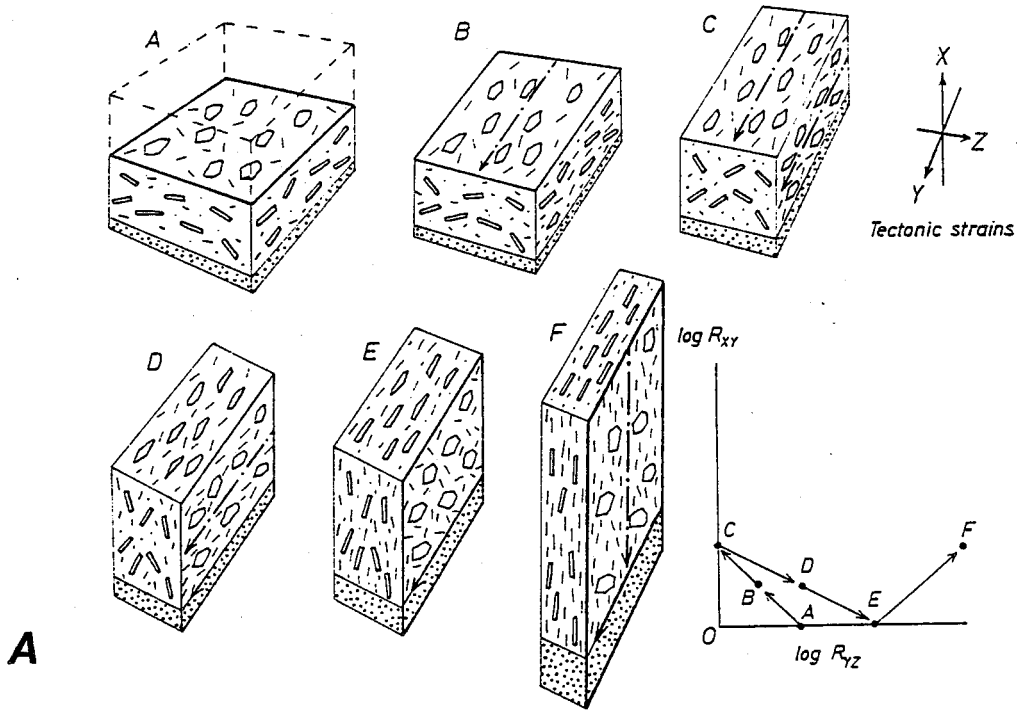

A

Figure 10.24. *Progressive stages in fabric development arising from the tectonic deformation of a shale.* A, *initial compacted shale;* B, *earliest deformation stage;* C, *pencil structure stage;* D, *embryonic cleavage stage;* E, *cleavage stage;* F, *cleavage with stretching lineation.*

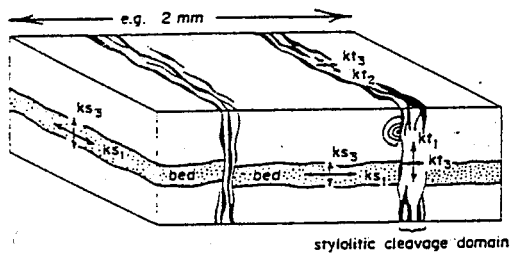

Fig. 8. Where a tectonic fabric develops a domainal texture, such as in stylolitic cleavage, there may be distinct contributions of magnetic anisotropy from different parts of the rock. Cleavage zones may contribute a tectonic susceptibility anisotropy while inter-cleavage domains may still retain a sedimentary magnetic fabric. The susceptibility determination for the rock blends the two fabrics.

B

Figure 2.8. This diagram illustrates two cases in which (a) fabric develops a number of different anisotropies during deformation due to the relationship between initial fabrics and strain (Ramsay and Huber, 1983) and (b) in magnetic fabrics where a domainal fabric exists. Different magnetic fabrics are present in the bedding and cleavage domains (Borradaile, 1988).

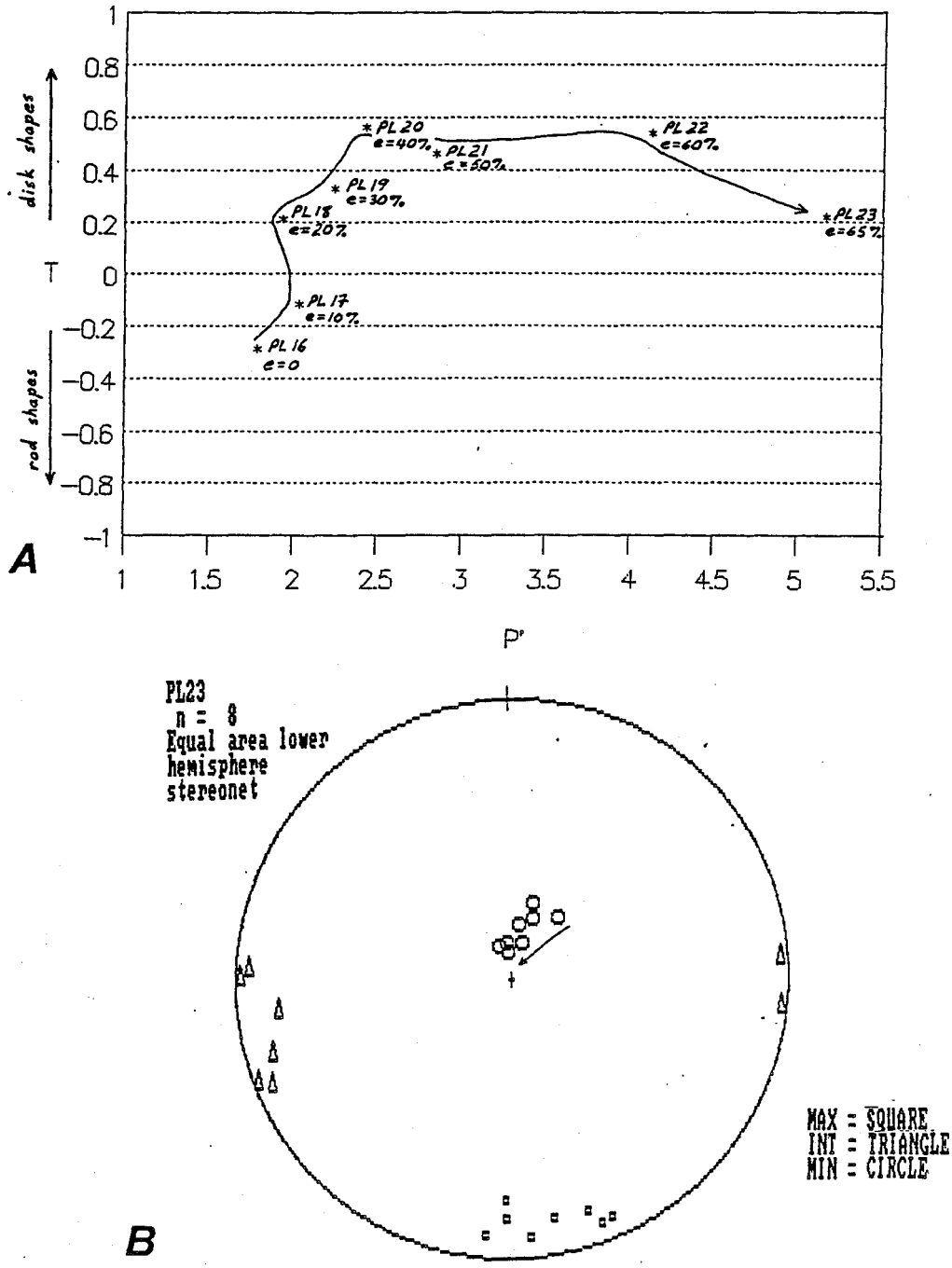

Figure 2.9. (a) P'–T diagram and (b) stereonet illustrating the progression of complex magnetic susceptibility fabrics during the second pure shear experiment performed on plasticene plus aluminum disks. Note that the calculated strains for each deformation increment are shown in the P'–T diagram.

Experiment # 3 (PL24-30)

The method for this experiment was similar to that for the previous ones, except that 5 cm^3 of plasticene containing only 25 aluminum disks was used. This size of sample allowed for a greater degree of strain to be achieved, with increments of 0, 12.5, 25, 37.5, 50, 62.5, and 75% shortening.

The deformation proceeded in a similar pattern to that of the previous experiments as seen in figure 2.10. The P'-T diagram illustrates a somewhat erratic increase in anisotropy and oblateness of fabric. The accompanying stereo-net illustrates the expected steady migration of the axis of minimum susceptibility towards parallelism with the compression direction.

Experiment # 4 (PL39-45)

This experiment made use of the same materials used in the first two pure shear experiments. The procedure was approximately the same, except that deformation ceased after 60% shortening. The overall pattern of deformation was very similar to that in experiment # 3 as figure 2.11 illustrates.

2.3.3. Discussion of pure shear results

Each experiment shows distinct changes in the character of electrical anisotropy as a result of deformation. Pure shear

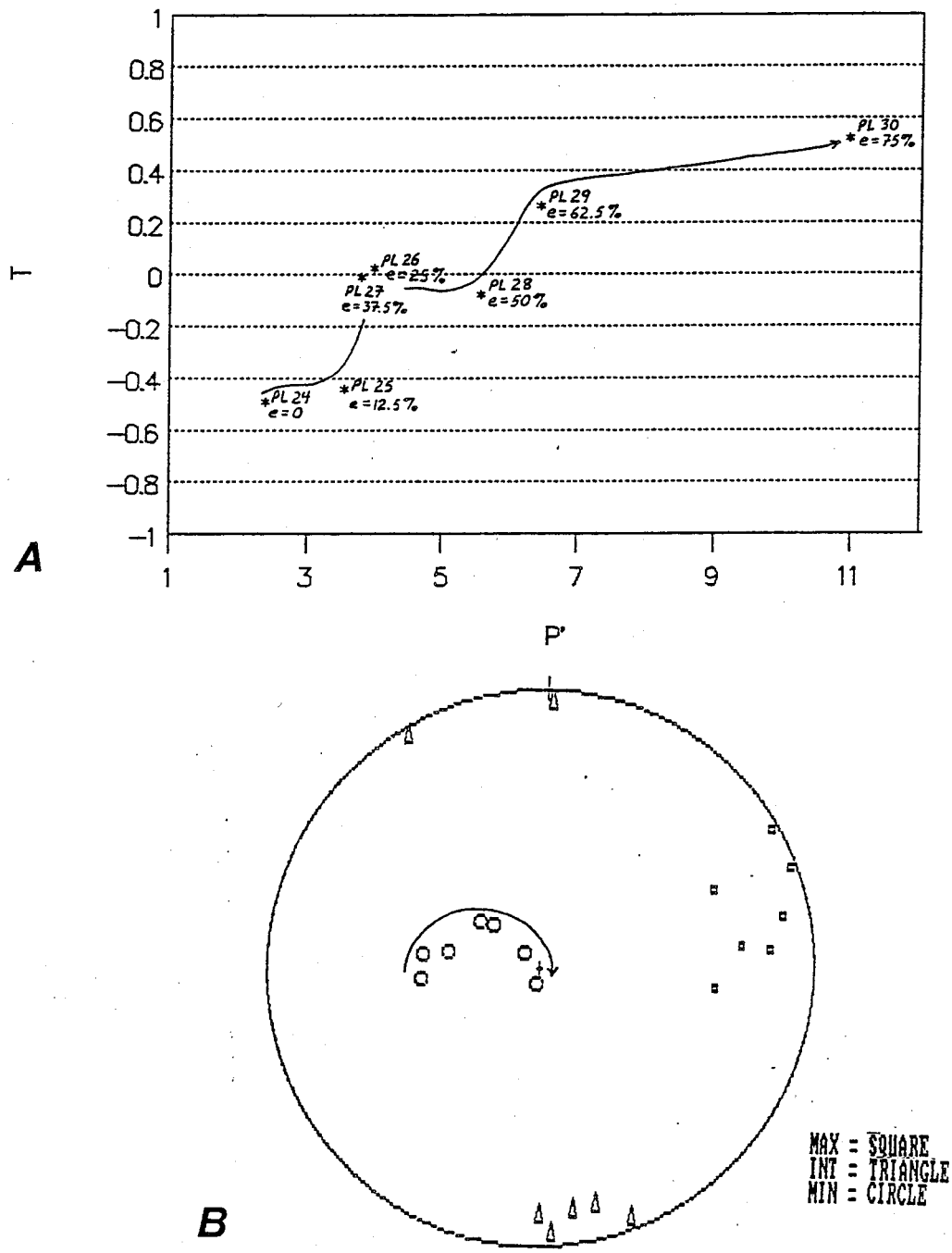

Figure 2.10. (a) P'-T diagram and (b) stereonet illustrating the progression of complex magnetic susceptibility fabrics during the third pure shear experiment performed on plasticene plus aluminum disks. Note that the calculated strains for each deformation increment are shown in the P'-T diagram.

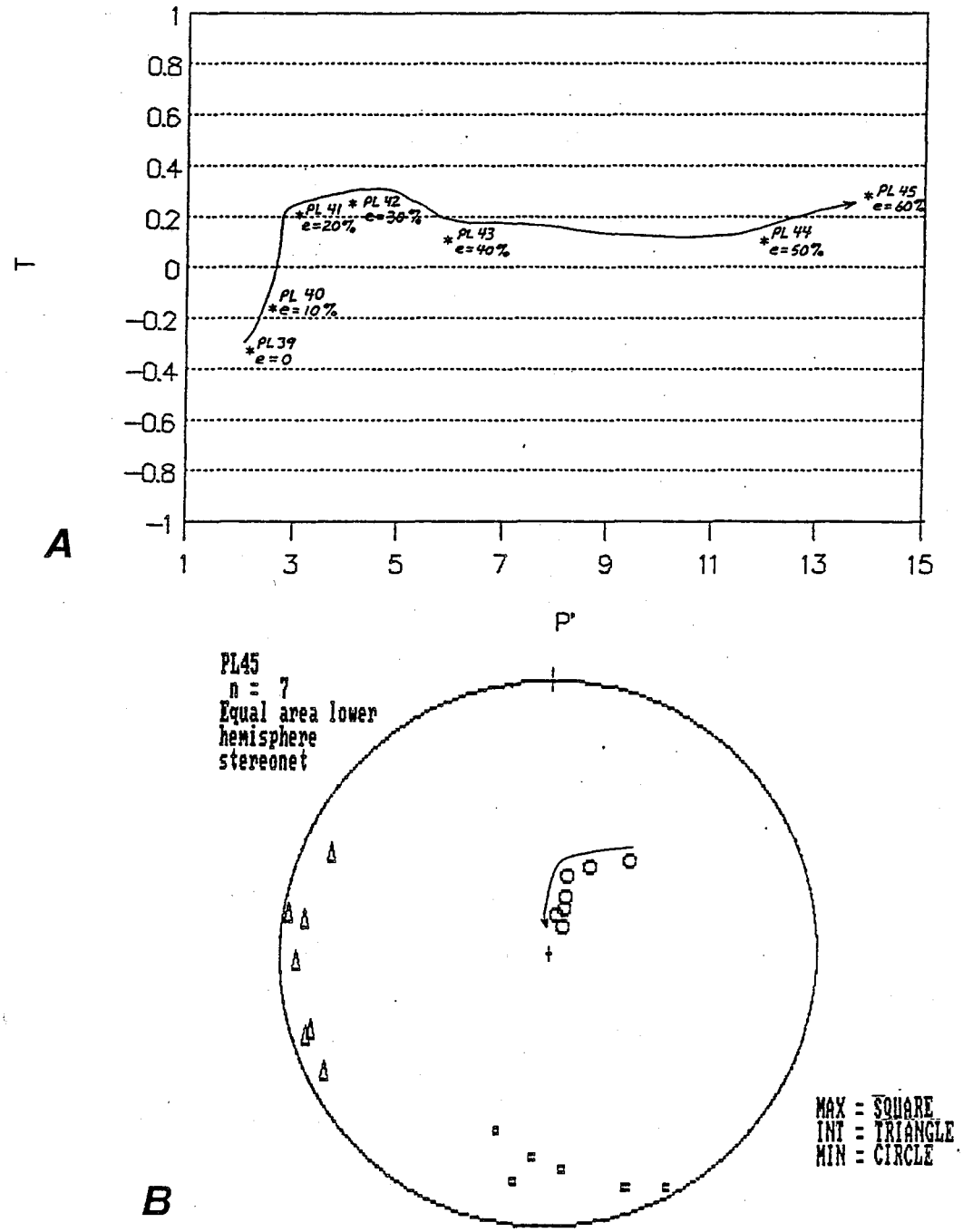

Figure 2.11. (a) P'-T diagram and (b) stereonet illustrating the progression of complex magnetic susceptibility fabrics during the fourth pure shear experiment performed on plasticene plus aluminum disks. Note that the calculated strains for each deformation increment are shown in the P'-T diagram.

deformation results show increased anisotropies with deformation as well as the general development of slightly oblate fabrics. The fabrics developed were not quite as oblate in character as expected, especially if one considers the kinetics of plasticene deformation to be the same as that for the study by Puumala (1989) in which AMS was studied using magnetite embedded in a plasticene matrix. In these experiments, the AMS fabric for magnetite developed a very strongly oblate character in pure shear experiments as shown in figure 2.12.

The fact that the aluminum particles had perfect disk shape would lead one to believe that strongly oblate ACMS fabrics should develop with increasing preferred dimensional orientation. However, the fabrics were less oblate than expected. This could be a function of the initial fabrics, which in general were prolate. It is also possible that the disks may have had some conductivity anisotropy derived from impurities in the aluminum or structural defects. Moreover, T values are small due to errors in definition of the principal susceptibility axes. Susceptibility values from the X-Y plane of strain were sometimes very low and difficult to reproduce. Standard deviations for some axial determinations were above 10%. It was also noticed that K''_{min} was generally defined with greater certainty (R95 often less than 5°) than K''_{int} and K''_{max}. This is a common occurence for specimens of highly oblate anisotropy.

The migration of the principal susceptibility axes indicates that the axes of ACMS rotate into parallelism with the principal

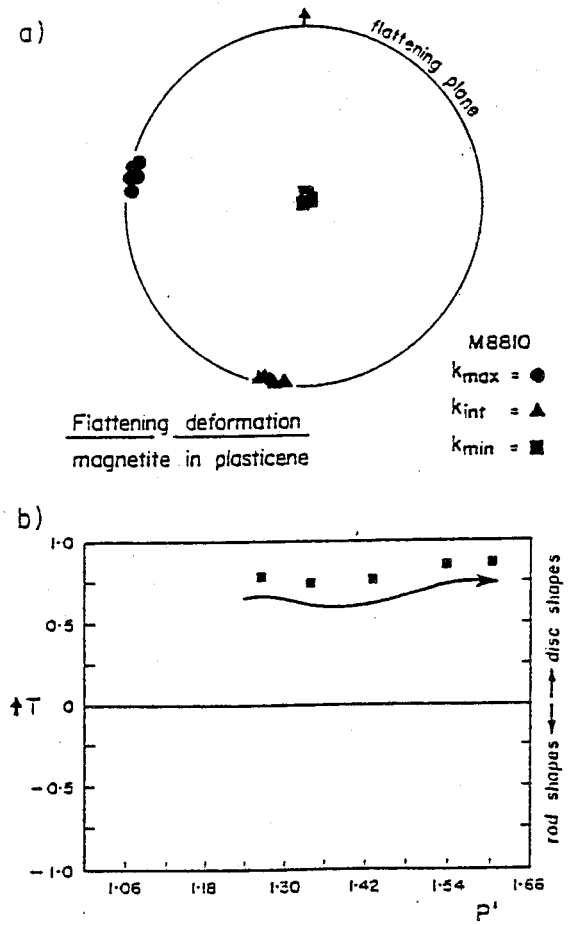

Figure 8. (a) Note the consistency in orientation of principal susceptibilities during experiment # 1. (b) The fabric becomes consistently more anisotropic with increasing deformation.

Figure 2.12. The development of magnetic susceptibility fabric in pure shear experiments performed on plasticene plus magnetite mixtures (Puumala, 1989) shows a similar pattern to that observed in the pure shear produced complex magnetic susceptibility fabrics in figures 2.7, 2.9, 2.10, and 2.11.

axes of the strain ellipsoid. This is particularly evident in the correspondence between the K''_{min} and X strain directions.

The sense of anisotropy in these experiments tend to mimic that of strain, with both being described by oblate ellipsoids. However, ACMS fabrics in these experiments tended to be less oblate than strain fabrics. This is to be expected, as the strains were assumed to have been perfectly oblate in character.

2.3.4 Simple shear data

Three successful simple shear experiments were performed. These will also be discussed individually.

Experiment # 1 (PL50-62)

The initial simple shear experiment utilized 8 cm^3 of plasticene containing 50 aluminum disks. Shear strains were applied to the specimen in increments of 0.3 from 0 to 3.2. In order to achieve shear strains of up to 3.2, the specimen had to be cut and re-assembled after approximately every three strain increments as illustrated previously in figure 2.6.

The stereo-net of figure 2.13 shows that K''_{min} was originally in a position much different from the shearing direction. As deformation proceeded, K''_{min} rotated progressively into the shearing direction with a plunge of approximately 45°. After reaching the shear direction, K''_{min} began rotating toward

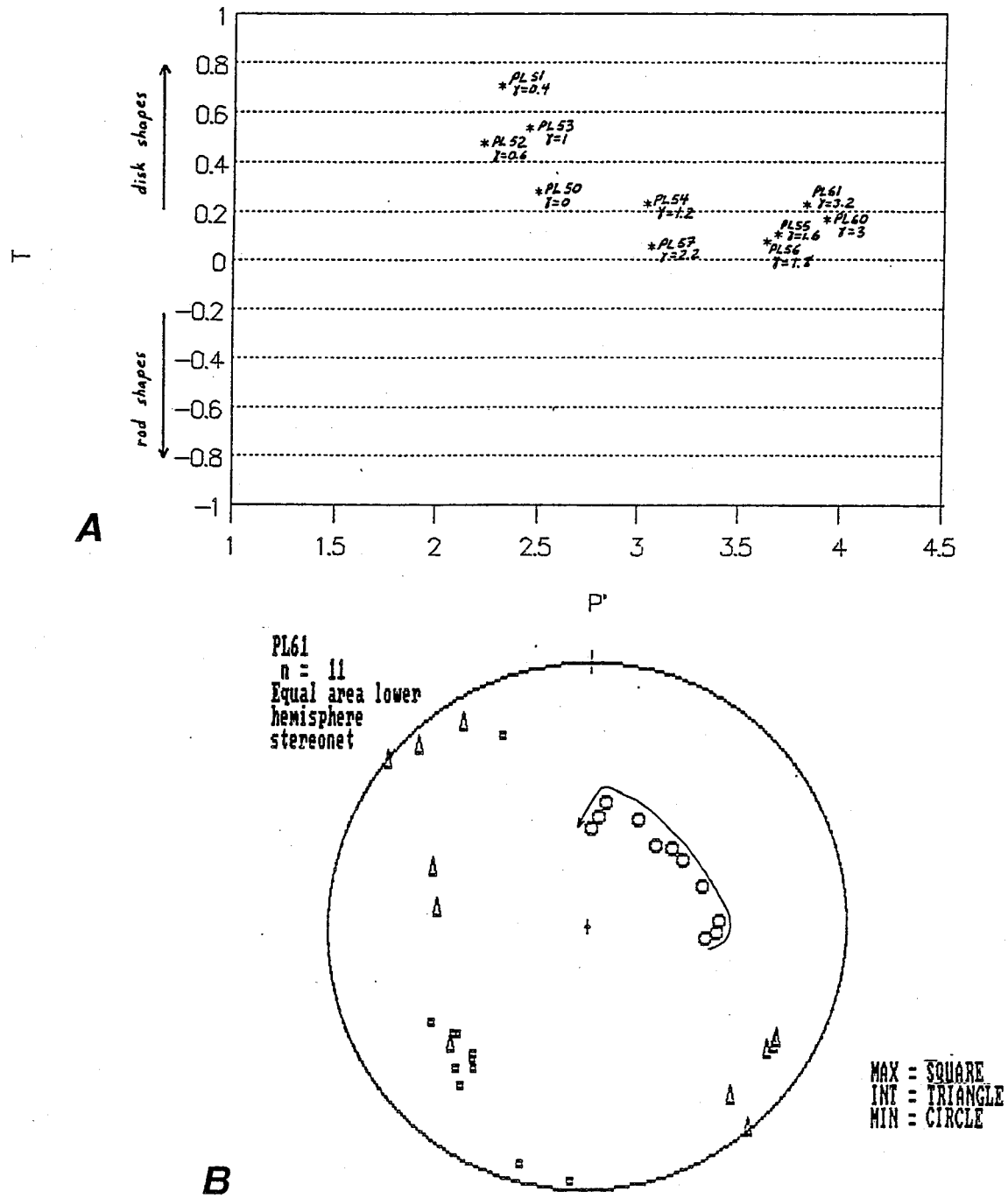

Figure 2.13. (a) P'-T diagram and (b) stereonet illustrating the progression of complex magnetic susceptibility fabrics during the first simple shear experiment performed on plasticene plus aluminum disks. Note that the calculated strains for each deformation increment are shown in the P'-T diagram.

the vertical as expected in simple shear. This is a very similar result to that discovered for AMS by Borradaile and Puumala (1989). Despite the ordered movement of K''_{min}, the other principal susceptibilities showed erratic development.

Figure 2.12 also illustrates a Jelinek-Hrouda diagram. This shows an erratic pattern of fabric development with strain. However, the diagram illustrates a tendency for the fabric to approach plane strain (T = 0) as is typical in simple shear, after beginning in the oblate field. The degree of anisotropy P' tended to increase with deformation, but was very erratic. This was undoubtedly due to the disruptive effect of specimen-cutting discussed earlier. The initial fabric also appears to have had a major effect upon the first few strain increments.

Experiment # 2 (PL63-73)

The materials and procedure were identical to those for the first simple shear experiment, except that the maximum shear strain produced was only 3.0. The relevant data pertaining to this experiment are illustrated in figure 2.14. The stereo-net shows rapid migration of the minimum resistive susceptibility toward near-parallelism with the shear direction. There was also a very slow subsequent rotation toward the vertical. The other principal axes also display a well defined migration as strain progressed. The P'-T diagram shows an interesting pattern of fabric development. Fabrics progressed from extreme prolateness

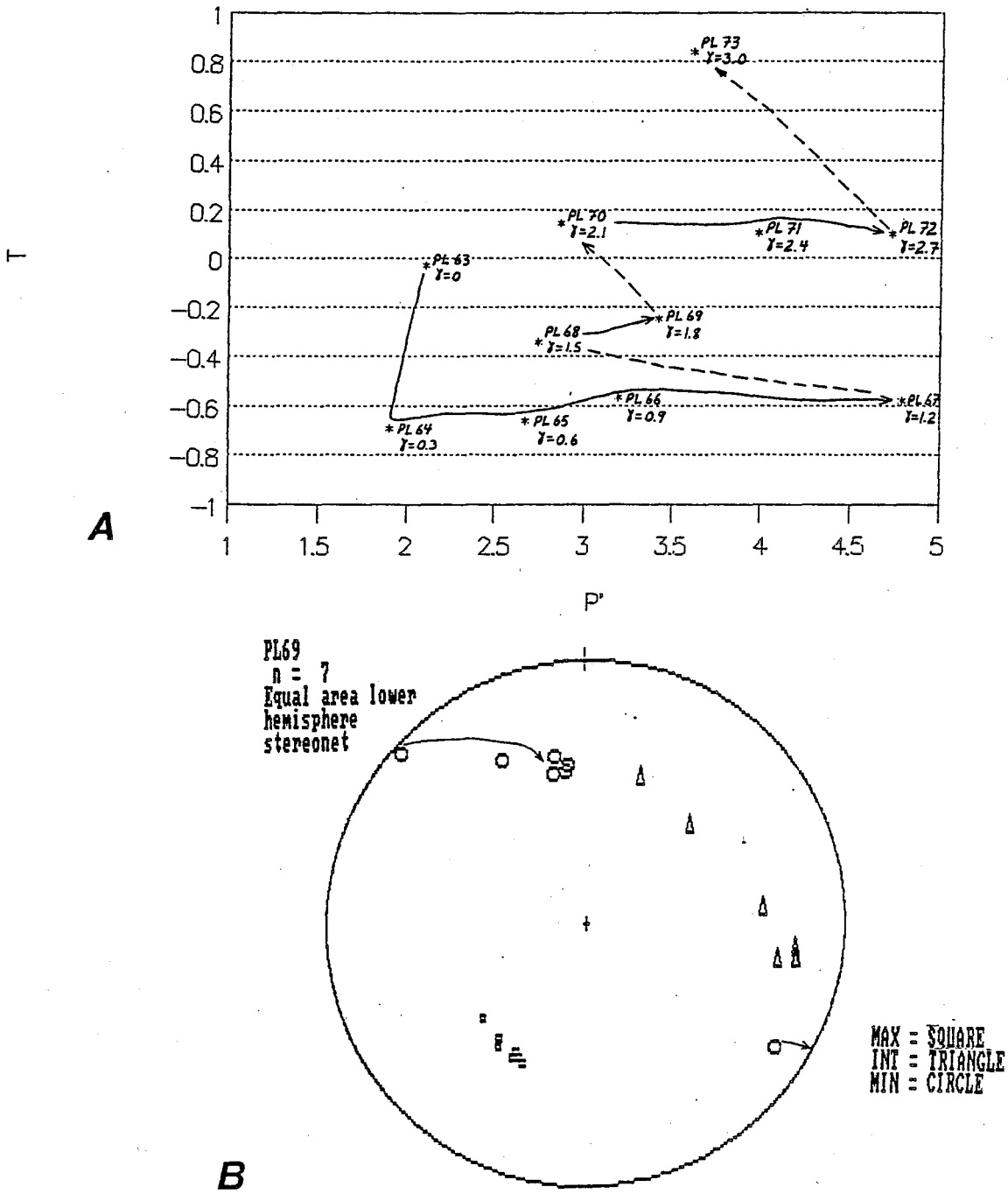

Figure 2.14. (a) P'–T diagram and (b) stereonet illustrating the progression of complex magnetic susceptibility fabrics during the second simple shear experiment performed on plasticene plus aluminum disks. Note that the calculated strains for each deformation increment are shown in the P'–T diagram.

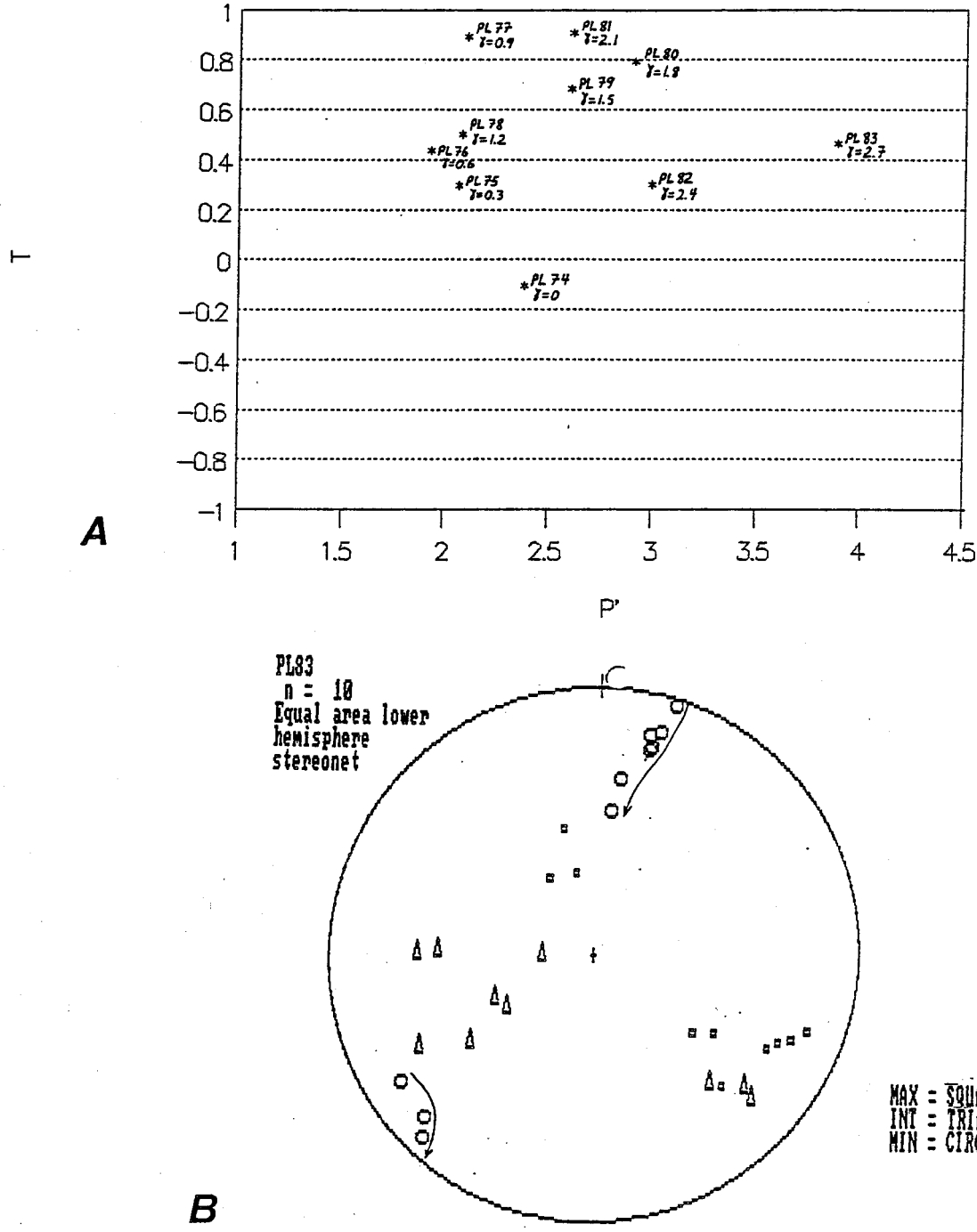

Figure 2.15. (a) P'-T diagram and (b) stereonet illustrating the progression of complex magnetic susceptibility fabrics during the third simple shear experiment performed on plasticene plus aluminum disks. Note that the calculated strains for each deformation increment are shown in the P'-T diagram.

toward plane strain, with a sudden jump into the oblate field for the final strain increment. The first strain increment produced a large jump from plane strain to the prolate field related to the initial shape and orientation of the ACMS ellipsoid. There are three marked discontinuities in the development of fabric, where the anisotropy (P') of the ellipsoid decreases. These all correspond to the strain increments between which the specimen was cut. Thus cutting has a major effect on anisotropy, causing a decrease, likely resulting from the disturbance of a number of aluminum disks. There is an apparent tendency toward plane strain similar to the first experiment if the final increment of strain. This may also be artificial if the other cuts affect the fabric similarly.

Experiment # 3 (PL74-PL83)

This experiment was identical to the other simple shear experiments, except it only achieved a shear strain of 2.7. Unfortunately, fabric development was extremely erratic, with little pattern evident in the P'-T diagram of figure 2.15. The later increments of shear do appear to show a general anisotropy increase, though. The poor fabrics were probably related to the specimen cut effect. Despite the erratic development of anisotropy, the migration of K''_{min} illustrated in figure 2.15 was once again well defined, proceeding as in the previous experiments. The sudden reversal of K''_{int} and K''_{min} shows a

sudden change in the ellipsoid related to its initial shape or more likely the cut following the third increment of strain.

2.3.5. Discussion of simple shear experiments

The simple shear deformation experiments appear to show that the K''_{min} axis of the ACMS ellipsoid tends to approach parallelism with the shear direction as deformation begins. Once this is achieved, this axis rotates progressively toward the vertical as is known to occur in nature. This also confirms the findings of AMS studies on plasticene-based aggregates (Borradaile and Puumala, 1989).

Unfortunately, ACMS fabric development in these experiments was erratic. This can be attributed largely to the experimental conditions, which were far from ideal. The small numbers of aluminum disks do not allow for statistical alignment of grains corresponding to strain. Also, only the disks within a few millimetres of the surface of each specimen are measured by the instrument due to the "skin effect". Probably 100 to 1000 much smaller grains per specimen would increase the correspondence between ACMS and strain. Despite these problems, there appear to be trends toward greater anisotropy with strain in each of the three experiments. Also, two experiments showed some evidence for a tendency toward plane strain fabrics, which were also observed by Borradaile and Puumala (1989).

2.4. Geological Implications

One might assume that aluminum is analogous to nearly electrically isotropic ore minerals such as pyrrhotite which has an anisotropy of only about 10% according to Krontiras et al. (1984). Therefore the foregoing experiments may have some geological relevance. The plasticene plus aluminum observations indicate that the principal axes of complex susceptibility should correspond to the principal strain axes in geological materials which contain conductive minerals having a shape-controlled anisotropy. This is assuming that deformed ore minerals develop preferred orientations as a result of tectonic strain. This indeed does occur and is summarized for a number of ore minerals in the reviews by Clark and Kelly (1976), McClay (1983), and Siemes and Hennig-Michaeli (1985). The preferred orientations developed are both dimensional and crystallographic. Which type occurs depends upon the conditions of stress and temperature at the time of deformation.

Preferred orientations of conductive minerals developed during deformation events thus should produce ACMS fabrics showing some relationship to strain, even if these are crystallographically controlled. It is possible that there may be difficulties in using ACMS to estimate strain values similar to that for AMS discussed by Borradaile and Mothersill (1984), but valuable data may be derived from the principal susceptibility axes. AMS can provide useful strain estimates in mineralogically

homogeneous rocks (Hrouda, 1987), especially where a single phase is responsible for the fabric. Since most ores contain only a limited number of highly conductive minerals such as chalcopyrite and pyrrhotite, it may be easier to obtain quantitative strain estimates using ACMS.

The success of the preceding experiments suggest that study of experimentally deformed ore minerals is justified.

3. EXPERIMENTALLY DEFORMED PYRRHOTITE AGGREGATES

3.1. Materials and Method

A number of deformation experiments were performed on aggregates of loose pyrrhotite having a grainsize in the range of 0.15 to 1.0 mm. The pyrrhotite was obtained by crushing specimens of massive sulphide from Shebandowan, Ontario which contained mostly pyrrhotite, and washing and sieving the grain aggregates.

The specimens were each deformed to varying degrees in a Donath triaxial deformation rig by pure shear. Specimens were protected in cylindrical teflon jackets with Berea sandstone disks at both ends to contain the aggregate. The purpose of the study was to determine if the ACMS fabrics measured in the deformed specimens showed any correspondence to calculated strain values and AMS fabrics. AMS fabrics have already been shown to have a correlation with strain (ie. Borradaile and Alford, 1987; Hrouda, 1987; Borradaile and Mothersill, 1984; Wood et al., 1976; and many others). Pyrrhotite was chosen for this experiment, as it is highly conductive and has a significant, measurable magnetic susceptibility. Its resistivity is only 2 to 160 x 10^{-6} Ω-m (Keller, 1982) and its magnetic susceptibility is 1.5 SI/volume (Carmichael, 1982). The specimen measurement procedure was the same as for the previous experiments, and the raw ACMS conductivity data were converted to resistive values for the purpose of graphical anisotropy interpretation in P'-T diagrams.

Two separate batches of pyrrhotite were used in these experiments. The first batch was used for specimens P002 to P008. This material contains many impurities which were recognized in polished section following ACMS measurement. There was about 70% pyrrhotite containing some pentlandite, 15% magnetite, and 15% chalcopyrite. The second batch was of much greater purity, containing about 95% pyrrhotite, with the remaining volume being comprised of pentlandite and chalcopyrite. The composition differences mean that the data for the two sample sets must be analysed separately.

Initially a specimen of known mass was hydrostatically compacted at a confining pressure of 150 MPa (1.5 kbars) in the triaxial rig for each batch of pyrrhotite. This allowed for determination of the ratio of mass : length of an "undeformed", but hydrostatically compacted specimen. "Undeformed" means that no differential stress was applied, although some preferred orientation of grains did develop in some cases due to initial pouring of aggregate into teflon tubes. By doing this test, the mass of specimens deformed using an applied differential stress could be used to calculate what the initial length of the specimen under a confining pressure of 1.5 kbars would be. Thus the measured length of a deformed specimen could be subtracted from its predicted initial length to calculate shortening. These measured strains were very unreliable, as the specimens typically cracked upon depressurization. One of these features is illustrated in the photomicrograph of figure 3.15. Thus other

means of strain calculation were used. These included the use of Rf/Ø analysis and chart recordings of piston displacement from the triaxial rig.

Differential stress was applied to specimens of 3/4" and 1/2" diameter under 1.5 kbars of confining pressure. This was done at a strain rate of approximately 10^{-4} s^{-1}. The 1/2" specimens provided greater strains, as they built up differential stress much more slowly and did not reach high enough values to potentially damage the triaxial rig. There was one drawback to the smaller specimens. This was that they did not provide as large an ACMS signal. Also, the deformation of specimens meant that they were variable in their shapes. However, this was not considered to be of great importance, as the conductive material was a number of grains much smaller than the bulk volume, similar to the situation in the aluminum plus plasticene experiments.

Figure 3.1 shows a typical differential stress versus strain curve. These charts were used as another method to calculate strains, after the elastic strain represented by the steeply sloping line at the end of the deformation (obtained during unloading) was subtracted. These charts were only obtained for deformations after experiment P013, as the chart recorder was not previously operational.

After each deformation experiment was completed, the specimens were impregnated with epoxy so that the specimens would remain intact for ACMS and AMS measurement. This process was also used in polished section preparation.

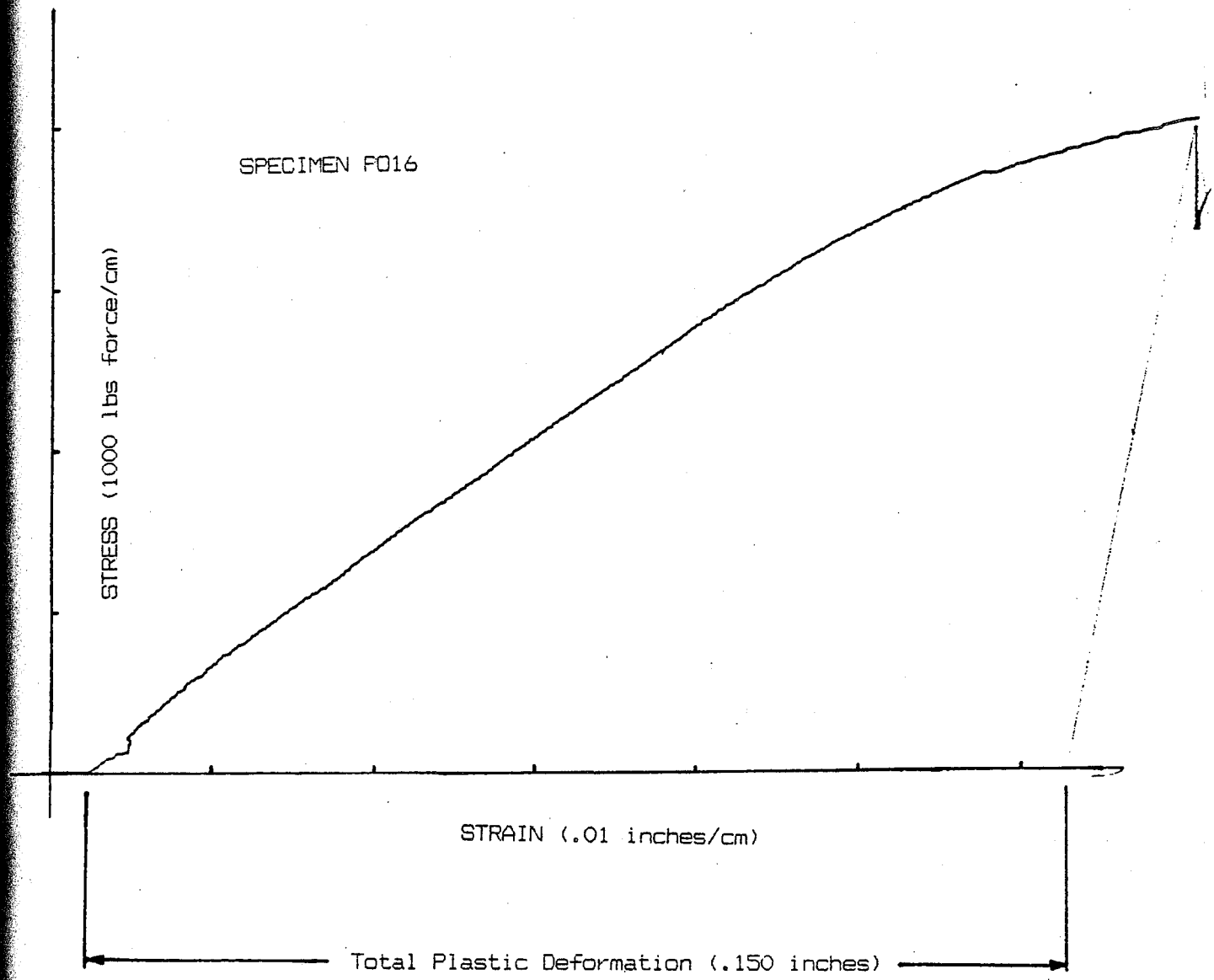

$$e = \frac{\text{plastic deformation}}{\text{initial length}} = \frac{.150}{.679} = 22.1\% \quad Rs = 1.454$$

where $Rs = (1 - e)^{-1.5}$ for three dimensional pure shear

Figure 3.1. A typical chart recording of a triaxial deformation is illustrated. Strain is plotted on the X-axis against differential stress. Rs is calculated by dividing the initial specimen length minus the total plastic deformation illustrated above by the initial estimated specimen length. Initial specimen length is calculated from a factor related to mass obtained from hydrostatically deformed specimens.

The electrical and mechanical properties of the materials used in these experiments will be discussed before the experimental data is presented.

3.2. Electrical Properties of Pyrrhotite

Pyrrhotite is a mineral which is variable in composition, having the chemical formula $Fe_{1-x}S$. Stoichiometric FeS is known as troilite and has many important differences from pyrrhotite. Magnetically, it is antiferromagnetic, while pyrrhotite is ferrimagnetic (Hirahara and Murakami, 1958). Troilite also has a much higher electrical anisotropy than pyrrhotite. Troilite is not commonly found on the surface of the earth, but is an important component of meteorites (Shuey, 1975). The structure of troilite, however, is similar to that of pyrrhotite, which has an iron deficiency. Natural pyrrhotite can be of hexagonal or monoclinic symmetry depending on the degree of iron deficiency. When iron comprises less than 47.2 % atomic weight, hexagonal symmetry gives way to monoclinic symmetry. Natural pyrrhotites are commonly intergrowths of these two varieties.

Three separate specimens of pyrrhotite were analysed using the X-ray diffraction technique in an effort to determine their composition. The first two specimens were obtained from the two batches of pyrrhotite used in this chapter, while the third specimen is representative of the Shebandowan ore for which ACMS data was obtained in chapter 5. Samples were prepared by crushing them to a fine powder along with approximately 40% by volume of NaCl which acts as a buffer. The specimens were then mounted on microscope slides in nail polish. The samples were analysed using Fe tube radiation. Results for each specimen are illustrated in

figures 3.2 to 3.4. Note that each specimen exhibits a double peak between the 2θ values 55.5 and 57. These are at the (102) reflection of hexagonal pyrrhotite (Scott, 1974). This double peak is characteristic of monoclinic pyrrhotite. If hexagonal pyrrhotite were present, only a single peak would appear and the iron content of the pyrrhotite could be estimated from the d-space value for this peak (Scott, 1974). However, the presence of monoclinic pyrrhotite and the resultant double peak for each specimen makes this calculation impossible. Although this data does not give an indication of the actual chemical formula of the three pyrrhotites, it does provide some valuable information about these specimens. For instance, the nearly equal intensities of the two peaks in figures 3.2 and 3.4 indicate that the pyrrhotite in these specimens is probably almost exclusively monoclinic (S. Kissin, personal communication). The unequal peaks of figure 3.3 indicate that monoclinic and hexagonal symmetries are probably both present. This may be part of the reason for the slightly lower magnetic susceptibilities of specimens from the second batch of pyrrhotite aggregate discussed later in this chapter. This is because monoclinic pyrrhotite is much more magnetically susceptible than hexagonal pyrrhotite (Shuey, 1975).

X-ray fluorescence (XRF), scanning electron microscope (SEM), atomic absorption (AA), and inductively coupled plasma (ICP) analyses were also attempted to determine the chemical composition of the pyrrhotites, but all obtained unsatisfactory results. Unfortunately, this means that no possible correlations

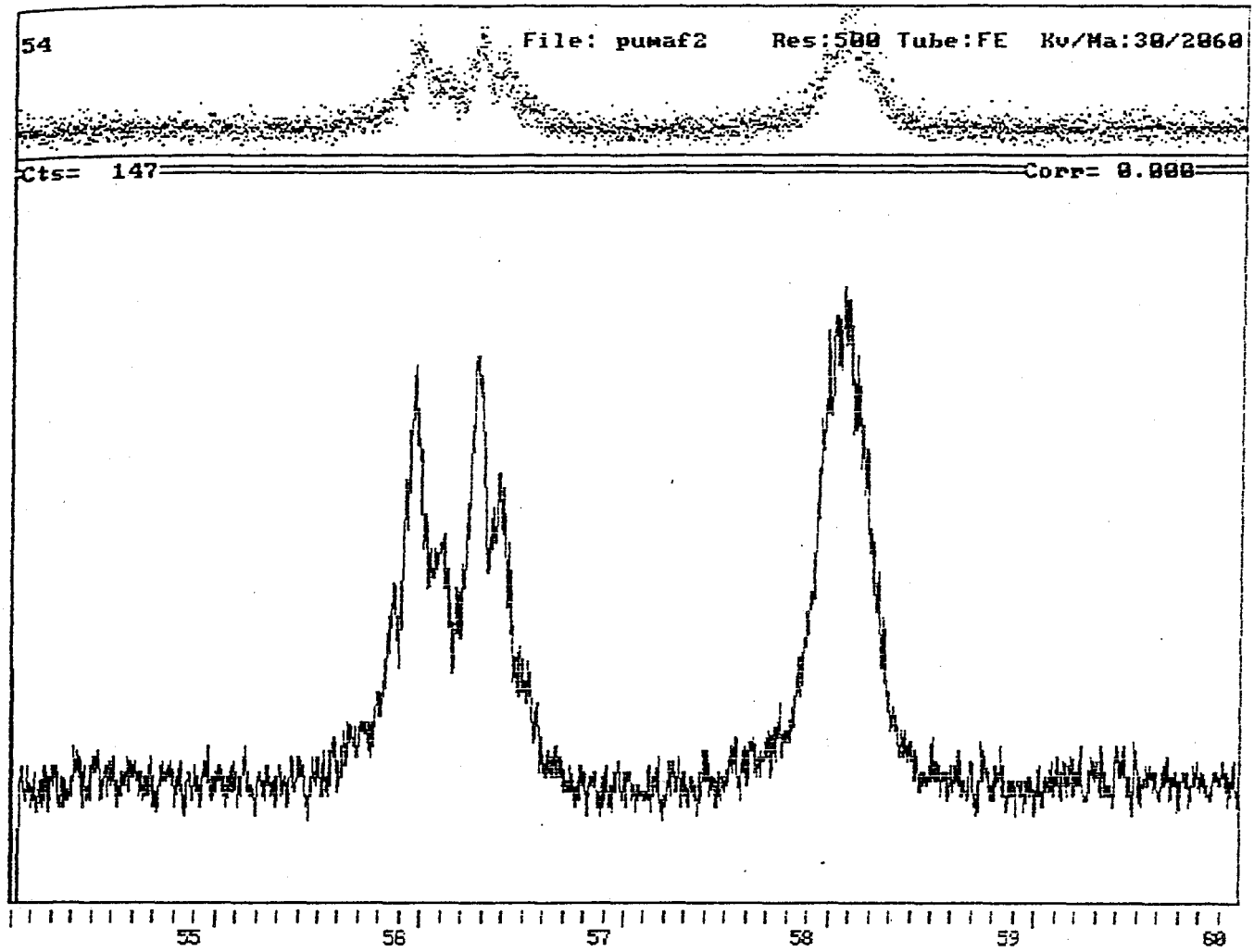

Figure 3.2. This is the X-ray diffraction trace for the pyrrhotite used in specimens P002 to P008 discussed in this chapter. The double peak indicates the presence of monoclinic pyrrhotite.

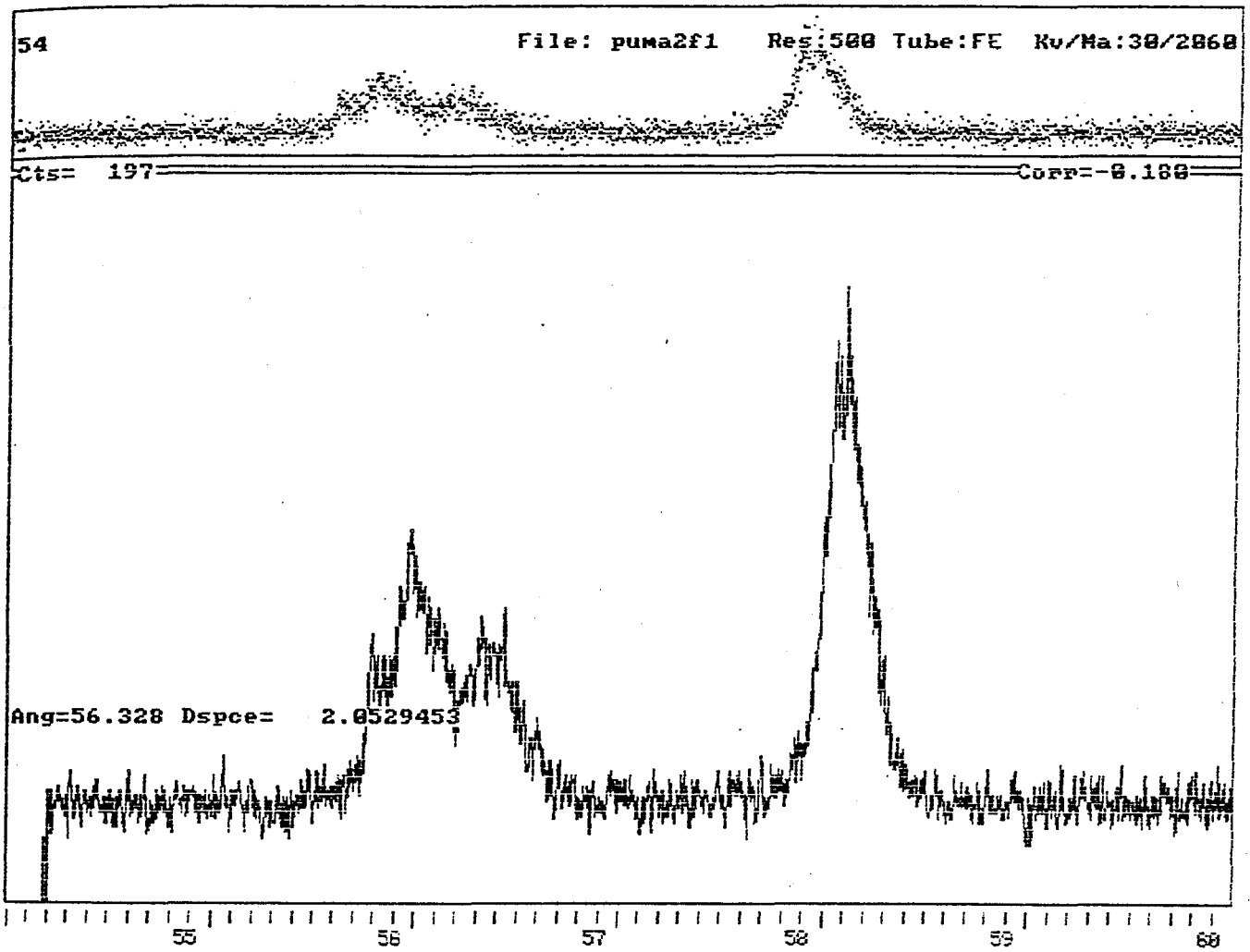

Figure 3.3. This pyrrhotite was used in specimens P009 to P028. The difference in height between the two peaks between 55.5 and 57 indicates that both hexagonal and monoclinic pyrrhotite were present in this specimen.

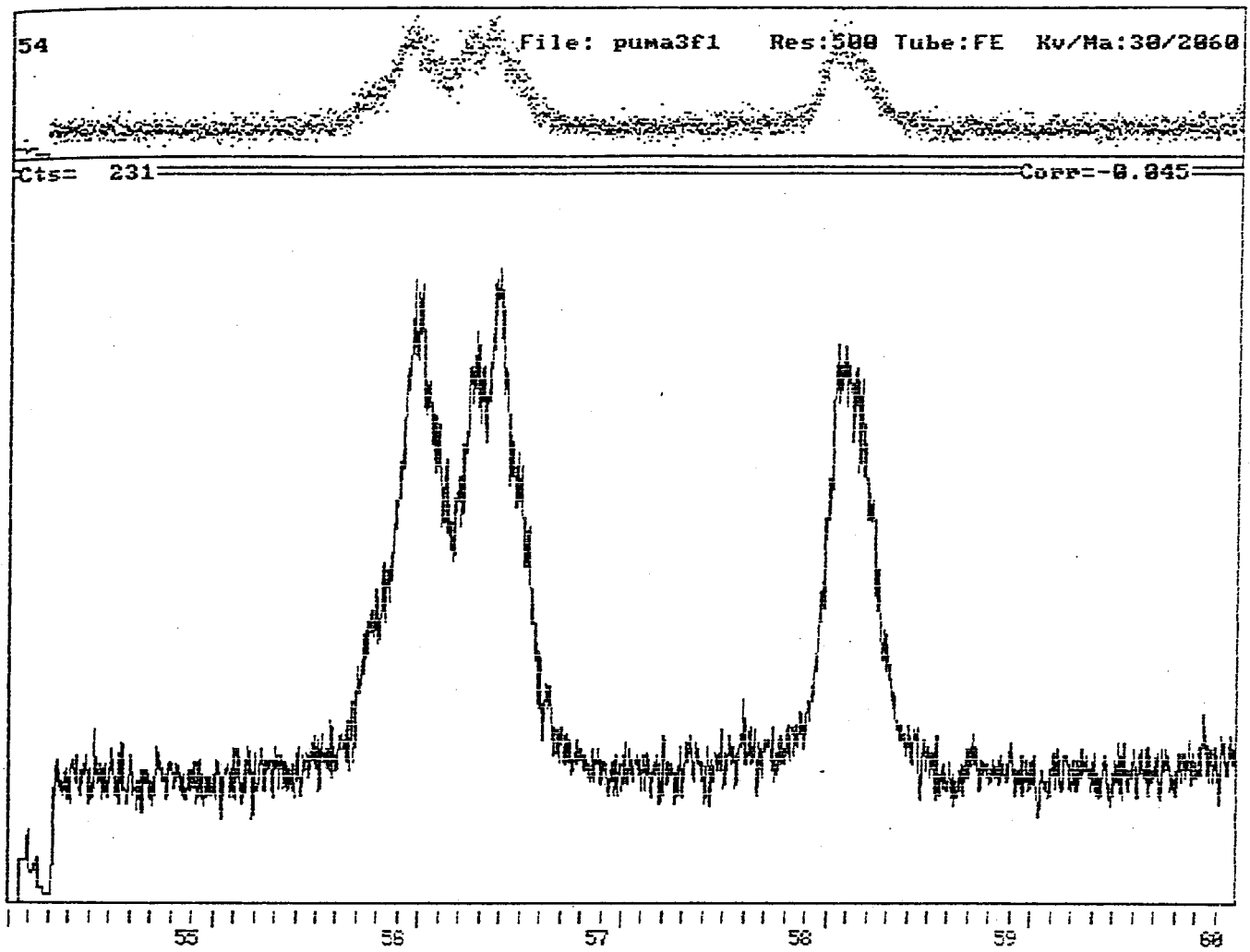

Figure 3.4. This massive pyrrhotite specimen from the Shebandowan mine is discussed in chapter 5 and, like the specimen of figure 3.2, contains monoclinic pyrrhotite.

between chemical composition and ACMS response for pyrrhotite can be made in this study.

The resistivity of pyrrhotite is quoted as 2 to 160 X 10^{-6} Ω-m (Keller, 1982). Four pieces of the pyrrhotite specimen SB02 were measured on a Hewlett-Packard 4192A impedence analyser upon which a resistivity of approximately 3.45 X 10^{-3} Ω-m was determined for each specimen. This is higher than expected, probably because of insufficient contact between specimen and instrument (M. Hawton, personal communication). Thus the true resistivities of the specimens are probably much lower.

Pyrrhotite is a mineral with an extremely high crystallographically controlled magnetic suscsptibility anisotropy (Schwartz, 1974), however, it only has a small electrical anisotropy of about 10%. The highest resistivity is parallel to the c-crystallographic axis (Krontiras et al., 1984), which is also the axis of least magnetic susceptibility. It is also important to note that the c-axis tends to become parallel to the maximum compressive strain axis during plastic deformation (Siemes and Hennig-Michaeli, 1985; McClay, 1983; and Clark and Kelly, 1976). Monoclinic and hexagonal pyrrhotite were considered essentially isotropic by Shuey (1975).

Pyrrhotite is a semiconductor. It has usually been assumed that charge carriers in pyrrhotite are holes associated with the iron vacancies. However, this is probably not the case, as conductivity should increase proportionately with iron deficiency, but pyrrhotite has nearly the same conductivity as

troilite (Shuey, 1975). This would make it essentially an intrinsic semiconductor. Sakkopolous et al. (1984) have shown that there probably is significant impurity-band or extrinsic semiconduction in pyrrhotite. They attribute this effect to the presence of such common impurities as Ni, Co, and Cu, as well as lattice defects (ie. vacancies).

The presence of pentlandite exsolution flames, which are illustrated in the photo of figure 3.16, should also affect the conductivity of the specimens used in this study, as pentlandite has a slightly lower resistivity of 1 to 11 x 10^{-6} Ω-m (Keller, 1982). Also, pentlandite is cubic and should thus have an exclusively shape controlled anisotropy.

3.3. Electrical Response of Magnetite and Chalcopyrite

The electrical properties of magnetite and chalcopyrite will be discussed briefly, as they are present in some of the specimens studied.

Magnetite has the lowest resistivity of any oxide, of the order of 52 x 10^{-6} Ω-m (Keller, 1982). This is in the same range of magnitude as for pyrrhotite, and therefore should have little effect on specimen bulk resistivities provided that this is also the case at the frequencies used by the ACMS coil. It is also cubic and should have no electrical anisotropy. Magnetite often contains exsolution lamellae of ilmenite which changes its overall resistivity. Figure 3.5 shows how resistivity increases with $FeTiO_4$ content.

Chalcopyrite has a resistivity of 150 to 9000 x 10^{-6} Ω-m. This is higher than the resistivity of pyrrhotite. Measurements on specimens of triaxially compacted loose chalcopyrite aggregate give lower conductive ACMS than measurements on similarly prepared pyrrhotite as shown in figure 3.6. Thus chalcopyrite in these specimens may have little effect on the results as it is a relatively minor constituent of most samples. Chalcopyrite also has a crystallographic resistivity anisotropy, with lower resistivity along its crystallographic c-axis. The ratio of maximum to minimum resistivity is 1.3 to 2.6 (Shuey, 1975).

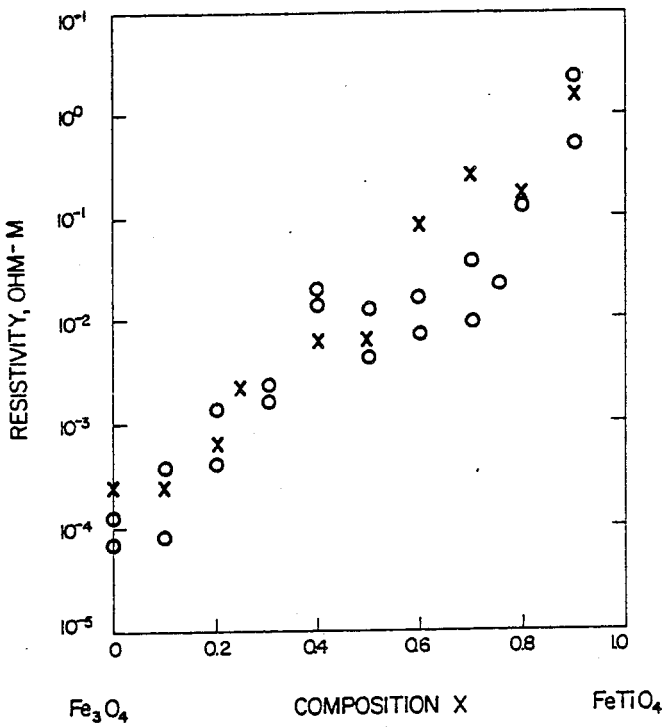

Fig. 22-1. Room-temperature resistivity of synthetic titanomagnetite as a function of composition. Crosses are for ceramics of O'Reilly and Banerjee (1965), circles are for single crystals of Stephenson (1969).

Figure 3.5. This diagram from Shuey (1975) shows that the resistivity of magnetite increases significantly with $FeTiO_4$ content.

PO1B SITE 1 CORE 1 SPEC 1 UNITS= SI v M= 6 NR= 2

SUSC.	DEC	INC	R95	EV	SDEV
MIN	60.63	5.13	63.0	8.1601E-05	1.673E-04
INT	329.80	9.18	63.1	4.2061E-04	1.296E-04
MAX	359.47	-79.46	5.4	3.0979E-03	1.970E-04

CP1B SITE 1 CORE 1 SPEC 1 UNITS= SI v M= 6 NR= 2

SUSC.	DEC	INC	R95	EV	SDEV
MIN	283.03	-22.64	58.2	8.3754E-05	9.803E-05
INT	17.87	-11.46	59.6	1.4039E-04	1.024E-04
MAX	312.82	64.33	15.9	6.3130E-04	5.023E-05

Figure 3.6. The data above are the determinations of the three principal conductive ACMS values for a specimen of crushed pyrrhotite (PO1B) and a similarly prepared specimen of chalcopyrite (CP1B). Each was triaxially deformed to a shortening of 5%. Notice that the EV values (ACMS in SI/mass) are higher for pyrrhotite, indicating that at least in this case, pyrrhotite has a higher conductive ACMS than chalcopyrite.

3.4. Deformation Characteristics of Pyrrhotite

Graf and Skinner (1970) experimentally deformed pyrrhotite to identify its methods of deformation. It was found to deform plastically in their tests at low temperatures and rapid strain rates. Cataclasis is only important at the lowest temperatures. Up to 250°C, translation gliding along (0001) and kinking dominate. Kinking results in striking deformation bands visible in cross-polarized light in polished section (Clark and Kelly, 1976). All of these features were apparent in the deformation experiments of this study. Above 250°C, at high pressures, pyrrhotite suddenly weakens and twinning develops. This transition is due to a change in the number and ordering of vacancies in pyrrhotite (Siemes and Hennig-Michaeli, 1985). Graf and Skinner (1970) also observed development of pyrite exsolution parallel to the basal plane of pyrrhotite at low temperatures. This was not observed in this study.

Slip along (0001), which is the only operative slip plane under most conditions will result in the rotation of these planes towards the plane of flattening. This is a strain induced preferred crystallographic orientation as described by Buerger (1928). Thus, since pyrrhotite has an electrical anisotropy, strained massive samples may exhibit ACMS fabrics with highest resistive susceptibility parallel to the maximum compressive strain. This is the opposite of what would be expected if anisotropy were strictly grain shape controlled. In loose

aggregates, the crystallographic anisotropy should not be a major factor.

3.5. Deformation Characteristics of Magnetite and Chalcopyrite

Once again, magnetite and chalcopyrite will be discussed, as they may have an effect on the first set of results. Room temperature deformation of magnetite results in twinning and slip along {111} (Siemes and Hennig-Michaeli, 1985). Also, the [110] crystallographic axis tends to become parallel to the axis of shortening. As magnetite has no crystallographic conductivity anisotropy, preferred crystallographic orientation has little effect on ACMS fabrics.

Chalcopyrite has been shown to develop strong preferred crystallographic orientations in natural specimens (Cox and Etheridge, 1983) as the result of glide along {112}. Hennig-Michaeli and Siemes (1987) found similar results in experimentally deformed chalcopyrite. As a result of this slip, {112} becomes parallel to the flattening plane. This combined with the strong resistivity anisotropy of chalcopyrite means that in massive specimens, the K''_{min} resistive complex susceptibility may not correspond to the axis of shortening.

3.6. Experimental Data

3.6.1. Complex magnetic susceptibility values

The values for bulk complex magnetic susceptibility for the specimens P002 to P028 range from 0.604 x 10^{-6} SI/mass to 7.56 x 10^{-6} SI/mass. This indicates that the conductivities of the specimens are extremely variable. There are many possible explanations for the disparity. The most likely reason is the presence of different shapes and sizes of spaces between grains as shown in the photomicrographs of figure 3.14. These spaces limit intergrain contacts and reduce the effective conducting surface area of the material being measured. The degree of strain should result in an increase of conductive CMS values with strain, as one would expect the grain contacts to become better, increasing conductivity. The graph of figure 3.7 shows the expected correlation when chart strain values are plotted against conductive bulk K". A number of factors may be important in any variability between K" values. One is the actual composition of the samples. The impurities such as pentlandite, magnetite, and chalcopyrite may have an effect on resistivity if they compose different proportions of different samples. Also, the internal features of pyrrhotite before and/or after experimental deformation may have some effect on resistivity. These features include dislocations, twins and microcracks. The degree of cataclasis occuring in these specimens may also affect bulk

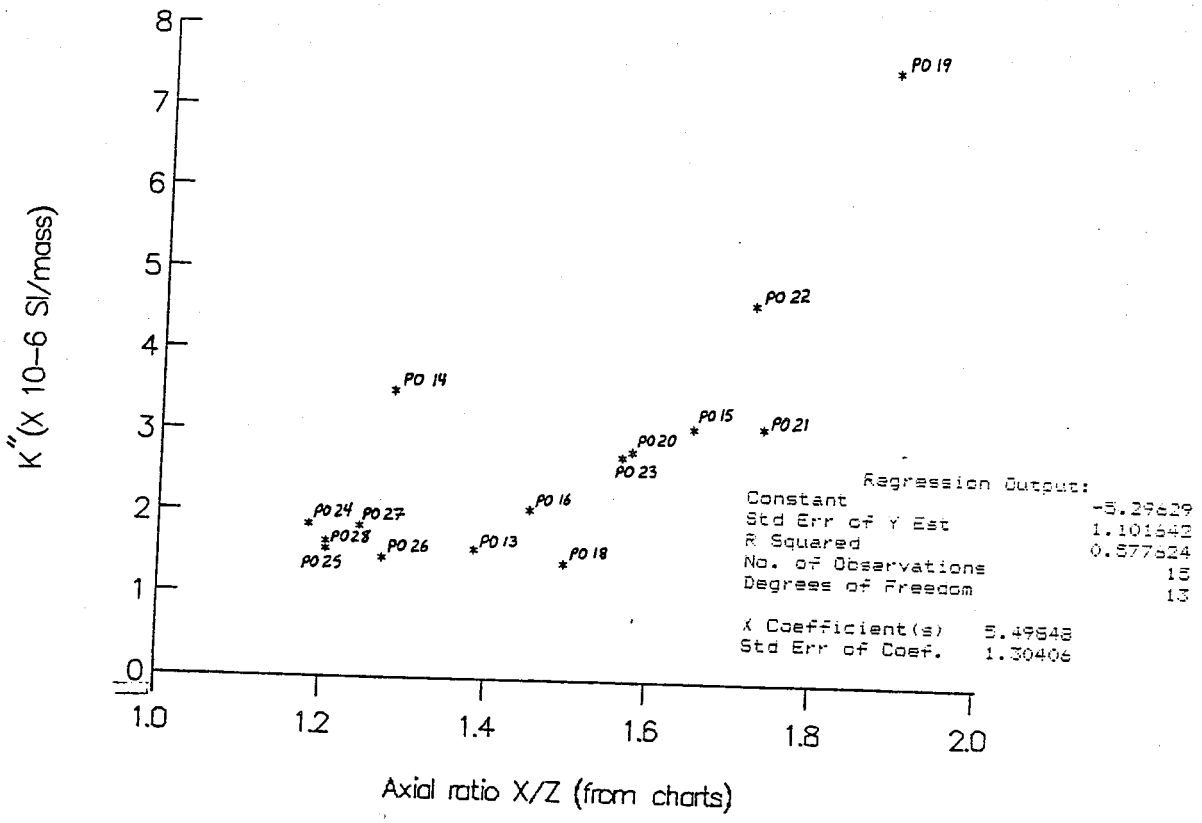

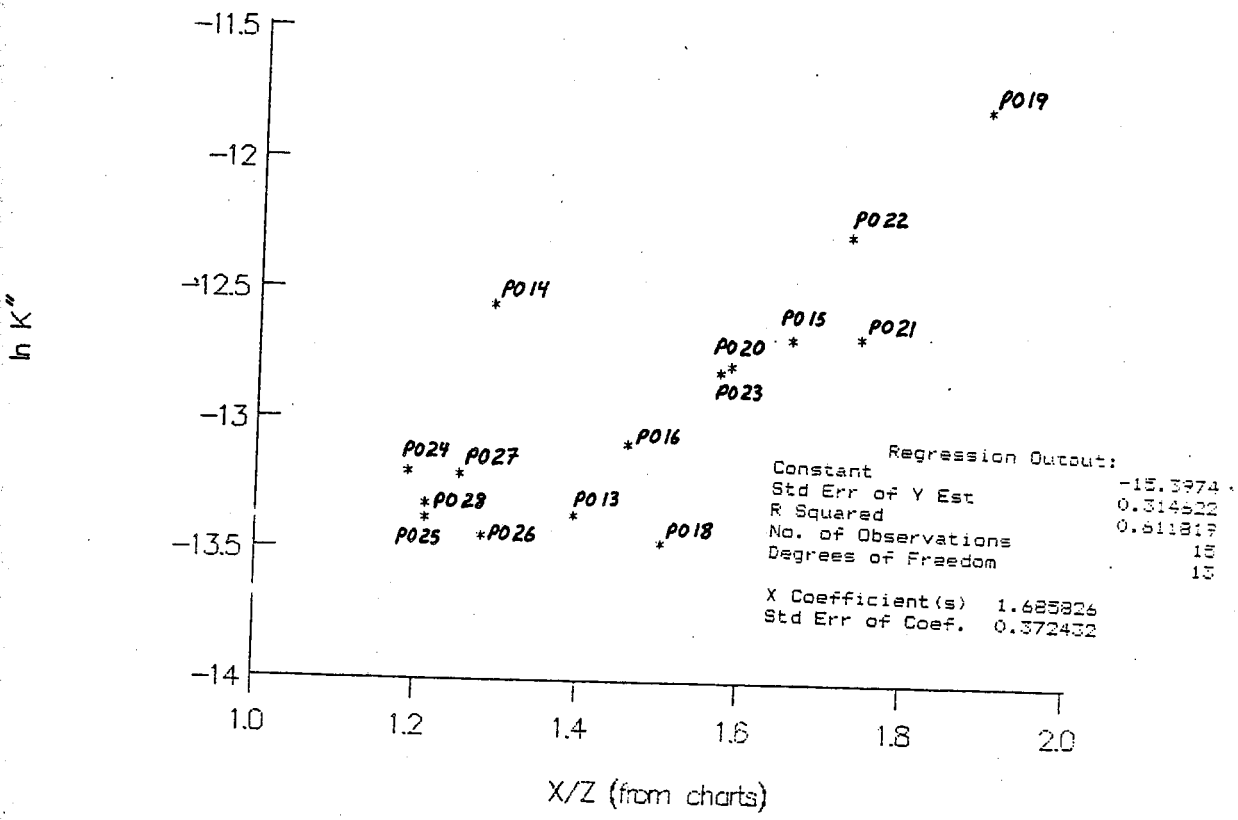

Figure 3.7. These diagrams illustrate that bulk complex magnetic susceptibility (conductive) generally increases as a function of strain calculated from chart recordings. Note that there is not a good linear relationship even when strain is plotted against ln K"(bulk).

conductive K".

3.6.2. ACMS fabric characteristics

The ACMS fabrics develop with a fairly consistent orientation of resistive K''_{min} parallel to the axis of compression. Each specimen had its ACMS measured 10 separate times to ensure that the axis of minimum susceptibility could be located consistently by the coil. The stereonets shown in figure 3.8 show the typical distribution of axes for these specimens. In most specimens, K''_{min} could be defined within the 95% confidence limits ("R95") of better than 5°. The axes are best defined at high strains and when bulk susceptibility is high.. The stereonet for the hydrostatically compacted specimen P010 shows that it developed a very poor fabric. This was expected, as this was one of the least deformed specimens. Better values were typically obtained from the most highly strained specimens. On the other hand, the axes of intermediate and maximum resistive susceptibility were never defined with precision (see data in appendix A). However, a plane in which these axes fall can be defined in all cases. The difficulty in defining these axes is in part due to the fabrics in most cases being nearly uniaxially oblate in character due to the pure shear deformation. The coil also often had some difficulty in detecting CMS in the foliation plane, as values were sometimes close to the detection limits of the coil. High standard deviations were typical of the K''_{max} and

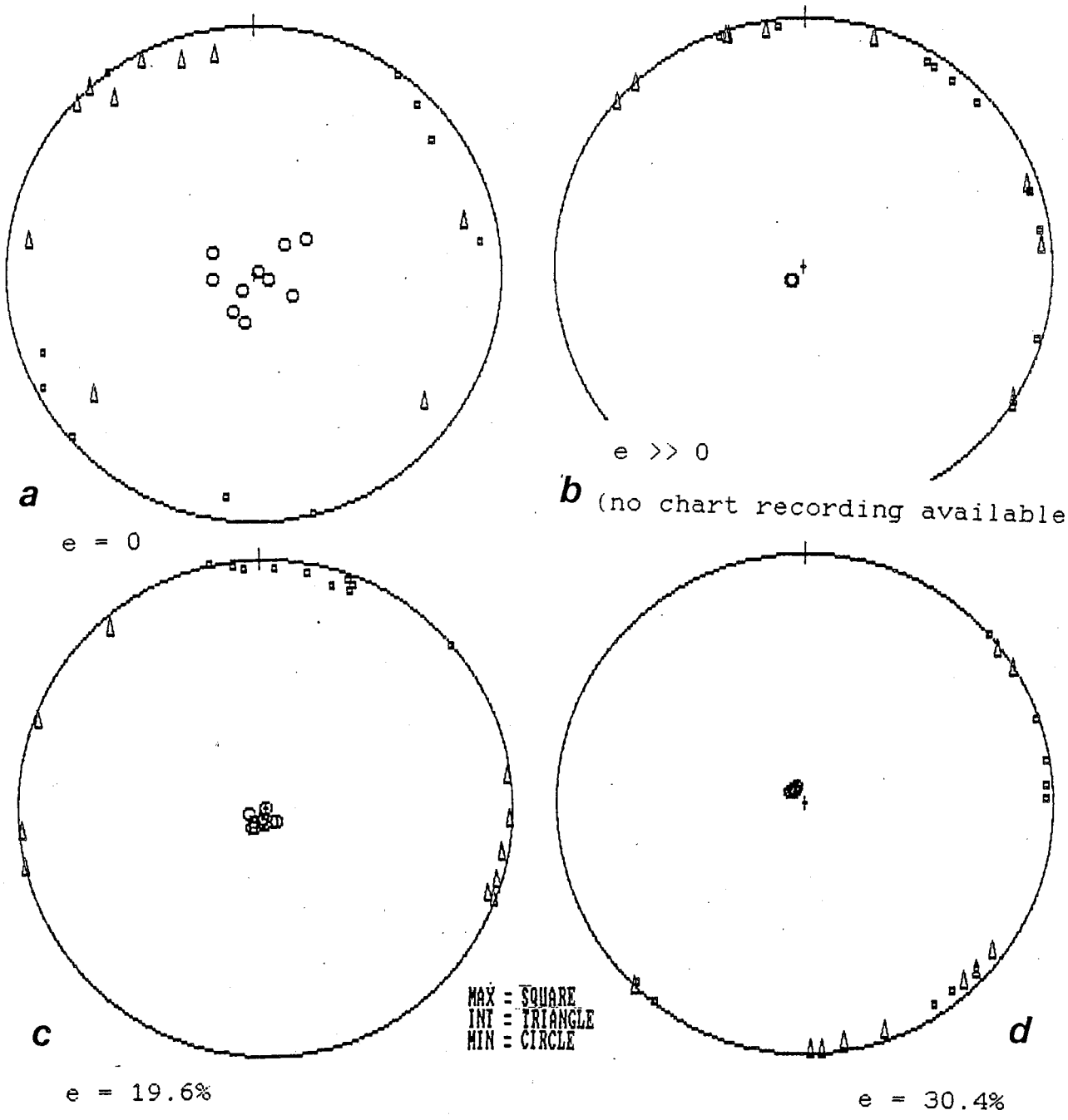

Figure 3.8. These are four typical principal axis distributions for ten separate ACMS measurements on a single pyrrhotite aggregate specimen. (a) P010 is a hydrostatically deformed specimen and all resistive ACMS principal axes are poorly defined. (b) P011 (c) P013 (d) P022 all show the typical well-defined K''_{min} and poorly defined K''_{int} and K''_{max} which fall within the plane of flattening.

K''_{int} values. The P'-T diagram of figure 3.9 illustrates that almost all specimens show strongly oblate resistive anisotropy. It should be noted, though, that standard deviations in T values were often quite high as the result of the poor precision in K''_{int} and K''_{max} determinations. Nonetheless, the consistency of oblate fabrics is significant. Values of bulk susceptibility for some specimens are quite variable over the 10 measurements, owing to the fact that the values are approaching the detection limits of the coil. This is illustrated by the table of figure 3.10. One unfortunate aspect of this low detection limit is that pyrite, the most common sulphide mineral, produces no ACMS signal.

There appears to be poor reproducibility of results when K'' is less than about 3×10^{-6} SI/mass. The 3/4" cores tend to give slightly better data than the 1/2" cores. All specimens from P002 to P014 were 3/4" and the rest were of 1/2" diameter.

Data obtained from massive specimens containing pyrrhotite and chalcopyrite obtain much more precise and reproducible ACMS values than the unconsolidated specimens, largely because of their much higher conductivities. Massive specimens will be discussed in more detail in chapter 5.

There may be a grain-size dependence upon CMS in the crushed pyrrhotite, as a specimen consisting of <0.15 mm material had a mean conductive ACMS of 7.09×10^{-7} SI/mass versus a minimum of 10.34×10^{-7} SI/mass for P009 to P028 which used the same pyrrhotite, except in the 0.15 to 1.0 mm grainsize range.

Pore water is not a factor in ACMS measurements as the

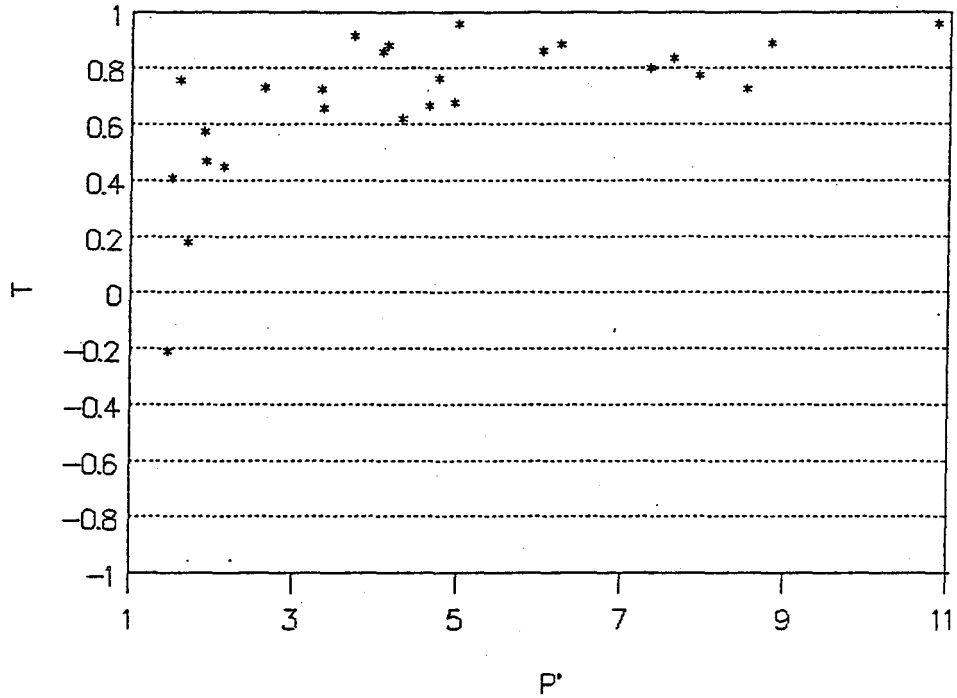

Figure 3.9. This P'– T diagram shows that the triaxially deformed pyrrhotite aggregates typically develop strongly oblate resistive ACMS fabrics typical of pure shear.

$K''_{(bulk)}$	P002 X 10E-6	P003	P004	P005	P006	P007	P008
1	0.669	0.6479	1.9387	0.6505	0.7223	1.8403	0.60959
2	0.7141	0.5653	1.8973	0.6257	0.7625	1.7455	0.63735
3	0.6843	0.583	1.9276	0.5762	0.7352	1.7176	0.63985
4	0.7366	0.5746	2.0016	0.6649	0.7025	1.7423	0.62004
5	0.7417	0.6733	1.9432	0.6071	0.7112	1.7077	0.62002
6	0.7015	0.647	1.9	0.6185	0.7212	1.6908	0.60238
7	0.6927	0.5825	1.9582	0.6379	0.7526	1.7673	0.60572
8	0.7314	0.6006	1.9429	0.6209	0.7264	1.7158	0.62572
9	0.7307	0.568	1.9023	0.6405	0.6899	1.6929	0.65294
10	0.6499	0.6009	1.9632	0.6355	0.7297	1.7669	0.64335
$K''_{avg.}$	0.70519	0.60431	1.9375	0.62777	0.72535	1.73871	0.625696
std.dev.	0.029512	0.036277	0.031016	0.023332	0.020604	0.042799	0.016298

	P009	P010	P011	P012	P013	P014	P015
1	2.3051	1.2026	4.0144	1.0608	1.5774	3.5365	3.0576
2	2.2802	1.1894	4.051	1.059	1.5585	3.5039	3.1381
3	2.3063	1.205	4.05	0.97445	1.6021	3.4853	3.0829
4	2.3278	1.2215	3.981	1.0049	1.5391	3.494	3.196
5	2.2734	1.1873	4.0739	0.98263	1.6059	3.5236	3.1923
6	2.2675	1.2367	4.0173	1.0473	1.544	3.5028	3.0326
7	2.3063	1.1857	4.0172	1.0515	1.5588	3.5027	3.2525
8	2.2828	1.1366	4.085	1.0246	1.577	3.5061	3.1245
9	2.2698	1.2218	4.0411	1.0516	1.5549	3.5087	3.015
10	2.2031	1.2354	4.0212	1.0844	1.5227	3.4517	3.0107
$K''_{avg.}$	2.28223	1.2022	4.03521	1.034118	1.56404	3.50153	3.11022
std.dev.	0.032363	0.028317	0.029482	0.034346	0.025341	0.021434	0.079895

	P016	P018	P019	P020	P021	P022	P023
1	2.0498	1.4686	7.4908	2.7274	3.1173	4.4437	2.6285
2	2.0798	1.4347	7.5872	2.9181	3.0641	4.607	2.8869
3	2.0663	1.4485	7.5011	2.9186	3.0753	4.7176	2.8587
4	2.078	1.3682	7.5773	2.8023	3.1804	4.6731	2.89
5	2.0335	1.4186	7.6094	2.9477	3.1737	4.7373	2.6986
6	2.0967	1.4779	7.5345	2.9251	3.0753	4.6265	2.8378
7	2.0672	1.4183	7.6201	2.6801	3.1586	4.6322	2.7789
8	2.0561	1.311	7.6072	2.8063	3.2744	4.6992	2.5731
9	2.0565	1.3917	7.5867	2.6061	3.1259	4.681	2.564
10	2.0615	1.4139	7.4917	2.7284	3.1118	4.643	2.6566
$K''_{avg.}$	2.06454	1.41514	7.5606	2.80601	3.13568	4.64606	2.73731
std.dev.	0.016686	0.046812	0.048581	0.112931	0.060525	0.07828	0.12211

$K''_{(bulk)}$	P024	P025	P026	P027	P028
1	1.8734	1.6188	1.4456	1.8723	1.6615
2	1.8458	1.5839	1.6336	1.8205	1.5785
3	1.9356	1.4372	1.2428	1.8896	1.565
4	1.858	1.6121	1.4092	1.7776	1.6074
5	1.8566	1.5864	1.4237	1.8895	1.6931
6	1.7882	1.4094	1.5297	1.807	1.6426
7	1.7683		1.4762	1.7656	1.6737
8	1.8287		1.4994	1.938	1.6063
9	1.7816		1.3682	1.7183	1.7107
10	1.8407		1.3769	1.7659	1.5411
$K''_{avg.}$	1.83769	1.5413	1.44053	1.82443	1.62799
std.dev.	0.047114	0.084757	0.099817	0.066583	0.054192

Figure 3.10. The average bulk conductive K" for the pyrrhotite aggregates is variable between measurements for some specimens as seen by the standard deviation values.

resistivity of pyrrhotite is several orders of magnitude lower than that of water and can not be detected on its own in the coil. Water typically has a resistivity of at least 1 Ω-m as opposed to 2 to 160 x 10^{-6} Ω-m in the case of pyrrhotite (Keller, 1982).

In conclusion, the ACMS method appears to be useful in detecting the axis of maximum compression in the deformed pyrrhotite aggregates. Thus we can conclude that preferred orientations of pyrrhotite grains must have an effect on ACMS despite the slight crystallographic electrical anisotropy. The P' values of up to 11 illustrated in figure 3.9 attest to this.

3.6.3. AMS fabric characteristics

Anisotropy of magnetic susceptibility data show remarkable precision in the definition of the three principal axes of susceptibility for all pyrrhotite specimens (see appendix B). This is undoubtedly due to the high magnetic susceptibility of pyrrhotite. Reproducibility of results between measurements on the same specimen is very good.

The Jelinek-Hrouda P'-T diagram of figure 3.11 shows that all specimens developed a strongly oblate magnetic fabric as the result of deformation. Also, the K_{min} AMS axis approximates the shortening direction in all cases. Example stereonets are illustrated in figure 3.12. Thus K''_{min}, K_{min}, and the maximum compressive strain directions approximately coincide for all

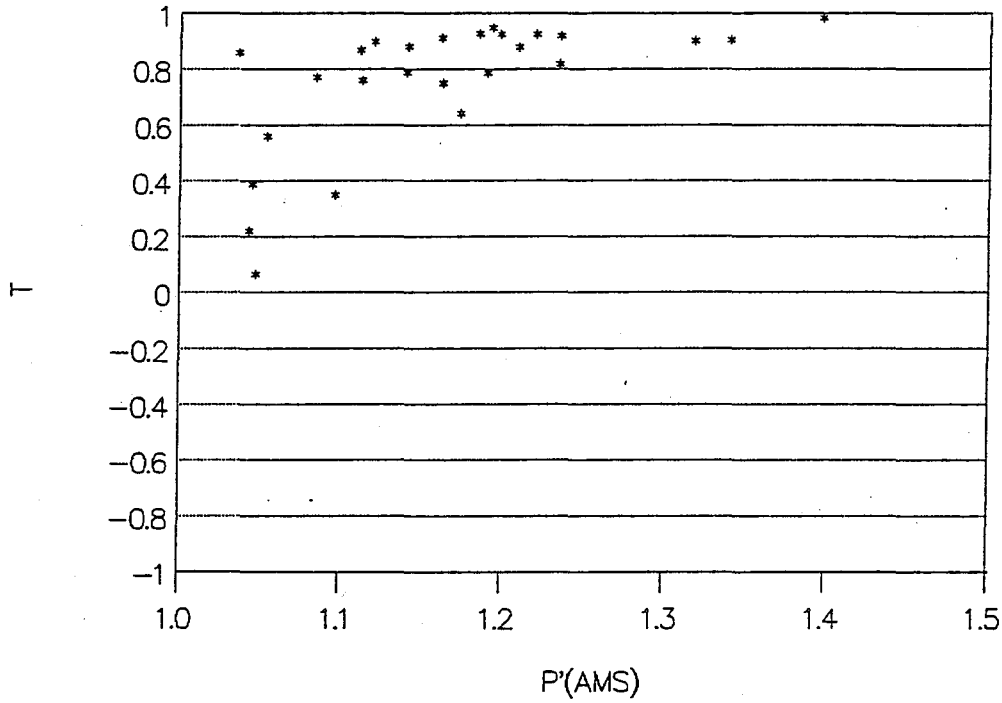

Figure 3.11. As with resistive ACMS fabrics, AMS fabrics for the pyrrhotite aggregates are generally strongly oblate, with T values greater than 1. Note that anisotropy P' is much lower in AMS.

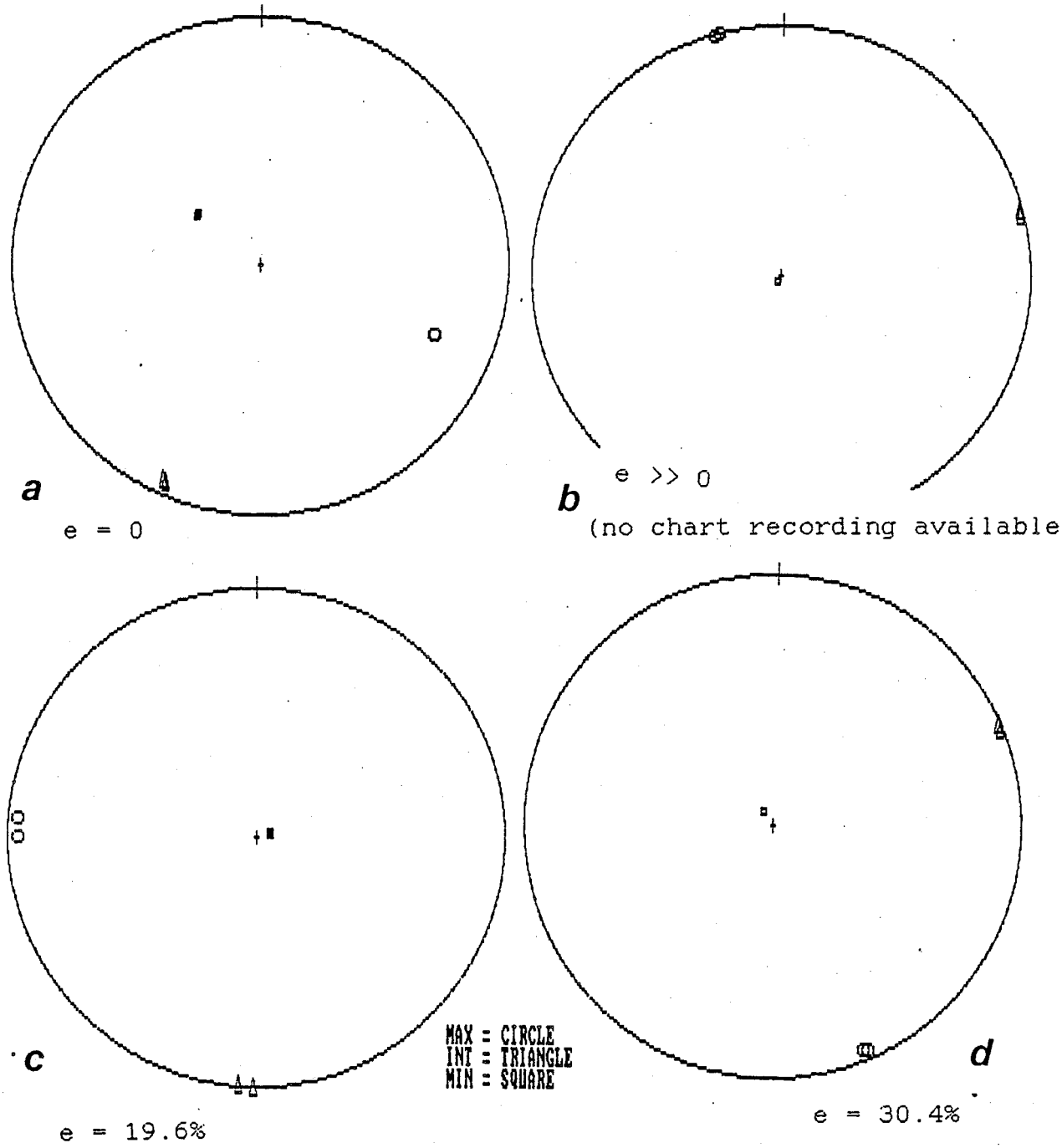

Figure 3.12. These stereonets show well-defined AMS fabrics for (a) P010 (b) P011 (c) P013 (d) P022. If one compares these stereonets to those for ACMS fabrics for the same specimens in figure 3.8, K_{min} and K''_{min} are nearly coincident.

specimens. This result permits us to suggest that ACMS will be useful in strain analyses to be performed on these specimens later.

The correspondence between AMS and strain ellipsoid axes indicates that there must be some crystallographic control on grain shapes. This is because pyrrhotite has a very strong crystallographic magnetic susceptibility anisotropy which controls its magnetic fabrics. If there was not a slight crystallographic preferred orientation, there would be no apparent AMS. Intracrystalline deformation is not believed to be much of a factor in the AMS fabrics, for well defined AMS is present in the hydrostatic specimens as well as the deformed specimens. Preferred orientations in the hydrostatically deformed specimens are probably due to gravity settling of the aggregate prior to the specimens being placed in the triaxial rig.

Bulk susceptibility values are reasonably consistent for the samples P002 to P008 as seen in the table of figure 3.13. These are much higher than the values for P009 to P028. This is probably because of the presence of magnetite in the first set of specimens. Magnetite has a magnetic susceptibility of 5.841 SI/volume (Borradaile et al., 1987) versus 1.5 SI/volume for pyrrhotite (Carmichael, 1982). Also, the first set of specimens appear to contain little hexagonal pyrrhotite, which is less susceptible than monoclinic pyrrhotite. The second set of specimens apparently contains hexagonal pyrrhotite as discussed earlier in section 3.2. The values for P009 to P028 are

SPECIMEN	K(bulk)g
P02	1.2088
P03	1.3844
P04	1.2423
P05	1.2735
P06	1.559
P07	1.4091
P08	1.543
P09	0.50135
P010	0.45246
P011	0.23244
P012	0.24673
P013	0.2321
P014	0.24384
P015	0.23492
P016	0.24778
P018	0.24222
P019	0.22163
P020	0.2296
P021	0.2005
P022	0.22656
P023	0.2262
P024	0.31921
P025	0.31512
P026	0.26007
P027	0.27799
P028	0.29284

Figure 3.13. These are the bulk magnetic susceptibility values for all specimens. P002 to P008 are from the first set of samples, which contained magnetite. Values for the samples P009 to P028 were quite consistent, except that the hydrostatically deformed specimens P009 and P010 are about twice as susceptible as the rest.

reasonably consistent as well, except that the hydrostatic specimens have roughly double the susceptibility of the deformed specimens. The reasons for this are unknown, but may be related to the effects of deformation. Variability between specimens is most likely due to small compositional differences between specimens.

3.7. Specimen Deformation Fabrics

After the pyrrhotite aggregates were deformed and AMS and ACMS fabrics measured, the specimens were cut in half to prepare polished sections. The polished sections were photographed to allow digitization for the purpose of strain analysis. They were also observed to examine mineralogy and textures.

3.7.1. P002-P008

These samples were obtained from a single specimen of massive sulphide. The mineralogy of each specimen is similar, with the major constituent being pyrrhotite which comprises 70% of the specimens by volume. The other important minerals in these aggregates are magnetite and chalcopyrite, each of which comprise about 15% of the volume. There is also a minor amount of gangue minerals and some pentlandite exsolved from pyrrhotite. Chalcopyrite occurs in these specimens almost exclusively as composite pyrrhotite-chalcopyrite grains derived from the sample crushing process. Magnetite occurs as both isolated and composite grains with pyrrhotite and/or chalcopyrite.

Most grains in all specimens are fractured. Many of these fractures were probably the result of the sample crushing procedure, since cracks are common in the hydrostatic sample P002. Otherwise, the grains in P002 show little evidence for prior deformation, as they lack evidence for twinning and

kinking.

After deformation, pore space is greatly reduced in all specimens. Each deformed specimen shows an increase in the amount of fracturing relative to P002, indicating that cataclasis is an important deformation mechanism. This is especially evident in the most highly deformed specimens, P004 and P007. Figure 3.14 illustrates an undeformed and deformed specimen for comparison. Before cataclasis occurs, much of the deformation is probably taken up by rigid-body rotation and particulate flow (Borradaile, 1981) to eliminate as much pore space as possible. These processes would be aided by the general compaction of the specimens. Once grains become pinned between other grains, cataclasis occurs. The process of cataclasis is made possible by the high strain rates of the experiment. After breaking, the grains are then able to flow by cataclastic flow. Rutter (1986) defines cataclastic flow along with a number of other deformation mechanisms and cassifies them as either brittle or plastic processes in an effort to eliminate the term "ductile" which applies to intragranular and cataclastic flow processes. Some cataclasis in these specimens is also the result of the unloading of confining pressure after the completion of deformation (see figure 3.15). All deformed specimens contain pressure release cracks perpendicular to the direction of applied stress.

Evidence for intragranular deformation is present in a number of grains which demonstrate undulatory extinction under cross-polarized light. However, there is no evidence for kinks as

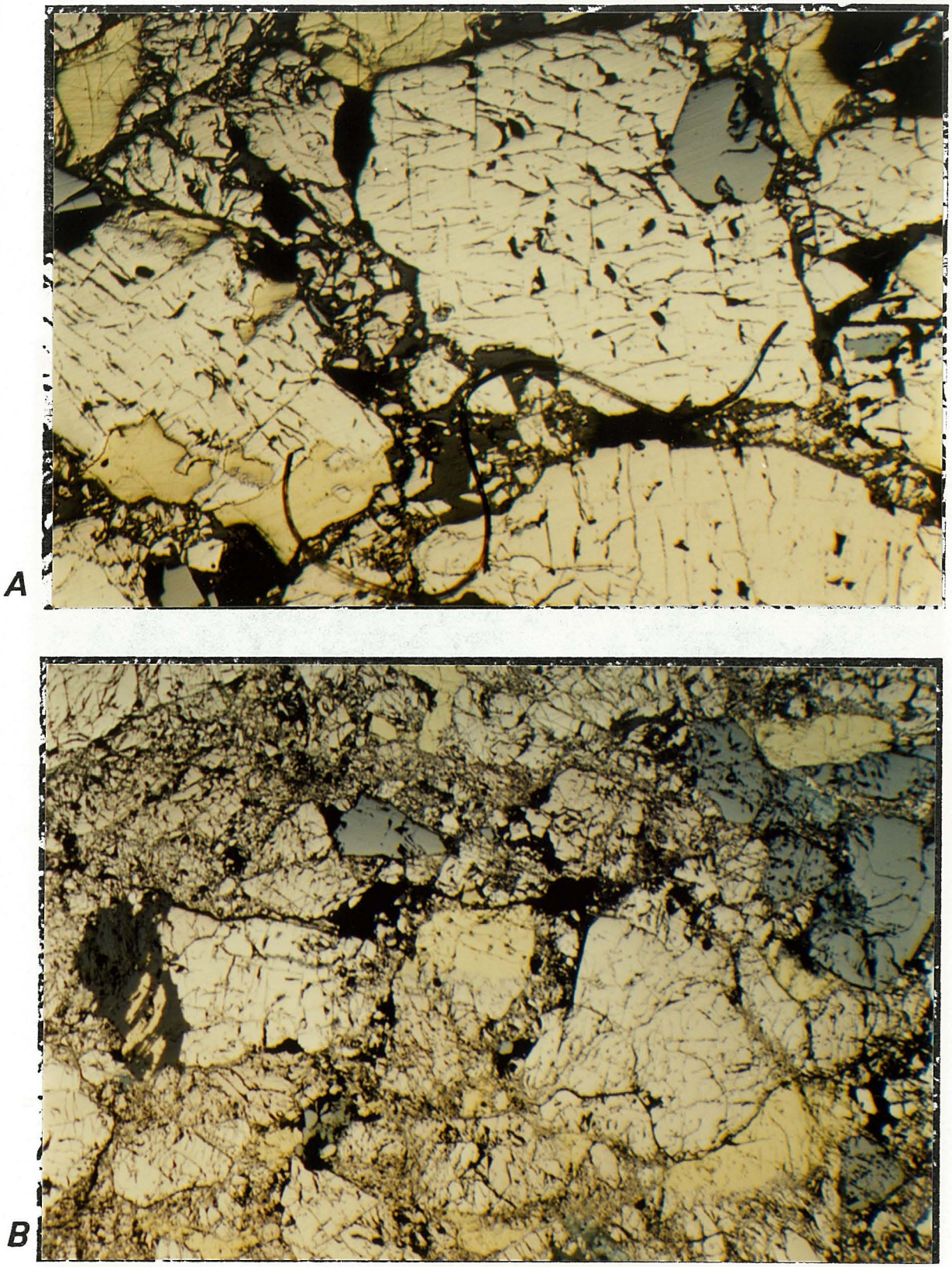

Figure 3.14. (a) P002 (b) P004. P002 is hydrostatically compacted while P004 has been exposed to differential stress. Note the extensive cracking and crushing of grains which has occured in P004 relative to P002.

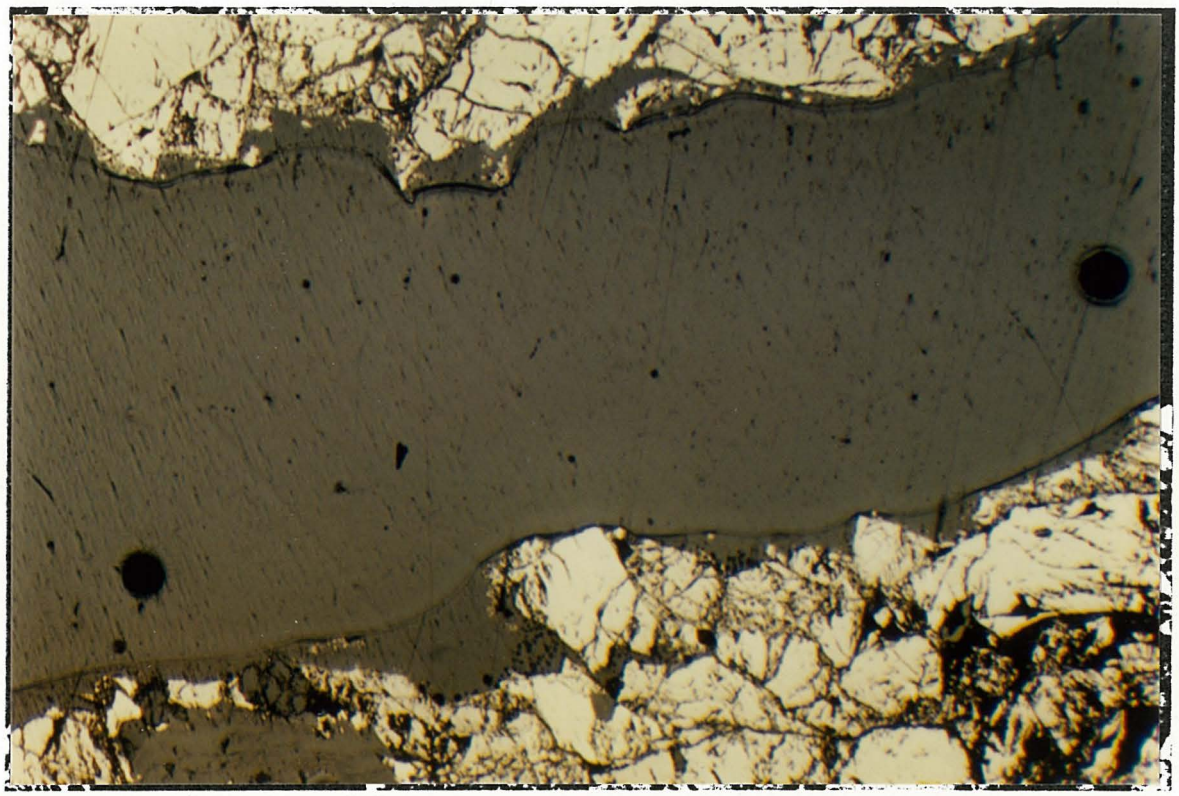

Figure 3.15. This photo illustrates a pressure-release crack in P018 which developed after deformation when differential stress was relaxed. This process contributes to cataclasis and disturbance of fabrics.

described by Clark and Kelly (1976), which are probably the same as the corrugation lamellae described by Ramdohr (1980), or deformation twins. Dependent particulate flow may have occured in these aggregates as well. This is a process in which the movement of particles is dependent upon intragranular deformation.

Many grains show more or less linear fractures similar to those of Graf and Skinner (1970) which are related to the directions of applied stress and are probably crystallographically controlled. Most fractures are irregular in shape, with some being smoothly curved and others can occur in closely spaced arrays sometimes being bent. Some of these features are illustrated in the photo of figure 3.16. The development of preferred dimensional orientations in many specimens was obvious. These preferred orientations were later confirmed in the strain analysis process.

Polishing of some specimens has resulted in some of the relatively unconsolidated material to be plucked from the surface of these sections, producing some large gaps between grains.

The chalcopyrite and magnetite exhibit no apparent plastic deformation features, only cataclastic textures similar to those seen in pyrrhotite.

3.7.2 P009-P028

These specimens were obtained from a second sample of crushed pyrrhotite ore. The composition of this material was

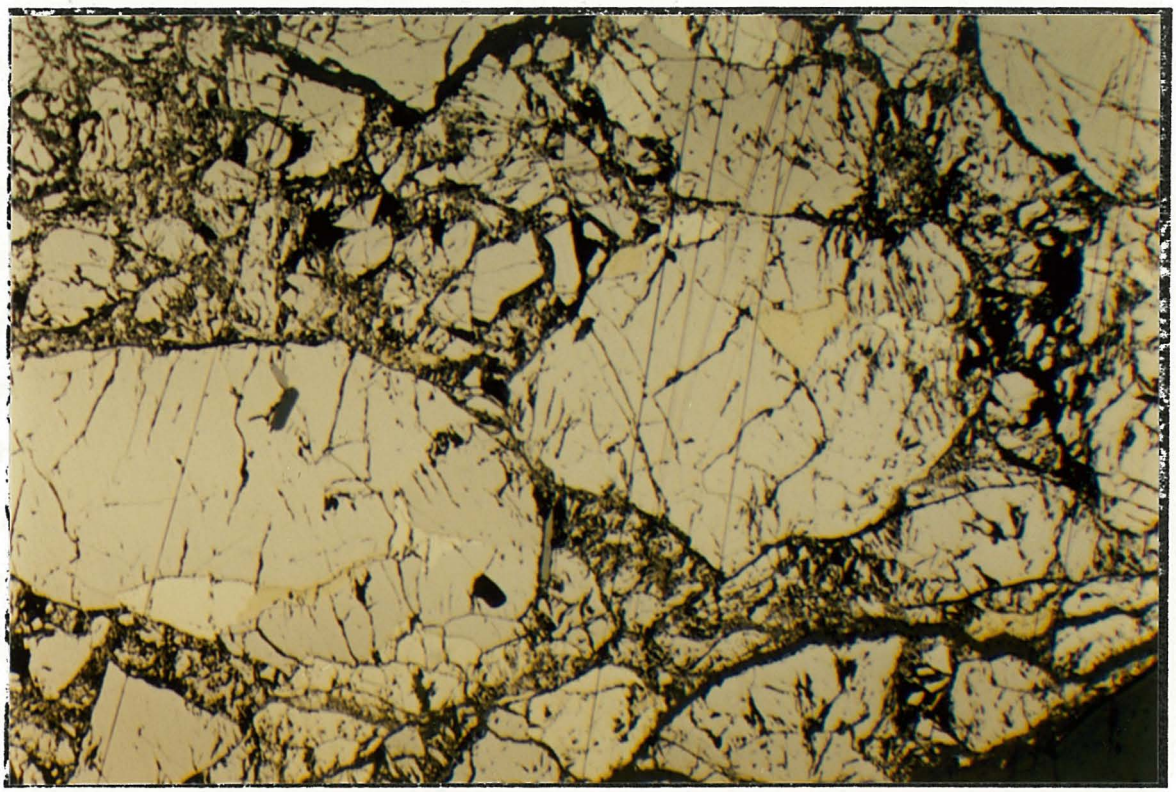

Figure 3.16. Note the concentration of cataclasis at the boundary between three grains near the top right of the photo. Cracks seem to radiate from the point of contact. Note that some fractures in the photo are irregular while others are linear, possibly following crystallographic planes. (P018)

vastly different from that of the first set of specimens. P009 to P028 generally contain about 95% pyrrhotite which contains pentlandite exsolution lamellae and composite chalcopyrite grains in approximately equal amounts.

P009 and P010, which were hydrostatically compacted, lack plastic deformation features, but many of the grains are cracked as a result of the specimen preparation process. The deformed specimens exhibit all of the same features as those seen in specimens P002 to P008. However, there is a striking feature seen in almost all of the second set of specimens in polished section under cross-polarized light which is absent from the first set. This feature appears to be kinking (corrugation lamellae) and is illustrated in figure 3.17. The lamellae are generally lensoid in shape and are often bent. These features are developed spectacularly in specimen P019, which is also the most highly deformed specimen. Grain boundaries have become very tight in this specimen (see figure 3.17), likely making plastic deformation the dominant deformation mechanism relative to cataclasis and particulate flow. The lamellae tend to be oriented preferentially at high angles to the compressive strain axis in this and other specimens. This is because kinking occurs in specimens which are not oriented favourably for slip to occur at high angles to the maximum compressive stress (Clark and Kelly, 1976). P019 also shows evidence for strong cataclasis.

It is unclear why specimens P009 to P028 have undergone a greater degree of plastic deformation than the previous

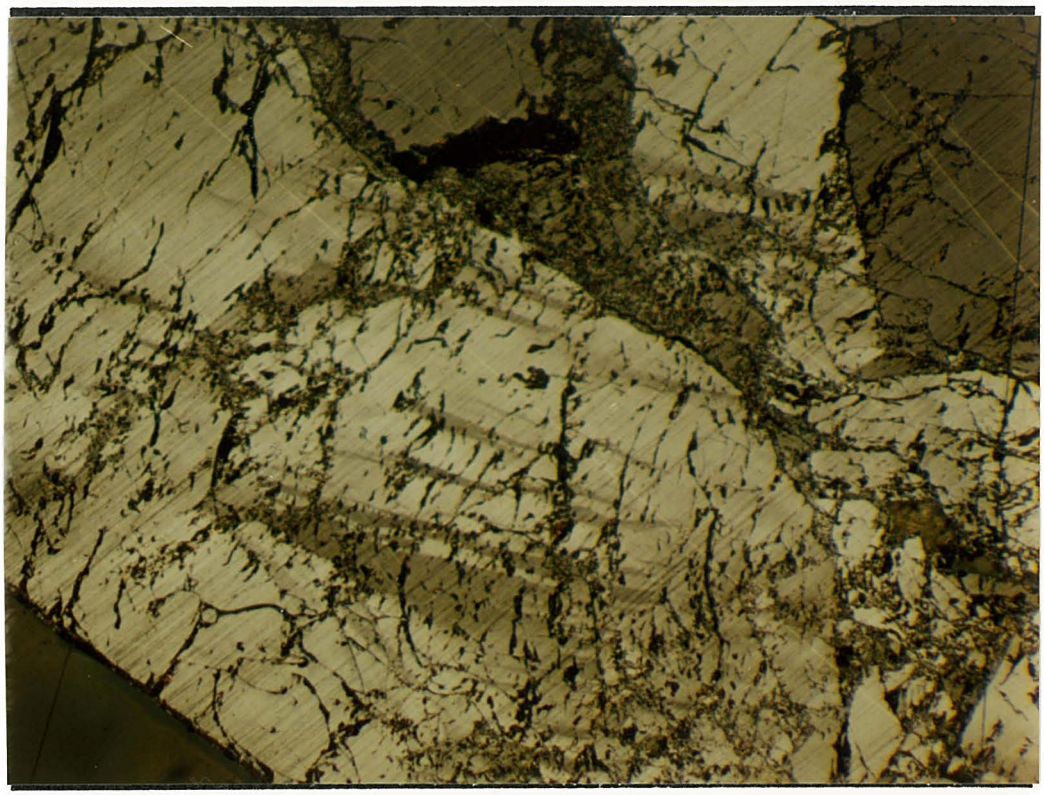

Figure 3.17. This photo of P019 taken in cross-polarized light illustrates kinks (corrugation lamellae). Note that the trace of the plane of flattening in this photo is horizontal and nearly parallel to the kink bands.

specimens. Perhaps compositional effects or the initial strain state of the grains had an effect on the features developed.

3.7.3. Relationship of textures to OMS data

It is clear that the development of preferred orientations in these specimens had an impact on their ACMS and AMS fabrics. The effects of cataclasis and crystal slip probably had an effect on the bulk ACMS values obtained. For example, the most highly deformed specimen, P019, had by far the highest bulk susceptibility as shown in figure 3.10, owing to the tighter grain contacts. On the other hand, the hydrostatically deformed specimens P002, P009, P010 have some of the lowest susceptibility values, as they have a large fraction of pore space. Some of the other low values may be attributed to grainsize reduction by cataclasis.

3.8. Strain Analysis

The amount of strain taken up by the specimens of pyrrhotite have been calculated from chart recordings for many of the specimens. Strain has also been calculated from data obtained by digitization of grain shapes. Photomicrographs of polished sections were taken perpendicular to the flattening plane of most specimens. Calculation of strain from the charts is straightforward and was discussed earlier.

3.8.1. Digitizing process

Pyrrhotite grain outlines were traced on a Zeiss-Kontron digitizing tablet having an active area of 280 x 260 mm. Ferromagnetic wires within the tablet arranged at regular intervals in the X and Y directions emit electronically induced magnetic pulses of constant frequency at a spatial interval of 68 µm, which defines the tablet resolution. When the tracing stylus traces a grain outline on the surface of the tablet, the computer determines coordinates from X and Y intercepts. The computer performs a number of arithmetic functions which can be used in strain analysis. The important calculations used for strain analysis in this study include the calculation of major and minor axes of each grain and the angular orientation of these axes. These numbers can be subsequently applied to Rf/Ø analysis.

3.8.2. Rf/Ø analysis

The Rf/Ø analysis technique (Ramsay, 1967; Ramsay and Huber, 1983) utilizes the shape and orientation of elliptical markers to obtain values for strain. This is on the assumption that the markers were initially spherical or elliptical. The Rf/Ø analysis utilizes the variables R_i, R_m, θ, ϕ, and R_f in two dimensions. Two analyses in, for example, the YZ and XZ planes of the finite strain ellipsoid can be used to obtain three-dimensional information. Figure 3.18 illustrates the relationship between the five variables above and their relationships to pre- and post-depositional fabrics. A number of assumptions are inherent in this strain analysis technique. First, the strain markers are assumed to have been initially circular or elliptical in cross-section. Secondly, there should be no significant viscosity contrast between the markers and their matrix. The third assumption is that the markers must undergo passive strain. Another matter of importance is that the principal axes of the strain ellipsoid must be known in order to perform the analysis. There can be problems in defining these axes, as preferred crystallographic orientations and preferred dimensional orientations in rock do not necessarily correspond perfectly to the flattening plane of the strain ellipsoid (Borradaile, 1987), although in most cases discrepancies are small. These problems can arise in rocks with non-coaxial strain histories as well as in rocks with pre-deformational preferred orientations. Also, the

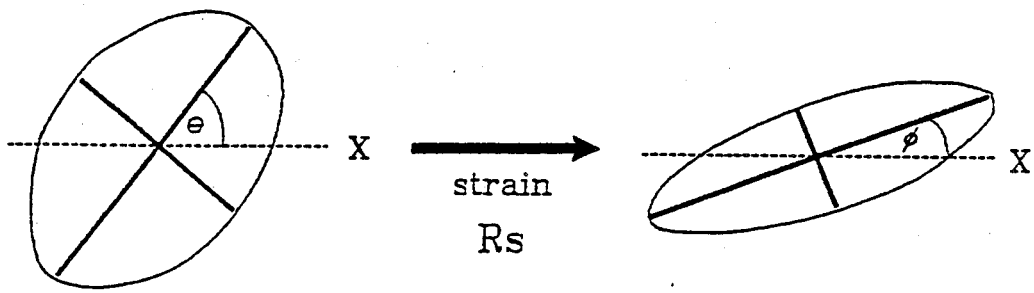

$$Ri = \frac{\text{long axis}}{\text{short axis}} \qquad Rf = \frac{\text{long axis}}{\text{short axis}}$$

Figure 8-2: Parameters used in the Rf/φ Technique:
where:

- Ri = initial undeformed particle axial ratio
- Rs = finite strain axial ratio
- Rf = final deformed particle axial ratio
- θ = angle between the Ri major axis and the maximum principle strain direction (X)
- φ = angle between the Rf major axis and the maximum principle strain direction (X)

Figure 3.18. This illustration was obtained from Spark (1990).

experiments of Means (1977) showed that flow of grains along microfaults within a material can have an effect on grain orientations.

In the pyrrhotite experiments, we know that there is a coaxial strain history and it is assumed that initial grain orientations were random, with some gravitational settling producing weak preferred orientations in the same orientation as those developed during deformation. Assuming that flow along microfaults was not important (no features in the specimens suggested this type of activity on a large scale), most preferred orientation in these specimens was probably the result of rigid-body rotation. This is what occurs in the March Model described by Tullis, 1976 and Tullis and Wood, 1975), however, its condition of non-impingement of rotating grains is violated. Preferred orientation is also probably facilitated by plastic deformation and cataclasis.Taking all of the above factors into account, it was assumed that the XY plane of the strain ellipsoid was normal to the vertical axis of compression in the triaxial rig. The data for phi mean in the table of figure 3.19 appear to confirm this, as most fall close to 90°.

The three assumptions for Rf/Ø analysis must be addressed for these specimens. The first is not met, as the grains are of irregular shape. However, the Zeiss digitizer converts the grains to equivalent ellipses for strain analysis. The second condition is met, as pyrrhotite is both the markers and the matrix. The third condition is partially met, as part of the deformation is

Specimen	Phi mean	Angular deviation	Skewness	#Grains
P002	77.88	46.46	.2714	58
P003	87.07	45.55	-.0949	64
P004	88.66	25.02	-.0472	60
P005	86.05	39.35	-.0429	105
P006	86.27	39.22	-.1301	102
P007	89.46	34.18	.0968	85
P008	98.42	38.00	-.2893	81
P009	96.03	45.88	-.4294	134
P010	89.16	40.56	.3219	125
P011	91.78	29.69	.7302	81
P012	96.73	28.87	-.5188	91
P013		NO DATA - FAULTED		
P014	89.86	31.62	-.0307	106
P015	88.16	35.45	.2707	103
P016	89.31	29.34	-.3464	113
P017		NO DATA - FAULTED		
P018	92.41	28.53	.0785	73
P019	88.52	19.14	-.9215	78
P020	98.18	25.9	-.1738	116
P021		NO DATA - FAULTED		
P022	83.88	34.84	.0823	102
P023	94.44	33.09	-.0032	111
P024	86.75	42.22	.2912	117
P025	90.41	38.22	.0583	123
P026	88.74	35.91	.2222	93
P027	94.71	39.18	.1336	134
P028	89.61	33.84	-.0215	121

Figure 3.19. This data for the orientation of the flattening plane in each pyrrhotite specimen was obtained from $R_f/\emptyset$ data and indicates that the flattening plane in all specimens is approximately at right angles to the direction of compression (0°).

taken up by plastic deformation in combination with particulate flow, rigid-body rotation, and cataclasis. Of course, it is almost impossible to meet all of these conditions in any geological material, however, the technique can give a reasonable estimate of strain and strain fabrics.

Knowing whether preferred orientations were present (ie. was θ random or not?) prior to strain is critical to the interpretation of Rf/Ø data. For example, sedimentary bedding fabrics often have preferred orientations as do earlier strain events (Borradaile, 1987). However, careful analysis of data, such as Rf versus Ø plots can make these identifiable.

The following equations from Ramsay (1967) form the basis for the Rf/Ø method:

$$\tan 2\emptyset = \frac{2\sqrt{R_m}(R_i - 1)\sin 2\theta}{(R_i + 1)(R_m - 1) + (R_i - 1)(R_m + 1)\cos 2\theta}$$

$$R_f = \frac{\tan^2\emptyset\ (1 + R_i \tan^2\theta) - R_m(\tan^2\theta + R_i)}{R_m\tan^2\emptyset\ (\tan^2\theta + R_i) - (1 + R_i\tan^2\theta)}$$

where $R = X / Y$. These equations are not solveable, as there are too many unknowns. Thus statistical/graphical methods are used to aid in their solution for a large number of particles. Tectonic strain can also be separated from initial shapes and orientations of markers (Ramsay, 1967; Dunnet, 1969; Lisle, 1977b; Ramsay and Huber, 1983). Initial bedding fabrics, etc. will not be considered for the pyrrhotite specimens, as they were not a major

factor in fabric analysis of these specimens.

In distribution diagrams (R_f versus Ø), in which initially random fabrics were present, there are two types of distribution which can occur. The first situation develops when maximum R_i is greater than strain (R_s). In this case, the data shows a fluctuation of 180° in the Ø values. The data has its highest concentration in the area of the maximum R_f value. The Ø value of the concentration of points defines the orientation of the long axis of the strain ellipse. Distribution of the data points about the maximum should be symmetric, or there was not an initial random fabric. The maximum and minimum values of the R_f/Ø envelope can be used to calculate the strain in the following way (Ramsay and Huber, 1983):

$$R_f max = R_s R_i min$$

$$R_f min = R_i max / R_s$$

Cross-multiplying or cross-dividing obtains:

$$(R_f max R_f min)^{1/2} = R_i max$$

$$(R_f max / R_f min)^{1/2} = R_s$$

Standard best-fit reference curves can also be used to determine the strains.

A second case develops when the maximum R_i is less than the strain R_s. This is what occurs when the fluctuation of data is less than 90°. The distribution has a form somewhat like that in figure 3.20. Once again the orientation of maximum frequency corresponds to the long axis of the strain ellipse. The strain can be calculated using the following formulae (Ramsay and Huber, 1983):

$$R_f max = R_s R_i max$$

$$R_f min = R_s / R_i max$$

Cross-multiplying or cross-dividing obtains:

$$(R_f max R_f min)^{1/2} = R_s$$

$$(R_f max / R_f min)^{1/2} = R_i max$$

Best-fit curves can also be used to analyse this data.

R_f versus Ø graphs for pyrrhotite are presented in appendix C. Data pertaining to the Ø mean and statistics are presented in figure 3.19. The Ø mean values show that the long axis of the strain ellipsoid lies approximately in the flattening plane of all samples, as it falls between 83° and 99° for all samples except the hydrostatic sample P002. Most data is not significantly skewed, meaning that initial fabrics were random.

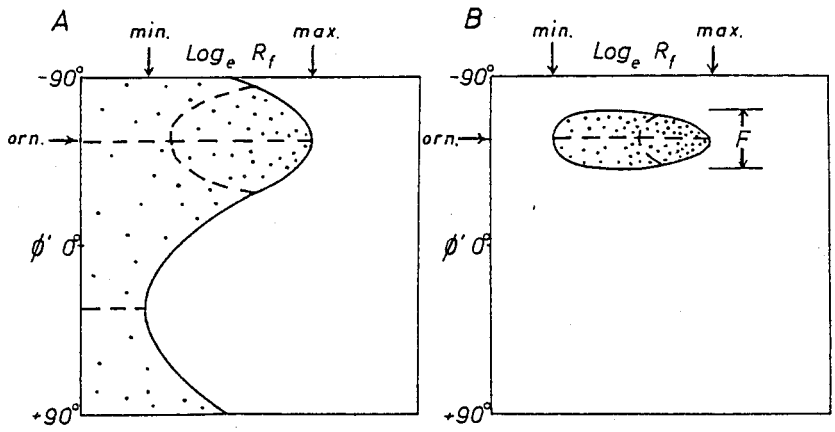

Figure 5.5. *Principal features of R_f/ϕ' plots used for computing the strain R_s. In A, where $R_i > R_s$ the data envelope is symmetric about the orientation of the long axis of the strain ellipse (orn.) and shows maximum and minimum R_f values. In B, where $R_s > R_i$, the data envelope is closed and the data points show a limited range of orientations defining the fluctuation F.*

Figure 3.20. The two Rf versus Ø plots above (Ramsay and Huber, 1983) illustrate the typical distribution of points when Ri > Rs and Ri < Rs respectively. The first case is typical of the distribution of Rf versus Ø for the digitized pyrrhotite aggregates.

The highest skewness values generally are found in specimens in which the fewest grains were digitized. In each specimen, at least 50 grains were digitized. The number of grains digitized depended on the quality of the specimens and availability of digitizable grains. Even the hydrostatically compacted specimens develop a weak preferred orientation parallel to the plane of settling of the grains in the sample's preparation, as discussed earlier. These initial preferred orientations have no effect on R_f/ϕ distributions, as they are parallel to the strain fabrics. They also may be considered the earliest part of the strain, since settling probably occured in all specimens before deformation commenced.

Almost all of the R_f/ϕ graphs show a fluctuation on the order of 180°. This makes sense, as strains were generally low, and less than the maximum R_i. Only sample P019, the most highly strained, shows a pattern with a fluctuation of data significantly less than 180°.

Curve fitting was not employed as ideal contours are difficult to obtain, and the number of data points is probably not sufficient in most cases to obtain a good fit. Thus, the linearization method, Robin's analysis, and harmonic means have been used to obtain strain estimates.

3.8.3. Linearization method

This is a technique which can be used to estimate strain in

specimens in which initially random grain orientations were present. Yu and Zheng (1984) noticed that the rearrangement of the relationship:

$$\cos \varnothing = \frac{\cosh 2\epsilon_f \cosh 2\epsilon_m - \cosh 2\epsilon_i}{\sinh 2\epsilon_f \sinh 2\epsilon_m}$$

where $\epsilon_f = \ln R_f$, $\epsilon_m = \ln R_m$, and $\epsilon_i = R_i$, which Dunnet (1969) derived from the original Ramsay equations listed earlier, obtains:

$$\cosh 2\epsilon_f = \tan 2\epsilon_m \sinh 2\epsilon_f \cos 2\varnothing + \frac{\cosh 2\epsilon_i}{\cosh 2\epsilon_m}$$

when divided by the hyperbolic cosine of $2\epsilon_m$. This is of the form $y = mx + b$ where $\cosh 2\epsilon_f = y$ and $\sinh 2\epsilon_f \cos 2\varnothing = x$. This is the equation of a line. A fitted regression line to $R_f/\varnothing$ data treated in this manner produces approximations for R_m and R_i. Tectonic strain can be estimated from the slope by halving it and taking the inverse function arctanh. Atheoretical initial shape axial ratio R_i can be derived from the y-intercept ($\cosh 2\epsilon_i / \cosh 2\epsilon_m$) of the line.

Linearization estimates were obtained by computer analysis of the digitized data, and results are presented in figure 3.21.

SPECIMEN	Rs (lin)	Rs (rob)	Rs (har)	e% chart	Rs chart
P02	1.436	1.115	1.576		
P03	1.267	1.147	1.586		
P04	1.789	1.604	1.874		
P05	1.489	1.229	1.622		
P06	1.268	1.206	1.561		
P07	1.442	1.342	1.635		
P08	1.286	1.213	1.603		
P09	1.263	1.115	1.567		
P010	1.29	1.187	1.617		
P011	1.455	1.382	1.584		
P012	1.411	1.416	1.687		
P013				19.6	1.387
P014	1.403	1.369	1.621	15.3	1.283
P015	1.349	1.342	1.646	28.4	1.651
P016	1.516	1.43	1.658	22.1	1.454
P018	1.548	1.486	1.728	23.6	1.497
P019	2.144	1.897	2.054	34.5	1.886
P020	1.679	1.56	1.778	26.2	1.577
P021				30.8	1.737
P022	1.248	1.364	1.641	30.4	1.722
P023	1.395	1.364	1.643	25.8	1.565
P024	1.341	1.173	1.539	10.6	1.183
P025	1.29	1.305	1.68	11.7	1.205
P026	1.502	1.307	1.667	14.9	1.274
P027	1.347	1.218	1.565	13.6	1.245
P028	1.751	1.327	1.645	11.7	1.205

Figure 3.21. These are the various strain values calculated from Rf/Ø data and chart recordings for each pyrrhotite specimen.

3.8.4. Harmonic means

Means of calculated R_f values of strain markers can be used as an estimate of R_s. Lisle (1977a) used computer modelling to demonstrate how various means depart from true R_s values (figure 3.22). Harmonic means provide the best estimates when compared with the arithmetic and geometric means. Harmonic means are calculated from the following relationship:

$$H = \frac{n}{1/R_{f1} + 1/R_{f2} + \ldots 1/R_{fn}}$$

Means are the simplest method of strain measurement, however, their accuracy is limited, especially for R_s values less than 2, where errors are greater than 10% of the true strain (Lisle, 1977a). Harmonic mean strain values in these pyrrhotite experiments were obtained during the digitizing process and are shown in figure 3.21. Strains in these specimens were low, with only one harmonic mean greater than 2, thus these values are interpreted to greatly overestimate strains in most cases.

3.8.5. Robin's analysis

Robin (1977) developed a mathematical treatment for $R_f/\emptyset$ data in which grain shapes need not be ellipsoids. This is well-suited to this study, as the sulphide grains were rarely

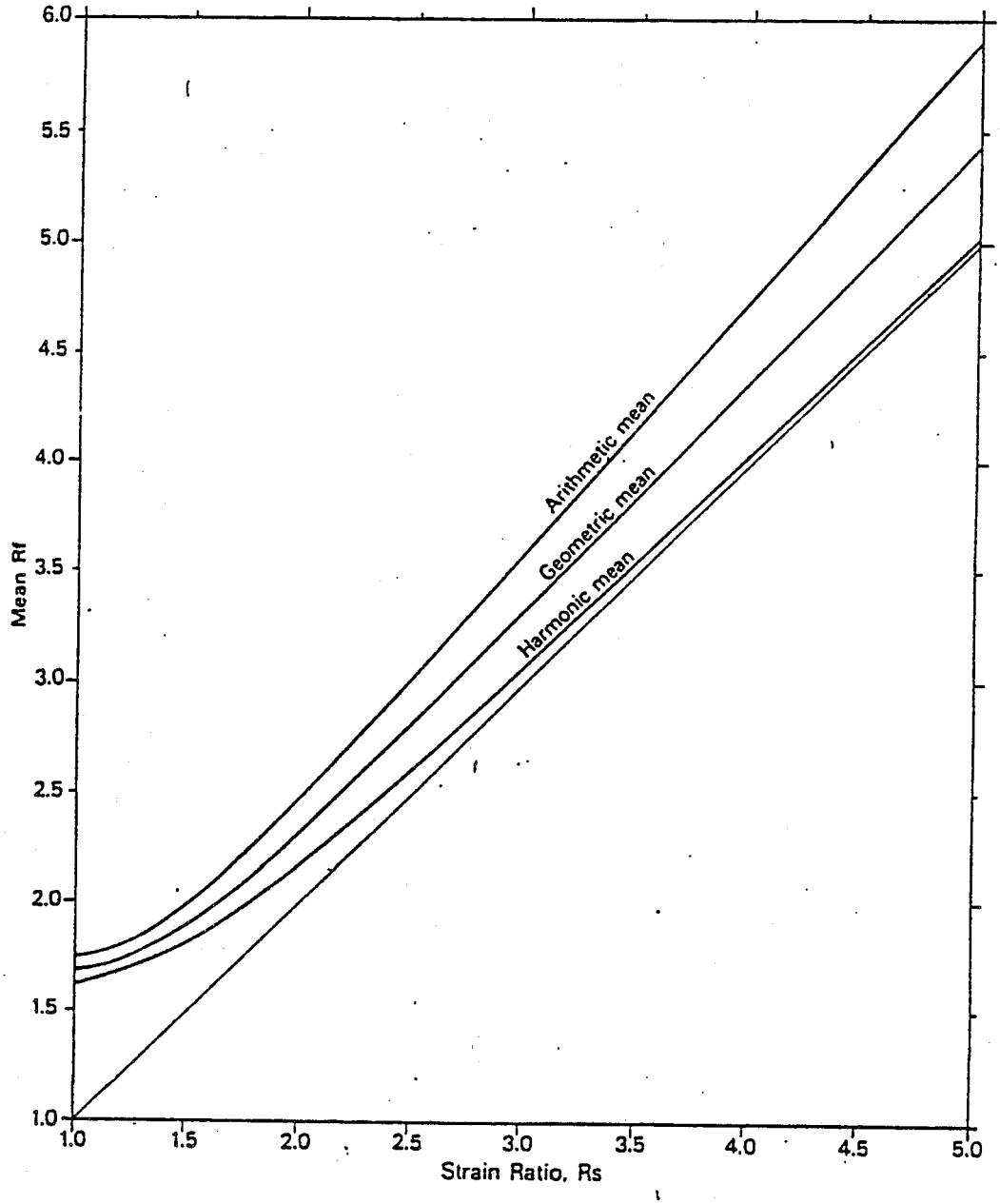

Figure 3.22. This diagram from Lisle (1977a) illustrates the deviation of various means from true strain as a function of Rs. Harmonic means give the best estimates, but are only useful when Rs is greater than 2.0.

ellipsoidal. Two lines parallel to the strain ellipse in a section being analysed are traced through the center of each grain. A logarithmic average process is used to calculate R_m. Robin strain estimates were calculated by computer analysis from the $R_f/\emptyset$ data to obtain the strain estimates shown in figure 3.21.

3.8.6. Comparison of strain analyses

The three strain analysis numbers along with the chart recorded strains, where available, are compared graphically in figure 3.23 for the specimen set P009 to P028. Notice that in most cases, the strain estimates from Robin's analysis are consistently among the lowest, and harmonic means are the highest. The linearization method, for the most part, gives intermediate values. There are a few exceptions to the rule, but note that there is a general pattern for all strain estimates to give similar relative strain estimates for most samples. Chart values appear to have a close relationship to values from Robin's analysis. Only P015, 22, and 23 show significant variation between the two. Only chart data is available for the faulted specimens P013 and P021. They were not digitized, as their fabrics were too disrupted to obtain meaningful strain estimates. P017 was not measured for strain or ACMS as it was destroyed when its protective jacket ruptured upon faulting. Assuming that the chart recordings are accurate, and that Robin's analysis is the

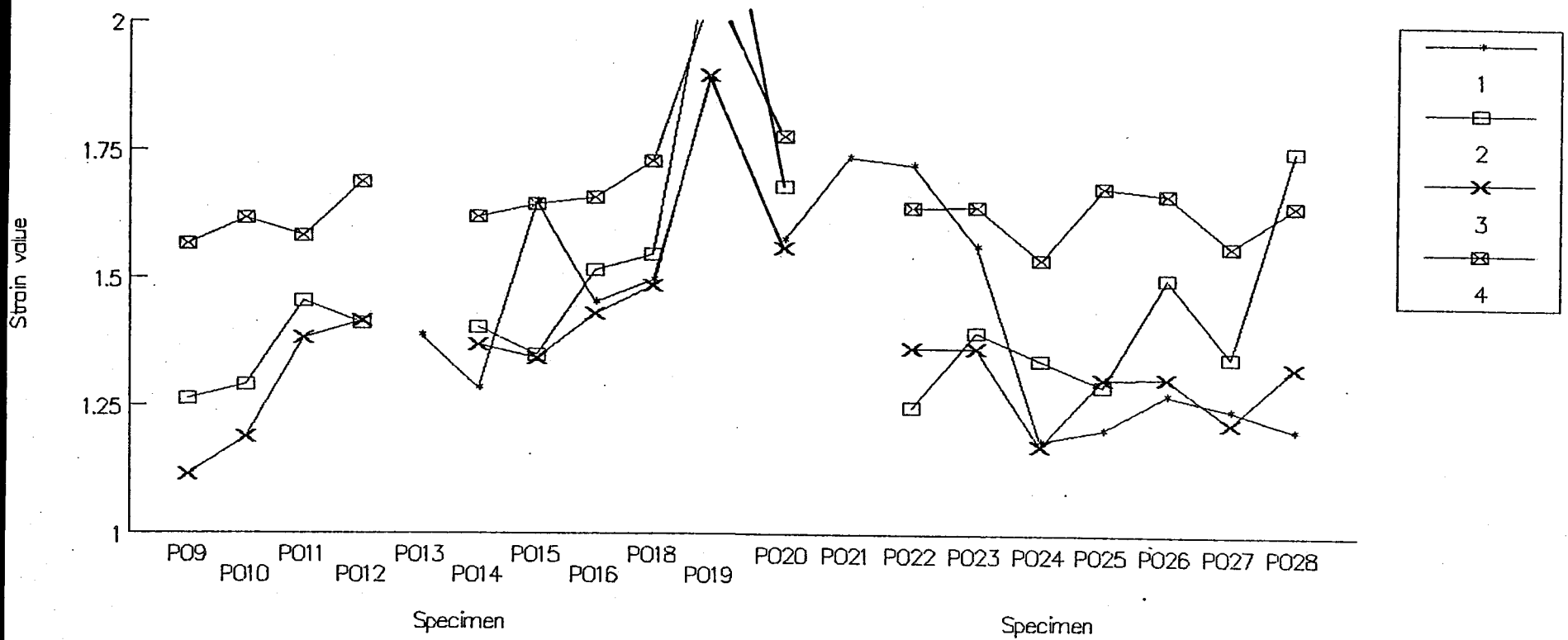

Figure 3.23. This diagram illustrates the relative magnitude of Rs as calculated from four different methods for the specimens P009 to P028. 1 = chart-recorded data, 2 = linearization method, 3 = Robin's analysis, and 4 = harmonic means. Note: No chart-recorded data is available for P009 to P012. P013 and P021 were faulted and not suitable for digitization. P017 faulted, rupturing its teflon jacket and making it unsuitable for strain or ACMS analysis.

best suited method for these specimens, (due to their odd shapes) these are probably the most reliable strain estimates. Harmonic means definitely overestimate strain, and linearization probably provides slight overestimates as well.

3.9. Comparison of ACMS Fabrics to Strain

3.9.1. P009-P028

This sample set will be discussed first, as it contains a greater amount of data, and patterns are much more apparent. ACMS anisotropy data was plotted against the strain estimates obtained from the linearization method, Robin's analysis, and the chart recordings in order to determine if a relationship exists between strain and ACMS. The data is illustrated in figures 3.24 to 3.26. P' (ACMS) plotted against linearization R_s shows that there may be a general increase in anisotropy with strain with the exception of specimens P019 and P028. P' versus Robin R_s shows a much better correlation, with the exception of the outlier P019. This is clearly not a linear relationship. Linear regression obtained an unacceptable value for R squared of 0.33356. An exponential curve with the equation $y = x^{6.34426} * 0.66287$ was fitted in figure 3.25b. In figure 3.25c, where ln R_s is plotted against ln P', the relationship is simplified to the linear form of $y = 6.34x - 0.41$. The fit is not perfect, and the relationship is probably more complex than this, but at least it appears to approximate a power law relationship. Note also that errors in the determination of P' and R_s may make this exponential correlation better or worse than it really is. Finally, the P' versus chart R_s diagram of figure 3.26 shows a somewhat more scattered distribution of data than the diagram of figure 3.25.

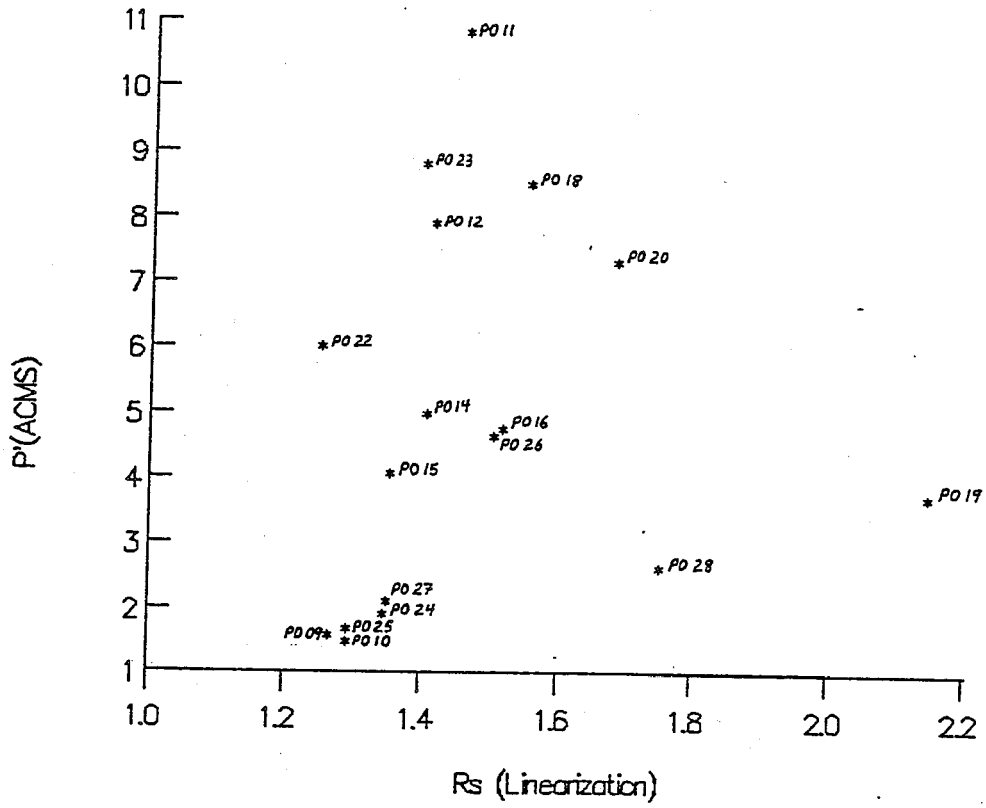

Figure 3.24. Rs (linearization) versus P'(ACMS) shows a possible weak positive correlation.

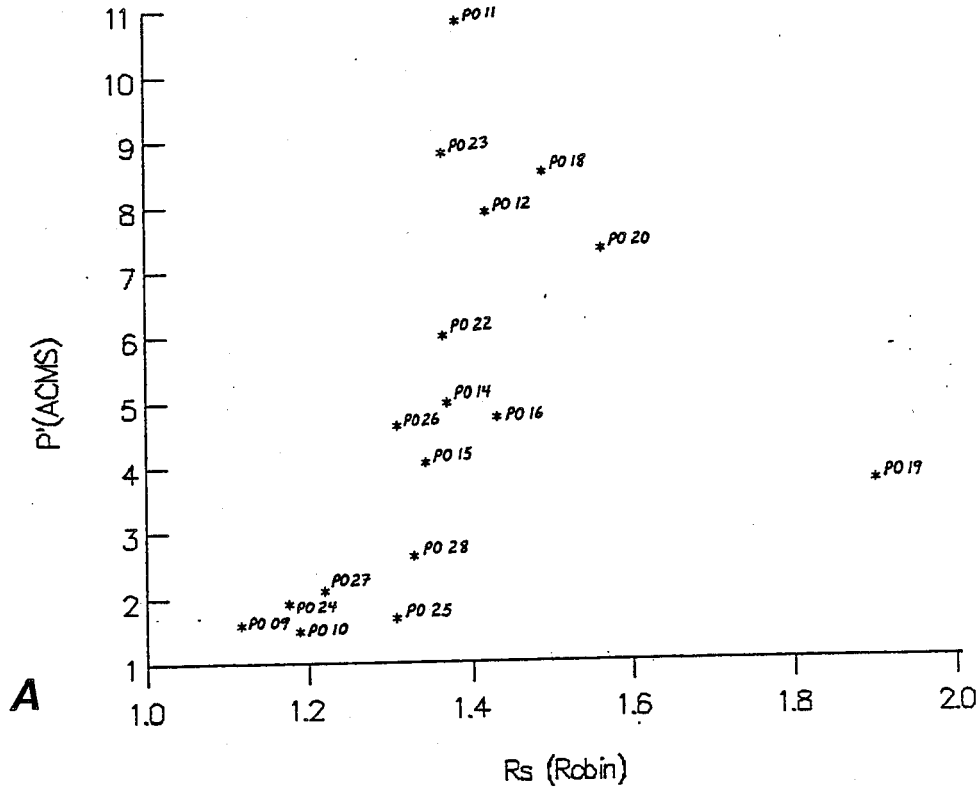

Figure 3.25. Rs (Robin) versus P' (ACMS) shows an interesting possible exponential relationship with the exception of the most highly deformed PO19. (a) This diagram illustrates all data from the second set of specimens. (b) Note the possible exponential relationship. (c) Plotting ln Rs versus ln P' produces a possible linear correlation with the equation: ln P' = 6.34(ln Rs) - 0.41.

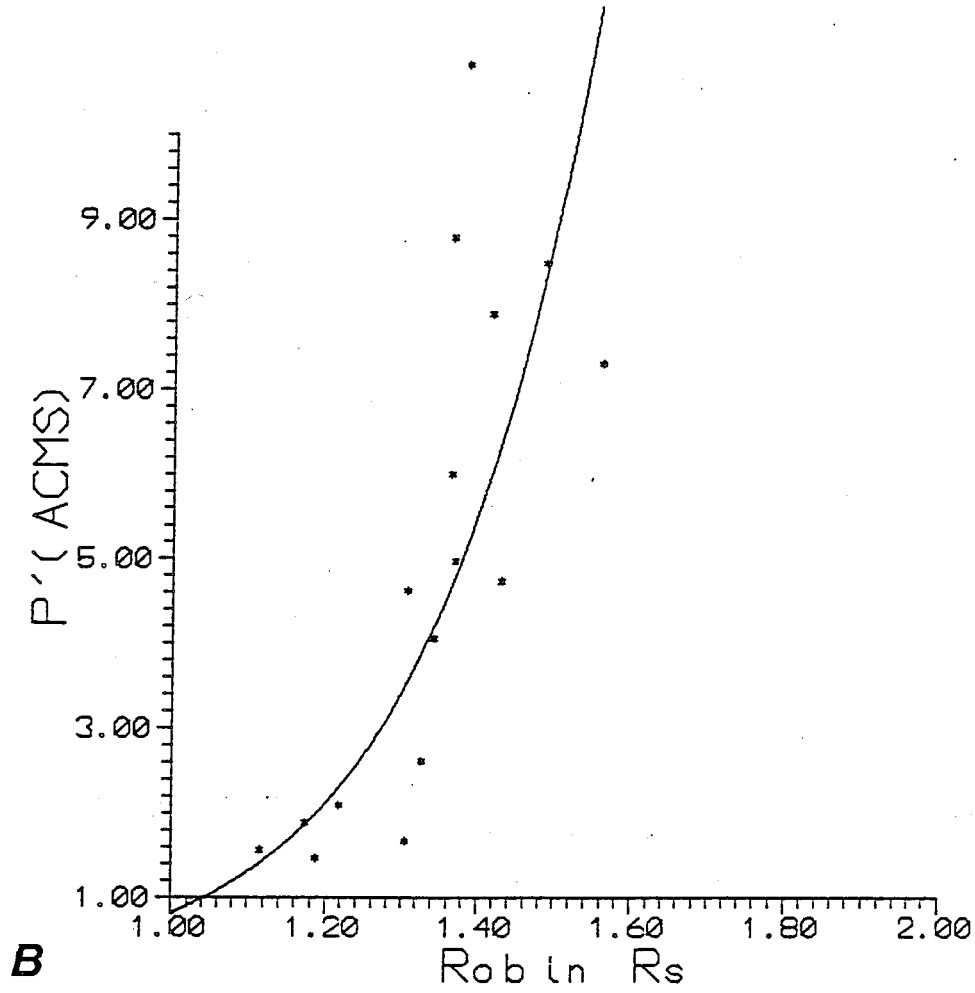

Figure 3.25. Rs (Robin) versus P' (ACMS) shows an interesting possible exponential relationship with the exception of the most highly deformed P019. (a) This diagram illustrates all data from the second set of specimens. (b) Note the possible exponential relationship. (c) Plotting ln Rs versus ln P' produces a possible linear correlation with the equation: ln P' = 6.34(ln Rs) - 0.41.

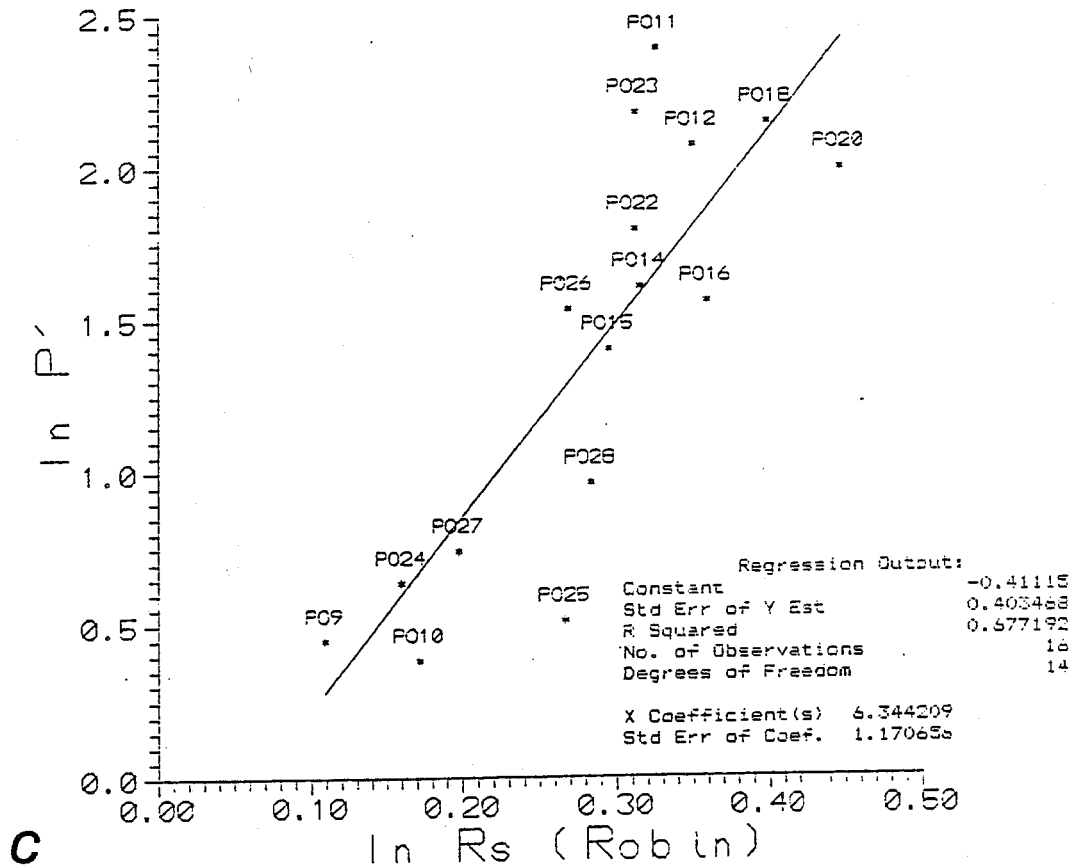

Figure 3.25. Rs (Robin) versus P' (ACMS) shows an interesting possible exponential relationship with the exception of the most highly deformed P019. (a) This diagram illustrates all data from the second set of specimens. (b) Note the possible exponential relationship. (c) Plotting ln Rs versus ln P' produces a possible linear correlation with the equation: ln P' = 6.34(ln Rs) - 0.41.

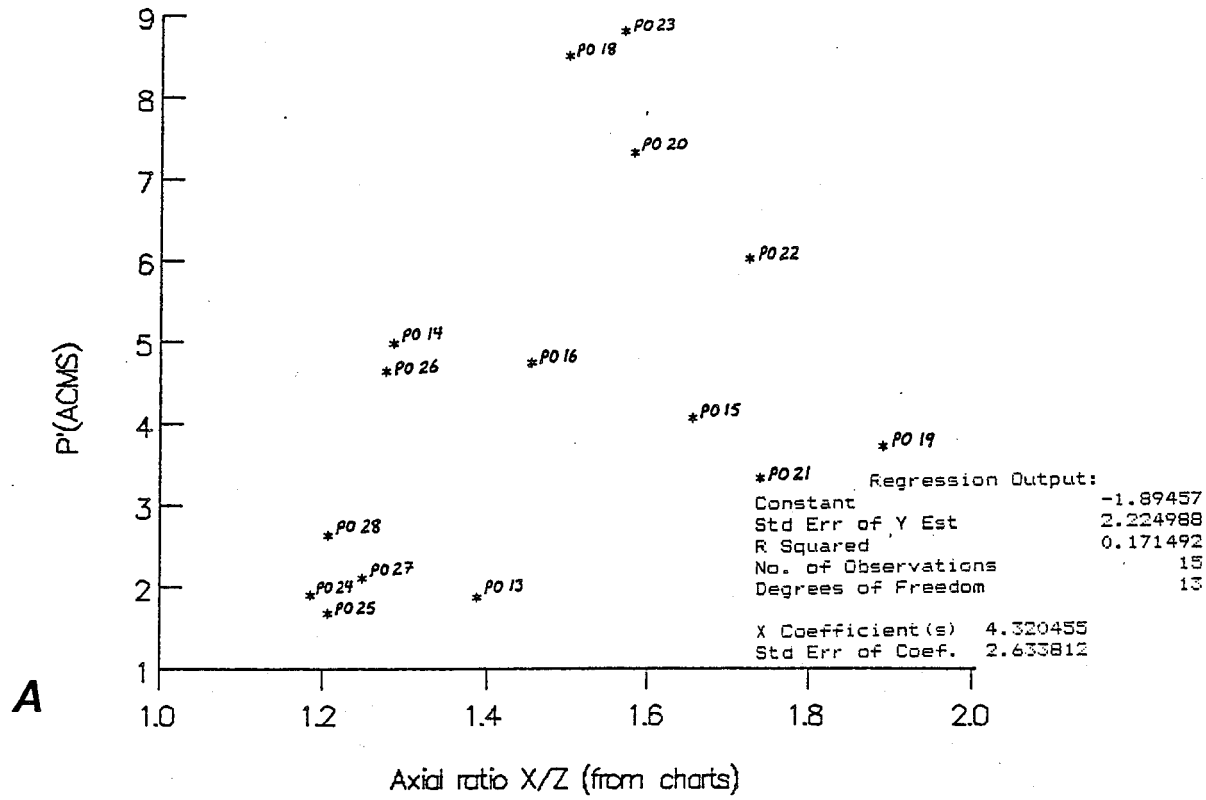

Figure 3.26. (a) This graph illustrates the distribution of chart strain versus P'(ACMS) for the second pyrrhotite specimen set, P009 to P028. Chart data was not available for P002 to P012. Note that there may be an initial trend toward higher P' with strain followed by a decrease in P' at higher strains. (b) This plot shows that there is not a good exponential relationship between chart Rs and P'(ACMS) for the same data which show the possible exponential relationship between Rs (Robin) and P'(ACMS).

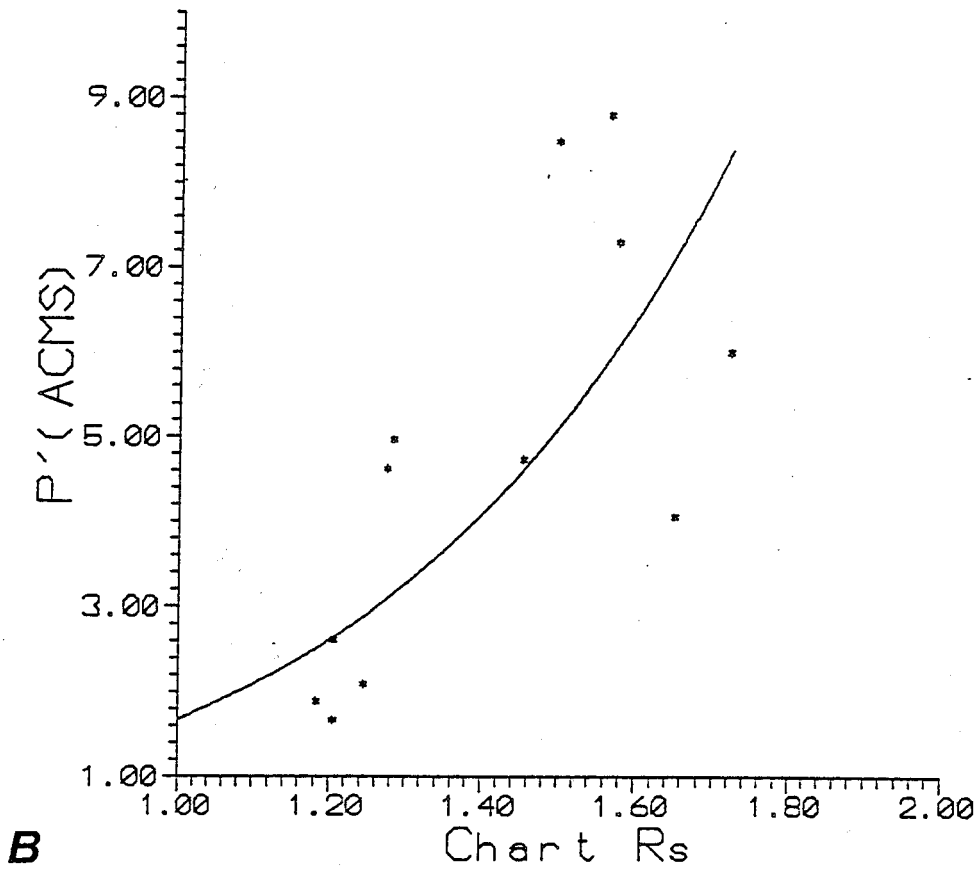

Figure 3.26. (a) This graph illustrates the distribution of chart strain versus P'(ACMS) for the second pyrrhotite specimen set, P009 to P028. Chart data was not available for P002 to P012. Note that there may be an initial trend toward higher P' with strain followed by a decrease in P' at higher strains. (b) This plot shows that there is not a good exponential relationship between chart Rs and P'(ACMS) for the same data which show the possible exponential relationship between Rs (Robin) and P'(ACMS).

The specimens P013 and P021 were faulted and are considered outliers due to the disturbance of ACMS fabrics. In general, there appears to be a strong positive correlation except in the case of P015, 19, and 22. Most of the data in this diagram is similar in distribution to that of figure 3.25, except for P015 and P022. Note that P009 to P012 have no chart recorded strains, although P009 and P010 can be said to have undergone "no strain". An exponential curve was fitted to this data as shown in figure 3.26b, but the relationship is poor. This may be attributed to the factors noted above. This finding thus raises the question: Which, if either of the relationships of figures 3.25 and 3.26 is closer to the true relationship between P' and R_m?

Interestingly, the answer may lie in the outlier specimen P019. This specimen underwent a large strain, much greater than any of the other specimens, yet it developed a much smaller ACMS than many lesser strained specimens. Apparently the high strains have resulted in tighter grain contacts. This can be seen in figure 3.14. Better grain contacts would make the specimen behave more as a single grain, reducing anisotropy as discussed earlier. This observation may therefore mean that there was an initial tendency toward greater ACMS as strain increased, likely influenced by reorientation of grains and cataclasis, however, after strain reached some critical value, grain contacts became tighter as strain progressed, reducing ACMS as strain increased. This may explain the pattern observed in figure 3.26a, as the three most highly strained specimens after P019, namely P020, 15,

and 22 show a possible trend toward decreased ACMS with strain. Such a trend is not as evident in figures 3.24 and 3.25a, but P018 and P020 in each may be part of such a trend in each. Thus, all of the strain analysis techniques may be showing a tendency toward decreased anisotropy as strains reach a critical value. In any case, it is clear that there is not a simple relationship.

Unfortunately, the experimental conditions of the deformation of P019 could not be duplicated in further experiments to determine with more certainty if the above proposed explanation is true. Most specimens (ie. P013, 17, and 21) faulted, or were determined to be in danger of faulting from chart observation before such strains could be achieved.

3.9.2. P002-P008

The strain versus ACMS data for these specimens are presented in figure 3.27. The P' versus linearization R_m plot shows a great amount of scatter and no apparent relationship. However, P' versus Robin R_m is remarkably similar to the equivalent diagram for P009 to P028 in figure 3.25. There is also an outlier specimen (P004) which underwent the largest amount of strain but exhibits a low ACMS. Unfortunately, there was insufficient chart data to plot P' against chart R_m. The data of figure 3.27 appear to confirm the belief that the Robin analysis method provides a better approximation of strain than the linearization method. It also appears to follow the same sort of

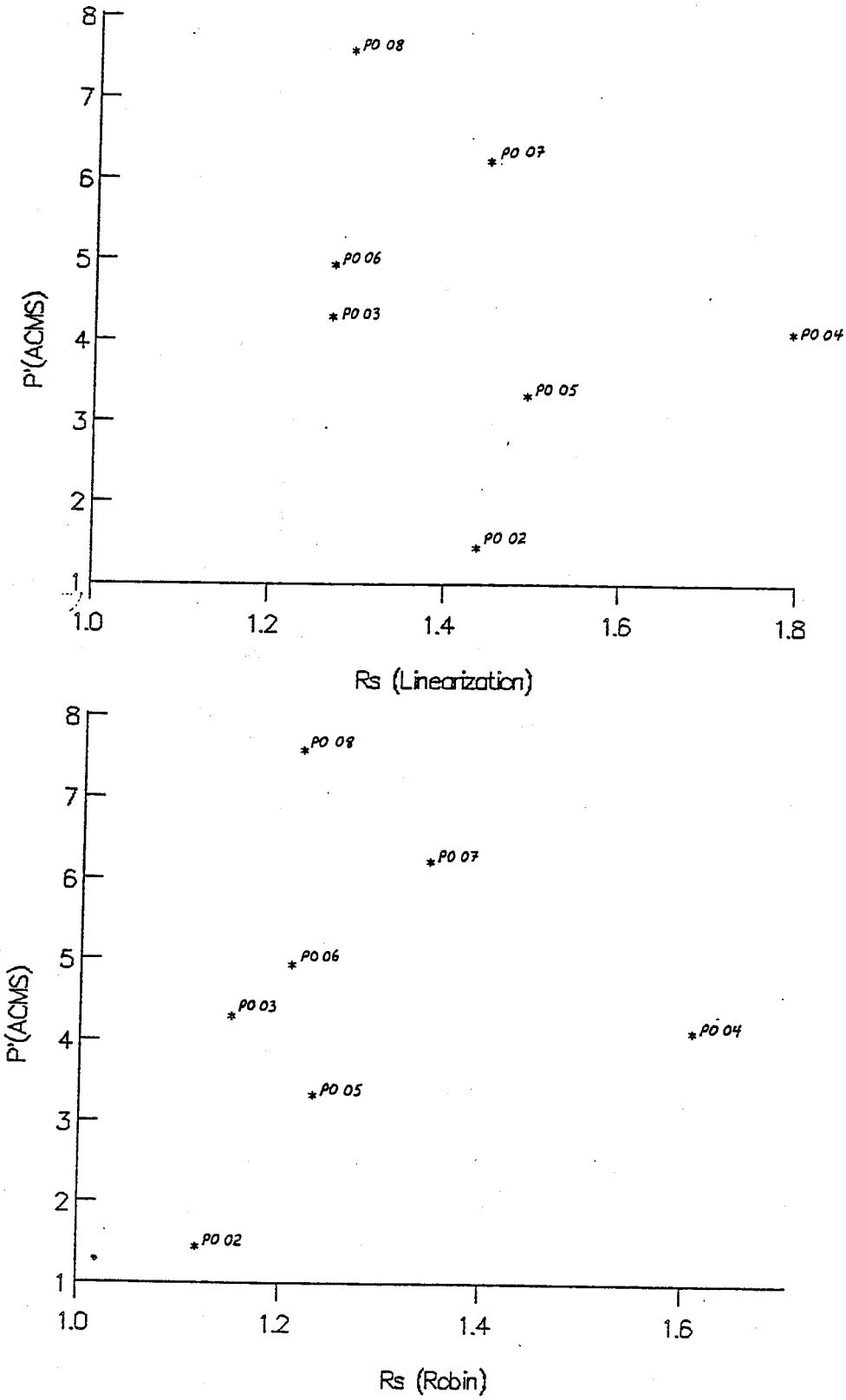

Figure 3.27. These are the plots of strain versus P' (ACMS) for specimens P002 to P008. The data distribution appears to be quite similar to that observed for P009 to P028, especially for the Robin strain data. Note that the most highly strained specimen (P004) is an outlier, just as P019 in the other set of specimens.

pattern of fabric development as interpreted for P009 to P028.

3.9.3. K''_{max} versus strain

The diagrams of figure 3.28 illustrate that in both sample sets there is a relationship between the magnitude of the maximum susceptibility axis and the magnitude of strain, especially when chart-recorded strains are used. This is the type of relationship observed by Borradaile and Hawton (1990) between conductivity and strain in talc aggregates deformed by triaxial deformation. The only difference is that in the pyrrhotite, the relationship appears to be closer to linear than logarithmic. This type of pattern is evidence that K''_{max} is influenced by the development of better preferred orientations of grains as deformation proceeds. Bulk susceptibility shows a similar relationship to strain, as shown earlier in figure 3.7. This may be because the other principal susceptibilities are affected by the tightening of grain boundaries in the compression direction as well as grain orientation, making them increase with strain as well. If susceptibility was solely a function of preferred orientation, all specimens would have approximately the same bulk susceptibility regardless of their strain state.

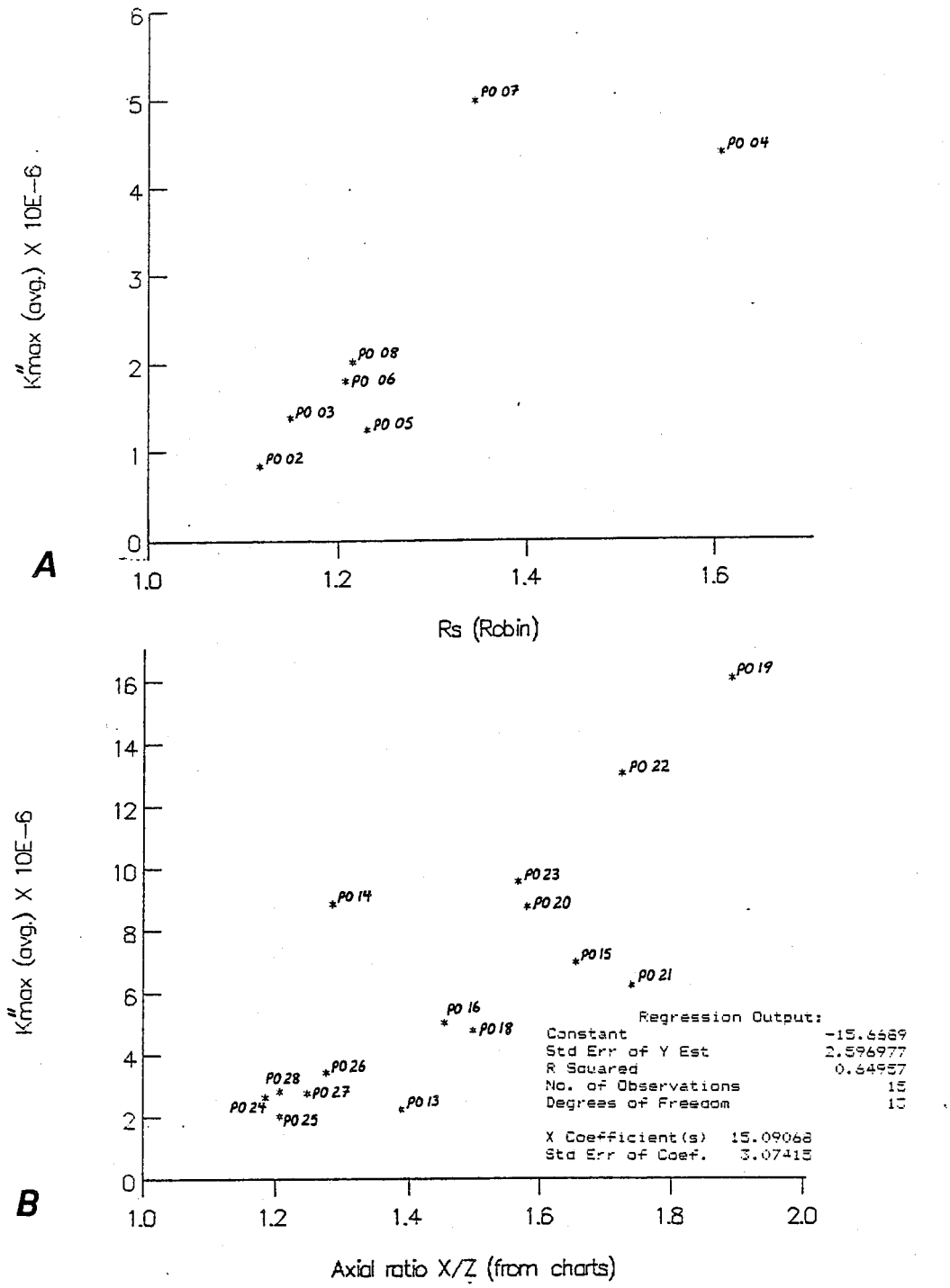

Figure 3.28. These diagrams show the relationship between conductive K''_{max} and Rs for all specimens. (a) Note the general increase of K''_{max} with strain for P002 to P008. (b) There is an approximately linear correlation between K''_{max} and strain from chart recordings for P009 to P028 of: $K''_{max} = 15.09Rs - 15.67$. (c) This distribution, using Rs (Robin) values is quite similar to that in (b) except for P011 and P022.

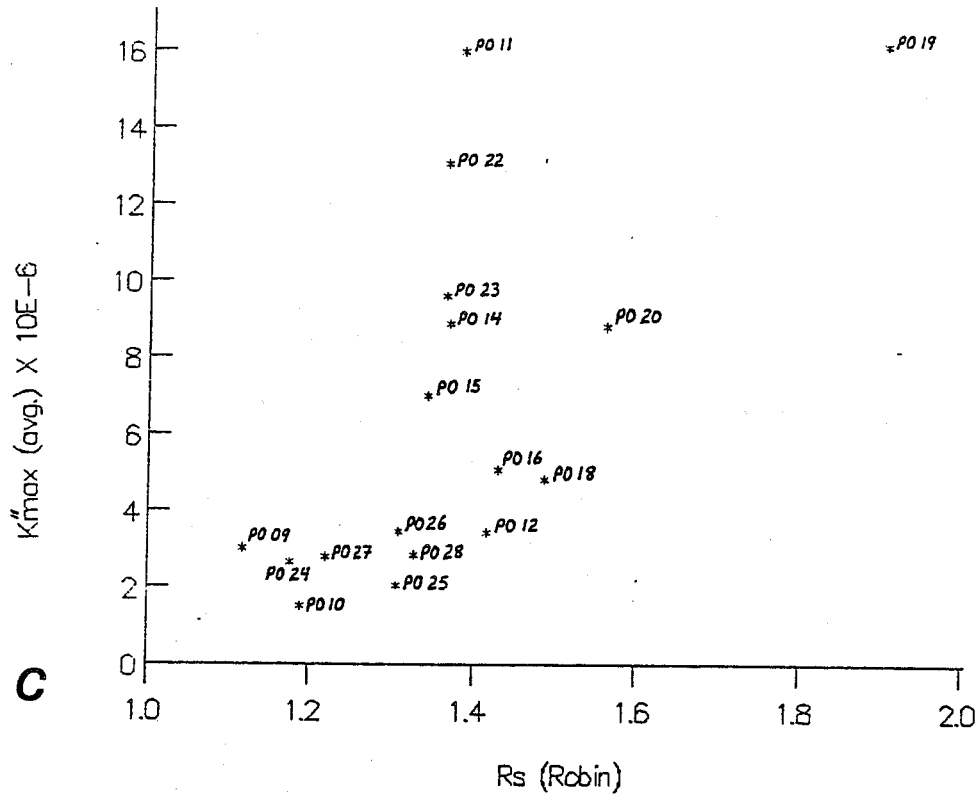

Figure 3.28. These diagrams show the relationship between conductive K''_{max} and Rs for all specimens. (a) Note the general increase of K''_{max} with strain for P002 to P008. (b) There is an approximately linear correlation between K''_{max} and strain from chart recordings for P009 to P028 of: $K''_{max} = 15.09Rs - 15.67$. (c) This distribution, using Rs (Robin) values is quite similar to that in (b) except for P011 and P022.

3.10. Comparison of AMS Fabrics to Strain

Similar plots of P' (AMS) versus the linearization, Robin and chart strains were plotted to determine if a relationship exists. Once again, the sample set P009 to P028 will be discussed first.

3.10.1. P009-P028

The P' (AMS) versus R_s data are illustrated in figure 3.29. Both Robin and chart strain values show fairly good linear relationships to P'. The equations for the lines are illustrated in figure 3.29. Note that the lines are of differing slope, but this can be attributed to differences in R_s values determined using two different techniques. Thus there is a nearly linear correlation between strain and AMS at least for the limited strains possible in these experiments. Thus it can not be said whether or not this might continue to higher values of R_s. Note that there is not quite as good a correlation between P' (AMS) and linearization strain. This is further evidence to suggest that linearization data is not as good as that from the two other strain analysis techniques. It appears that the chart recorded strains provide the most consistent results if the graphical relationships to date are examined.

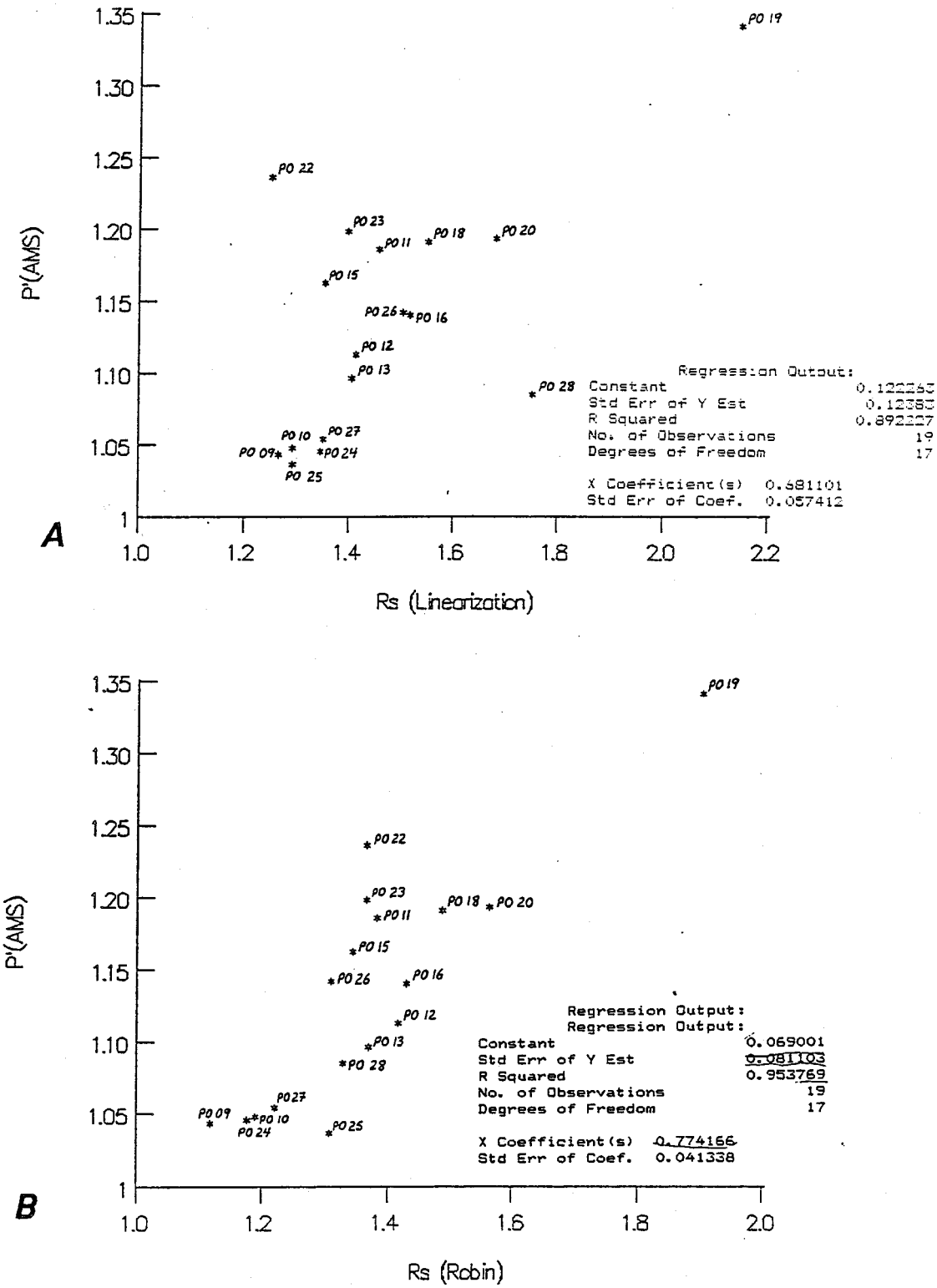

Figure 3.29. There appears to be a linear correlation between strain and P' (AMS) for the pyrrhotite aggregates P009 to P028, especially in graphs (b), where P' = 0.77Rs + 0.07 and (c), where P' = 0.33 Rs + 0.67. The differing slopes may be a function of the over- or under-estimation of strain by the two methods. Note that chart-recordings and Rf/Ø data were not available for all specimens and may account for some discrepancy. In any case, there appears to be a strong correlation between strain and AMS for these specimens. This once again illustrates the usefulness of AMS as a strain analysis tool.

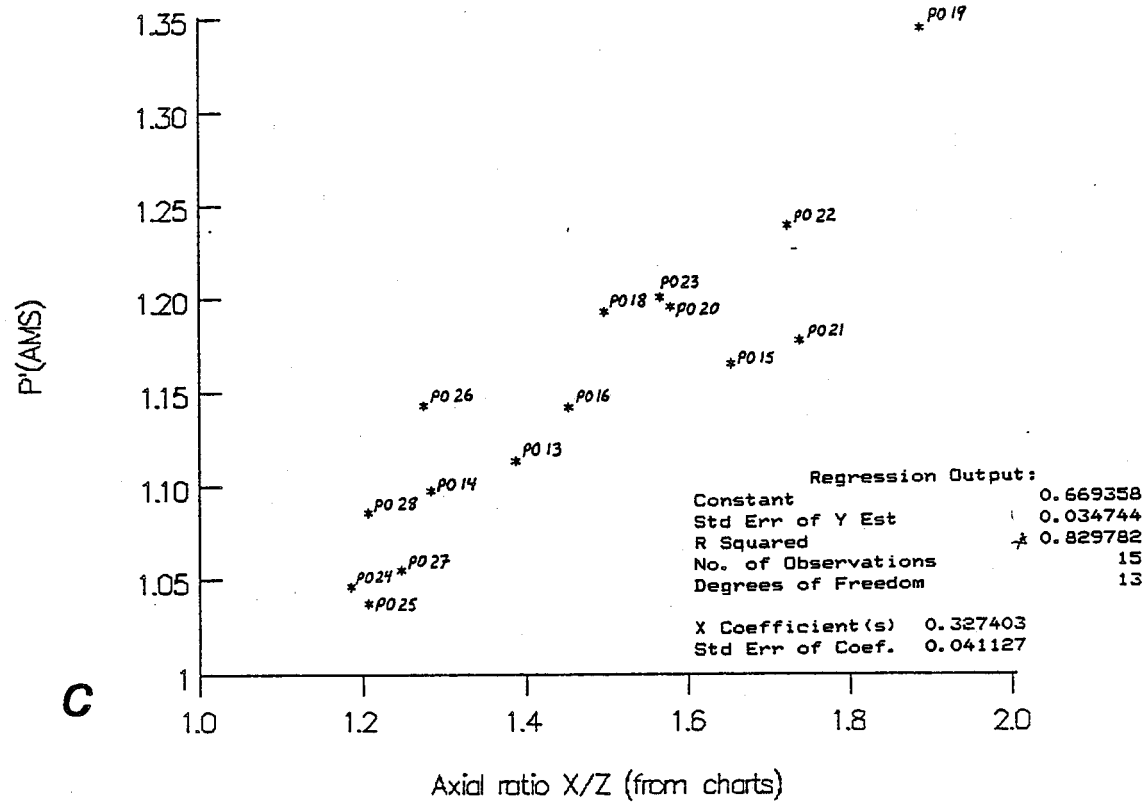

Figure 3.29. There appears to be a linear correlation between strain and P' (AMS) for the pyrrhotite aggregates P009 to P028, especially in graphs (b), where P' = 0.77Rs + 0.07 and (c), where P' = 0.33 Rs + 0.67. The differing slopes may be a function of the over- or under-estimation of strain by the two methods. Note that chart-recordings and Rf/Ø data were not available for all specimens and may account for some discrepancy. In any case, there appears to be a strong correlation between strain and AMS for these specimens. This once again illustrates the usefulness of AMS as a strain analysis tool.

3.10.2. P002-P008

The diagrams of figure 3.30 show that there is no apparent relationship between P' (AMS) and strain in these specimens. The mixed composition of these specimens may have been a factor in this lack of a relationship. Also, no chart recorded strains are available for comparison.

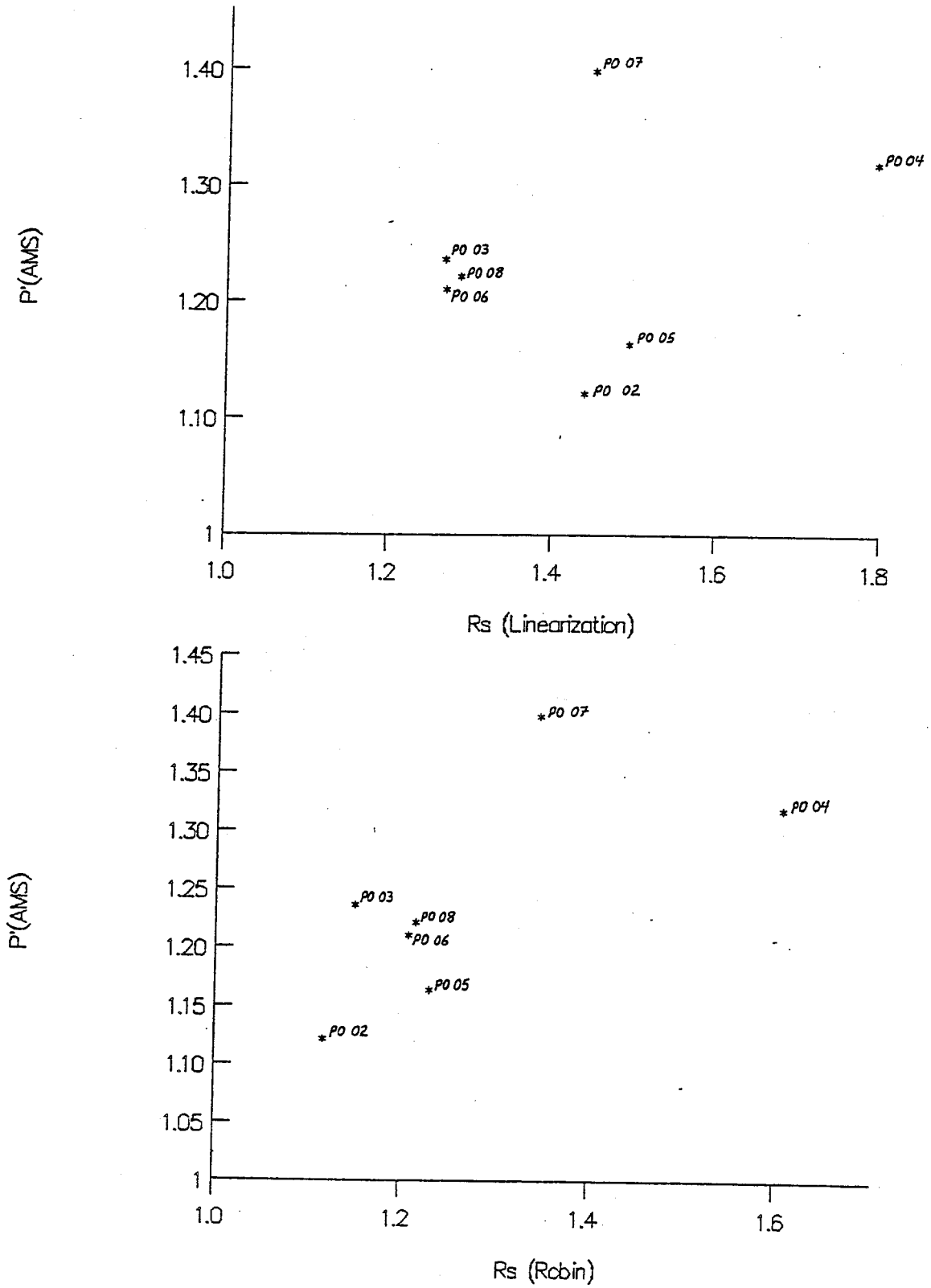

Figure 3.30. No obvious patterns are evident in these plots of strain versus P'(AMS) for P002 to P008.

3.11. Relationship Between P'(AMS) and P'(ACMS)

The relationships between the two anisotropies for both data sets are illustrated in figure 3.31. In each case there is a slight apparent tendency toward mutual increase. This is attributable to the fact that the two anisotropies are both related to strain to some extent.

Figure 3.32 illustrates dramatically that P'(ACMS) is much higher than P'(AMS) in most specimens. This may be an important finding, as one of the major disadvantages of magnetic susceptibility analysis is that anisotropies are generally quite low (Borradaile, 1988).

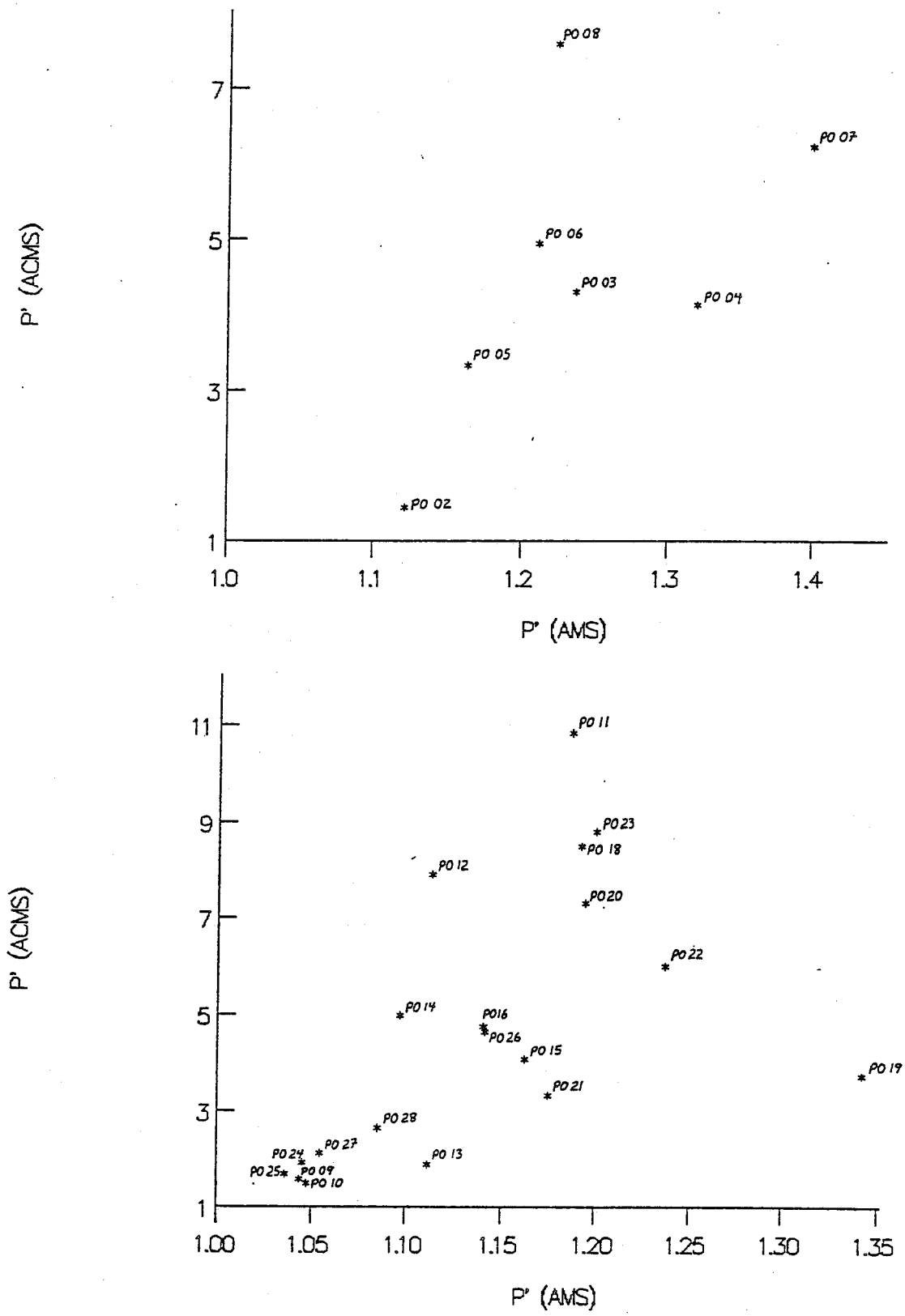

Figure 3.31. These P' (AMS) versus P' (ACMS) plots bear some resemblance to strain versus P' (ACMS) plots, owing to the strong correlation between strain and P' (AMS) in P009 to P028.

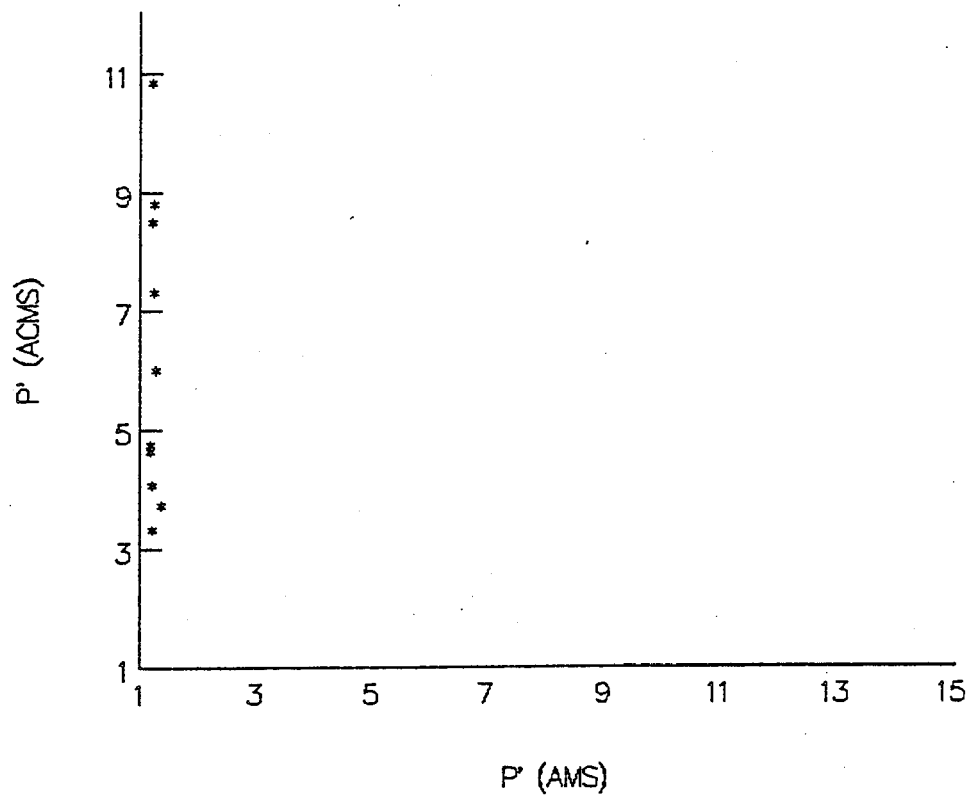

Figure 3.32. The X and Y axes of this diagram are of equal scale to illustrate the relative magnitudes of ACMS and AMS anisotropies in P009 to P028. Obviously, P'(ACMS) developed much more strongly.

3.12. Discussion of Results

The experiments performed on loose pyrrhotite aggregates showed without a doubt that there was a relationship between the principal directions of the strain ellipsoid and the corresponding axes of the strain ellipsoid. Thus it was possible to determine if there was a correlation between the magnitude of anisotropy and calculated strain. There appears to be a correlation, however, it is complicated. A power law relationship may exist up to some critical strain, after which a peak ACMS is attained and a subsequent drop in anisotropy occurs as grain contacts become better. This relationship indicates that the prospects for quantitative correlation between ACMS and strain are not good, especially at high strain. At extremely high strains, when grain boundaries are not a major factor (Shuey, 1975), it would be expected that any anisotropy of resistivity would be crystallographic. At this point, there may be a totally different relationship between strain and ACMS in massive specimens. This would probably not be so much of a factor in disseminated sulphides, as continuity between sulphide grains is broken and grain shapes should continue to play a role. The following chapter involves experimental deformation of a partially disseminated sulphide.

4. PYRRHOTITE PLUS TALC EXPERIMENTS

4.1. Materials and Method

These experiments were similar to those described in the previous chapter, except that the materials used were pyrrhotite from the same source used for specimens P009 to P028 and talc in the grainsize 74 to 150 μm. The proportions by volume were approximately 70% pyrrhotite and 30% talc in the unconsolidated state. Thus this also includes pore space between grains of each mineral and the values are not necessarily precise. They also changed as the result of compaction in the triaxial rig. The proportions noted above were used because smaller amounts of pyrrhotite did not provide measurable results (see figure 4.1). Once again, ACMS and AMS measurements were performed on these specimens to test their relationship to strain.

ACMS OUTPUT: Conductivity parameters

TP04 SITE 1 CORE 1 SPEC 1 UNITS= SI m M= 6 NR= 2 13:53:50 06-11-1990

SUSC.	DEC	INC	R95	EV	SDEV
MIN	64.93	-2.41	42.6	4.1220E-07	2.307E-08
INT	337.15	42.60	61.2	5.1077E-07	4.310E-09
MAX	332.32	-47.30	63.0	5.7655E-07	2.511E-08

ACMS OUTPUT: Conductivity parameters

TP04 SITE 1 CORE 1 SPEC 2 UNITS= SI m M= 6 NR= 2 13:57:55 06-11-1990

SUSC.	DEC	INC	R95	EV	SDEV
MIN	307.07	37.89	38.3	4.6400E-07	1.271E-08
INT	48.65	14.46	44.8	5.5496E-07	3.651E-08
MAX	335.59	-48.48	38.3	6.2174E-07	4.164E-08

ACMS OUTPUT: Conductivity parameters

TP04 SITE 1 CORE 1 SPEC 3 UNITS= SI m M= 6 NR= 2 14:02:09 06-11-1990

SUSC.	DEC	INC	R95	EV	SDEV
MIN	356.23	-13.50	22.0	3.9050E-07	1.987E-08
INT	275.26	33.15	69.8	4.9414E-07	5.412E-08
MAX	67.29	53.51	70.8	6.2207E-07	8.399E-08

ACMS OUTPUT: Conductivity parameters

TP04 SITE 1 CORE 1 SPEC 4 UNITS= SI m M= 6 NR= 2 14:06:36 06-11-1990

SUSC.	DEC	INC	R95	EV	SDEV
MIN	314.28	5.37	37.7	3.9738E-07	7.369E-09
INT	36.58	-54.94	73.3	5.5646E-07	7.642E-09
MAX	48.00	34.53	63.0	6.0283E-07	1.500E-08

ACMS OUTPUT: Conductivity parameters

TP04 SITE 1 CORE 1 SPEC 5 UNITS= SI m M= 6 NR= 2 14:12:02 06-11-1990

SUSC.	DEC	INC	R95	EV	SDEV
MIN	13.34	3.33	74.5	4.9736E-07	6.037E-08
INT	282.21	18.71	104.9	5.1144E-07	4.817E-08
MAX	293.04	-70.98	72.9	6.2849E-07	2.620E-08

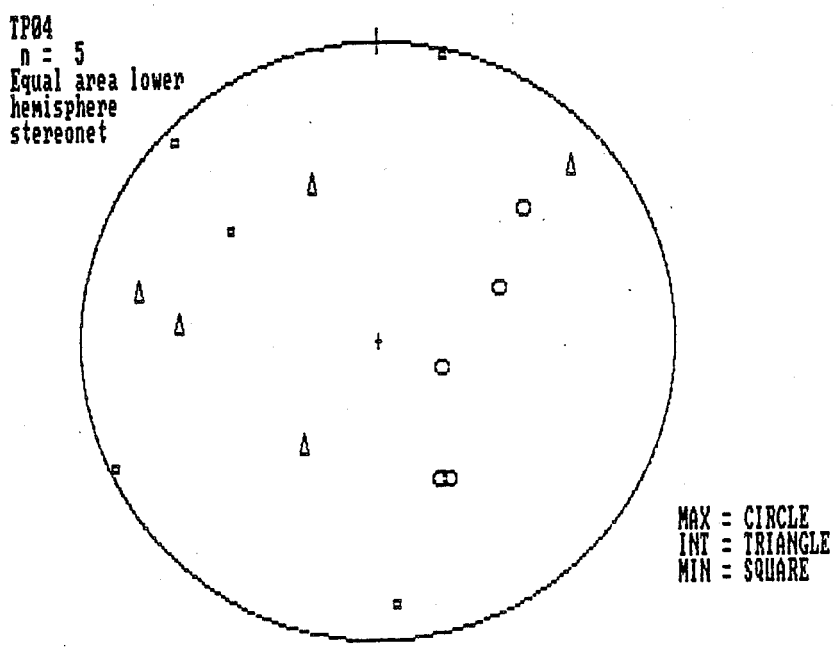

A

Figure 4.1. (a) This is conductive ACMS data for the specimen TP04 which contained 50 volume % of pyrrhotite and talc. Note that the axes of susceptibility are poorly defined and that standard deviations for K" values are high, as conductivities are very low. The specimen was shortened by 12 %. (b) When 70 volume % pyrrhotite plus 30 volume % talc were deformed, as in TP09, conductive K''_{max} (the same as resistive K''_{min} used earlier) is well defined and much more conductive. Despite the poor definition of K''_{int} and K''_{min}, they define the plane of flattening, where conductivity is lowest.

TP09 SITE 1 CORE 1 SPEC 1 UNITS= SI m M= 6 NR= 2 11:47:36 07-24-1990

SUSC.	DEC	INC	R95	EV	SDEV
MIN	312.28	3.51	85.3	5.5296E-07	5.910E-09
INT	42.40	2.06	85.3	5.9491E-07	4.776E-08
MAX	342.80	-85.93	0.2	2.4939E-06	4.925E-09

ACMS OUTPUT: Conductivity parameters

TP09 SITE 1 CORE 1 SPEC 2 UNITS= SI m M= 6 NR= 2 11:51:54 07-24-1990

SUSC.	DEC	INC	R95	EV	SDEV
MIN	296.41	3.12	60.3	5.4286E-07	7.867E-08
INT	26.49	1.46	60.3	6.4437E-07	8.442E-09
MAX	321.60	-86.56	0.6	2.4645E-06	1.259E-08

ACMS OUTPUT: Conductivity parameters

TP09 SITE 1 CORE 1 SPEC 3 UNITS= SI m M= 6 NR= 2 11:55:57 07-24-1990

SUSC.	DEC	INC	R95	EV	SDEV
MIN	317.13	2.28	65.6	5.8832E-07	5.896E-08
INT	47.25	3.11	65.6	6.5303E-07	5.426E-10
MAX	11.01	-86.14	1.9	2.4768E-06	6.676E-08

ACMS OUTPUT: Conductivity parameters

TP09 SITE 1 CORE 1 SPEC 4 UNITS= SI m M= 6 NR= 2 12:00:00 07-24-1990

SUSC.	DEC	INC	R95	EV	SDEV
MIN	293.18	3.86	8.9	4.7842E-07	5.427E-08
INT	23.24	1.03	8.9	6.2812E-07	7.622E-09
MAX	314.24	-86.00	3.3	2.5092E-06	7.929E-09

ACMS OUTPUT: Conductivity parameters

TP09 SITE 1 CORE 1 SPEC 5 UNITS= SI m M= 6 NR= 2 12:03:56 07-24-1990

SUSC.	DEC	INC	R95	EV	SDEV
MIN	291.56	3.65	29.4	5.2851E-07	2.378E-08
INT	21.34	-0.06	29.6	5.3796E-07	7.936E-09
MAX	292.41	-86.35	4.2	2.4701E-06	8.398E-08

ACMS OUTPUT: Conductivity parameters

TP09 SITE 1 CORE 1 SPEC 6 UNITS= SI m M= 6 NR= 2 12:07:28 07-24-1990

SUSC.	DEC	INC	R95	EV	SDEV
MIN	294.15	3.98	1.5	5.0314E-07	2.253E-08
INT	24.20	0.84	2.3	6.6830E-07	3.505E-08
MAX	306.27	-85.93	2.5	2.3596E-06	3.296E-08

ACMS OUTPUT: Conductivity parameters

TP09 SITE 1 CORE 1 SPEC 7 UNITS= SI m M= 6 NR= 2 12:11:00 07-24-1990

SUSC.	DEC	INC	R95	EV	SDEV
MIN	306.83	3.63	1.6	4.1111E-07	6.713E-08
INT	36.97	2.23	1.7	6.2004E-07	3.336E-08
MAX	338.52	-85.73	0.8	2.4883E-06	2.559E-08

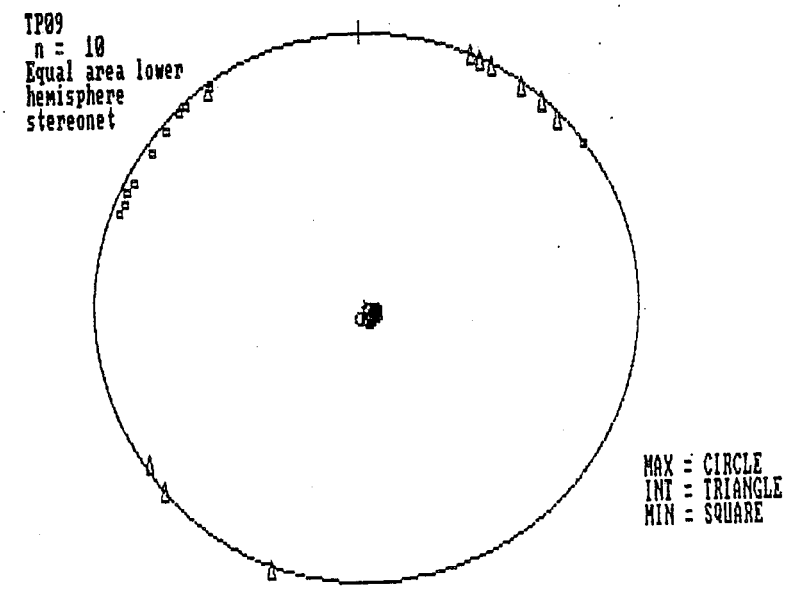

B

Figure 4.1. (a) This is conductive ACMS data for the specimen TP04 which contained 50 volume % of pyrrhotite and talc. Note that the axes of susceptibility are poorly defined and that standard deviations for K" values are high, as conductivities are very low. The specimen was shortened by 12 %. (b) When 70 volume % pyrrhotite plus 30 volume % talc were deformed, as in TP09, conductive K''_{max} (the same as resistive K''_{min} used earlier) is well defined and much more conductive. Despite the poor definition of K''_{int} and K''_{min}, they define the plane of flattening, where conductivity is lowest.

4.2. Electrical Properties of Talc

The electrical properties of experimentally deformed talc aggregates were studied by Borradaile and Hawton (1990). They used the same talc used in this experiment. Results of conductivity measurements on talc at 88% relative humidity are summarized in figure 4.2. Note that for all strains at 10^5 Hz, which is the approximate frequency of ACMS measurements, conductivity is less than 100×10^{-6} S/m, which corresponds to 10^4 Ω·m. This is several orders of magnitude higher than the resistivity of pyrrhotite, and well out of the sensitivity limits of the ACMS coil. Figure 4.1 illustrates the effect which talc has on measurements when greater than 30% of the volume of a specimen consists of talc. Thus the ACMS signals in the following specimens are dominantly controlled by the pyrrhotite.

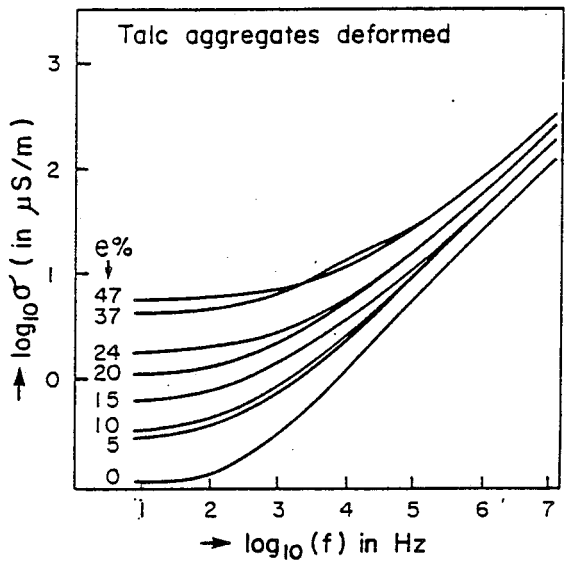

Fig. 4. Conductivity (σ) of specimens parallel to the direction of loading of the talc aggregates, as a function of the frequency, f. Measured at 88% relative humidity.

A

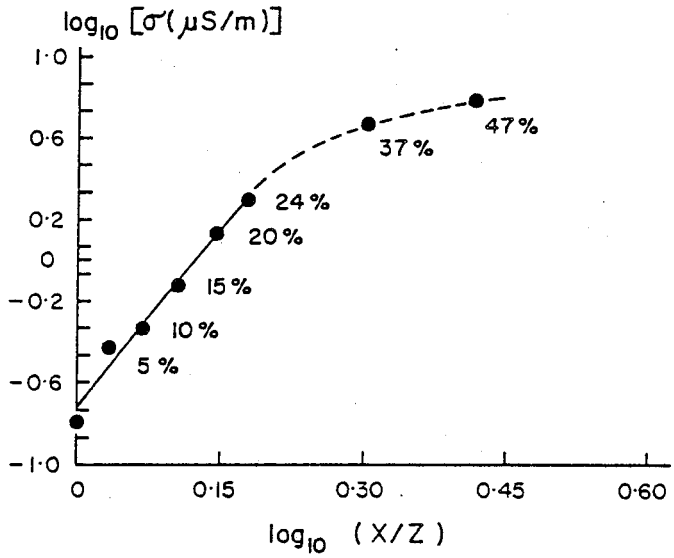

B

Fig. 6. Logarithmic plot (base 10) of conductivity (σ) vs. strain ratio (X/Z). The approximately linear relationship for the six most weakly strained specimens should be noted.

Figure 4.2. (a) Note that conductivity in talc aggregates measured parallel to the direction of compression of triaxial deformation increases as a function of strain and frequency. Note that these conductivities are not detectable in the ACMS coil, as they are too low. (b) Notice the linear logarithmic relationship between strain and conductivity below 24% strain. This appears to have some similarity to the possible logarithmic relationship between strain and ACMS in pyrrhotite aggregates discussed in chapter 3. Both diagrams are from Borradaile and Hawton (1990).

4.3. Deformation Textures

Polished sections were prepared from the seven specimens TP06 to TP12, for which ACMS and AMS were measured to study the textures developed in pyrrhotite. Talc was not examined as it does not influence the ACMS fabrics. The pyrrhotite plus talc specimens appear to have deformed somewhat differently than the pyrrhotite specimens discussed in the previous chapter. The differences are due to the presence of the fine-grained talc matrix. Cataclasis is much less prevalent and occurs only where pyrrhotite grains impinge, occurs as seen in figure 4.3. Some undulatory extinction was evident in pyrrhotite, but kinking was not present, even though this was the same pyrrhotite used for experiments P009 to P028. This is because much of the deformation was taken up by the softer, finer-grained talc. This is evident when one compares the relative volume of matrix in the hydrostatically compacted specimen TP07 and the most highly deformed specimen TP10 illustrated in the photomicrographs of figure 4.4. The specimen TP07 contains an estimated 25 to 30 volume percent talc, while TP10 appears to contain only 10 to 15% talc. Very strong preferred orientations of pyrrhotite grains were developed in these specimens, and can be seen easily in figures 4.3 and 4.4.

The textures observed in these specimens indicate that the deformation mechanisms operative in pyrrhotite were rigid-body rotation combined with some minor plastic and cataclastic

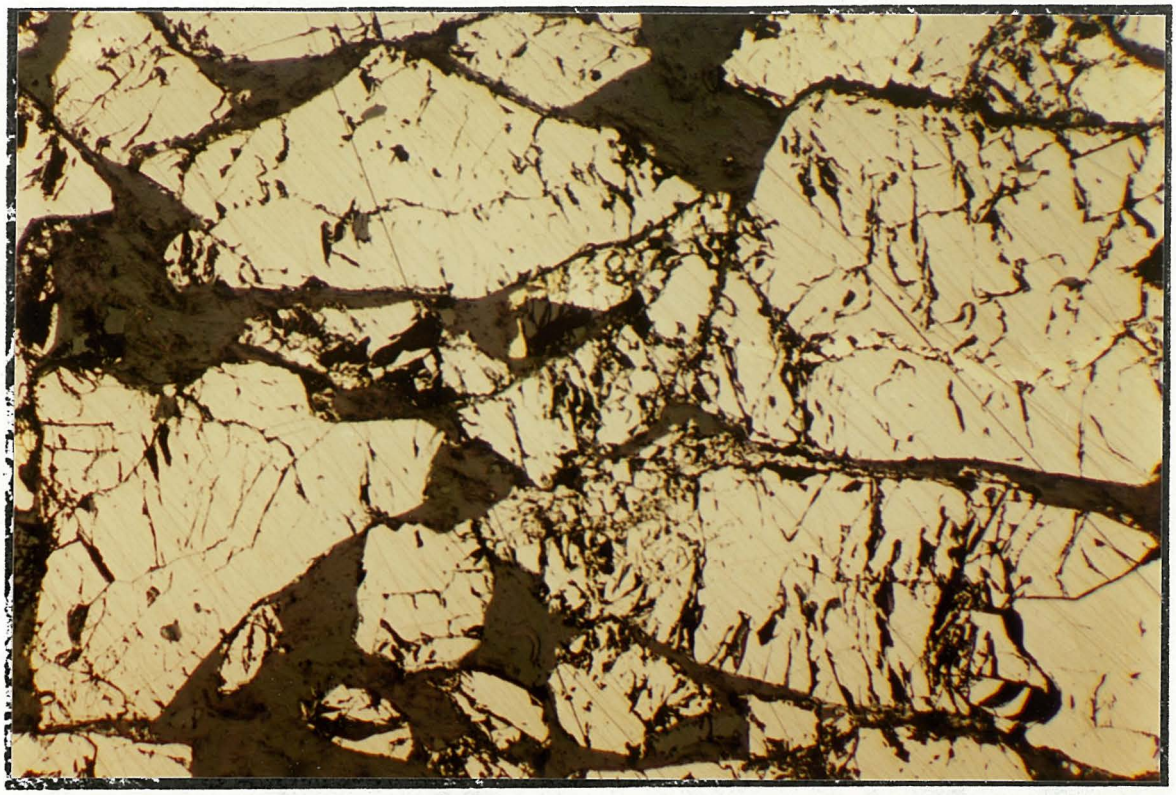

A

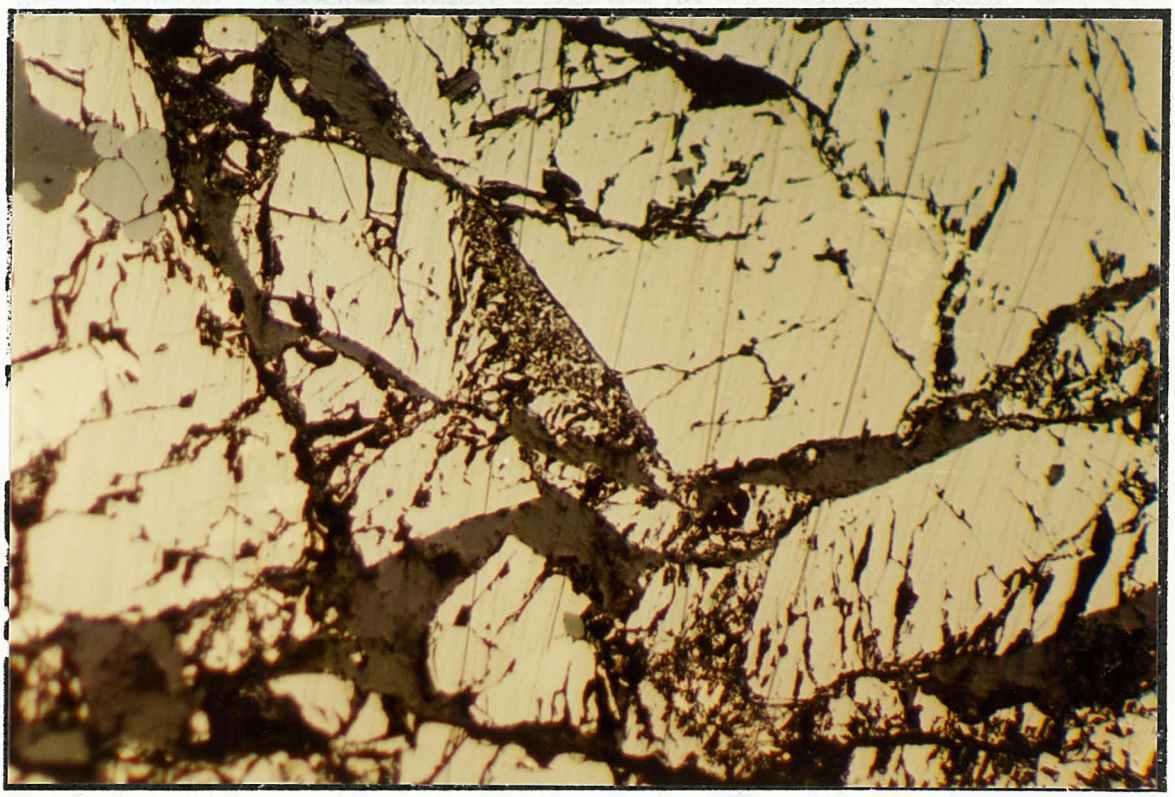

B

Figure 4.3. These photos of (a) TP06 and (b) TP 08 illustrate that cataclasis is only prevalent in locations where pyrrhotite grains impinge on one another. This is evident in the concentration of fracturing at the junction of the three large grains at the center of photo (a). Cataclasis is extremely well developed in the grain at the center of photo (b).

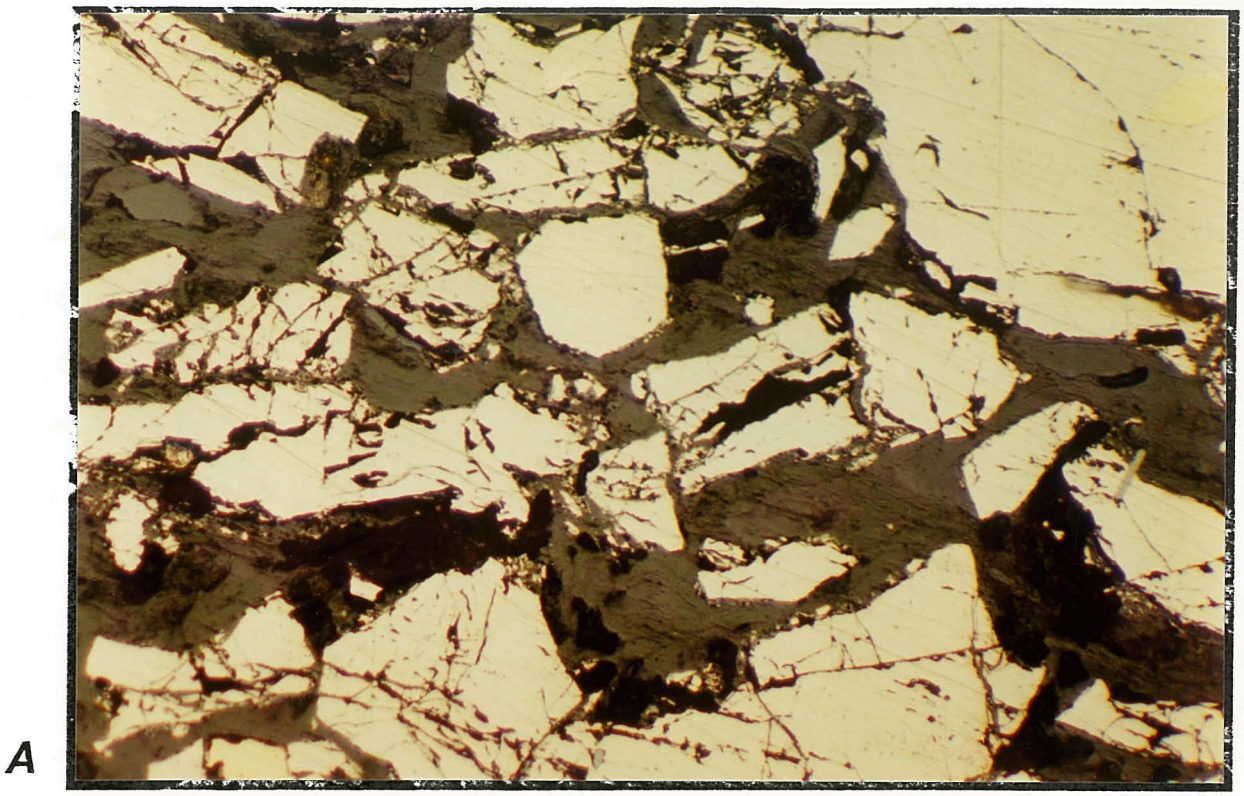

A

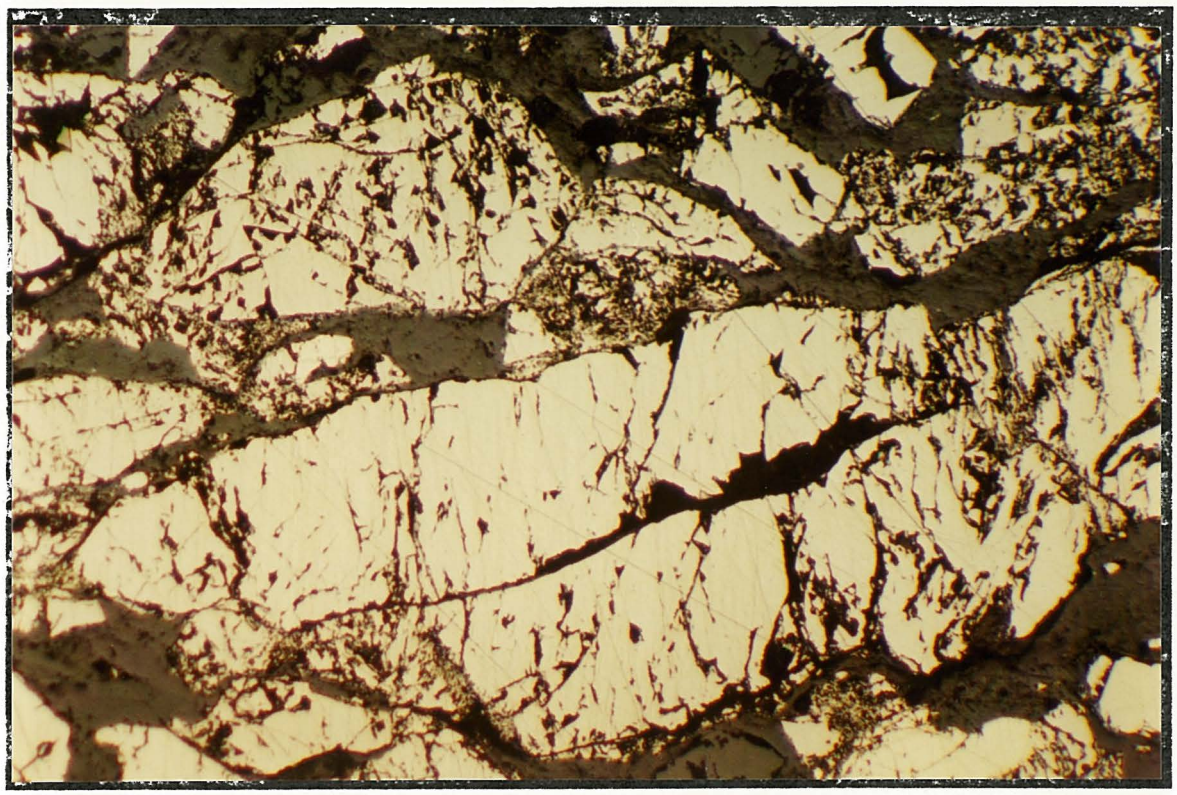

B

Figure 4.4. The volume taken up by talc is much greater in the hydrostatically deformed TP07 of photo (a) than in TP10, which was the most highly deformed specimen, illustrated in photo (b). Note the strong preferred dimensional orientations of grains.

deformation. The fine-grained talc matrix probably helps in the development of preferred dimensional orientations, as it reduces impingement between pyrrhotite grains and promotes rigid-body rotation. The mode of rotation may approximate the March Model, which will be discussed later.

4.4. ACMS Fabrics and Their Relationship to Strain and AMS

The bulk, conductive, complex-susceptibility values in these experiments illustrated in figure 4.5 are much lower than those for pyrrhotite in the previous chapter. This is due to the lesser degree of contact between adjacent conducting grains, reducing conductive surface area. Once again, dominantly oblate ACMS fabrics were developed, with resistive K''_{min} occuring in the axis of shortening as seen in figure 4.6.

As in the pyrrhotite experiments of chapter 3, conductive K''_{bulk} and K''_{max} were plotted against strain in figure 4.7 to determine if there is a correlation. Only chart-recorded strains were used for this data, as they were shown to be quite reliable in the experiments of the previous chapter. The correlations are not as good as those obtained in P009 to P028, but there seems to be a slight trend toward an increase in K'' with greater deformation. The reason for the relatively poor relationship may be explained when one considers that slightly differing relative proportions of talc and pyrrhotite may be present in each specimen. This is possible since the material was mixed at once for all the samples, but it may not have been distributed homogeneously among the specimens. Also, some specimens contain regions of small-scale heterogeneous distribution throughout their volume which may affect their bulk conductivity fabrics. These factors underline the possible complexities of dealing with specimens of disseminated sulphide. It must also be noted that

K″ vals	TP06	TP07	TP08	TP09	TP10	TP11	TP12
1	0.52387	1.1056	0.65137	0.93627	0.77196	0.30627	0.5378
2	0.51352	1.1967	0.64265	0.95187	0.71972	0.34389	0.54233
3	0.49373	1.1632	0.67794	0.98373	0.7575	0.4	0.57158
4	0.49097	1.1739	0.68962	0.91031	0.76262	0.37931	0.56081
5	0.53018	1.1763	0.71331	0.92089	0.74399	0.3351	0.56511
6	0.48993		0.71241	0.92589	0.71507	0.37068	0.55561
7	0.54867		0.63185	0.85931	0.72132	0.39453	0.53133
8	0.48945		0.67305	0.90071	0.77097	0.3715	0.52641
9	0.5438		0.67593	0.91963	0.78991	0.33523	0.54005
10	0.53352		0.68844	0.98446	0.71916	0.31027	0.54552
K″avg.	0.515764	1.16314	0.675657	0.929307	0.747222	0.354678	0.547655
std.dev.	0.022187	0.030744	0.025956	0.035799	0.02569	0.031593	0.01421

Kmax vals	TP06	TP07	TP08	TP09	TP10	TP11	TP12
1	1.0775	1.2622	1.2498	2.4939	2.1337	0.71731	1.1714
2	1.0607	1.2665	1.2448	2.4645	2.0784	0.74734	1.2171
3	1.0578	1.2281	1.2373	2.4768	2.0159	0.81268	1.1581
4	1.015	1.2221	1.2283	2.5092	2.1117	0.75836	1.1137
5	1.0831	1.2473	1.2182	2.4701	2.0271	0.77721	1.1616
6	1.1008		1.2351	2.3596	2.0489	0.70994	1.0442
7	1.1253		1.1556	2.4883	2.087	0.7625	1.1072
8	1.1022		1.1685	2.474	2.0725	0.76035	1.1076
9	1.1058		1.1951	2.4445	2.0153	0.71313	1.0131
10	1.1499		1.2059	2.4952	2.0678	0.75092	1.0589
K″max(avg)	1.08781	1.24524	1.21386	2.46761	2.06583	0.750974	1.11529
std. dev.	0.036091	0.017738	0.030568	0.039939	0.03768	0.030056	0.060245

Figure 4.5. Conductive bulk K" values and K''_{max} values for each pyrrhotite plus talc specimen and their standard deviations are listed. Note that K" values are much smaller than for the pyrrhotite specimens in chapter 3.

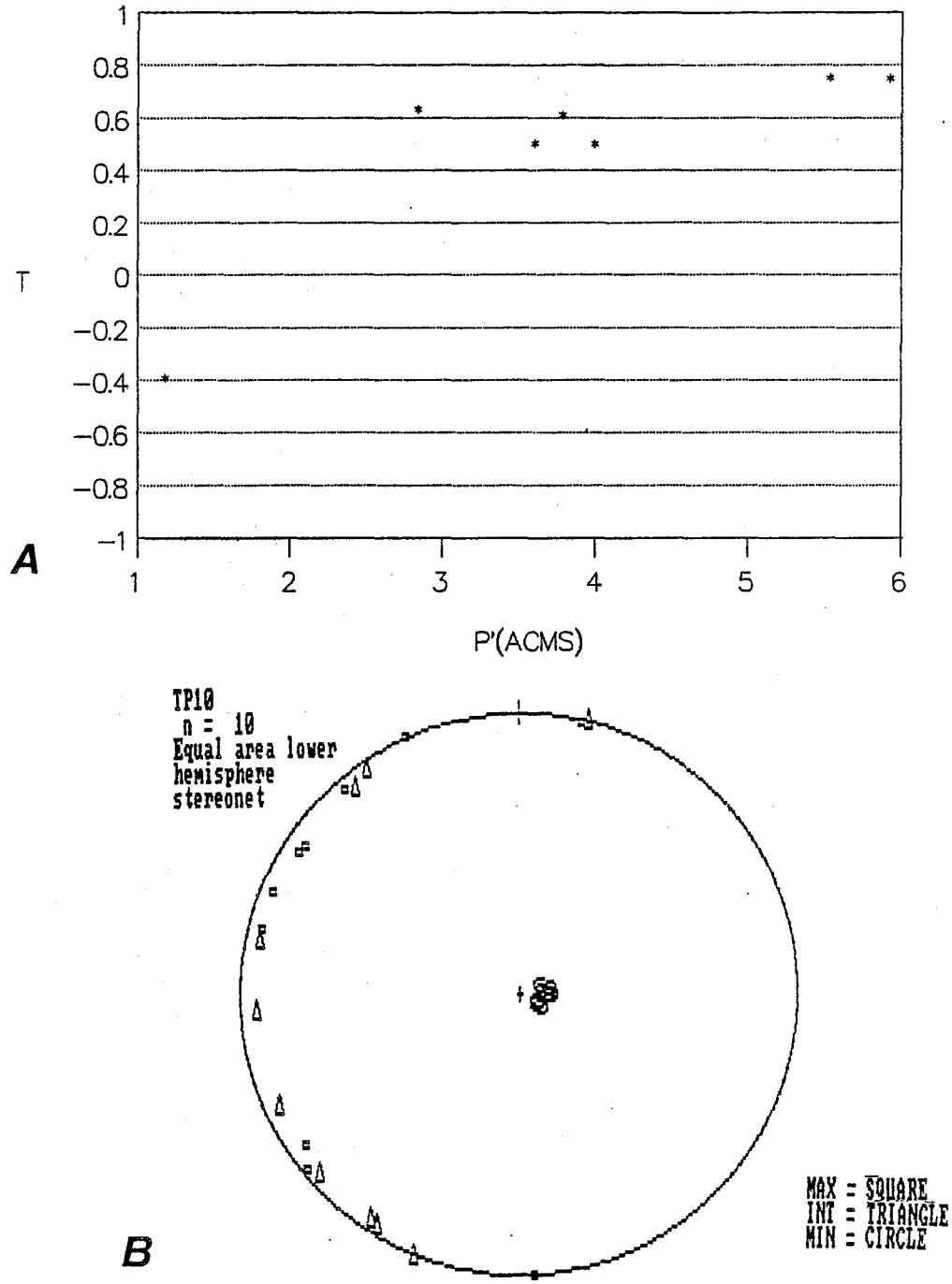

Figure 4.6. (a) Except for the hydrostatically deformed specimen TP07, all pyrrhotite plus talc specimens exhibited oblate resistive ACMS fabrics. (b) This is a typical distribution of resistive K" principal axes for 10 separate anisotropy measurements on a single sample. Note that K''_{min} is nearly vertical, parallel to the compression direction of the triaxial rig. As in the pyrrhotite specimens, K''_{int} and K''_{max} are poorly defined within the flattening plane. This poor definition is probably due to a combination of low K" values and oblate anisotropy.

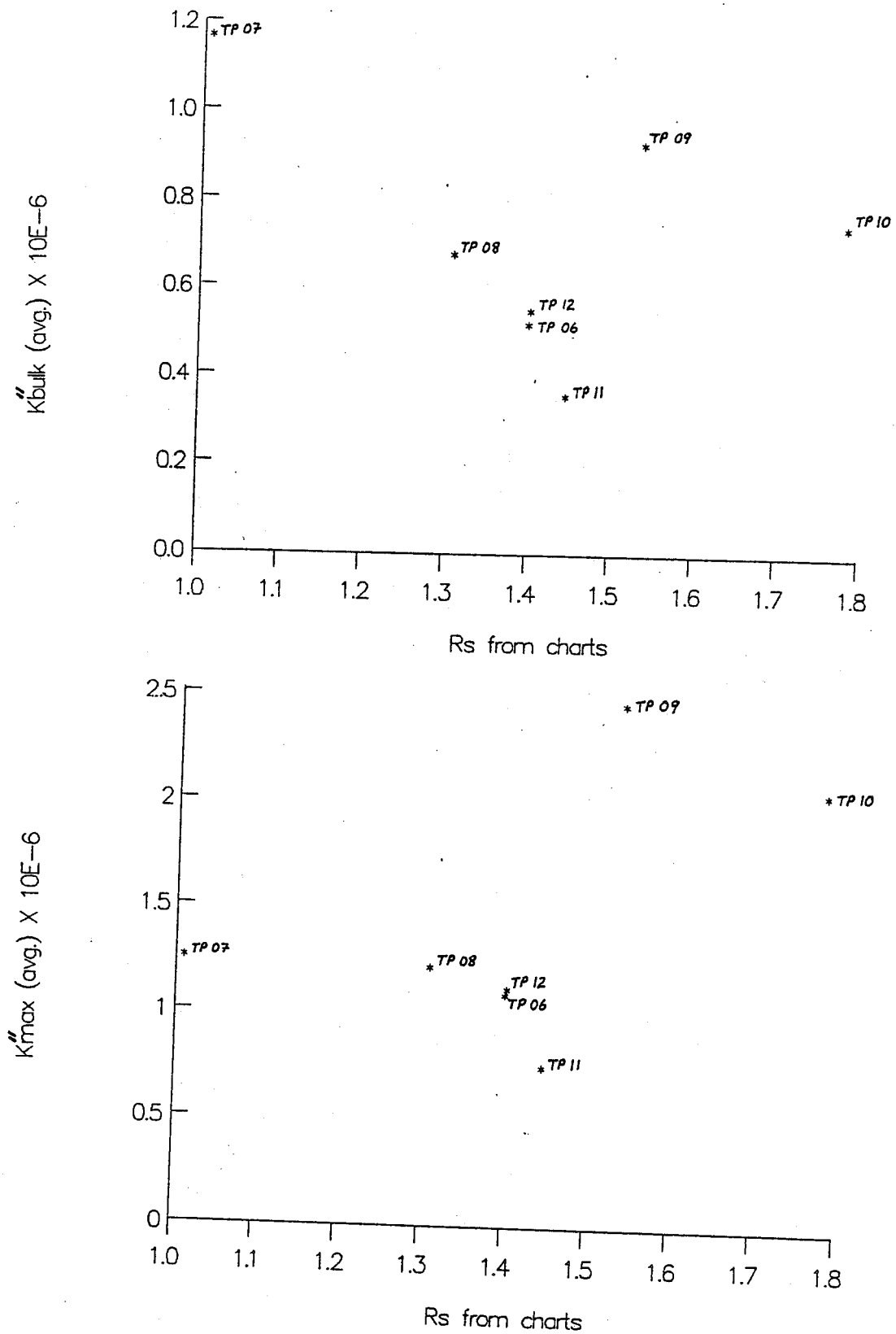

Figure 4.7. K"$_{bulk}$ and K"$_{max}$ show no definite relationships to strain, but there may be a slight tendency toward increased K" values with strain.

not enough data is present in the above diagrams to make definite conclusions.

Figure 4.8 illustrates the relationship between resistive P' and chart strain. There is a very strong correlation, with an apparent linear correlation over the limited range of strains possible in these experiments. The greatest degree of shortening achieved was only 31.9% for TP10. When P'(ACMS) is plotted against P'(AMS), there is also a good correlation. This is because, except for a single outlier, AMS anisotropy also appears to show a linear increase with strain.

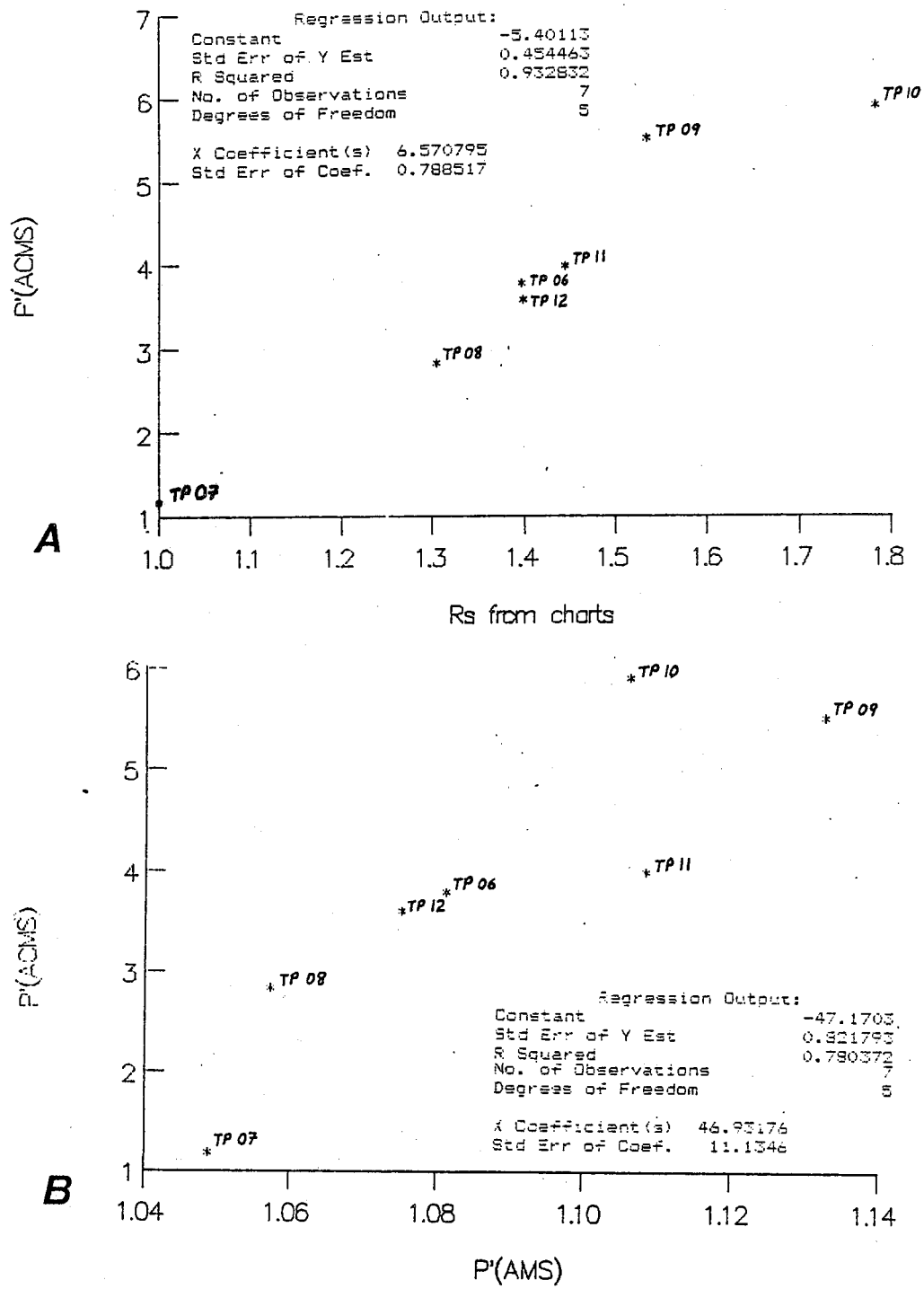

Figure 4.8. Note the apparent linear correlations between (a) P'(ACMS) and Rs, (b) P'(ACMS) and P'(AMS), and (c) P'(AMS) and Rs developed in the pyrrhotite plus talc specimens. The equations for the lines are, P'(ACMS) = 6.57Rs - 5.40, P'(ACMS) = 47P'(AMS) - 47, P'(AMS) = 0.098Rs + 0.95.

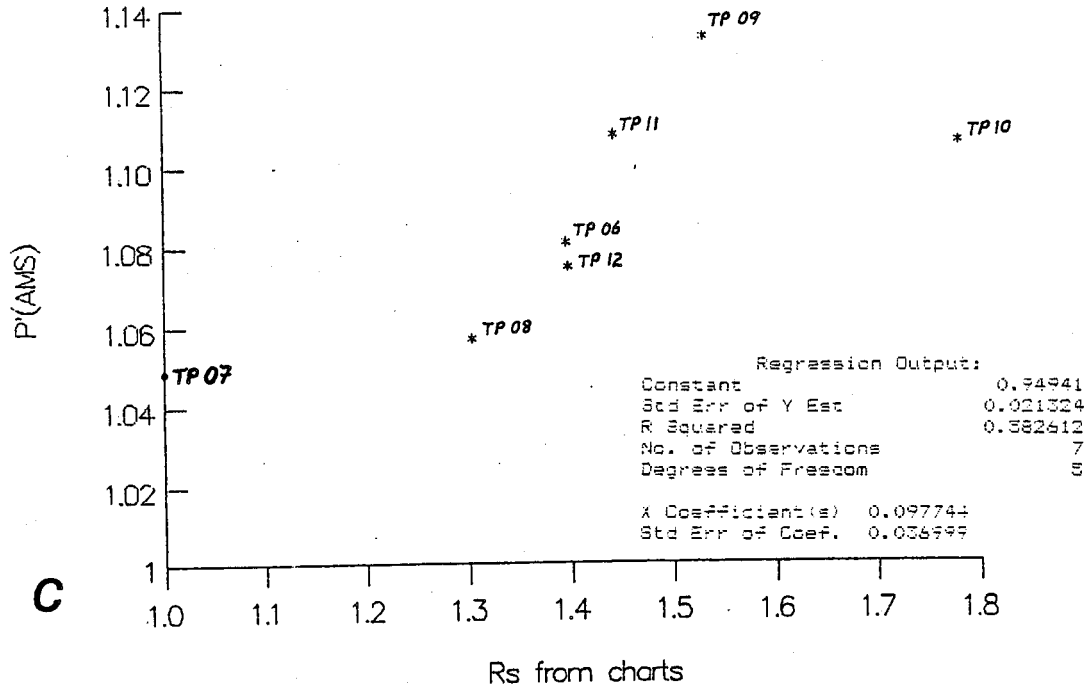

Figure 4.8. Note the apparent linear correlations between (a) P'(ACMS) and Rs, (b) P'(ACMS) and P'(AMS), and (c) P'(AMS) and Rs developed in the pyrrhotite plus talc specimens. The equations for the lines are, P'(ACMS) = 6.57Rs - 5.40, P'(ACMS) = 47P'(AMS) - 47, P'(AMS) = 0.098Rs + 0.95.

4.5. Discussion of Results

The strong correlation between strain and resistive P' values in these experiments relative to those of chapter 3 is undoubtedly influenced by the presence of the talc matrix. The talc is of much lower viscosity than pyrrhotite and allows the pyrrhotite grains embedded within it to rotate more freely, approximating the March Model discussed by Tullis (1976). Figure 4.9 illustrates the basic principle of the model. The model is not followed perfectly, as there is extensive impingement between pyrrhotite grains resulting in cataclasis and intragranular deformation. The March Model requires that a logarithmic relationship exists between grain preferred orientation and strain (Tullis, 1976). The equation for this relationship is:

$$\ln \rho = -3\epsilon_d$$

where ρ is the orientation of poles to tabular bodies in the principal compressive strain direction and ϵ_d is the natural deviatoric strain defined as:

$$\epsilon_d = \ln [\ l'/l_o(V/V_o)^{-1/3}\ ]$$

where l' is the final length of the strained material, l_o is its initial length, V is its volume after strain, and V_o is its initial volume. By examining figure 4.9, it is clear that grains

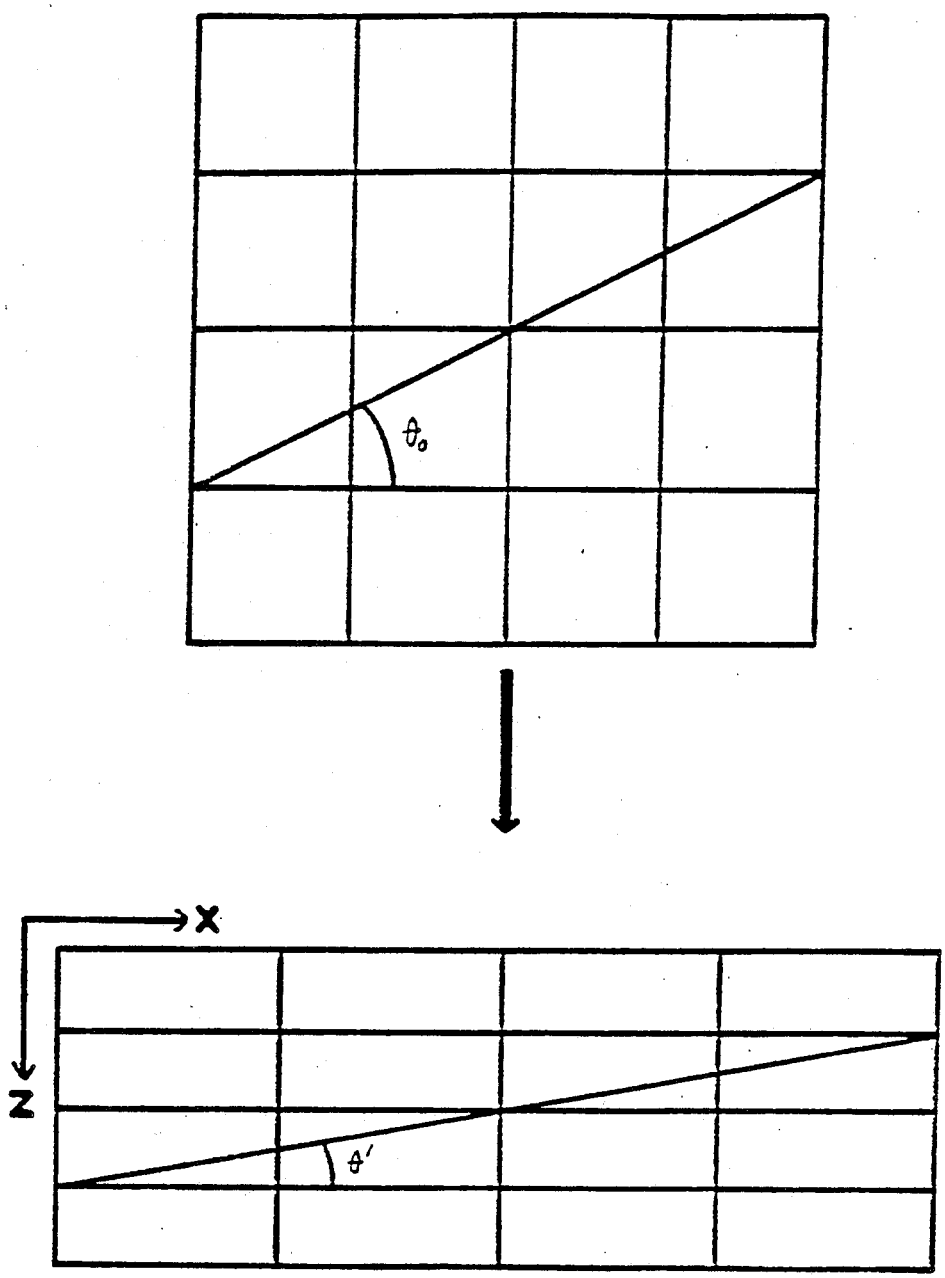

Figure 14. This diagram shows how a planar marker horizon would be expected to rotate during pure shear using the March Model. This can be related to the degree of deformation in X and Z as follows: $\tan \theta' / \tan \theta_0 = Z / X$.

Figure 4.9. Illustration of the rotation of passive planar markers explained by the March Model. This may partially explain the development of preferred orientations of pyrrhotite in the pyrrhotite plus talc mixtures.

will rotate more quickly when they are at low angles to the compressive stress direction. Thus as strains become high in coaxial strain and the grains are aligned at a higher angle to the compressive stress, they will rotate progressively more slowly. We may be seeing evidence for this type of trend in the P' versus R_s diagram of figure 4.7, as the most highly strained specimen is not quite on the linear trend of the less highly strained specimens. Such an interpretation is only speculative, as there is not sufficient data to confirm such a trend. There is also no way of knowing what will happen at higher strains. Perhaps at high strains a relationship similar to that in the pyrrhotite specimens will develop as the talc becomes further compressed and contact between adjacent pyrrhotite grains improves.

Despite these problems, it is clear that there is a relationship between the degree of preferred orientation of the sulphide grains and ACMS. Thus disseminated sulphide preferred orientations might potentially be analysed using the ACMS technique, provided that they behave in a similar fashion to these experimentally deformed aggregates.

5. PRELIMINARY INVESTIGATION OF ACMS IN DEFORMED MASSIVE PYRRHOTITE AND ITS IMPLICATIONS FOR EXPERIMENTAL DATA

5.1. Introduction

Natural massive ore specimens were obtained from the INCO Shebandowan mine located approximately 100 km west of Thunder Bay, Ontario. The specimens consist largely of strongly deformed pyrrhotite containing significant quantities of pentlandite and chalcopyrite, which make it a rich Ni-Cu ore. These minerals are all clearly visible in the photomicrograph of figure 5.1.

These specimens were obtained to provide a preliminary indication of the relationship between ACMS fabrics and strain fabrics in a tectonically deformed ore. The fact that this ore is largely pyrrhotite allows for the comparison of ACMS data for these specimens with data obtained from the experimentally deformed pyrrhotite aggregates. A detailed study of the mine was not carried out, as time was limited.

The ore has been strongly deformed and exhibits a fabric defined by the preferred dimensional orientation of grains as well as by parallel bands of pentlandite. AMS fabrics, which indicate preferred crystallographic orientation of pyrrhotite (Schwarz, 1974), display a magnetic foliation essentially parallel to the observed fabrics. AMS has been shown to be very useful in defining preferred orientations in massive pyrrhotite,

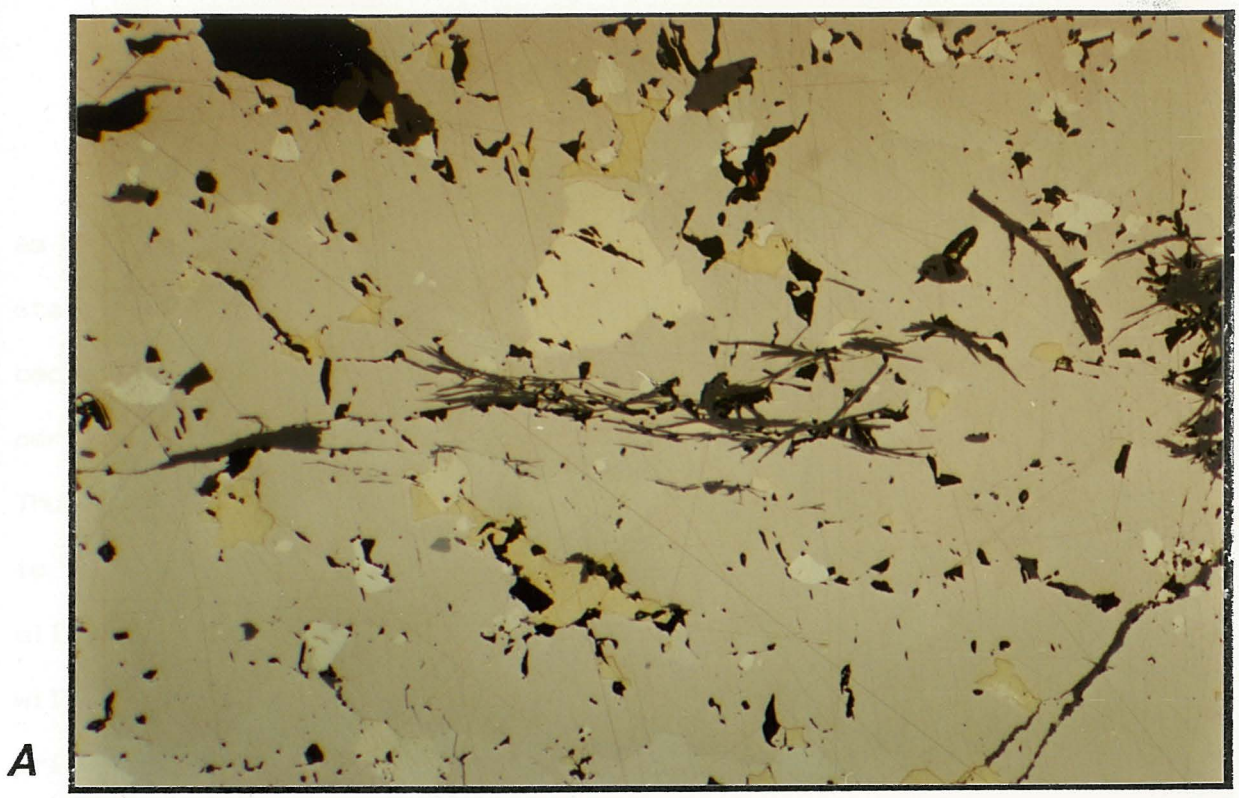

A

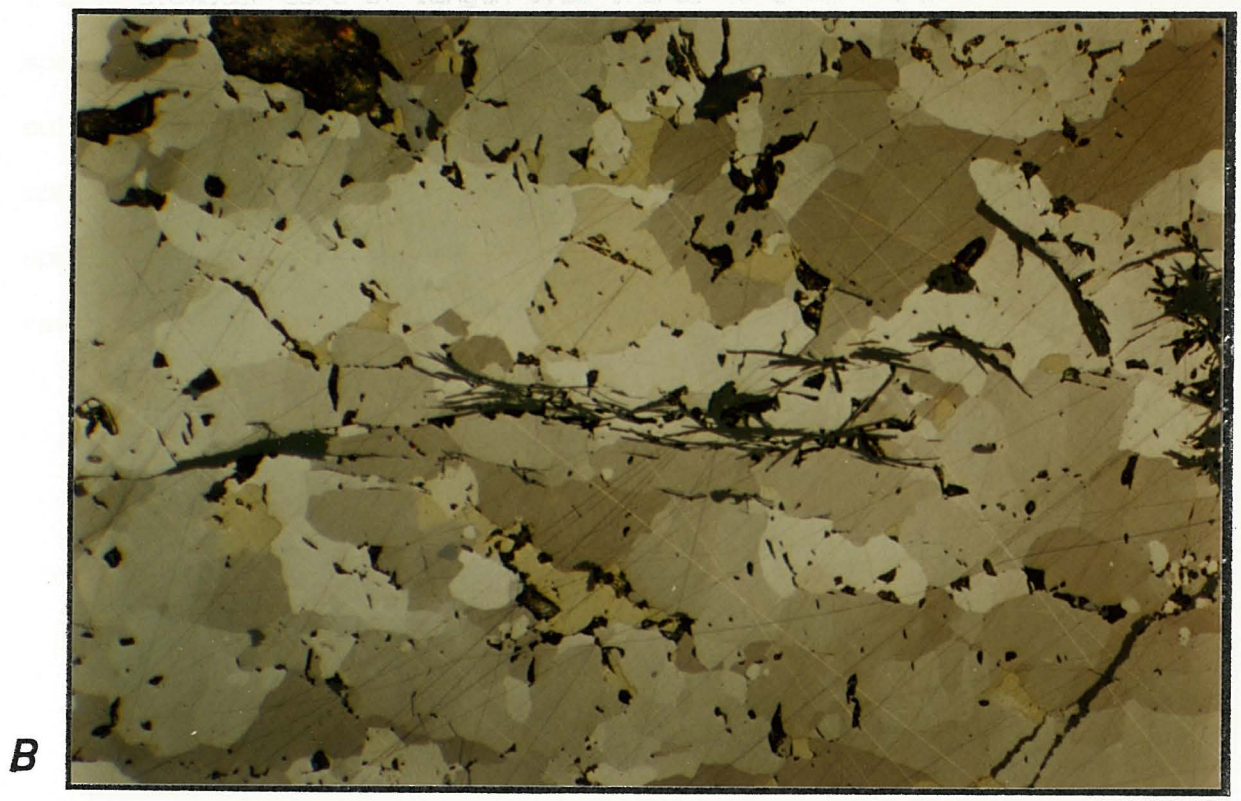

B

Figure 5.1. These photomicrographs illustrate the same section of SB02 under (a) plane-polarized light and (b) cross-polarized light. (a) The yellow mineral is chalcopyrite, the white mineral is pentlandite, and the predominant mineral (grey) is pyrrhotite. Notice the preferred orientation of the gangue phyllosilicates. (b) Pyrrhotite grains are recognizable under crossed polarizers. Note that there is an apparent preferred dimensional orientation.

as K_{min} is known to be parallel to the c-axis of pyrrhotite. As stated earlier in section 3.4, deformed pyrrhotite tends to become oriented by crystal slip so that the c-axis is perpendicular to the plane of flattening of the strain ellipsoid. Thus the simplest way to compare tectonic fabrics to ACMS fabrics is to use AMS fabrics to represent tectonic fabrics. The AMS ellipsoids will not give a quantitative estimate of strain, but will give an indication as to the orientation of the three principal axes of strain. Each of the specimens was prepared as a 1 inch diameter core of length 0.82 inches to ensure that no specimen shape effect was present (Sarvas, 1988). Massive sulphide specimens have tight grain contacts which may make the specimens behave as a single grain electrically. Thus the specimen must be of nearly isotropic shape to ensure reliable results.

5.2. Results of ACMS Measurements

Figure 5.2 compares stereonet projections of ACMS fabrics versus AMS fabrics for each of the massive specimens studied. There is a slight obliquity between the principal axes of the ACMS and AMS ellipsoids for each specimen. This observation is different from what was seen in the deformed pyrrhotite aggregates of chapter 3, where ACMS fabrics were consistently approximately coaxial with AMS fabrics. Another very important difference is that resistive K''_{max} tends to be closest to K_{min} of AMS in all of the massive specimens. In the experimentally deformed material, resistive K''_{min} was always subparallel to K_{min} of AMS. Another major difference is the extremely low ACMS anisotropies in the massive specimens compared to the unconsolidated aggregates. A number of anisotropies (P') are illustrated in figure 5.3 for comparison. All of the above observations appear to indicate that crystallographically controlled, rather than grain shape controlled anisotropy is responsible for the ACMS fabrics of the massive pyrrhotite specimens. Evidence for this interpretation includes the low crystallographic electrical anisotropy of pyrrhotite and the observation of Krontiras et al. (1984) that hexagonal pyrrhotite is most resistive parallel to its crystallographic c-axis. It should be noted, however, that the specimens used in this study contain mostly monoclinic pyrrhotite, which has a slightly different crystal structure than hexagonal pyrrhotite and is not

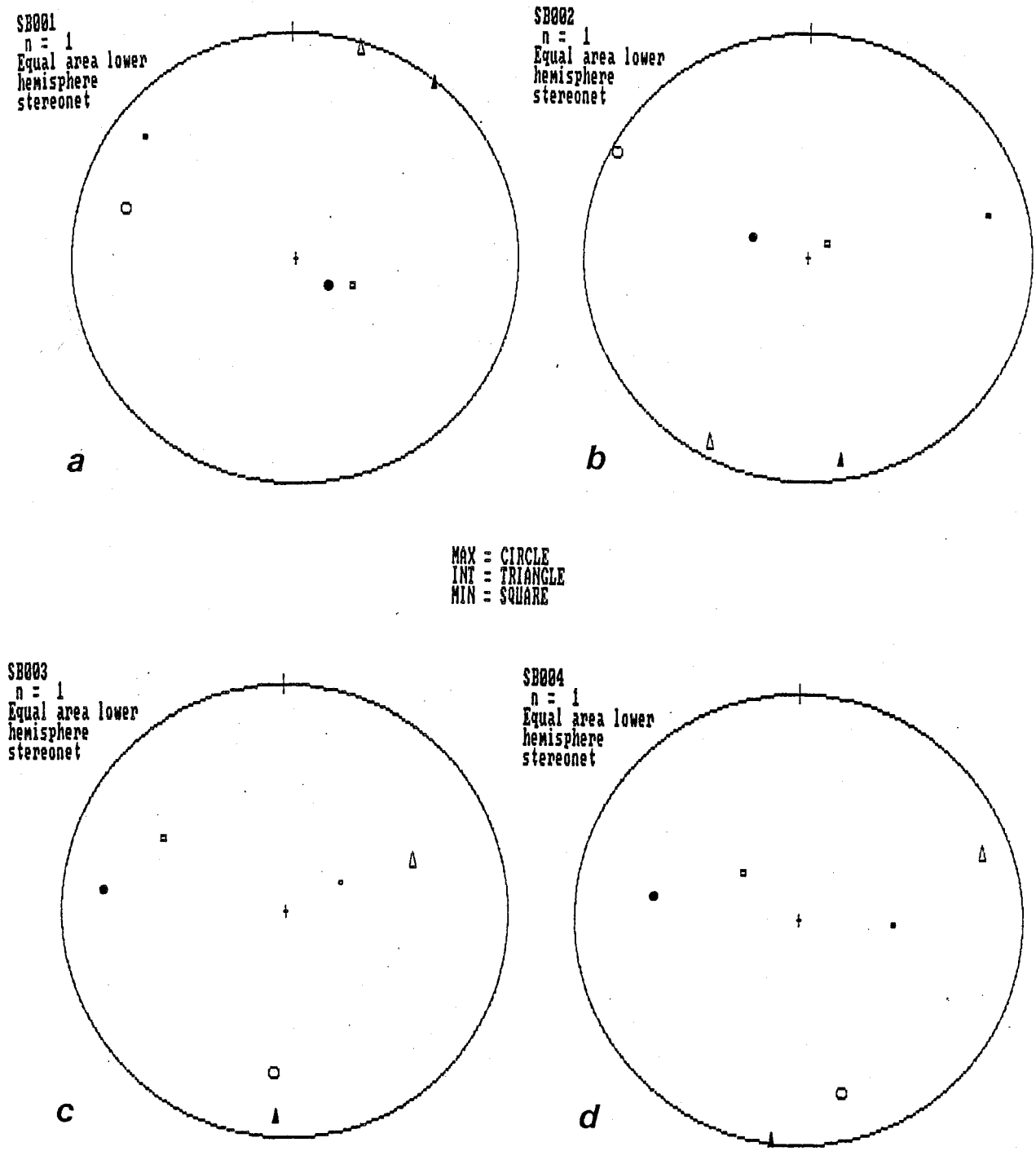

Figure 5.2. Each of these stereonets illustrate ACMS fabrics represented by filled markers and AMS fabrics represented by open markers. The specimens are (a) SB01 (b) SB02 (c) SB03 (d) SB04 (e) SB05 (f) SB09. Note the obliquity between the ACMS and AMS principal axes. K''_{max} tends to be closest to K_{min} unlike in the triaxially deformed loose aggregates. Also, K''_{min} is closest to K_{max} in a, b, e, and f, but closest to K_{int} in stereonets c and d. SB09 is a stringer sulphide sample which exhibits similar characteristics to the massive specimens SB01 to SB05.

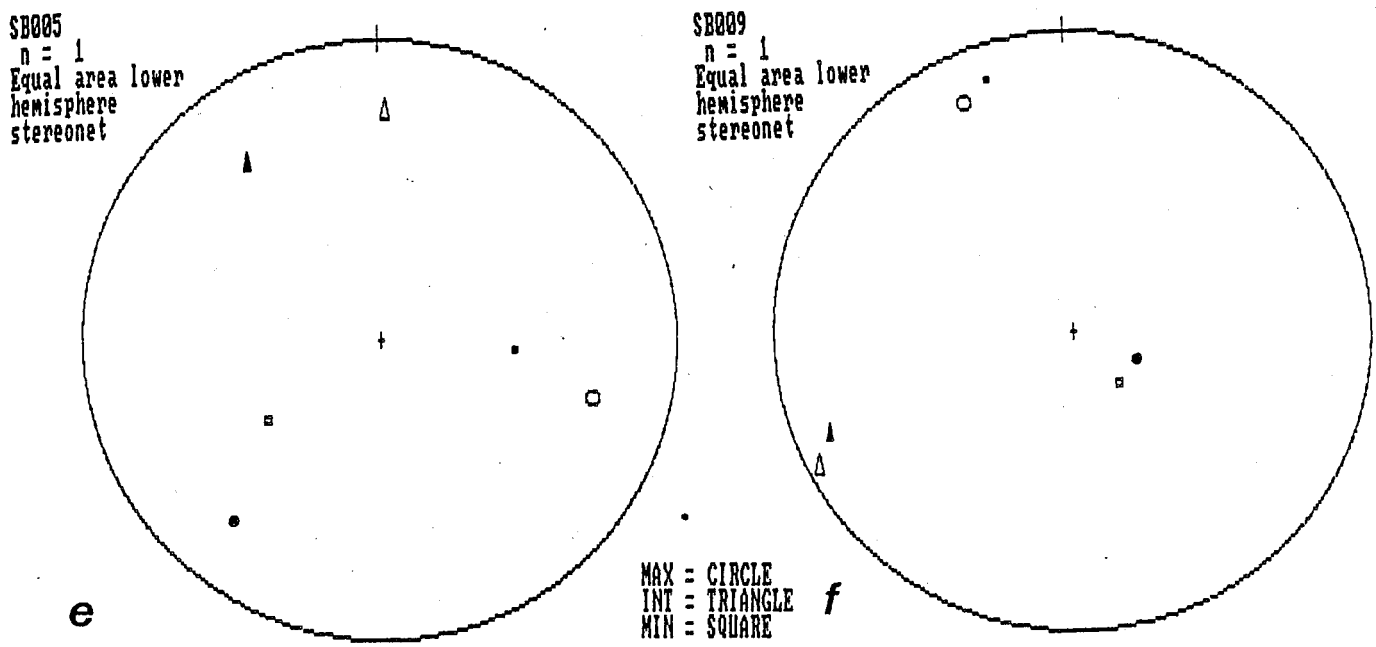

Figure 5.2. Each of these stereonets illustrate ACMS fabrics represented by filled markers and AMS fabrics represented by open markers. The specimens are (a) SB01 (b) SB02 (c) SB03 (d) SB04 (e) SB05 (f) SB09. Note the obliquity between the ACMS and AMS principal axes. K''_{max} tends to be closest to K_{min} unlike in the triaxially deformed loose aggregates. Also, K''_{min} is closest to K_{max} in a, b, e, and f, but closest to K_{int} in stereonets c and d. SB09 is a stringer sulphide sample which exhibits similar characteristics to the massive specimens SB01 to SB05.

P' (massive)	P' (loose aggregates)
SB01 = 1.0894	P002 to P008:
SB02 = 1.1869	high - P00 = 7.57
SB03 = 1.1215	low - P002 = 1.43
SB04 = 1.0622	P009 to P028:
SB05 = 1.1720	high - P011 = 10.82
SB09 = 1.3394	low - P010 = 1.47

Figure 5.3. Note that all massive specimens have lower P' than even the least anisotropic loose aggregates from chapter 3. This would suggest that grain-shape is not a factor in the ACMS fabrics observed in the massive specimens, whereas it is important in the loose aggregates.

as well understood electrically. Thus, the above interpretation may not be entirely correct. If monoclinic pyrrhotite behaves slightly differently from hexagonal pyrrhotite, this may be an explanation for the obliquity between AMS and ACMS principal axes. This is entirely speculative, and the obliquity may in fact be influenced by the minerals chalcopyrite and pentlandite, which have different electrical properties than pyrrhotite. ACMS fabrics would be much easier to interpret in an ore which contains only a single conductive mineral, or a mineral which is less complex structurally than pyrrhotite.

5.3. Comparison of Loose Aggregate and Massive Specimen Data

Obviously, the loose pyrrhotite aggregates and massive pyrrhotite ore behaved much differently during deformation to produce such widely differing ACMS fabric characteristics. It is probable that the natural ore deformed by plastic mechanisms while the experimentally deformed aggregates deformed largely by rigid body rotation, particulate flow, and cataclasis. Therefore, the way in which electrical anisotropy developed in the triaxial deformation experiments seem to have little relationship to how it developed in the massive specimens. Despite this, the triaxial deformation experiments did provide some insight into the operation of the ACMS coil and showed that it is effective in identifying electrical anisotropy.

5.4. Discussion

Unfortunately, this test of the ability of ACMS to identify strained fabrics in a massive pyrrhotite ore was not sucessful. The prospects for the use of ACMS on other massive sulphides depend on the distribution of conducting minerals within the specimen and the degree to which the electrical properties correspond to strained fabrics. Thus it is apparent that the next step in the use of ACMS technique should be to study the ACMS of single crystals of conducting minerals. This would provide further insight into the electrical properties of conducting minerals at high frequency (ie. monoclinic pyrrhotite) and aid in the interpretation of ACMS fabrics observed in deformed ores which contain more than a single conducting phase.

There are only a small number of common ore minerals which are sufficiently conductive to be measured using the ACMS technique, limiting its application. It is especially unfortunate that the most common sulphide mineral, pyrite cannot be detected by the ACMS coil. In addition, two minerals which are sufficiently conductive, pyrrhotite and magnetite have significant, easily measurable magnetic susceptibilities which have proven relationships to strained rock fabrics. Thus the future use of ACMS shold be concentrated on investigating electrical properties of minerals.

REFERENCES

Archie, G.E. (1942). The electrical resistivity log as an aid in determining some reservoir characteristics. Trans. AIME, 146, 54-62.

Borradaile, G.J. (1981). Particulate flow and the formation of rock cleavage. Tectonophysics, 72, 305-321.

Borradaile, G.J. (1987). Analysis of strained sedimentary fabrics: review and tests. Can. J. Earth Sci., 24, 442-455.

Borradaile, G.J. (1988). Magnetic fabrics, petrofabrics and strain. Tectonophysics, 156, 1-20.

Borradaile, G.J. and Mothersill, J.S. (1984). Coaxial deformed and magnetic fabrics without simply correlated magnitudes of principal values. Physics of the Earth and Planetary Interiors, 35, 294-300.

Borradaile, G.J. and Alford, C. (1987). Relationship between magnetic susceptibility and strain in laboratory experiments. Tectonophysics, 133, 121-135.

Borradaile, G.J., Keeler, W., Alford, C., and Sarvas, P. (1987). Anisotropy of magnetic susceptibility of some metamorphic minerals. Physics of the Earth and Planetary Interiors, 48, 161-166.

Borradaile, G.J. and Puumala, M.A. (1989). Synthetic magnetic fabrics in a plasticene medium. Tectonophysics, 164, 73-78.

Borradaile, G.J. and Hawton, M. (1990). Dielectric anisotropy and strain of experimentally deformed talc aggregates. Phys. Earth Planet. Inter., 62, 323-328.

Brace, W.F. and Orange, A.S. (1968). Further studies of the effects of pressure on electrical resistivity of rocks. Journal of Geophysical Research, 73, 5407-5420.

Buerger, M.J. (1928). The plastic deformation of ore minerals. A preliminary investigation: Galena, sphalerite, chalcopyrite, pyrrhotite, and pyrite. Part I. The American Mineralogist, 13, 1-17.

Carmichael, R.S. (1982). Magnetic properties of minerals and rocks. In CRC handbook of physical constants for rocks, R.C. Weast and M.J. Ashe, editors. CRC Press, Boca Raton, Florida, 229-287.

Clark, B.R. and Kelly, W.C. (1976). Experimental deformations of common sulphide minerals. In The physics and chemistry of minerals and rocks: an introduction to modern texture analysis, R.G.J. Strens, editor. John Wiley and Sons Ltd., London, 51-70.

Cox, S.F. and Etheridge, M.A. (1984). Deformation microfabric development in chalcopyrite fault zones, Mt. Lyell, Tasmania. Journal of Structural Geology, 6, 167-182.

Drury, M.J. and Hyndman, R.D. (1979). The electrical resistivity of oceanic basalts. Journal of Geophysical Research, 84, 4537-4545.

Dunnet, D. (1969). A technique of finite strain analysis using elliptical particles. Tectonophysics, 7, 307-325.

Flinn, D. (1958). On the nappe structure of north-east Shetland. Quart. Journ. Geol. Soc. Lond., 114, 107-136.

Flinn, D. (1965). On the symmetry principle and the deformation ellipsoid. Geol. Mag., 102, 36-45.

Graf, J.L. and Skinner, B.J. (1970). Strength and deformation of pyrite and pyrrhotite. Economic Geology, 65, 206-215.

Hawton, M. and Borradaile, G. (1989). Dielectric determination of rock fabric anisotropy. Physics of the Earth and Planetary Interiors, 56, 371-376.

Hennig-Michaeli, C. and Siemes, H. (1987), Experimental deformation of chalcopyrite single crystals at 200°C. Tectonophysics, 135, 217-232.

Hill, D.G. (1972). A laboratory investigation of electrical anisotropy in Precambrian rocks. Geophysics, 37, 1022-1036.

Hirihara, E. and Murakami, M. (1958). Magnetic and electrical anisotropies of iron sulfide single crystals. J. Phys. Chem. Solids, 7, 281-289.

Hrouda, F. (1987). Mathematical model relationships between the paramagnetic anisotropy and strain in slates. Tectonophysics , 142, 323-327.

Jelinek, V. (1981). Characterization of the magnetic fabrics of rocks. Tectonophysics, 79, T63-T67.

Keller, G.V. (1982). Electrical properties of rocks and minerals. In CRC handbook of physical properties of rocks, volume I. R.S. Carmichael, editor. CRC Press, Boca Raton, Florida, 217-293.

Keller, G.V. and Frischnecht, F.C. (1966). Electrical methods in geophysical prospecting. Pergamon Press, Oxford. 519p.

Kip, A.F. (1969). Fundamentals of electricity and magnetism. McGraw-Hill, New York. 630p.

Kittel, C. (1966). Introduction to Solid State Physics. John Wiley and Sons, New York. 648p.

Krontiras, C., Pomoni, K., and Theodossiou, A. (1984). Resistivity anisotropy of pyrrhotite. J. Appl. Phys., 55, 3894-3895.

Lisle, R.J. (1977a). Estimation of the tectonic strain ratio from the mean shape of deformed elliptical markers. Geologie en Mijnbouw, 56, 140-144.

Lisle, R.J. (1977b). Clastic grain shape and orientation in relation to cleavage from the Aberystwyth Grits, Wales. Tectonophysics, 60, 263-267.

March, A. (1932). Mathematische theorie der regelung nach der kornegestalt bei affiner deformation. Zeitschr. Kristallographie, 81, 285-289.

McClay, K.R. (1983). Fabrics of deformed sulphides, Geologische Rundschau, 72, 469-491.

Meaden, G.T. (1965). Electrical resistance of metals. Plenum Press, New York. 218p.

Means, W.D. (1977). A deformation experiment in transmitted light. Earth and Planetary Science Letters, 35, 169-179.

Morrow, C. and Brace, W.F. (1981). Electrical resistivity changes in tuffs due to stress. Journal of Geophysical Research, 86, 2929-2934.

Nowina, S. and Strangway, D.W. (1982). Petrofabric and dielectric anisotropy in rock. Can. J. Earth Sci., 19, 36-54.

Parkhomenko, E.I. (1967). Electrical properties of rock. Plenum Press, New York. 314p.

Parkhomenko, E.I. (1982). Electrical resistivity of minerals and rocks at high temperature and pressure. Reviews of Geophysics and Space Physics, 20, 193-218.

Puumala, M. (1989). Experimental investigation of magnetic fabrics in simulated geological materials. B.Sc. Thesis, Lakehead University, Thunder Bay, Ontario.

Ramdohr, P. (1980). The ore minerals and their intergrowths, volume 2. Pergamon Press, Frankfurt. 1207 p.

Ramsay, J.G. (1967). Folding and fracturing of rocks. McGraw-Hill, New York. 568p.

Ramsay, J.G., and Huber, M.I. (1983). The techniques of modern structural geology. Academic Press, London. 307p.

Robin, P.F. (1977). Determination of geologic strain using randomly oriented strain markers of any shape. Tectonophysics, 42, T7-T16.

Rutter, E.H. (1986). On the nomenclature of mode of failure transitions in rocks. Tectonophysics, 122, 381-387.

Sakkopolous, S., Vitoratos, E., and Argyreas, T. (1984). Impurity band conduction in natural pyrrhotite. J. Appl. Phys., 55, 595-597.

Sarvas, P. (1988). The structure and magnetic fabric of the Quetico metasedimentary rocks in the Calm Lake-Perch Lake area, near Atikokan, Northwestern Ontario. M.Sc. Thesis, Lakehead University, Thunder Bay, Ontario.

Schwarz, E.J. (1974). Magnetic fabric in massive sulphide deposits. Canadian Journal of Earth Sciences, 11, 1669-1675.

Scott, S.D. (1974). Experimental methods in sulfide synthesis. In Mineralogical Society of America short course notes, volume 1: Sulfide mineralogy. Southern Printing Company, Blacksburg, Virginia, S1-S38.

Shankland, T.J. (1975). Electrical conduction in rocks and minerals: parameters for interpretation. Physics of the Earth and Planetary Interiors, 10, 209-219.

Shuey, R.T. (1975). Semiconducting ore minerals. Elsevier, New York. 415p.

Siemes, H. and Hennig-Michaeli, C. (1985). Ore minerals, In The physics and chemistry of minerals and rocks: an introduction to modern texture analysis, R.G.J. Strens, editor. John Wiley and Sons Ltd., London, 51-70.

Spark, R.N. (1990). Magnetic fabrics and boundary structure at the Quetico/Shebandowan Subprovince boundary near Kashabowie, NW Ontario. M.Sc. Thesis, Lakehead University, Thunder Bay, Ontario.

Tuck, G.J. and Stacey, F.D. (1978). Dielectric anisotropy as a petrofabric indicator. Tectonophysics, 50, 1-11.

Tullis, T.E. (1976). Experiments on the origin of slaty cleavage and schistosity. Geological Society of America Bulletin, 87, 745-753.

Tullis, T.E. and Wood, D.S. (1975). Correlation of finite strain from both reduction bodies and preferred orientation of mica in slate from Wales. Geol. Soc. Am. Bull., 86, 632-638.

Wood, D.S, Oertel, G., Singh, J., and Bennet, H.F. (1976). Strain and anisotropy in rocks. Phil. Trans. R. Soc. Lond., A., 283, 27-42.

Worthington, P.F. (1981). The influence of formation anisotropy upon resistivity-porosity relationships. SPWLA Logging Symposium, Transactions. 25p.

Yu, H. and Zheng, Y. (1984). A statistical analysis applied to the Rf/Ø method. Tectonophysics, 110, 151-155.

APPENDIX A: ACMS Raw Data for Loose Aggregates

The P' and T values calculated from all ACMS and AMS measurements on pyrrhotite and pyrrhotite plus talc aggregates are listed at the beginning of appendix A. These are accompanied by the strain data for each specimen. These were the data used for numerous diagrams in chapters 3 and 4.

Appendix A also contains the raw data obtained from ACMS measurements performed on all pyrrhotite aggregates (P002 to P028) and all talc plus pyrrhotite aggregates (TP06 to TP12) used in this study. Ten separate measurements were performed on all specimens except P025 (6) and TP07 (5). The CMS values for the three principal axes of the ACMS ellipsoid were determined by the computer in each measurement, and are presented in the form of conductive susceptibilities. These were subsequently converted to resistive susceptibilities for the purpose of data presentation in chapters 3 and 4. Stereonets illustrating the position of the three principal conductive complex magnetic susceptibilities for each measurement are also provided for all specimens, except P010, 11, 13, and 22, for which stereonets illustrating the three principal resistive susceptibilities are illustrated in chapter 3. These give an indication of how consistent the axial determinations were, and hence, how well-defined the ACMS ellipsoid was. The data contain a number of headings, the meanings of which are listed below.

MIN = conductive K''_{min}

INT = conductive K''_{int}

MAX = conductive K''_{max}

DEC = declination of principal susceptibility axis in degrees

INC = inclination of principal susceptibility axis in degrees

R95 = angular deviation of the principal susceptibility direction

EV = magnitude of ACMS (in SI/volume X 1000 for P002 to P008 and in SI/mass for all others)

SDEV = standard deviation of principal axis ACMS values

SPECIMEN	Rs (lin)	Rs (rob)	Rs (har)	e% chart	Rs chart	P' (ACMS)	T(cond)	T(res)	P' (AMS)	T (AMS)
P02	1.436	1.115	1.576			1.4344	0.2157	-0.2157	1.1202	0.8938
P03	1.267	1.147	1.586			4.2894	-0.6168	0.6168	1.2352	0.8132
P04	1.789	1.604	1.874			4.1204	-0.8768	0.8768	1.3184	0.8976
P05	1.489	1.229	1.622			3.3178	-0.6551	0.6551	1.1627	0.7451
P06	1.268	1.206	1.561			4.9195	-0.6709	0.6709	1.2101	0.8751
P07	1.442	1.342	1.635			6.2121	-0.8801	0.8801	1.3973	0.9775
P08	1.286	1.213	1.603			7.5727	-0.8337	0.8337	1.221	0.9207
P09	1.263	1.115	1.567			1.5663	-0.7536	0.7536	1.0431	0.2176
P010	1.29	1.187	1.617			1.4674	-0.4025	0.4025	1.0475	0.0612
P011	1.455	1.382	1.584			10.8158	-0.9543	0.9543	1.1853	0.9213
P012	1.411	1.416	1.687			7.8827	-0.7725	0.7725	1.1125	0.7541
P013				19.6	1.387	1.8673	-0.5696	0.5696	1.1113	0.8636
P014	1.403	1.369	1.621	15.3	1.283	4.9689	-0.9532	0.9532	1.0958	0.3464
P015	1.349	1.342	1.646	28.4	1.651	4.0549	-0.8552	0.8552	1.1618	0.9074
P016	1.516	1.43	1.658	22.1	1.454	4.732	-0.7613	0.7613	1.14	0.7843
P018	1.548	1.486	1.728	23.6	1.497	8.4773	-0.723	0.723	1.1903	0.7818
P019	2.144	1.897	2.054	34.5	1.886	3.7063	-0.9131	0.9131	1.3407	0.8988
P020	1.679	1.56	1.778	26.2	1.577	7.2921	-0.797	0.797	1.1931	0.9435
P021				30.8	1.737	3.3029	-0.7218	0.7218	1.1739	0.6374
P022	1.248	1.364	1.641	30.4	1.722	5.9917	-0.8602	0.8602	1.2354	0.9144
P023	1.395	1.364	1.643	25.8	1.565	8.7834	-0.8833	0.8833	1.1982	0.9195
P024	1.341	1.173	1.539	10.6	1.183	1.8919	-0.4636	0.4636	1.0451	0.3833
P025	1.29	1.305	1.68	11.7	1.205	1.6668	-0.176	0.176	1.036	0.8559
P026	1.502	1.307	1.667	14.9	1.274	4.624	-0.6632	0.6632	1.1413	0.8755
P027	1.347	1.218	1.565	13.6	1.245	2.0985	-0.4462	0.4462	1.0539	0.5561
P028	1.751	1.327	1.645	11.7	1.205	2.6161	-0.7256	0.7256	1.0842	0.7656
TP06				19.6	1.3939	3.7877	-0.6068	0.6068	1.081	0.9764
TP07				0	1	1.1797	0.3975	-0.3975	1.0484	0.6883
TP08				16.1	1.3012	2.8351	-0.6278	0.6278	1.057	0.9339
TP09				24.7	1.5304	5.5305	-0.7478	0.7478	1.1325	0.8155
TP10				31.9	1.7794	5.9246	-0.746	0.746	1.1059	0.848
TP11				21.6	1.4405	3.994	-0.4977	0.4977	1.1081	0.8718
TP12				19.9	1.3949	3.5991	-0.4999	0.4999	1.0748	0.9367

This table summarizes all strain data as well as all complex magnetic susceptibility and magnetic susceptibility data for each pyrrhotite aggregate and each talc plus pyrrhotite aggregate discussed in chapters 3 and 4. Rs (lin) = liearization strain, Rs (rob) = Robin strain, Rs (har) = strain from harmonic means, e% chart = % shortening from chart recording data, Rs chart = strain calculated from charts by the formula $Rs = (1-e)^{-1.5}$, P'(ACMS) = anisotropy degree of the ACMS ellipsoid, T(cond) = anisotropy sense of the conductive ACMS ellipsoid, T(res) = anisotropy sense of the resistive ACMS ellipsoid, P'(AMS) = anisotropy degree of the AMS ellipsoid, and T(AMS) = anisotropy sense of the AMS ellipsoid. Graphical relationships between many of these variables are presented in chapters 3 and 4.

Specimen	P'	std. dev.	T	std. dev.
P002	1.4344	.2186	-.2157	.3031
P002	4.2894	.4919	.6168	.1331
P004	4.1204	.1363	.8768	.0477
P005	3.3178	.3081	.6551	.2368
P006	4.9195	.3070	.6709	.1318
P007	6.2121	.2397	.8801	.0545
P008	7.5727	.3374	.8337	.1044
P009	1.5663	.0404	.7536	.1297
P010	1.4674	.0939	.4025	.2060
P011	10.8158	.1492	.9543	.0164
P012	7.8827	.5856	.7725	.1101
P013	1.8673	.0529	.5696	.1550
P014	4.9689	.0665	.9532	.0287
P015	4.0549	.1630	.8552	.0784
P016	4.7320	.1732	.7613	.1089
P018	8.4773	.4357	.7230	.1772
P019	3.7063	.0715	.9131	.0437
P020	7.2921	.4558	.7970	.1181
P021	3.3029	.1400	.7218	.1136
P022	5.9917	.2501	.8602	.0967
P023	8.7834	.6287	.8833	.0618
P024	1.8919	.1320	.4636	.1717
P025	1.6668	.1180	.1760	.3104
P026	4.6240	.7137	.6632	.1616
P027	2.0985	.1355	.4462	.1499
P028	2.6161	.1939	.7256	.1894
TP06	3.7877	.2750	.6068	.2519
TP07	1.1797	.0878	-.3975	.1576
TP08	2.8351	.2342	.6278	.2057
TP09	5.5305	.4605	.7478	.1031
TP10	5.9246	.4247	.7460	.0915
TP11	3.9940	.7754	.4977	.2736
TP12	3.5991	.3258	.4999	.2154

The ACMS P' and T data were calculated from ten separate ACMS measurements performed on each specimen, except in the cases of P025 and TP07 where six and five measurements were made respectively due to extremely weak and difficult to reproduce fabrics. This table illustrates the standard deviations for each value. Note that some standard deviations are quite high, especially for T. This can be attributed to the relatively low conductivities of some specimens. T values have been converted from conductive to resistive (achieved by multiplying by -1). Similar data was not compiled for AMS, as results were highly reproducible and only two measurements were performed on each specimen.

P002 SITE 1 CORE 1 SPEC 1 UNITS= SI v M= 6 NR= 2 12:18:36 12-18-1989

SUSC.	DEC	INC	R95	EV	SDEV
MIN	302.54	21.85	33.8	1.6004E-03	9.692E-05
INT	32.07	-1.19	37.6	2.0393E-03	7.508E-05
MAX	299.08	-68.12	19.7	2.5553E-03	2.846E-05

Hydrostatically compacted po

P02E SITE 1 CORE 1 SPEC 1 UNITS= SI v M= 6 NR= 2 11:45:26 01-11-1990

SUSC.	DEC	INC	R95	EV	SDEV
MIN	23.92	32.69	58.6	1.8275E-03	2.021E-04
INT	87.08	-35.13	71.4	2.3483E-03	1.060E-04
MAX	323.88	-37.88	48.6	2.6481E-03	6.695E-05

P02F SITE 1 CORE 1 SPEC 1 UNITS= SI v M= 6 NR= 2 11:51:27 01-11-1990

SUSC.	DEC	INC	R95	EV	SDEV
MIN	320.11	7.79	19.8	1.8052E-03	1.806E-04
INT	51.78	12.03	33.2	2.1846E-03	9.852E-05
MAX	17.89	-75.60	35.9	2.4381E-03	3.409E-05

P02G SITE 1 CORE 1 SPEC 1 UNITS= SI v M= 6 NR= 2 11:56:06 01-11-1990

SUSC.	DEC	INC	R95	EV	SDEV
MIN	276.92	48.92	54.4	1.7919E-03	3.795E-05
INT	28.35	17.67	88.4	2.1314E-03	1.440E-04
MAX	311.56	-35.65	73.9	2.4242E-03	3.235E-04

P02H SITE 1 CORE 1 SPEC 1 UNITS= SI v M= 6 NR= 2 12:05:53 01-11-1990

SUSC.	DEC	INC	R95	EV	SDEV
MIN	0.70	-8.08	33.0	1.8059E-03	6.080E-05
INT	84.86	35.61	87.0	2.2453E-03	2.048E-04
MAX	281.63	53.20	82.7	2.6875E-03	1.600E-04

P02I SITE 1 CORE 1 SPEC 1 UNITS= SI v M= 6 NR= 2 12:12:22 01-11-1990

SUSC.	DEC	INC	R95	EV	SDEV
MIN	344.80	34.91	19.4	2.0051E-03	2.527E-04
INT	57.08	-23.56	61.8	2.2166E-03	8.402E-05
MAX	300.51	-45.73	58.0	2.4455E-03	1.223E-04

P02J SITE 1 CORE 1 SPEC 1 UNITS= SI v M= 6 NR= 2 12:16:50 01-11-1990

SUSC.	DEC	INC	R95	EV	SDEV
MIN	319.05	-9.21	5.8	1.3487E-03	1.461E-04
INT	57.74	-43.00	49.6	2.2627E-03	1.372E-04
MAX	39.54	45.53	49.8	2.5057E-03	6.002E-05

P02B SITE 1 CORE 1 SPEC 1 UNITS= SI v M= 6 NR= 2 14:22:17 01-04-1990

SUSC.	DEC	INC	R95	EV	SDEV
MIN	302.71	1.66	83.8	2.0745E-03	1.242E-04
INT	34.05	38.87	109.2	2.1346E-03	5.380E-05
MAX	30.66	-51.08	77.0	2.2908E-03	1.737E-04

P02C SITE 1 CORE 1 SPEC 1 UNITS= SI v M= 6 NR= 2 14:26:25 01-04-1990

SUSC.	DEC	INC	R95	EV	SDEV
MIN	313.79	19.83	18.5	1.6390E-03	8.130E-06
INT	315.98	-70.16	38.0	2.2477E-03	3.681E-05
MAX	44.04	0.69	36.4	2.4230E-03	1.323E-04

P02D SITE 1 CORE 1 SPEC 1 UNITS= SI v M= 6 NR= 2 14:31:08 01-04-1990

SUSC.	DEC	INC	R95	EV	SDEV
MIN	41.03	17.11	21.7	1.9297E-03	6.451E-05
INT	289.63	49.86	55.8	2.3078E-03	1.526E-04
MAX	323.49	-35.01	52.8	2.4998E-03	5.540E-05

P02J
n = 10
Equal area lower hemisphere stereonet

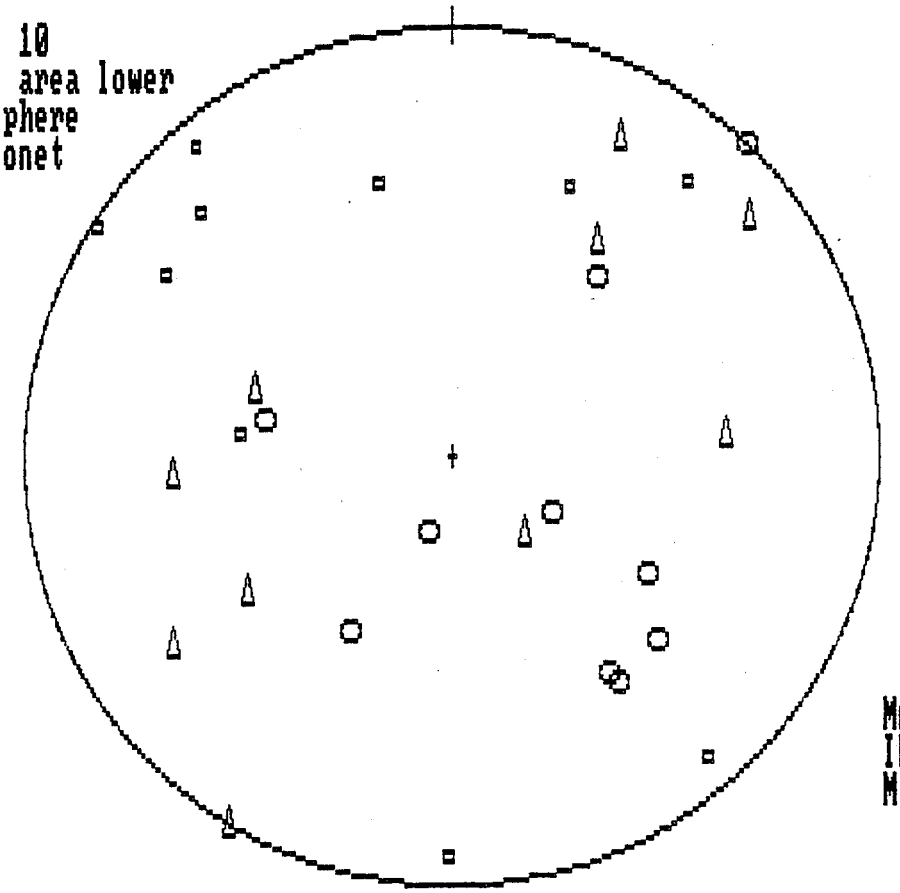

MAX = CIRCLE
INT = TRIANGLE
MIN = SQUARE

P03E SITE 1 CORE 1 SPEC 1 UNITS= SI v M= 6 NR= 2 12:28:02 01-11-1990

SUSC.	DEC	INC	R95	EV	SDEV
MIN	68.09	6.18	29.6	1.4207E-03	5.289E-06
INT	337.73	3.32	29.8	1.6255E-03	9.256E-05
MAX	39.63	-82.98	4.3	4.4543E-03	1.002E-04

P03F SITE 1 CORE 1 SPEC 1 UNITS= SI v M= 6 NR= 2 12:32:35 01-11-1990

SUSC.	DEC	INC	R95	EV	SDEV
MIN	62.29	2.27	45.3	1.2879E-03	7.253E-05
INT	332.42	-3.31	45.3	1.6141E-03	1.370E-05
MAX	297.93	85.98	2.1	4.3912E-03	5.158E-05

P03G SITE 1 CORE 1 SPEC 1 UNITS= SI v M= 6 NR= 2 12:37:07 01-11-1990

SUSC.	DEC	INC	R95	EV	SDEV
MIN	284.17	-0.13	52.3	1.1373E-03	1.124E-04
INT	14.17	0.74	52.3	1.4040E-03	2.885E-05
MAX	20.72	-89.25	2.6	4.1705E-03	5.076E-05

P03H SITE 1 CORE 1 SPEC 1 UNITS= SI v M= 6 NR= 2 12:42:10 01-11-1990

SUSC.	DEC	INC	R95	EV	SDEV
MIN	71.08	2.48	34.0	1.0709E-03	9.732E-05
INT	340.99	2.10	35.2	1.5636E-03	1.257E-04
MAX	30.78	-86.75	9.1	4.3603E-03	1.469E-04

P03I SITE 1 CORE 1 SPEC 1 UNITS= SI v M= 6 NR= 2 12:46:32 01-11-1990

SUSC.	DEC	INC	R95	EV	SDEV
MIN	317.09	-3.32	7.1	1.0025E-03	1.449E-04
INT	46.77	5.43	10.6	1.4025E-03	7.653E-05
MAX	78.43	-83.63	8.0	4.3927E-03	1.749E-04

P03J SITE 1 CORE 1 SPEC 1 UNITS= SI v M= 6 NR= 2 12:50:47 01-11-1990

SUSC.	DEC	INC	R95	EV	SDEV
MIN	334.99	-2.64	77.1	1.1752E-03	1.155E-04
INT	65.07	-1.87	76.6	1.3509E-03	6.463E-05
MAX	10.47	86.77	9.7	4.6070E-03	2.411E-05

P003 SITE 1 CORE 1 SPEC 1 UNITS= SI v M= 6 NR= 2 12:25:55 12-18-1989

SUSC.	DEC	INC	R95	EV	SDEV
MIN	345.93	2.96	84.1	1.3186E-03	3.876E-05
INT	76.39	8.93	84.1	1.5474E-03	1.895E-04
MAX	57.76	-80.59	0.8	4.4912E-03	2.182E-04

16.1% strained po

P03B SITE 1 CORE 1 SPEC 1 UNITS= SI v M= 6 NR= 2 13:49:44 01-04-1990

SUSC.	DEC	INC	R95	EV	SDEV
MIN	19.32	2.66	20.6	1.0530E-03	1.178E-05
INT	289.45	-2.69	18.8	1.3189E-03	7.357E-05
MAX	64.67	-86.21	9.2	4.3846E-03	5.669E-04

P03C SITE 1 CORE 1 SPEC 1 UNITS= SI v M= 6 NR= 2 13:55:17 01-04-1990

SUSC.	DEC	INC	R95	EV	SDEV
MIN	320.69	-2.13	32.6	1.0051E-03	3.724E-06
INT	50.58	3.20	32.7	1.4783E-03	1.077E-04
MAX	84.24	-86.16	2.7	4.4944E-03	2.664E-05

P03D SITE 1 CORE 1 SPEC 1 UNITS= SI v M= 6 NR= 2 14:00:20 01-04-1990

SUSC.	DEC	INC	R95	EV	SDEV
MIN	310.46	-2.58	5.4	9.3285E-04	1.131E-04
INT	40.34	2.51	5.6	1.5152E-03	6.841E-05
MAX	86.10	-86.39	4.1	4.5241E-03	9.633E-05

P03J
n = 10
Equal area lower hemisphere stereonet

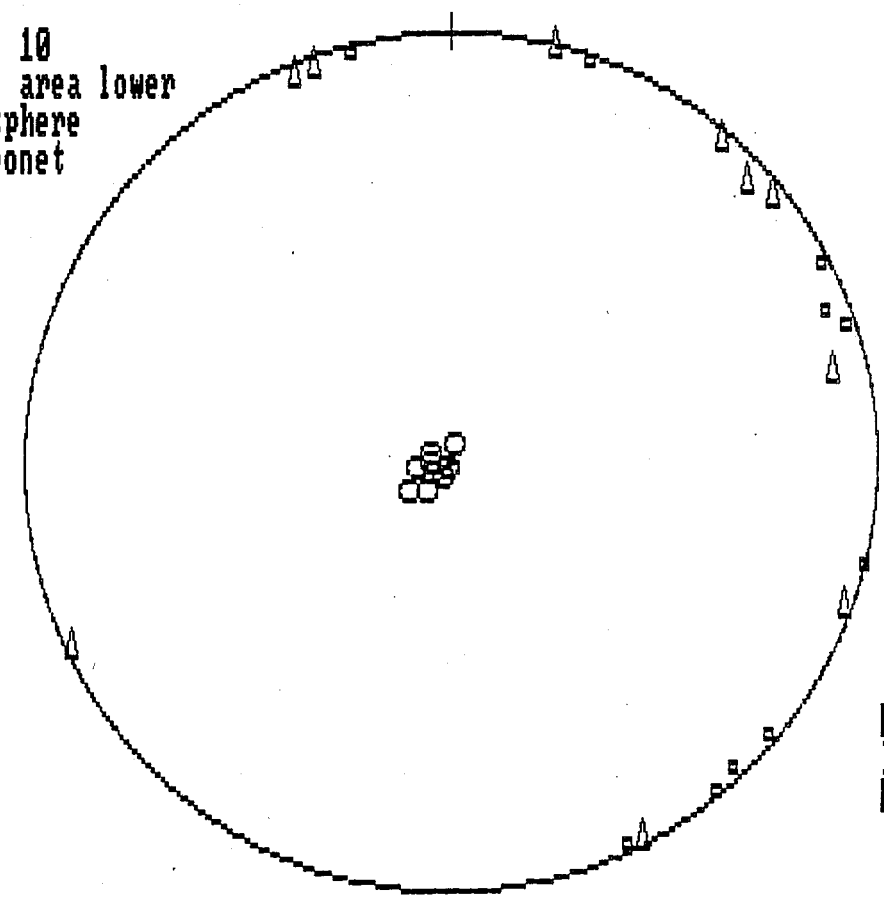

MAX = CIRCLE
INT = TRIANGLE
MIN = SQUARE

P04D SITE 1 CORE 1 SPEC 1 UNITS= SI v M= 6 NR= 2 14:15:04 01-11-1990

SUSC.	DEC	INC	R95	EV	SDEV
MIN	33.06	0.52	8.3	3.7691E-03	7.469E-06
INT	303.06	-0.62	7.6	4.0459E-03	2.026E-05
MAX	84.06	-89.18	1.8	1.2702E-02	2.214E-04

P04E SITE 1 CORE 1 SPEC 1 UNITS= SI v M= 6 NR= 2 14:20:04 01-11-1990

SUSC.	DEC	INC	R95	EV	SDEV
MIN	63.39	-0.64	1.5	3.5798E-03	5.302E-05
INT	333.39	1.48	1.2	3.8535E-03	1.381E-04
MAX	310.14	-88.39	1.1	1.2846E-02	7.396E-05

P04F SITE 1 CORE 1 SPEC 1 UNITS= SI v M= 6 NR= 2 14:25:44 01-11-1990

SUSC.	DEC	INC	R95	EV	SDEV
MIN	282.98	2.21	14.2	3.4708E-03	1.350E-05
INT	13.07	-0.01	14.1	3.7955E-03	3.485E-05
MAX	280.77	-87.79	0.6	1.2576E-02	4.240E-05

P04G SITE 1 CORE 1 SPEC 1 UNITS= SI v M= 6 NR= 2 14:30:34 01-11-1990

SUSC.	DEC	INC	R95	EV	SDEV
MIN	327.72	0.13	85.7	3.7351E-03	4.925E-05
INT	57.83	-2.38	85.8	3.8662E-03	1.787E-04
MAX	59.93	87.62	1.9	1.2558E-02	7.120E-05

P04H SITE 1 CORE 1 SPEC 1 UNITS= SI v M= 6 NR= 2 14:36:13 01-11-1990

SUSC.	DEC	INC	R95	EV	SDEV
MIN	53.17	-3.88	11.1	3.5190E-03	1.076E-06
INT	323.24	1.22	11.2	4.0845E-03	1.526E-04
MAX	70.72	85.94	2.9	1.2323E-02	3.747E-05

P04I SITE 1 CORE 1 SPEC 1 UNITS= SI v M= 6 NR= 2 14:41:41 01-11-1990

SUSC.	DEC	INC	R95	EV	SDEV
MIN	286.26	3.05	27.6	3.4551E-03	4.774E-05
INT	16.17	-1.87	27.8	3.7650E-03	1.089E-04
MAX	74.63	86.43	2.1	1.2782E-02	3.791E-04

P04J SITE 1 CORE 1 SPEC 1 UNITS= SI v M= 6 NR= 2 14:46:16 01-11-1990

SUSC.	DEC	INC	R95	EV	SDEV
MIN	68.20	-0.70	33.5	3.6428E-03	5.861E-05
INT	338.21	1.88	33.5	3.8984E-03	1.571E-04
MAX	317.88	-87.99	0.8	1.2869E-02	8.979E-05

P04A SITE 1 CORE 1 SPEC 1 UNITS= SI v M= 6 NR= 2 10:25:35 01-03-1990

SUSC.	DEC	INC	R95	EV	SDEV
MIN	76.67	-1.55	23.0	3.5819E-03	2.877E-05
INT	346.78	4.72	23.0	3.8244E-03	1.400E-04
MAX	328.59	-85.03	0.9	1.2848E-02	5.933E-05

P04B SITE 1 CORE 1 SPEC 1 UNITS= SI v M= 6 NR= 2 10:30:28 01-03-1990

SUSC.	DEC	INC	R95	EV	SDEV
MIN	317.92	3.58	30.5	3.4348E-03	1.390E-04
INT	47.81	-1.98	30.5	3.8046E-03	2.036E-05
MAX	288.87	-85.90	0.9	1.2622E-02	5.114E-05

P04C SITE 1 CORE 1 SPEC 1 UNITS= SI v M= 6 NR= 2 10:37:31 01-03-1990

SUSC.	DEC	INC	R95	EV	SDEV
MIN	270.72	4.01	16.0	3.6445E-03	3.657E-05
INT	1.23	1.98	15.7	3.8011E-03	1.797E-05
MAX	297.48	-85.51	1.6	1.2488E-02	2.020E-04

P04J
n = 10
Equal area lower hemisphere stereonet

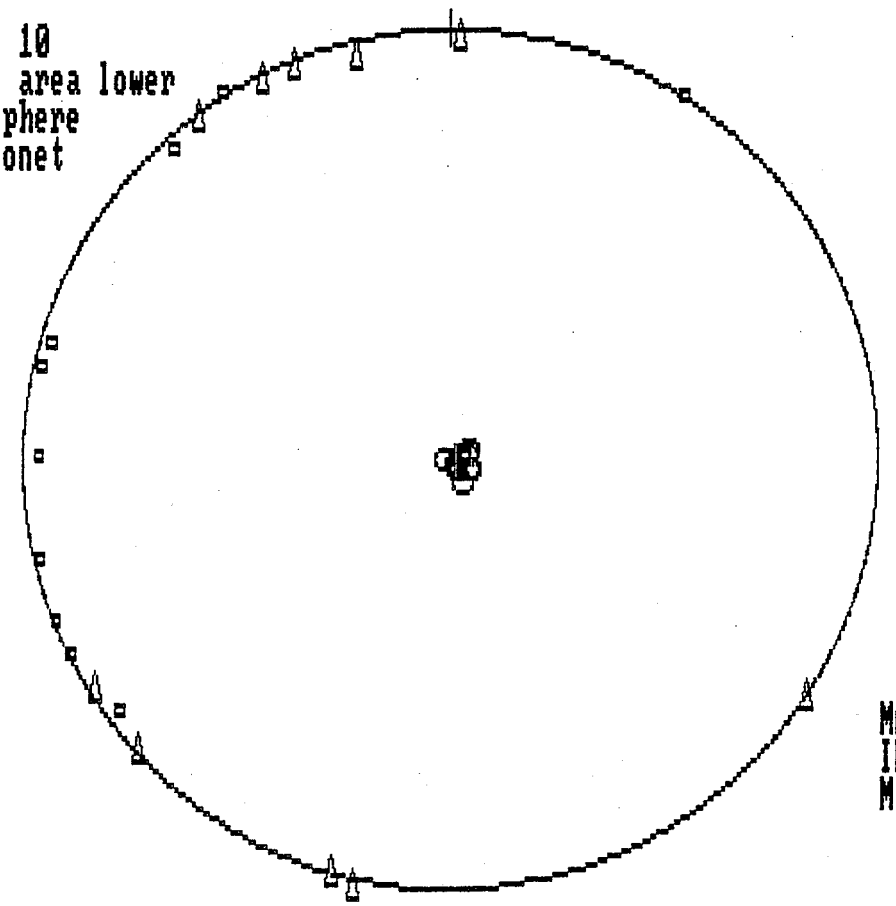

MAX = CIRCLE
INT = TRIANGLE
MIN = SQUARE

POSD SITE 1 CORE 1 SPEC 1 UNITS= SI v M= 6 NR= 2 14:57:45 01-11-1990

SUSC.	DEC	INC	R95	EV	SDEV
MIN	55.89	-1.20	8.2	1.1111E-03	8.809E-05
INT	325.99	4.69	15.1	1.7289E-03	1.172E-04
MAX	311.58	-85.16	14.9	3.4553E-03	4.870E-05

POSE SITE 1 CORE 1 SPEC 1 UNITS= SI v M= 6 NR= 2 15:02:20 01-11-1990

SUSC.	DEC	INC	R95	EV	SDEV
MIN	359.09	-6.94	35.8	9.8445E-04	5.961E-05
INT	89.31	-2.06	35.9	1.4577E-03	1.771E-04
MAX	15.79	82.76	3.6	3.5203E-03	1.261E-04

POSF SITE 1 CORE 1 SPEC 1 UNITS= SI v M= 6 NR= 2 15:06:36 01-11-1990

SUSC.	DEC	INC	R95	EV	SDEV
MIN	86.47	-6.76	29.0	1.2267E-03	6.819E-06
INT	356.72	2.36	28.8	1.3476E-03	6.377E-05
MAX	285.91	-82.84	7.0	3.2317E-03	8.040E-05

POSG SITE 1 CORE 1 SPEC 1 UNITS= SI v M= 6 NR= 2 15:10:51 01-11-1990

SUSC.	DEC	INC	R95	EV	SDEV
MIN	29.83	2.23	56.2	1.1320E-03	1.416E-04
INT	299.57	6.73	56.3	1.5271E-03	1.785E-04
MAX	318.02	-82.90	9.6	3.3906E-03	2.598E-04

POSH SITE 1 CORE 1 SPEC 1 UNITS= SI v M= 6 NR= 2 15:15:52 01-11-1990

SUSC.	DEC	INC	R95	EV	SDEV
MIN	44.51	-5.21	67.4	1.2024E-03	6.444E-05
INT	314.61	1.48	67.4	1.2322E-03	4.227E-05
MAX	60.48	84.59	2.5	3.6476E-03	2.288E-05

POSI SITE 1 CORE 1 SPEC 1 UNITS= SI v M= 6 NR= 2 15:19:38 01-11-1990

SUSC.	DEC	INC	R95	EV	SDEV
MIN	39.89	-0.20	54.9	1.2598E-03	9.651E-05
INT	309.90	-0.18	55.4	1.3359E-03	5.367E-05
MAX	349.66	89.72	12.0	3.5251E-03	3.838E-05

POSJ SITE 1 CORE 1 SPEC 1 UNITS= SI v M= 6 NR= 2 15:23:18 01-11-1990

SUSC.	DEC	INC	R95	EV	SDEV
MIN	8.13	1.99	49.1	1.1725E-03	1.827E-04
INT	278.13	-0.19	49.2	1.4056E-03	1.951E-04
MAX	14.65	-88.00	3.9	3.5167E-03	1.111E-04

P05A SITE 1 CORE 1 SPEC 1 UNITS= SI v M= 6 NR= 2 10:45:38 01-03-1990

SUSC.	DEC	INC	R95	EV	SDEV
MIN	358.22	5.16	35.6	1.2574E-03	1.200E-04
INT	87.51	-7.70	35.0	1.3941E-03	1.028E-04
MAX	301.74	-80.71	6.7	3.5468E-03	8.477E-05

P05B SITE 1 CORE 1 SPEC 1 UNITS= SI v M= 6 NR= 2 10:50:56 01-03-1990

SUSC.	DEC	INC	R95	EV	SDEV
MIN	326.77	-1.11	25.1	1.1685E-03	3.609E-05
INT	56.74	1.39	25.1	1.3462E-03	2.150E-05
MAX	275.03	88.22	4.9	3.5166E-03	2.168E-04

P05C SITE 1 CORE 1 SPEC 1 UNITS= SI v M= 6 NR= 2 10:56:06 01-03-1990

SUSC.	DEC	INC	R95	EV	SDEV
MIN	330.04	5.51	22.1	9.0279E-04	1.834E-04
INT	59.69	-3.68	21.2	1.3581E-03	2.328E-04
MAX	296.08	-83.37	6.7	3.5246E-03	3.457E-05

P05J
n = 10
Equal area lower hemisphere stereonet

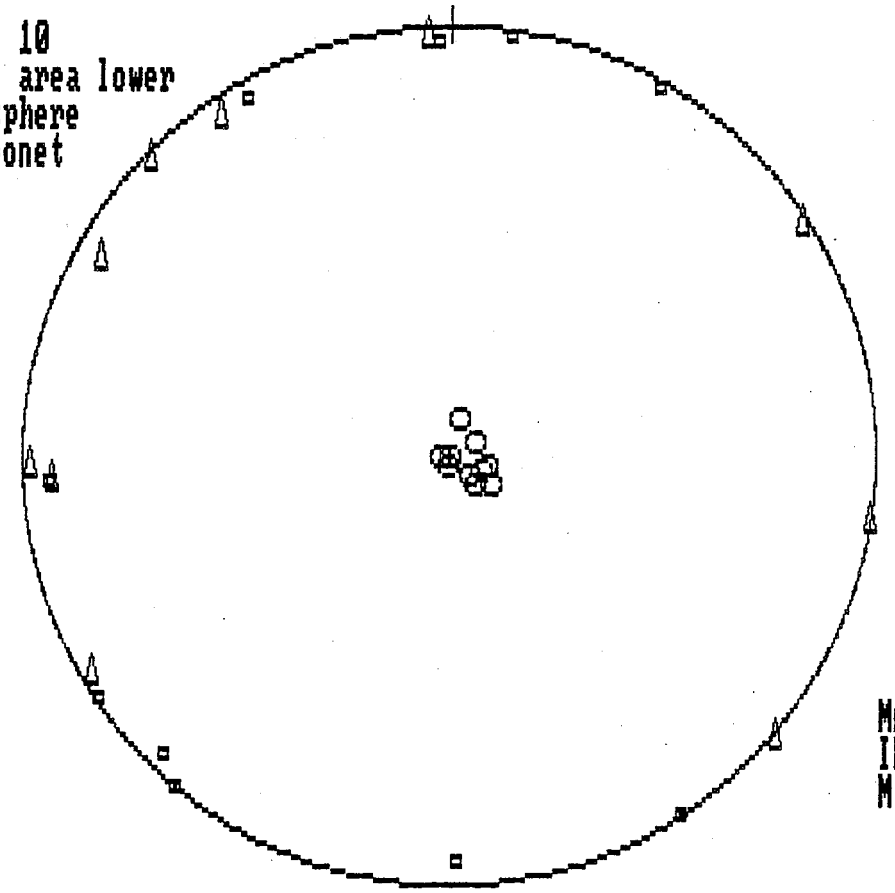

MAX = CIRCLE
INT = TRIANGLE
MIN = SQUARE

ACMS OUTPUT: Conductivity parameters

P06D SITE 1 CORE 1 SPEC 1 UNITS= SI m M= 6 NR= 2 11:08:22 01-15-1990

SUSC.	DEC	INC	R95	EV	SDEV
MIN	19.66	3.19	20.3	3.6600E-04	9.822E-06
INT	289.33	5.92	20.6	5.2668E-04	1.198E-05
MAX	317.79	-83.27	5.0	1.7982E-03	4.097E-05

ACMS OUTPUT: Conductivity parameters

P06E SITE 1 CORE 1 SPEC 1 UNITS= SI m M= 6 NR= 2 11:13:15 01-15-1990

SUSC.	DEC	INC	R95	EV	SDEV
MIN	347.30	7.05	24.5	3.9106E-04	4.223E-05
INT	77.26	-0.47	24.5	4.9364E-04	4.268E-07
MAX	343.36	-82.93	2.2	1.8630E-03	4.981E-05

ACMS OUTPUT: Conductivity parameters

P06F SITE 1 CORE 1 SPEC 1 UNITS= SI m M= 6 NR= 2 11:17:47 01-15-1990

SUSC.	DEC	INC	R95	EV	SDEV
MIN	319.74	7.86	58.5	3.8398E-04	1.026E-04
INT	49.69	-0.47	58.5	5.3811E-04	3.887E-05
MAX	316.19	-82.12	2.1	1.8150E-03	9.485E-06

ACMS OUTPUT: Conductivity parameters

P06G SITE 1 CORE 1 SPEC 1 UNITS= SI m M= 6 NR= 2 11:23:16 01-15-1990

SUSC.	DEC	INC	R95	EV	SDEV
MIN	40.36	3.56	11.2	4.0985E-04	3.460E-05
INT	309.98	6.03	8.9	5.8995E-04	1.242E-04
MAX	340.75	-82.99	6.8	1.7624E-03	9.592E-05

ACMS OUTPUT: Conductivity parameters

P06H SITE 1 CORE 1 SPEC 1 UNITS= SI m M= 6 NR= 2 11:28:04 01-15-1990

SUSC.	DEC	INC	R95	EV	SDEV
MIN	312.31	5.69	34.6	3.8962E-04	4.788E-05
INT	42.59	2.86	34.8	5.4912E-04	2.906E-05
MAX	339.21	-83.63	5.4	1.7907E-03	6.254E-05

ACMS OUTPUT: Conductivity parameters

P06I SITE 1 CORE 1 SPEC 1 UNITS= SI m M= 6 NR= 2 11:32:31 01-15-1990

SUSC.	DEC	INC	R95	EV	SDEV
MIN	323.20	5.96	72.8	4.1160E-04	7.876E-05
INT	53.50	0.02	73.2	4.6193E-04	3.642E-05
MAX	322.59	-84.04	4.9	1.7264E-03	4.717E-05

ACMS OUTPUT: Conductivity parameters

P06J SITE 1 CORE 1 SPEC 1 UNITS= SI m M= 6 NR= 2 11:36:59 01-15-1990

SUSC.	DEC	INC	R95	EV	SDEV
MIN	60.65	0.67	52.5	4.5011E-04	1.350E-05
INT	330.58	9.13	52.5	4.8471E-04	3.474E-05
MAX	334.81	-80.84	2.9	1.7805E-03	7.862E-06

P06A SITE 1 CORE 1 SPEC 1 UNITS= SI v M= 6 NR= 2 11:31:57 01-03-1990

SUSC.	DEC	INC	R95	EV	SDEV
MIN	60.90	1.22	12.0	1.0428E-03	3.351E-05
INT	330.71	8.82	11.8	1.3723E-03	4.418E-05
MAX	338.69	-81.10	2.2	4.8215E-03	5.676E-05

P06B SITE 1 CORE 1 SPEC 1 UNITS= SI v M= 6 NR= 2 11:37:22 01-03-1990

SUSC.	DEC	INC	R95	EV	SDEV
MIN	32.10	6.42	3.6	1.1701E-03	8.633E-06
INT	301.39	6.31	7.9	1.4870E-03	6.075E-05
MAX	347.23	-80.97	7.9	4.6652E-03	5.166E-05

P06C SITE 1 CORE 1 SPEC 1 UNITS= SI v M= 6 NR= 2 11:42:51 01-03-1990

SUSC.	DEC	INC	R95	EV	SDEV
MIN	23.84	5.77	70.7	1.1635E-03	4.046E-05
INT	293.04	7.93	70.7	1.3177E-03	1.774E-04
MAX	329.50	-80.17	2.3	4.7451E-03	2.705E-04

P06J
n = 10
Equal area lower hemisphere stereonet

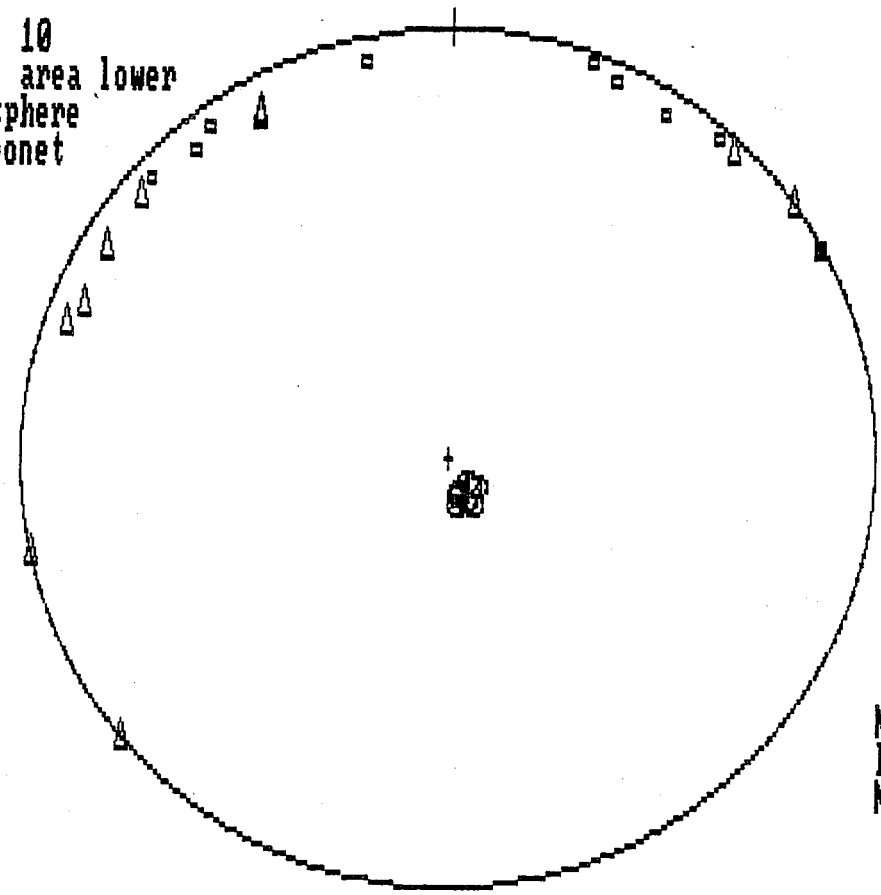

MAX = CIRCLE
INT = TRIANGLE
MIN = SQUARE

ACMS OUTPUT: Conductivity parameters

P07G SITE 1 CORE 1 SPEC 1 UNITS= SI m M= 6 NR= 2 12:34:39 01-15-1990

SUSC.	DEC	INC	R95	EV	SDEV
MIN	338.16	-1.98	1.6	9.7240E-04	2.687E-05
INT	68.23	-2.40	1.6	1.1433E-03	1.925E-06
MAX	28.72	86.89	0.5	4.9644E-03	7.763E-05

ACMS OUTPUT: Conductivity parameters

P07A SITE 1 CORE 1 SPEC 1 UNITS= SI m M= 6 NR= 2 11:55:00 01-15-1990

SUSC.	DEC	INC	R95	EV	SDEV
MIN	46.97	-2.75	44.2	1.0471E-03	8.552E-05
INT	316.95	-0.76	44.4	1.1902E-03	3.618E-05
MAX	31.35	87.14	2.0	4.9999E-03	1.961E-05

ACMS OUTPUT: Conductivity parameters

P07B SITE 1 CORE 1 SPEC 1 UNITS= SI m M= 6 NR= 2 11:59:19 01-15-1990

SUSC.	DEC	INC	R95	EV	SDEV
MIN	58.65	-3.12	45.6	9.8187E-04	2.008E-05
INT	328.62	-0.86	45.6	1.0799E-03	6.750E-05
MAX	43.02	86.76	1.3	5.0144E-03	1.916E-05

ACMS OUTPUT: Conductivity parameters

P07C SITE 1 CORE 1 SPEC 1 UNITS= SI m M= 6 NR= 2 12:14:52 01-15-1990

SUSC.	DEC	INC	R95	EV	SDEV
MIN	11.05	-2.46	59.7	9.9941E-04	3.776E-05
INT	281.13	1.71	59.7	1.0210E-03	4.660E-05
MAX	45.91	87.00	1.5	4.9651E-03	2.506E-05

ACMS OUTPUT: Conductivity parameters

P07D SITE 1 CORE 1 SPEC 1 UNITS= SI m M= 6 NR= 2 12:19:35 01-15-1990

SUSC.	DEC	INC	R95	EV	SDEV
MIN	311.27	-0.72	8.9	9.9271E-04	4.347E-05
INT	41.27	-1.25	9.0	1.0661E-03	1.615E-05
MAX	11.53	88.56	0.4	4.9964E-03	2.537E-05

ACMS OUTPUT: Conductivity parameters

P07E SITE 1 CORE 1 SPEC 1 UNITS= SI m M= 6 NR= 2 12:24:02 01-15-1990

SUSC.	DEC	INC	R95	EV	SDEV
MIN	315.05	-0.34	24.9	9.7517E-04	1.347E-05
INT	44.99	-4.74	24.9	1.0245E-03	9.166E-06
MAX	41.08	85.25	2.3	4.9840E-03	1.176E-05

ACMS OUTPUT: Conductivity parameters

P07F SITE 1 CORE 1 SPEC 1 UNITS= SI m M= 6 NR= 2 12:30:32 01-15-1990

SUSC.	DEC	INC	R95	EV	SDEV
MIN	310.59	-0.19	14.4	9.1002E-04	5.878E-05
INT	40.34	-4.10	14.2	1.0736E-03	3.225E-05

P07H SITE 1 CORE 1 SPEC 1 UNITS= SI m M= 6 NR= 2 12:39:14 01-15-1990

SUSC.	DEC	INC	R95	EV	SDEV
MIN	86.23	-2.53	49.3	9.6617E-04	4.784E-05
INT	356.10	-2.21	49.3	1.0468E-03	7.471E-05
MAX	44.97	86.63	1.3	4.9940E-03	1.125E-05

ACMS OUTPUT: Conductivity parameters

P07I SITE 1 CORE 1 SPEC 1 UNITS= SI m M= 6 NR= 2 12:42:45 01-15-1990

SUSC.	DEC	INC	R95	EV	SDEV
MIN	316.82	-0.68	74.3	9.2533E-04	5.981E-05
INT	46.85	-3.38	74.2	1.0570E-03	6.763E-05
MAX	35.50	86.56	0.5	4.9592E-03	2.793E-05

ACMS OUTPUT: Conductivity parameters

P07J SITE 1 CORE 1 SPEC 1 UNITS= SI m M= 6 NR= 2 12:46:40 01-15-1990

SUSC.	DEC	INC	R95	EV	SDEV
MIN	62.66	-2.80	50.9	1.0166E-03	5.219E-05
INT	332.63	-0.92	50.9	1.0946E-03	1.538E-05
MAX	44.24	87.05	1.2	4.9558E-03	4.884E-05

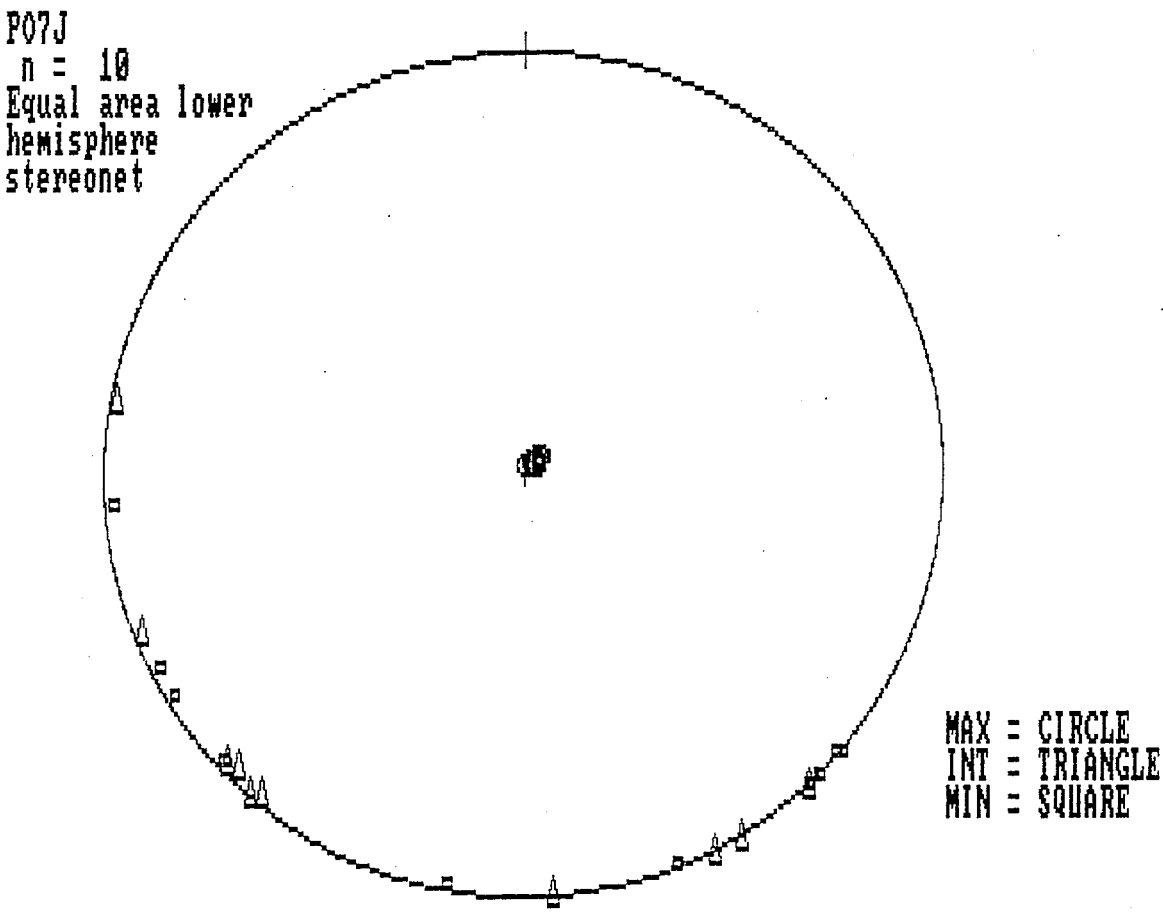

ACMS OUTPUT: Conductivity parameters

P08D SITE 1 CORE 1 SPEC 1 UNITS= SI m M= 6 NR= 2 14:13:50 01-15-1990

SUSC.	DEC	INC	R95	EV	SDEV
MIN	49.57	3.20	79.6	3.2831E-04	7.280E-06
INT	319.47	1.99	79.7	3.6256E-04	4.014E-05
MAX	17.55	-86.23	2.4	2.0022E-03	3.237E-05

ACMS OUTPUT: Conductivity parameters

P08E SITE 1 CORE 1 SPEC 1 UNITS= SI m M= 6 NR= 2 14:19:30 01-15-1990

SUSC.	DEC	INC	R95	EV	SDEV
MIN	48.81	2.36	40.6	3.1160E-04	4.796E-05
INT	318.68	3.15	39.5	3.8242E-04	1.511E-05
MAX	355.58	-86.06	5.2	1.9998E-03	8.688E-05

ACMS OUTPUT: Conductivity parameters

P08F SITE 1 CORE 1 SPEC 1 UNITS= SI m M= 6 NR= 2 14:24:53 01-15-1990

SUSC.	DEC	INC	R95	EV	SDEV
MIN	26.57	1.95	41.7	3.0024E-04	4.267E-05
INT	296.53	1.18	41.9	3.7397E-04	1.318E-06
MAX	355.07	-87.72	3.6	1.9463E-03	3.222E-05

ACMS OUTPUT: Conductivity parameters

P08G SITE 1 CORE 1 SPEC 1 UNITS= SI m M= 6 NR= 2 14:29:29 01-15-1990

SUSC.	DEC	INC	R95	EV	SDEV
MIN	301.07	2.33	74.3	3.0978E-04	3.751E-05
INT	31.24	4.40	74.3	3.5581E-04	8.957E-06
MAX	3.22	-85.02	1.9	2.0158E-03	2.526E-05

ACMS OUTPUT: Conductivity parameters

P08H SITE 1 CORE 1 SPEC 1 UNITS= SI m M= 6 NR= 2 14:33:41 01-15-1990

SUSC.	DEC	INC	R95	EV	SDEV
MIN	43.29	1.45	62.9	3.3184E-04	1.738E-05
INT	313.22	3.07	62.9	3.6826E-04	4.332E-05
MAX	338.52	-86.61	2.7	2.0042E-03	1.830E-05

ACMS OUTPUT: Conductivity parameters

P08I SITE 1 CORE 1 SPEC 1 UNITS= SI m M= 6 NR= 2 14:47:06 01-15-1990

SUSC.	DEC	INC	R95	EV	SDEV
MIN	357.08	4.07	69.2	3.6429E-04	4.240E-05
INT	86.99	0.69	69.4	3.8232E-04	2.699E-05
MAX	6.71	-85.87	3.2	1.9982E-03	1.364E-05

ACMS OUTPUT: Conductivity parameters

P08J SITE 1 CORE 1 SPEC 1 UNITS= SI m M= 6 NR= 2 14:51:33 01-15-1990

SUSC.	DEC	INC	R95	EV	SDEV
MIN	60.15	3.22	20.8	2.9115E-04	3.667E-05
INT	329.74	7.24	20.5	4.4338E-04	7.316E-05
MAX	353.96	-82.07	3.9	2.0623E-03	6.151E-05

P08A SITE 1 CORE 1 SPEC 1 UNITS= SI v M= 6 NR= 2 11:50:34 01-03-1990

SUSC.	DEC	INC	R95	EV	SDEV
MIN	78.09	0.70	50.3	8.2749E-04	3.855E-05
INT	348.04	4.80	50.3	9.5415E-04	7.928E-05
MAX	356.32	-85.15	6.3	5.3000E-03	9.218E-05

P08B SITE 1 CORE 1 SPEC 1 UNITS= SI v M= 6 NR= 2 11:56:36 01-03-1990

SUSC.	DEC	INC	R95	EV	SDEV
MIN	273.30	0.53	42.8	8.9574E-04	1.009E-04
INT	3.37	5.65	42.5	1.0166E-03	2.019E-05
MAX	358.02	-84.32	5.4	5.2522E-03	6.089E-05

P08C SITE 1 CORE 1 SPEC 1 UNITS= SI v M= 6 NR= 2 12:03:56 01-03-1990

SUSC.	DEC	INC	R95	EV	SDEV
MIN	46.78	4.60	80.8	9.3567E-04	9.228E-06
INT	316.55	3.07	80.8	9.7822E-04	3.024E-05
MAX	12.86	-84.47	1.9	5.2875E-03	5.224E-05

P08J
n = 10
Equal area lower hemisphere stereonet

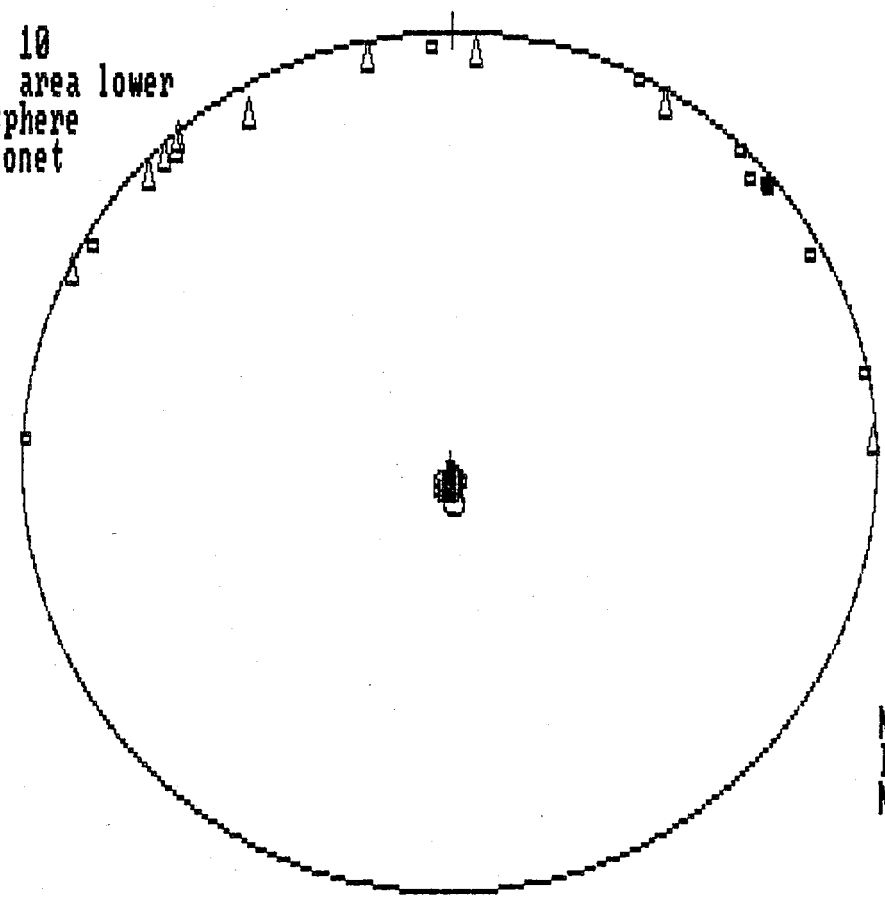

MAX = CIRCLE
INT = TRIANGLE
MIN = SQUARE

ACMS OUTPUT: Conductivity parameters

P09A SITE 1 CORE 1 SPEC 1 UNITS= SI m M= 6 NR= 2 15:11:14 03-07-1990

SUSC.	DEC	INC	R95	EV	SDEV
MIN	326.15	-11.13	86.9	1.9958E-06	3.860E-08
INT	55.01	5.83	86.8	2.0556E-06	1.178E-08
MAX	297.81	77.40	11.4	2.8886E-06	6.068E-08

ACMS OUTPUT: Conductivity parameters

P09B SITE 1 CORE 1 SPEC 1 UNITS= SI m M= 6 NR= 2 15:18:26 03-07-1990

SUSC.	DEC	INC	R95	EV	SDEV
MIN	89.20	17.32	66.4	1.9972E-06	2.643E-08
INT	1.61	-6.95	66.2	2.0340E-06	5.242E-08
MAX	292.63	71.22	5.5	3.0140E-06	1.263E-08

ACMS OUTPUT: Conductivity parameters

P09C SITE 1 CORE 1 SPEC 1 UNITS= SI m M= 6 NR= 2 15:22:55 03-07-1990

SUSC.	DEC	INC	R95	EV	SDEV
MIN	0.57	-8.30	48.3	1.9930E-06	5.488E-09
INT	87.67	15.87	48.3	2.0532E-06	9.526E-09
MAX	297.08	71.93	5.2	2.9967E-06	8.869E-08

ACMS OUTPUT: Conductivity parameters

P09D SITE 1 CORE 1 SPEC 1 UNITS= SI m M= 6 NR= 2 15:27:13 03-07-1990

SUSC.	DEC	INC	R95	EV	SDEV
MIN	308.99	-14.15	9.6	1.9837E-06	5.328E-08
INT	37.88	4.41	9.5	2.1290E-06	2.951E-09
MAX	290.97	75.15	2.1	2.9856E-06	2.872E-08

ACMS OUTPUT: Conductivity parameters

P09E SITE 1 CORE 1 SPEC 1 UNITS= SI m M= 6 NR= 2 15:31:31 03-07-1990

SUSC.	DEC	INC	R95	EV	SDEV
MIN	270.89	-16.68	10.3	1.9503E-06	1.762E-08
INT	3.43	-8.48	10.2	2.0454E-06	2.781E-08
MAX	299.37	71.18	4.2	2.9441E-06	1.236E-07

ACMS OUTPUT: Conductivity parameters

P09F SITE 1 CORE 1 SPEC 1 UNITS= SI m M= 6 NR= 2 15:36:11 03-07-1990

SUSC.	DEC	INC	R95	EV	SDEV
MIN	333.54	-14.23	6.1	1.8631E-06	8.360E-09
INT	61.77	6.95	10.4	2.0873E-06	2.329E-08
MAX	306.42	74.10	10.9	2.9967E-06	5.893E-08

ACMS OUTPUT: Conductivity parameters

P09G SITE 1 CORE 1 SPEC 1 UNITS= SI m M= 6 NR= 2 15:41:36 03-07-1990

SUSC.	DEC	INC	R95	EV	SDEV
MIN	294.22	-13.69	16.2	1.9791E-06	3.898E-08
INT	24.61	-1.61	16.9	2.0812E-06	3.413E-08
MAX	301.19	76.21	6.0	2.9772E-06	3.286E-09

ACMS OUTPUT: Conductivity parameters

P09H SITE 1 CORE 1 SPEC 1 UNITS= SI m M= 6 NR= 2 16:09:16 03-07-1990

SUSC.	DEC	INC	R95	EV	SDEV
MIN	319.13	-16.87	3.3	1.9574E-06	7.171E-09
INT	46.55	8.45	9.2	2.0430E-06	1.266E-08
MAX	290.94	71.02	8.8	2.9734E-06	1.021E-07

ACMS OUTPUT: Conductivity parameters

P09I SITE 1 CORE 1 SPEC 1 UNITS= SI m M= 6 NR= 2 16:13:37 03-07-1990

SUSC.	DEC	INC	R95	EV	SDEV
MIN	311.28	-15.81	12.6	1.8955E-06	2.712E-08
INT	40.21	3.79	13.9	2.0939E-06	6.023E-08
MAX	297.08	73.72	10.4	2.9453E-06	2.150E-08

ACMS OUTPUT: Conductivity parameters

P09J SITE 1 CORE 1 SPEC 1 UNITS= SI m M= 6 NR= 2 16:17:40 03-07-1990

SUSC.	DEC	INC	R95	EV	SDEV
MIN	87.43	11.75	77.1	2.0306E-06	3.614E-08
INT	358.64	-6.24	76.9	2.0716E-06	4.905E-09
MAX	296.11	76.66	5.3	2.9030E-06	1.042E-07

P09J
n = 10
Equal area lower hemisphere stereonet

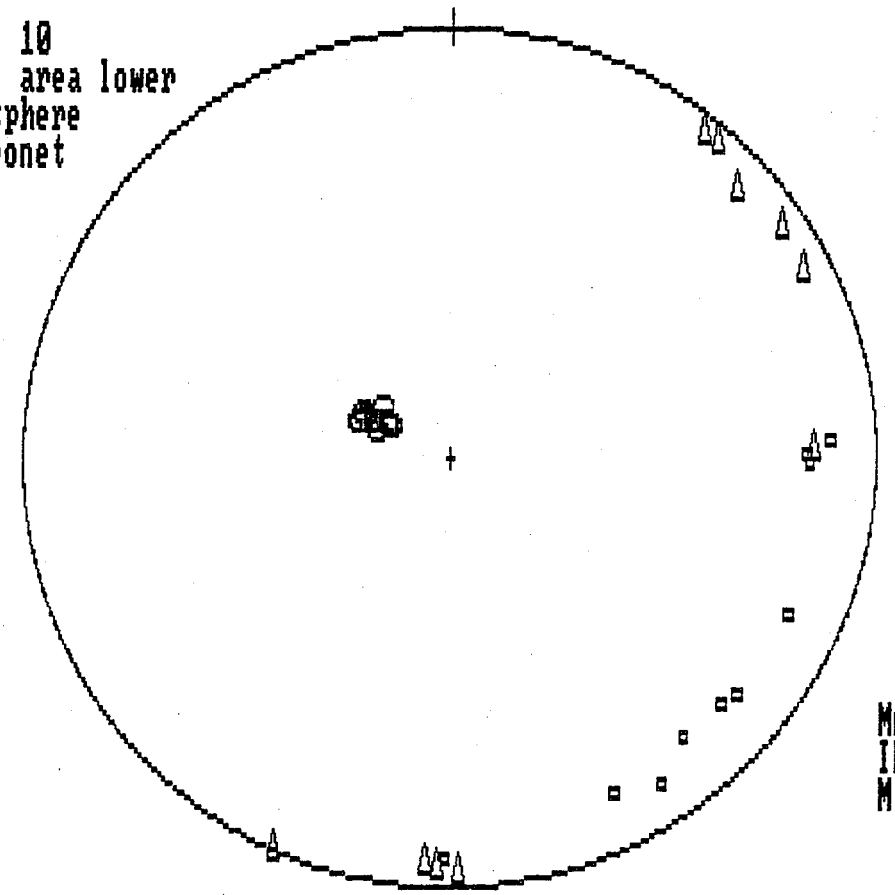

MAX = CIRCLE
INT = TRIANGLE
MIN = SQUARE

ACMS OUTPUT: Conductivity parameters

P10A SITE 1 CORE 1 SPEC 1 UNITS= SI m M= 6 NR= 2 16:57:57 03-07-1990

SUSC.	DEC	INC	R95	EV	SDEV
MIN	48.54	-1.93	81.8	1.0286E-06	3.058E-08
INT	318.54	0.24	83.2	1.1663E-06	1.021E-07
MAX	56.71	88.05	15.3	1.4493E-06	4.904E-08

ACMS OUTPUT: Conductivity parameters

P10B SITE 1 CORE 1 SPEC 1 UNITS= SI m M= 6 NR= 2 17:01:59 03-07-1990

SUSC.	DEC	INC	R95	EV	SDEV
MIN	7.42	-10.61	35.4	1.0561E-06	1.035E-08
INT	279.06	8.67	36.8	1.1705E-06	2.756E-08
MAX	47.54	76.23	11.3	1.3607E-06	2.271E-08

ACMS OUTPUT: Conductivity parameters

P10C SITE 1 CORE 1 SPEC 1 UNITS= SI m M= 6 NR= 2 17:06:21 03-07-1990

SUSC.	DEC	INC	R95	EV	SDEV
MIN	346.27	-1.60	34.0	1.0154E-06	4.819E-08
INT	75.89	13.31	35.1	1.1477E-06	2.703E-08
MAX	83.00	-76.59	8.8	1.5008E-06	1.369E-08

ACMS OUTPUT: Conductivity parameters

P10D SITE 1 CORE 1 SPEC 1 UNITS= SI m M= 6 NR= 2 17:10:48 03-07-1990

SUSC.	DEC	INC	R95	EV	SDEV
MIN	61.99	-3.77	86.7	1.0938E-06	1.808E-09
INT	332.22	3.52	88.0	1.1256E-06	3.069E-08
MAX	285.16	-84.84	14.5	1.4799E-06	3.640E-08

ACMS OUTPUT: Conductivity parameters

P10E SITE 1 CORE 1 SPEC 1 UNITS= SI m M= 6 NR= 2 17:15:00 03-07-1990

SUSC.	DEC	INC	R95	EV	SDEV
MIN	81.55	8.48	46.2	1.0038E-06	1.563E-08
INT	349.89	10.98	49.2	1.0847E-06	2.073E-09
MAX	28.47	-76.06	16.9	1.5363E-06	7.717E-08

ACMS OUTPUT: Conductivity parameters

P10F SITE 1 CORE 1 SPEC 1 UNITS= SI m M= 6 NR= 2 17:19:10 03-07-1990

SUSC.	DEC	INC	R95	EV	SDEV
MIN	53.72	11.73	5.3	1.0353E-06	3.943E-08
INT	321.47	10.69	7.4	1.1638E-06	3.746E-08
MAX	10.21	-74.02	7.6	1.5693E-06	4.215E-08

ACMS OUTPUT: Conductivity parameters

P10G SITE 1 CORE 1 SPEC 1 UNITS= SI m M= 6 NR= 2 17:23:20 03-07-1990

SUSC.	DEC	INC	R95	EV	SDEV
MIN	69.67	-9.81	22.6	1.0376E-06	5.266E-08
INT	341.50	10.46	16.5	1.1148E-06	1.802E-08
MAX	297.41	-75.58	15.8	1.4403E-06	1.328E-08

ACMS OUTPUT: Conductivity parameters

MIN	323.69	0.85	12.4	9.0421E-07	8.978E-08
INT	53.38	-20.54	16.0	1.1068E-06	4.767E-08
MAX	55.94	69.44	11.7	1.4665E-06	8.441E-09

ACMS OUTPUT: Conductivity parameters

P10I SITE 1 CORE 1 SPEC 1 UNITS= SI m M= 6 NR= 2 17:31:07 03-07-1990

SUSC.	DEC	INC	R95	EV	SDEV
MIN	36.36	2.08	16.4	1.0054E-06	2.318E-08
INT	306.92	-15.20	28.7	1.1936E-06	1.556E-08
MAX	298.77	74.65	25.8	1.5193E-06	5.656E-08

ACMS OUTPUT: Conductivity parameters

P10J SITE 1 CORE 1 SPEC 1 UNITS= SI m M= 6 NR= 2 17:37:39 03-07-1990

SUSC.	DEC	INC	R95	EV	SDEV
MIN	44.17	6.07	41.6	1.0664E-06	3.864E-08
INT	314.07	0.91	45.7	1.1780E-06	9.259E-09
MAX	35.50	-83.87	19.5	1.5004E-06	2.511E-08

ACMS OUTPUT: Conductivity parameters

P11A SITE 1 CORE 1 SPEC 1 UNITS= SI m M= 6 NR= 2 10:46:30 03-08-1990

SUSC.	DEC	INC	R95	EV	SDEV
MIN	46.78	5.86	3.1	1.9790E-06	4.338E-08
INT	317.05	0.48	6.1	2.0415E-06	3.272E-08
MAX	42.26	-84.13	0.4	1.6007E-05	6.982E-09

ACMS OUTPUT: Conductivity parameters

P11B SITE 1 CORE 1 SPEC 1 UNITS= SI m M= 6 NR= 2 10:51:08 03-08-1990

SUSC.	DEC	INC	R95	EV	SDEV
MIN	38.59	5.85	16.6	1.9837E-06	9.352E-10
INT	311.01	0.09	15.5	2.0939E-06	5.820E-08
MAX	38.28	-84.16	0.2	1.6000E-05	2.967E-08

ACMS OUTPUT: Conductivity parameters

P11C SITE 1 CORE 1 SPEC 1 UNITS= SI m M= 6 NR= 2 10:55:31 03-08-1990

SUSC.	DEC	INC	R95	EV	SDEV
MIN	80.91	4.54	36.6	1.9873E-06	6.146E-09
INT	350.57	4.08	36.7	2.0887E-06	2.879E-08
MAX	38.76	-83.89	0.3	1.5998E-05	4.510E-08

ACMS OUTPUT: Conductivity parameters

P11D SITE 1 CORE 1 SPEC 1 UNITS= SI m M= 6 NR= 2 11:01:00 03-08-1990

SUSC.	DEC	INC	R95	EV	SDEV
MIN	339.27	2.96	1.6	1.9285E-06	9.945E-09
INT	69.50	5.15	1.5	2.0494E-06	2.538E-08
MAX	39.51	-84.05	0.5	1.5958E-05	3.754E-08

ACMS OUTPUT: Conductivity parameters

P11E SITE 1 CORE 1 SPEC 1 UNITS= SI m M= 6 NR= 2 11:05:02 03-08-1990

SUSC.	DEC	INC	R95	EV	SDEV
MIN	71.30	4.83	47.4	2.0103E-06	7.781E-09
INT	341.06	2.97	47.4	2.1123E-06	6.209E-08
MAX	39.55	-84.32	0.1	1.5916E-05	3.142E-09

ACMS OUTPUT: Conductivity parameters

P11F SITE 1 CORE 1 SPEC 1 UNITS= SI m M= 6 NR= 2 11:09:15 03-08-1990

SUSC.	DEC	INC	R95	EV	SDEV
MIN	353.63	3.82	38.3	1.9519E-06	3.836E-08
INT	83.87	4.56	38.3	2.0836E-06	1.254E-08
MAX	43.80	-84.05	0.2	1.5936E-05	6.449E-08

ACMS OUTPUT: Conductivity parameters

P11G SITE 1 CORE 1 SPEC 1 UNITS= SI m M= 6 NR= 2 11:13:30 03-08-1990

SUSC.	DEC	INC	R95	EV	SDEV
MIN	32.93	5.79	59.3	2.0064E-06	1.499E-08
INT	302.18	-0.99	58.9	2.0236E-06	3.478E-09
MAX	42.03	-84.14	0.7	1.5960E-05	2.840E-08

ACMS OUTPUT: Conductivity parameters

P11H SITE 1 CORE 1 SPEC 1 UNITS= SI m M= 6 NR= 2 11:18:35 03-08-1990

SUSC.	DEC	INC	R95	EV	SDEV
MIN	71.69	5.15	31.7	2.0091E-06	4.032E-08
INT	341.41	3.25	31.7	2.1272E-06	1.017E-08
MAX	39.25	-83.91	0.1	1.5944E-05	4.468E-08

ACMS OUTPUT: Conductivity parameters

P11I SITE 1 CORE 1 SPEC 1 UNITS= SI m M= 6 NR= 2 11:22:48 03-08-1990

SUSC.	DEC	INC	R95	EV	SDEV
MIN	31.07	5.81	17.4	1.9702E-06	4.348E-08
INT	301.14	-1.24	17.9	2.1053E-06	5.116E-08
MAX	43.19	-84.06	0.3	1.5904E-05	2.132E-08

ACMS OUTPUT: Conductivity parameters

P11J SITE 1 CORE 1 SPEC 1 UNITS= SI m M= 6 NR= 2 11:27:06 03-08-1990

SUSC.	DEC	INC	R95	EV	SDEV
MIN	286.80	-2.06	23.1	1.9912E-06	1.586E-08
INT	16.70	5.14	23.3	2.0610E-06	3.268E-08
MAX	38.57	-84.47	0.3	1.5839E-05	2.469E-08

ACMS OUTPUT: Conductivity parameters

P12A SITE 1 CORE 1 SPEC 1 UNITS= SI m M= 6 NR= 2 12:48:13 03-08-1990

SUSC.	DEC	INC	R95	EV	SDEV
MIN	10.12	-1.29	21.8	5.2568E-07	6.611E-10
INT	280.08	-2.29	21.9	6.8391E-07	5.048E-09
MAX	309.37	87.38	2.4	3.3190E-06	6.231E-08

ACMS OUTPUT: Conductivity parameters

P12B SITE 1 CORE 1 SPEC 1 UNITS= SI m M= 6 NR= 2 12:52:08 03-08-1990

SUSC.	DEC	INC	R95	EV	SDEV
MIN	55.08	1.10	4.1	5.2694E-07	2.083E-08
INT	325.02	0.10	4.3	6.7414E-07	5.544E-08
MAX	57.55	-88.90	1.5	3.3424E-06	1.234E-08

ACMS OUTPUT: Conductivity parameters

P12C SITE 1 CORE 1 SPEC 1 UNITS= SI m M= 6 NR= 2 12:56:10 03-08-1990

SUSC.	DEC	INC	R95	EV	SDEV
MIN	340.62	-3.40	40.6	4.5163E-07	6.458E-08
INT	70.45	2.83	40.7	5.9816E-07	8.020E-09
MAX	300.72	85.57	1.7	3.4237E-06	3.356E-08

ACMS OUTPUT: Conductivity parameters

P12D SITE 1 CORE 1 SPEC 1 UNITS= SI m M= 6 NR= 2 13:00:11 03-08-1990

SUSC.	DEC	INC	R95	EV	SDEV
MIN	320.44	-2.35	2.7	4.4447E-07	1.571E-08
INT	50.36	2.00	3.0	6.7596E-07	1.697E-08
MAX	279.90	86.92	2.0	3.3759E-06	9.714E-08

ACMS OUTPUT: Conductivity parameters

P12E SITE 1 CORE 1 SPEC 1 UNITS= SI m M= 6 NR= 2 13:07:08 03-08-1990

SUSC.	DEC	INC	R95	EV	SDEV
MIN	21.02	-0.74	44.4	4.7863E-07	1.456E-08
INT	290.98	-3.96	44.4	5.9076E-07	2.373E-08
MAX	301.55	85.97	0.7	3.3542E-06	3.839E-08

ACMS OUTPUT: Conductivity parameters

P12F SITE 1 CORE 1 SPEC 1 UNITS= SI m M= 6 NR= 2 13:12:28 03-08-1990

SUSC.	DEC	INC	R95	EV	SDEV
MIN	13.86	1.76	52.1	5.4873E-07	3.402E-08
INT	283.94	-2.54	52.2	6.0805E-07	4.611E-08
MAX	69.23	-86.91	2.4	3.4414E-06	4.353E-08

ACMS OUTPUT: Conductivity parameters

P12G SITE 1 CORE 1 SPEC 1 UNITS= SI m M= 6 NR= 2 13:16:53 03-08-1990

SUSC.	DEC	INC	R95	EV	SDEV
MIN	289.69	-3.09	70.4	5.8193E-07	7.345E-09
INT	19.78	0.41	68.1	6.0708E-07	2.944E-08
MAX	281.91	86.88	1.1	3.2892E-06	2.255E-08

ACMS OUTPUT: Conductivity parameters

P12H SITE 1 CORE 1 SPEC 1 UNITS= SI m M= 6 NR= 2 13:20:52 03-08-1990

SUSC.	DEC	INC	R95	EV	SDEV
MIN	40.20	-0.41	82.7	5.3055E-07	1.999E-08
INT	310.19	-3.18	82.8	6.1775E-07	6.839E-08
MAX	317.36	86.79	1.8	3.2809E-06	3.272E-08

ACMS OUTPUT: Conductivity parameters

P12I SITE 1 CORE 1 SPEC 1 UNITS= SI m M= 6 NR= 2 13:24:21 03-08-1990

SUSC.	DEC	INC	R95	EV	SDEV
MIN	44.46	3.26	13.9	4.8318E-07	3.970E-08
INT	314.60	-2.56	13.9	6.9278E-07	8.919E-08
MAX	82.67	-85.85	1.4	3.4727E-06	3.593E-09

ACMS OUTPUT: Conductivity parameters

P12J SITE 1 CORE 1 SPEC 1 UNITS= SI m M= 6 NR= 2 13:28:09 03-08-1990

SUSC.	DEC	INC	R95	EV	SDEV
MIN	16.34	1.99	66.1	5.7930E-07	6.769E-09
INT	286.48	-4.13	66.1	6.4577E-07	7.033E-08
MAX	80.67	-85.41	3.2	3.4068E-06	1.803E-08

P12J
n = 10
Equal area lower hemisphere stereonet

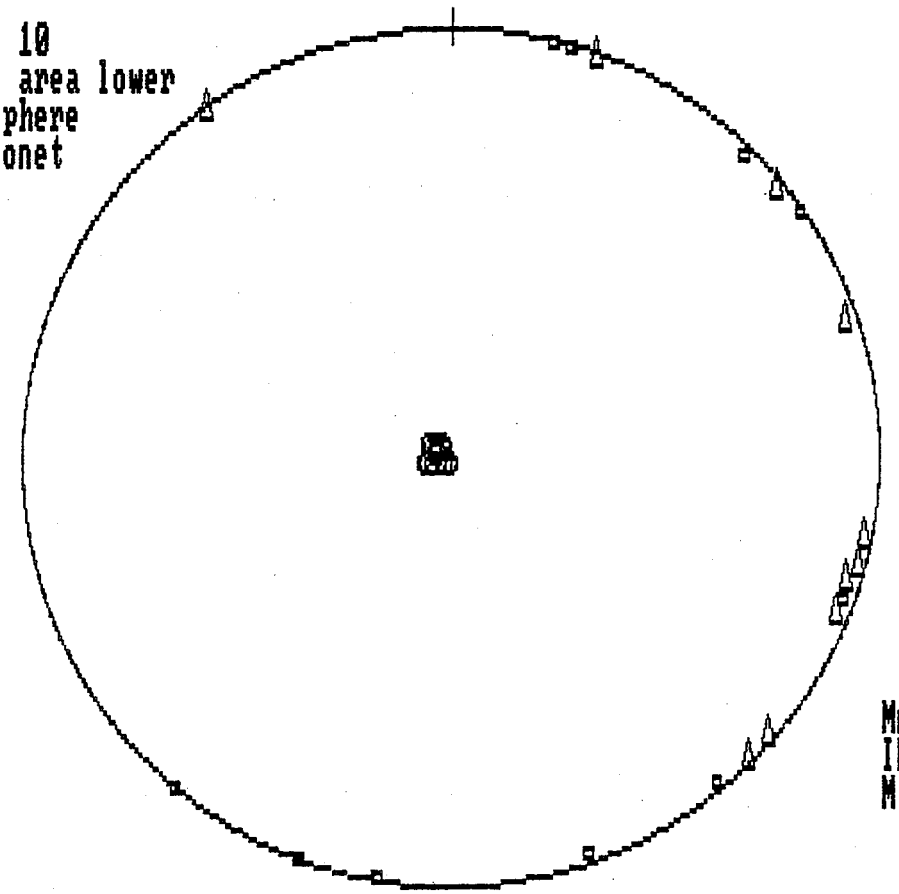

MAX = CIRCLE
INT = TRIANGLE
MIN = SQUARE

ACMS OUTPUT: Conductivity parameters

P13A SITE 1 CORE 1 SPEC 1 UNITS= SI m M= 6 NR= 2 16:19:40 03-08-1990

SUSC.	DEC	INC	R95	EV	SDEV
MIN	11.52	5.08	24.1	1.2629E-06	1.875E-08
INT	281.81	-3.24	23.6	1.3854E-06	2.362E-08
MAX	44.21	-83.97	6.7	2.2427E-06	5.018E-08

ACMS OUTPUT: Conductivity parameters

P13B SITE 1 CORE 1 SPEC 1 UNITS= SI m M= 6 NR= 2 16:23:41 03-08-1990

SUSC.	DEC	INC	R95	EV	SDEV
MIN	21.57	3.79	2.8	1.2273E-06	3.678E-09
INT	291.87	-4.53	3.2	1.4287E-06	2.486E-08
MAX	71.83	-84.09	2.4	2.1578E-06	4.197E-08

ACMS OUTPUT: Conductivity parameters

P13C SITE 1 CORE 1 SPEC 1 UNITS= SI m M= 6 NR= 2 16:27:54 03-08-1990

SUSC.	DEC	INC	R95	EV	SDEV
MIN	23.07	4.69	8.7	1.2962E-06	1.353E-08
INT	292.95	1.50	1.7	1.4249E-06	6.294E-09
MAX	5.22	-85.08	8.8	2.2258E-06	3.035E-08

ACMS OUTPUT: Conductivity parameters

P13D SITE 1 CORE 1 SPEC 1 UNITS= SI m M= 6 NR= 2 16:35:22 03-08-1990

SUSC.	DEC	INC	R95	EV	SDEV
MIN	356.13	4.80	12.3	1.1827E-06	3.414E-08
INT	86.01	-1.40	11.7	1.3829E-06	8.849E-10
MAX	339.68	-85.00	4.0	2.2282E-06	3.622E-08

ACMS OUTPUT: Conductivity parameters

P13E SITE 1 CORE 1 SPEC 1 UNITS= SI m M= 6 NR= 2 16:39:57 03-08-1990

SUSC.	DEC	INC	R95	EV	SDEV
MIN	18.09	7.71	9.2	1.2409E-06	1.755E-08
INT	288.41	-2.38	8.6	1.4759E-06	4.294E-08
MAX	35.47	-81.92	3.8	2.2606E-06	7.178E-08

ACMS OUTPUT: Conductivity parameters

P13F SITE 1 CORE 1 SPEC 1 UNITS= SI m M= 6 NR= 2 16:44:17 03-08-1990

SUSC.	DEC	INC	R95	EV	SDEV
MIN	353.72	3.15	20.1	1.1786E-06	2.679E-08
INT	83.80	1.49	20.2	1.3895E-06	2.452E-09
MAX	19.20	-86.52	4.6	2.2465E-06	3.160E-08

ACMS OUTPUT: Conductivity parameters

P13G SITE 1 CORE 1 SPEC 1 UNITS= SI m M= 6 NR= 2 16:48:38 03-08-1990

SUSC.	DEC	INC	R95	EV	SDEV
MIN	50.47	0.16	80.3	1.2960E-06	1.630E-08
INT	320.60	5.48	80.2	1.3160E-06	3.825E-08
MAX	321.83	-84.52	4.3	2.2198E-06	8.696E-09

ACMS OUTPUT: Conductivity parameters

P13H SITE 1 CORE 1 SPEC 1 UNITS= SI m M= 6 NR= 2 16:53:27 03-08-1990

SUSC.	DEC	INC	R95	EV	SDEV
MIN	22.72	7.39	2.6	1.2008E-06	3.280E-08
INT	292.84	-0.95	3.2	1.4490E-06	7.815E-08
MAX	30.19	-82.54	2.0	2.2529E-06	2.677E-08

ACMS OUTPUT: Conductivity parameters

P13I SITE 1 CORE 1 SPEC 1 UNITS= SI m M= 6 NR= 2 16:58:05 03-08-1990

SUSC.	DEC	INC	R95	EV	SDEV
MIN	3.58	4.89	35.7	1.2371E-06	1.538E-08
INT	273.67	-1.04	35.7	1.3715E-06	3.876E-08
MAX	15.74	-85.00	2.9	2.2149E-06	6.479E-08

ACMS OUTPUT: Conductivity parameters

P13J SITE 1 CORE 1 SPEC 1 UNITS= SI m M= 6 NR= 2 17:02:08 03-08-1990

SUSC.	DEC	INC	R95	EV	SDEV
MIN	348.35	0.14	12.2	1.1803E-06	4.155E-08
INT	78.34	-0.05	12.5	1.3759E-06	2.690E-08
MAX	302.20	-89.83	7.9	2.1730E-06	3.757E-08

ACMS OUTPUT: Conductivity parameters

P14A SITE 1 CORE 1 SPEC 1 UNITS= SI m M= 6 NR= 2 11:54:22 03-13-1990

SUSC.	DEC	INC	R95	EV	SDEV
MIN	56.98	0.27	34.1	2.1585E-06	1.290E-08
INT	326.98	1.47	34.4	2.3268E-06	1.207E-07
MAX	336.84	-88.50	0.6	8.8030E-06	4.308E-08

ACMS OUTPUT: Conductivity parameters

P14B SITE 1 CORE 1 SPEC 1 UNITS= SI m M= 6 NR= 2 11:59:19 03-13-1990

SUSC.	DEC	INC	R95	EV	SDEV
MIN	25.10	0.91	82.0	2.1927E-06	3.437E-10
INT	295.24	0.38	82.2	2.2115E-06	1.923E-08
MAX	1.55	-89.01	0.7	8.8680E-06	5.253E-08

ACMS OUTPUT: Conductivity parameters

P14C SITE 1 CORE 1 SPEC 1 UNITS= SI m M= 6 NR= 2 12:03:54 03-13-1990

SUSC.	DEC	INC	R95	EV	SDEV
MIN	71.25	0.13	35.0	2.1512E-06	1.082E-08
INT	341.38	1.26	34.9	2.2260E-06	4.412E-08
MAX	343.78	-88.74	0.8	8.8378E-06	7.193E-08

ACMS OUTPUT: Conductivity parameters

P14D SITE 1 CORE 1 SPEC 1 UNITS= SI m M= 6 NR= 2 12:08:43 03-13-1990

SUSC.	DEC	INC	R95	EV	SDEV
MIN	33.24	0.49	35.1	2.1690E-06	1.946E-08
INT	303.25	0.96	35.0	2.2343E-06	1.115E-08
MAX	330.04	-88.92	0.1	8.7984E-06	1.323E-08

ACMS OUTPUT: Conductivity parameters

P14E SITE 1 CORE 1 SPEC 1 UNITS= SI m M= 6 NR= 2 12:13:08 03-13-1990

SUSC.	DEC	INC	R95	EV	SDEV
MIN	11.59	0.95	61.2	2.1988E-06	2.637E-08
INT	281.54	-0.16	61.1	2.2451E-06	6.132E-08
MAX	23.07	-89.03	0.6	8.8586E-06	7.537E-09

ACMS OUTPUT: Conductivity parameters

P14F SITE 1 CORE 1 SPEC 1 UNITS= SI m M= 6 NR= 2 12:18:05 03-13-1990

SUSC.	DEC	INC	R95	EV	SDEV
MIN	45.68	0.31	61.5	2.1648E-06	3.853E-09
INT	315.74	-0.10	61.6	2.2648E-06	9.777E-08
MAX	36.42	-89.70	1.0	8.7626E-06	1.326E-08

ACMS OUTPUT: Conductivity parameters

P14G SITE 1 CORE 1 SPEC 1 UNITS= SI m M= 6 NR= 2 12:22:31 03-13-1990

SUSC.	DEC	INC	R95	EV	SDEV
MIN	320.36	0.82	75.4	2.1978E-06	2.303E-08
INT	50.26	0.41	75.6	2.2132E-06	9.300E-09
MAX	347.69	-89.09	0.7	8.8313E-06	6.582E-08

ACMS OUTPUT: Conductivity parameters

P14H SITE 1 CORE 1 SPEC 1 UNITS= SI m M= 6 NR= 2 12:27:11 03-13-1990

SUSC.	DEC	INC	R95	EV	SDEV
MIN	279.65	0.46	3.6	2.1642E-06	4.952E-08
INT	9.67	0.99	3.8	2.2393E-06	8.048E-09
MAX	345.15	-88.91	1.1	8.8897E-06	5.942E-08

ACMS OUTPUT: Conductivity parameters

P14I SITE 1 CORE 1 SPEC 1 UNITS= SI m M= 6 NR= 2 12:31:51 03-13-1990

SUSC.	DEC	INC	R95	EV	SDEV
MIN	32.55	0.81	43.9	2.1926E-06	4.634E-08
INT	302.59	0.70	45.1	2.2332E-06	7.952E-09
MAX	350.80	-88.93	1.4	8.8180E-06	2.395E-08

ACMS OUTPUT: Conductivity parameters

P14J SITE 1 CORE 1 SPEC 1 UNITS= SI m M= 6 NR= 2 12:36:27 03-13-1990

SUSC.	DEC	INC	R95	EV	SDEV
MIN	304.53	0.30	33.2	2.0948E-06	4.657E-08
INT	34.52	0.47	33.1	2.2175E-06	5.590E-09
MAX	4.57	-89.44	0.9	8.8497E-06	7.059E-09

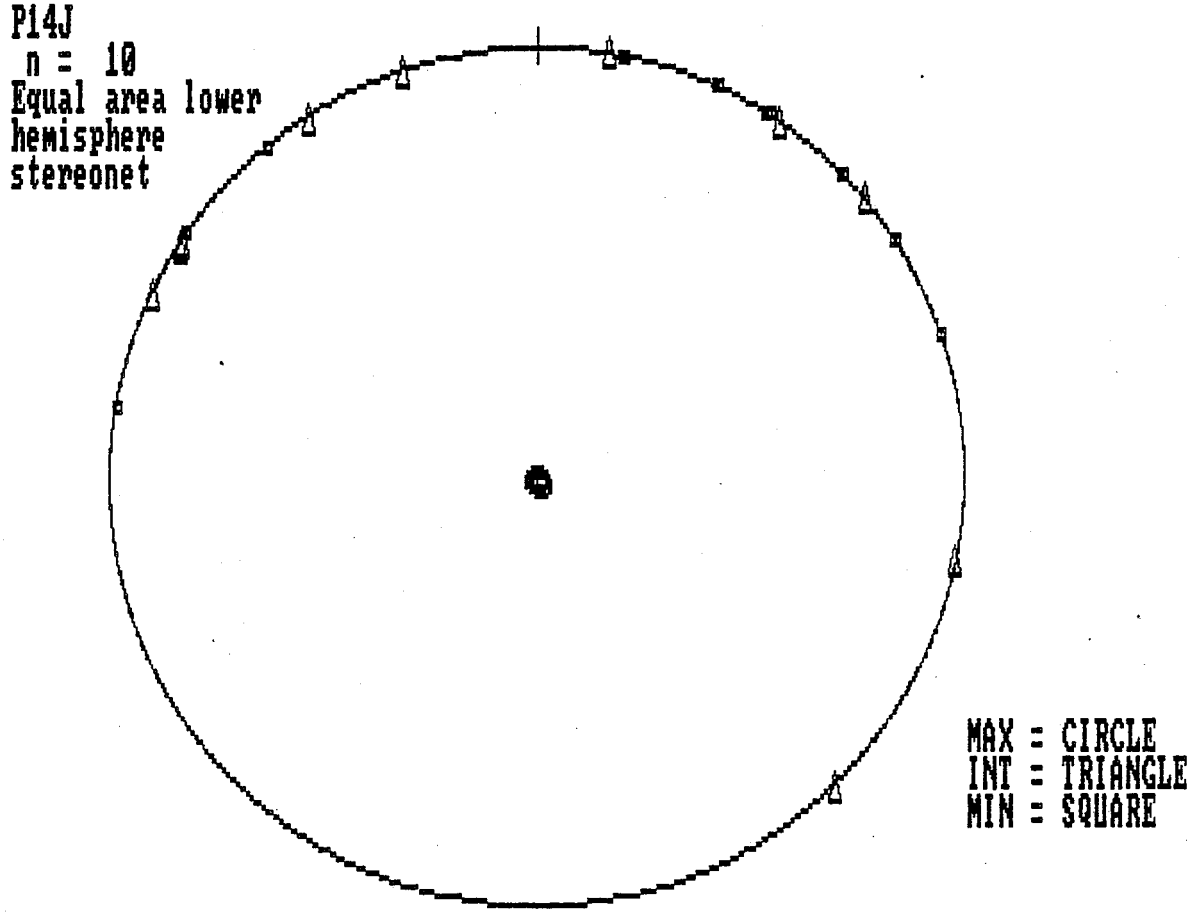

ACMS OUTPUT: Conductivity parameters

P15A SITE 1 CORE 1 SPEC 1 UNITS= SI m M= 6 NR= 2 12:19:36 03-14-1990

SUSC.	DEC	INC	R95	EV	SDEV
MIN	311.29	-6.64	75.7	1.9459E-06	7.668E-08
INT	40.98	2.74	75.8	2.1146E-06	8.558E-08
MAX	288.62	82.81	2.4	6.9444E-06	2.489E-08

ACMS OUTPUT: Conductivity parameters

P15B SITE 1 CORE 1 SPEC 1 UNITS= SI m M= 6 NR= 2 12:24:43 03-14-1990

SUSC.	DEC	INC	R95	EV	SDEV
MIN	28.46	0.24	21.8	2.0603E-06	4.686E-09
INT	298.43	-6.96	21.7	2.2110E-06	9.685E-08
MAX	296.62	83.04	2.9	6.7812E-06	3.245E-08

ACMS OUTPUT: Conductivity parameters

P15C SITE 1 CORE 1 SPEC 1 UNITS= SI m M= 12 NR= 2 12:33:26 03-14-1990

SUSC.	DEC	INC	R95	EV	SDEV
MIN	12.08	-0.53	16.8	1.9153E-06	5.449E-08
INT	282.03	-7.28	16.8	2.2219E-06	1.482E-08
MAX	286.15	82.70	1.4	6.8826E-06	4.762E-08

ACMS OUTPUT: Conductivity parameters

P15D SITE 1 CORE 1 SPEC 1 UNITS= SI m M= 6 NR= 2 12:38:19 03-14-1990

SUSC.	DEC	INC	R95	EV	SDEV
MIN	42.00	4.50	70.7	2.0955E-06	2.396E-10
INT	312.53	-6.81	70.8	2.2222E-06	1.164E-07
MAX	278.81	81.82	2.4	7.0080E-06	9.117E-08

ACMS OUTPUT: Conductivity parameters

P15E SITE 1 CORE 1 SPEC 1 UNITS= SI m M= 6 NR= 2 12:43:02 03-14-1990

SUSC.	DEC	INC	R95	EV	SDEV
MIN	35.60	5.43	21.6	2.0151E-06	4.922E-08
INT	306.26	-6.97	21.6	2.2674E-06	2.468E-08
MAX	88.01	-81.14	0.8	7.1173E-06	1.097E-07

ACMS OUTPUT: Conductivity parameters

P15F SITE 1 CORE 1 SPEC 1 UNITS= SI m M= 6 NR= 2 12:48:07 03-14-1990

SUSC.	DEC	INC	R95	EV	SDEV
MIN	50.50	4.21	84.4	1.9681E-06	1.187E-08
INT	320.99	-6.91	84.4	2.0250E-06	6.959E-08
MAX	289.40	81.90	1.7	6.9954E-06	1.047E-07

ACMS OUTPUT: Conductivity parameters

P15G SITE 1 CORE 1 SPEC 1 UNITS= SI m M= 6 NR= 2 12:52:28 03-14-1990

SUSC.	DEC	INC	R95	EV	SDEV
MIN	55.49	6.17	13.4	2.0233E-06	6.126E-08
INT	325.97	-4.50	13.4	2.4421E-06	1.308E-07
MAX	271.90	82.36	1.7	6.9611E-06	9.650E-08

ACMS OUTPUT: Conductivity parameters

P15H SITE 1 CORE 1 SPEC 1 UNITS= SI m M= 6 NR= 2 13:40:40 03-14-1990

SUSC.	DEC	INC	R95	EV	SDEV
MIN	314.39	-7.18	68.6	1.9936E-06	6.006E-08
INT	43.61	6.29	68.6	2.1417E-06	8.127E-08
MAX	272.78	80.44	2.0	7.1413E-06	9.137E-09

ACMS OUTPUT: Conductivity parameters

P15I SITE 1 CORE 1 SPEC 1 UNITS= SI m M= 6 NR= 2 13:45:00 03-14-1990

SUSC.	DEC	INC	R95	EV	SDEV
MIN	48.81	3.85	51.3	1.9767E-06	2.969E-08
INT	319.16	-5.44	51.2	2.0261E-06	1.503E-08
MAX	283.71	83.33	2.7	6.8402E-06	6.737E-08

ACMS OUTPUT: Conductivity parameters

P15J SITE 1 CORE 1 SPEC 1 UNITS= SI m M= 6 NR= 2 13:49:24 03-14-1990

SUSC.	DEC	INC	R95	EV	SDEV
MIN	331.56	-4.92	30.5	1.8733E-06	1.544E-07
INT	61.29	3.18	30.6	2.1081E-06	2.975E-08
MAX	298.47	84.14	1.6	6.9081E-06	7.396E-08

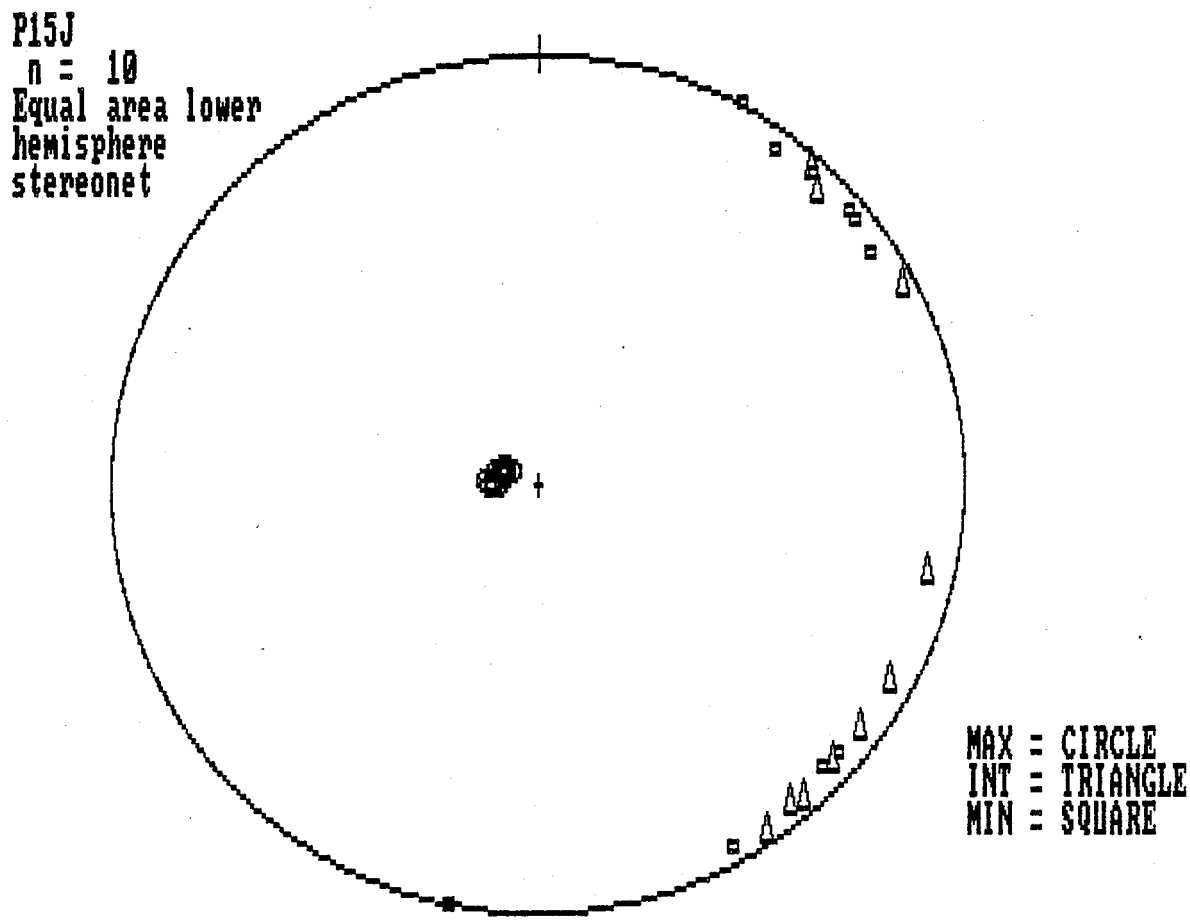

ACMS OUTPUT: Conductivity parameters

P16A SITE 1 CORE 1 SPEC 1 UNITS= SI m M= 6 NR= 2 14:07:12 03-14-1990

SUSC.	DEC	INC	R95	EV	SDEV
MIN	308.03	-1.89	71.2	1.2361E-06	1.016E-07
INT	38.23	-5.89	71.2	1.4127E-06	6.338E-08
MAX	20.30	83.81	1.3	4.9300E-06	8.290E-08

ACMS OUTPUT: Conductivity parameters

P16B SITE 1 CORE 1 SPEC 1 UNITS= SI m M= 6 NR= 2 14:11:55 03-14-1990

SUSC.	DEC	INC	R95	EV	SDEV
MIN	354.41	-5.65	21.0	1.2235E-06	1.507E-09
INT	84.12	2.88	21.6	1.4579E-06	9.853E-08
MAX	327.19	83.65	5.0	5.0413E-06	1.667E-07

ACMS OUTPUT: Conductivity parameters

P16C SITE 1 CORE 1 SPEC 1 UNITS= SI m M= 6 NR= 2 14:16:26 03-14-1990

SUSC.	DEC	INC	R95	EV	SDEV
MIN	22.45	-7.19	63.4	1.1569E-06	9.407E-08
INT	292.06	-3.12	63.3	1.4876E-06	2.144E-07
MAX	358.72	82.15	2.7	5.1240E-06	7.810E-09

ACMS OUTPUT: Conductivity parameters

P16D SITE 1 CORE 1 SPEC 1 UNITS= SI m M= 6 NR= 2 14:20:56 03-14-1990

SUSC.	DEC	INC	R95	EV	SDEV
MIN	57.84	-5.47	25.1	1.2363E-06	8.902E-08
INT	327.47	-3.88	25.1	1.4518E-06	9.697E-08
MAX	22.28	83.28	3.6	4.9972E-06	2.797E-08

ACMS OUTPUT: Conductivity parameters

P16E SITE 1 CORE 1 SPEC 1 UNITS= SI m M= 6 NR= 2 14:25:19 03-14-1990

SUSC.	DEC	INC	R95	EV	SDEV
MIN	45.00	-5.44	13.2	1.0826E-06	2.419E-08
INT	314.62	-3.96	13.1	1.5310E-06	1.865E-07
MAX	8.73	83.27	1.6	5.0715E-06	4.680E-08

ACMS OUTPUT: Conductivity parameters

P16F SITE 1 CORE 1 SPEC 1 UNITS= SI m M= 6 NR= 2 14:29:39 03-14-1990

SUSC.	DEC	INC	R95	EV	SDEV
MIN	40.08	-3.22	29.8	1.1989E-06	5.713E-09
INT	310.02	-1.23	29.9	1.5562E-06	3.140E-08
MAX	19.11	86.55	2.4	4.9385E-06	1.096E-07

ACMS OUTPUT: Conductivity parameters

P16G SITE 1 CORE 1 SPEC 1 UNITS= SI m M= 6 NR= 2 14:33:58 03-14-1990

SUSC.	DEC	INC	R95	EV	SDEV
MIN	49.51	-3.41	8.2	1.2649E-06	1.023E-07
INT	319.21	-5.00	7.6	1.3909E-06	1.221E-07
MAX	353.67	83.95	3.7	5.0194E-06	3.672E-09

ACMS OUTPUT: Conductivity parameters

P16H SITE 1 CORE 1 SPEC 1 UNITS= SI m M= 6 NR= 2 14:39:29 03-14-1990

SUSC.	DEC	INC	R95	EV	SDEV
MIN	35.11	-4.04	76.6	1.2109E-06	3.251E-11
INT	304.86	-3.60	76.5	1.4006E-06	2.040E-07
MAX	353.27	84.58	5.4	5.1234E-06	1.795E-07

ACMS OUTPUT: Conductivity parameters

P16I SITE 1 CORE 1 SPEC 1 UNITS= SI m M= 6 NR= 2 14:44:29 03-14-1990

SUSC.	DEC	INC	R95	EV	SDEV
MIN	26.96	-6.89	52.0	1.2693E-06	6.900E-08
INT	296.66	-2.62	52.1	1.3921E-06	1.272E-07
MAX	5.96	82.62	0.3	4.9199E-06	1.234E-08

ACMS OUTPUT: Conductivity parameters

P16J SITE 1 CORE 1 SPEC 1 UNITS= SI m M= 6 NR= 2 14:49:07 03-14-1990

SUSC.	DEC	INC	R95	EV	SDEV
MIN	61.14	-3.43	78.9	1.2700E-06	2.084E-08
INT	330.93	-3.51	78.9	1.3476E-06	5.433E-08
MAX	15.33	85.09	1.3	5.1168E-06	2.129E-08

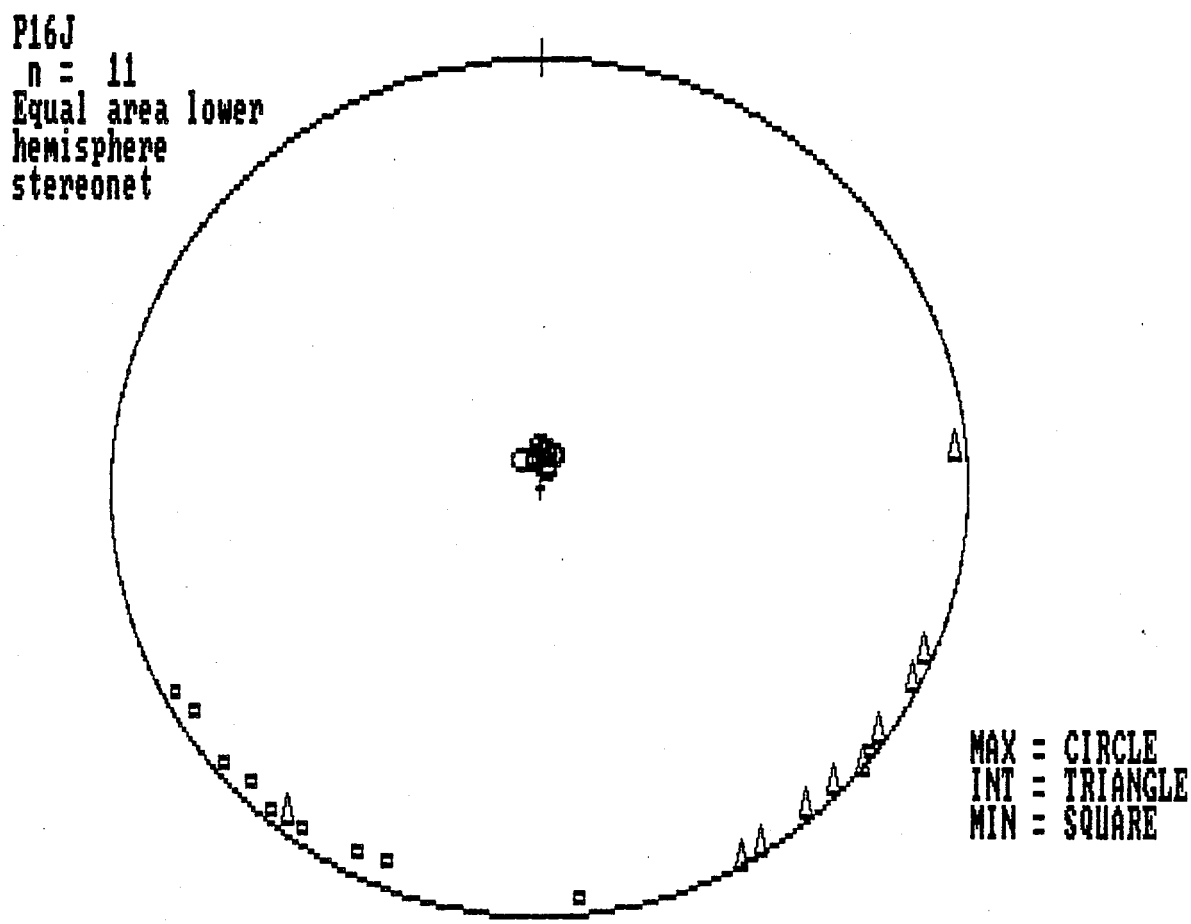

ACMS OUTPUT: Conductivity parameters

P18A SITE 1 CORE 1 SPEC 1 UNITS= SI m M= 6 NR= 2 11:28:09 03-15-1990

SUSC.	DEC	INC	R95	EV	SDEV
MIN	300.65	-7.13	45.1	7.8327E-07	2.106E-08
INT	30.90	-2.12	45.2	8.6300E-07	4.901E-08
MAX	317.35	82.56	3.2	4.6841E-06	9.150E-08

ACMS OUTPUT: Conductivity parameters

P18B SITE 1 CORE 1 SPEC 1 UNITS= SI m M= 6 NR= 2 11:33:12 03-15-1990

SUSC.	DEC	INC	R95	EV	SDEV
MIN	37.47	-4.17	7.5	5.8919E-07	7.807E-08
INT	306.88	-7.98	3.9	1.0458E-06	2.075E-07
MAX	334.78	80.98	6.9	4.7906E-06	1.221E-07

ACMS OUTPUT: Conductivity parameters

P18C SITE 1 CORE 1 SPEC 1 UNITS= SI m M= 6 NR= 2 11:37:27 03-15-1990

SUSC.	DEC	INC	R95	EV	SDEV
MIN	23.53	-2.98	48.6	6.9818E-07	1.261E-07
INT	293.24	-5.73	48.3	8.8144E-07	1.675E-07
MAX	320.82	83.53	6.8	4.9363E-06	8.453E-08

ACMS OUTPUT: Conductivity parameters

P18D SITE 1 CORE 1 SPEC 1 UNITS= SI m M= 6 NR= 2 11:41:38 03-15-1990

SUSC.	DEC	INC	R95	EV	SDEV
MIN	297.73	-5.36	17.6	5.9144E-07	5.001E-08
INT	28.17	-4.68	18.1	9.1387E-07	5.148E-08
MAX	339.09	82.88	4.6	4.7365E-06	1.402E-07

ACMS OUTPUT: Conductivity parameters

P18E SITE 1 CORE 1 SPEC 1 UNITS= SI m M= 12 NR= 2 11:49:35 03-15-1990

SUSC.	DEC	INC	R95	EV	SDEV
MIN	299.55	-7.53	87.3	7.2842E-07	3.571E-08
INT	29.57	-0.63	87.4	8.1915E-07	4.377E-08
MAX	304.40	82.45	6.1	4.7829E-06	3.747E-08

ACMS OUTPUT: Conductivity parameters

P18F SITE 1 CORE 1 SPEC 1 UNITS= SI m M= 6 NR= 2 11:54:40 03-15-1990

SUSC.	DEC	INC	R95	EV	SDEV
MIN	45.04	-1.15	59.9	6.1759E-07	1.474E-08
INT	314.91	-6.64	59.8	1.0808E-06	4.200E-07
MAX	324.78	83.26	6.2	4.8341E-06	9.072E-08

ACMS OUTPUT: Conductivity parameters

P18G SITE 1 CORE 1 SPEC 1 UNITS= SI m M= 6 NR= 2 11:59:18 03-15-1990

SUSC.	DEC	INC	R95	EV	SDEV
MIN	354.95	-6.59	61.1	7.5722E-07	9.680E-08
INT	84.67	2.24	61.1	7.7696E-07	9.647E-08
MAX	335.96	83.03	2.1	4.8470E-06	1.391E-07

ACMS OUTPUT: Conductivity parameters

P18H SITE 1 CORE 1 SPEC 1 UNITS= SI m M= 6 NR= 2 12:04:06 03-15-1990

SUSC.	DEC	INC	R95	EV	SDEV
MIN	38.82	-4.57	53.4	6.5082E-07	1.626E-07
INT	308.31	-6.42	53.4	7.3585E-07	1.943E-07
MAX	344.07	82.11	3.2	4.7029E-06	6.243E-08

ACMS OUTPUT: Conductivity parameters

P18I SITE 1 CORE 1 SPEC 1 UNITS= SI m M= 6 NR= 2 12:08:29 03-15-1990

SUSC.	DEC	INC	R95	EV	SDEV
MIN	50.25	-3.05	20.9	6.2374E-07	1.706E-08
INT	319.90	-6.70	20.9	9.1569E-07	1.089E-07
MAX	344.60	82.64	1.1	4.7176E-06	9.358E-08

ACMS OUTPUT: Conductivity parameters

P18J SITE 1 CORE 1 SPEC 1 UNITS= SI m M= 6 NR= 2 12:12:55 03-15-1990

SUSC.	DEC	INC	R95	EV	SDEV
MIN	41.25	-4.83	51.0	6.7901E-07	2.742E-08
INT	310.69	-6.68	51.2	8.7262E-07	1.635E-07
MAX	346.86	81.74	2.4	4.7689E-06	8.067E-08

P18J
n = 10
Equal area lower hemisphere stereonet

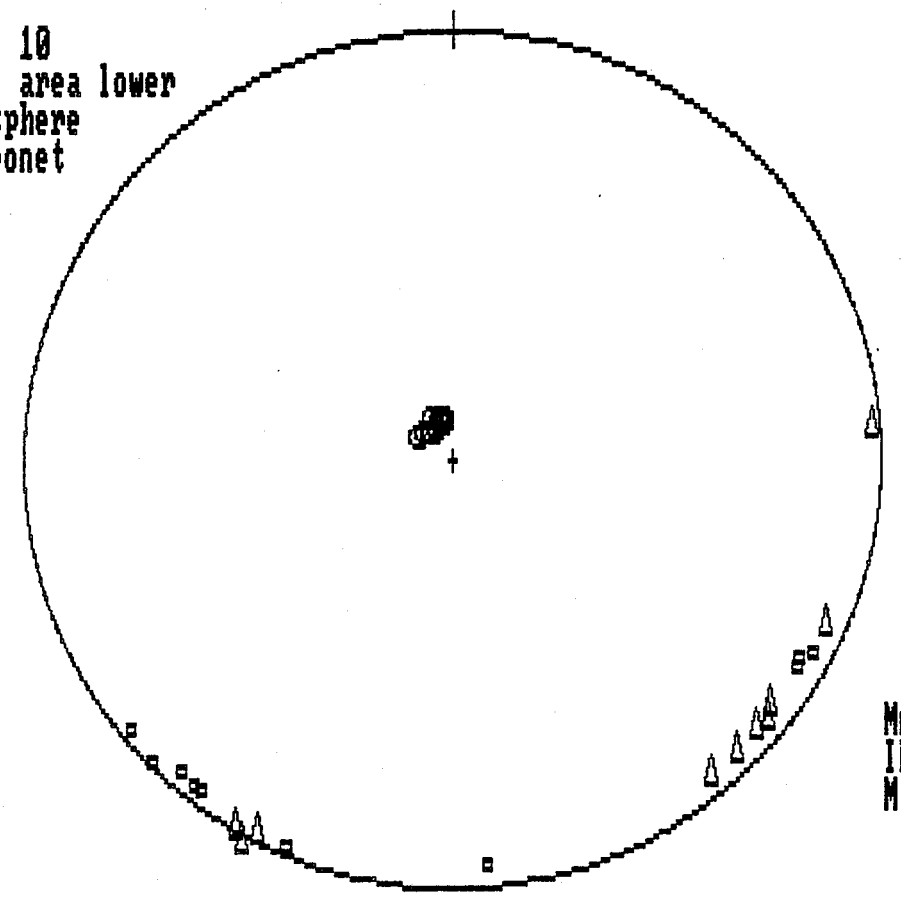

MAX = CIRCLE
INT = TRIANGLE
MIN = SQUARE

ACMS OUTPUT: Conductivity parameters

P19A SITE 1 CORE 1 SPEC 1 UNITS= SI m M= 6 NR= 2 14:00:27 03-27-1990

SUSC.	DEC	INC	R95	EV	SDEV
MIN	310.23	8.23	18.7	4.9433E-06	9.769E-08
INT	41.37	7.85	18.7	5.2852E-06	4.466E-08
MAX	354.45	-78.58	1.5	1.6083E-05	1.221E-07

ACMS OUTPUT: Conductivity parameters

P19B SITE 1 CORE 1 SPEC 1 UNITS= SI m M= 6 NR= 2 14:05:41 03-27-1990

SUSC.	DEC	INC	R95	EV	SDEV
MIN	7.16	11.99	52.0	5.0757E-06	1.050E-07
INT	276.71	2.38	52.0	5.3284E-06	2.095E-07
MAX	355.63	-77.77	2.0	1.6144E-05	2.400E-07

ACMS OUTPUT: Conductivity parameters

P19C SITE 1 CORE 1 SPEC 1 UNITS= SI m M= 6 NR= 2 14:10:34 03-27-1990

SUSC.	DEC	INC	R95	EV	SDEV
MIN	311.09	9.45	5.3	4.8810E-06	5.809E-08
INT	42.33	7.41	5.3	5.3972E-06	1.558E-07
MAX	349.84	-77.95	0.5	1.6016E-05	8.629E-10

ACMS OUTPUT: Conductivity parameters

P19D SITE 1 CORE 1 SPEC 1 UNITS= SI m M= 6 NR= 2 14:15:27 03-27-1990

SUSC.	DEC	INC	R95	EV	SDEV
MIN	26.07	10.79	12.0	5.0078E-06	8.361E-08
INT	295.09	5.17	12.0	5.3451E-06	1.091E-07
MAX	359.86	-78.01	1.4	1.6247E-05	1.619E-07

ACMS OUTPUT: Conductivity parameters

P19E SITE 1 CORE 1 SPEC 1 UNITS= SI m M= 6 NR= 2 14:20:19 03-27-1990

SUSC.	DEC	INC	R95	EV	SDEV
MIN	37.29	8.61	15.7	5.0778E-06	2.295E-09
INT	305.99	8.52	15.7	5.4672E-06	1.213E-08
MAX	351.92	-77.84	0.6	1.5866E-05	1.531E-08

ACMS OUTPUT: Conductivity parameters

P19F SITE 1 CORE 1 SPEC 1 UNITS= SI m M= 6 NR= 2 14:26:01 03-27-1990

SUSC.	DEC	INC	R95	EV	SDEV
MIN	45.27	7.57	67.6	5.1142E-06	6.784E-09
INT	314.08	9.06	67.5	5.2025E-06	7.552E-08
MAX	354.60	-78.16	1.3	1.6070E-05	1.826E-08

ACMS OUTPUT: Conductivity parameters

P19G SITE 1 CORE 1 SPEC 0 UNITS= SI m M= 6 NR= 2 14:31:12 03-27-1990

SUSC.	DEC	INC	R95	EV	SDEV
MIN	67.63	3.55	71.5	5.1474E-06	8.001E-08
INT	336.93	11.32	71.5	5.3807E-06	1.398E-07
MAX	354.77	-78.12	0.9	1.5970E-05	1.407E-07

ACMS OUTPUT: Conductivity parameters

P19H SITE 1 CORE 1 SPEC 1 UNITS= SI m M= 6 NR= 2 14:37:36 03-27-1990

SUSC.	DEC	INC	R95	EV	SDEV
MIN	333.66	10.20	78.6	5.1247E-06	7.928E-08
INT	64.54	4.98	78.6	5.3459E-06	1.328E-07
MAX	0.20	-78.63	1.9	1.6063E-05	9.367E-08

ACMS OUTPUT: Conductivity parameters

P19I SITE 1 CORE 1 SPEC 1 UNITS= SI m M= 6 NR= 2 14:42:11 03-27-1990

SUSC.	DEC	INC	R95	EV	SDEV
MIN	22.58	11.76	19.2	5.1679E-06	3.951E-08
INT	291.50	5.75	19.1	5.2095E-06	2.373E-08
MAX	355.89	-76.88	1.1	1.6214E-05	9.143E-08

ACMS OUTPUT: Conductivity parameters

P19J SITE 1 CORE 1 SPEC 1 UNITS= SI m M= 6 NR= 2 14:46:49 03-27-1990

SUSC.	DEC	INC	R95	EV	SDEV
MIN	80.08	0.60	40.7	4.9869E-06	3.713E-08
INT	350.01	11.63	40.7	5.1849E-06	7.253E-08
MAX	352.97	-78.36	1.0	1.6256E-05	1.296E-07

P19J
n = 10
Equal area lower hemisphere stereonet

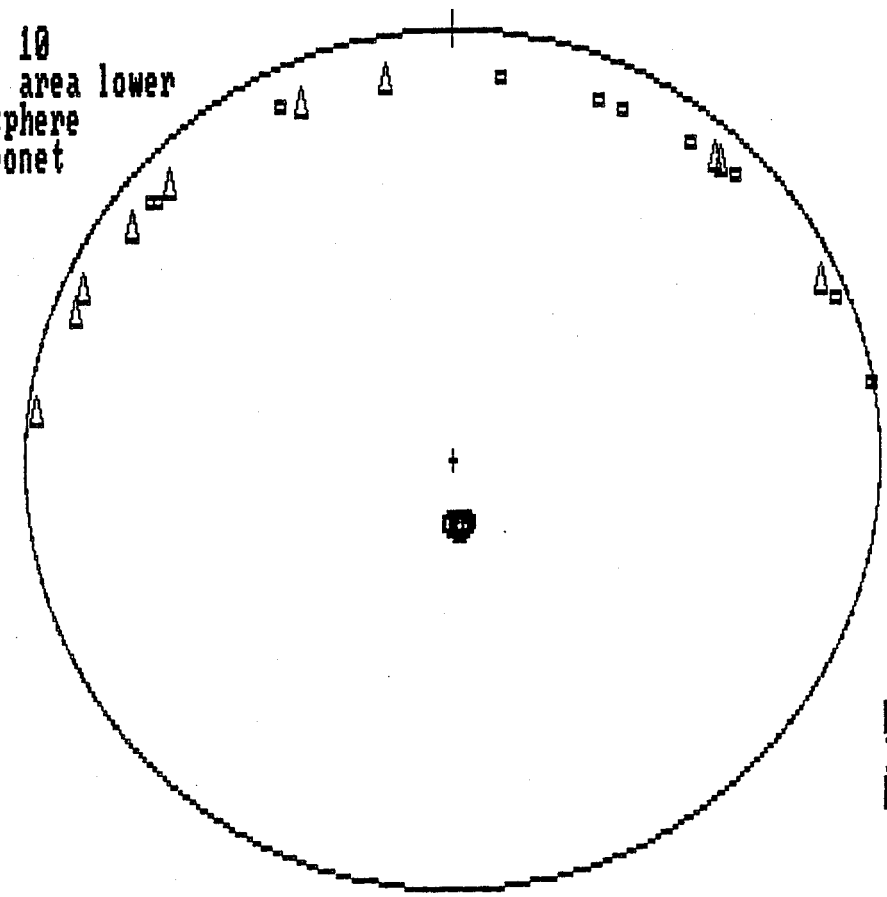

MAX = CIRCLE
INT = TRIANGLE
MIN = SQUARE

ACMS OUTPUT: Conductivity parameters

P20A SITE 1 CORE 1 SPEC 1 UNITS= SI m M= 6 NR= 2 10:56:46 04-02-1990

SUSC.	DEC	INC	R95	EV	SDEV
MIN	83.83	-0.24	53.6	1.4265E-06	7.755E-08
INT	353.80	1.56	53.6	1.6379E-06	1.402E-07
MAX	345.69	-88.42	1.9	8.6803E-06	4.889E-08

ACMS OUTPUT: Conductivity parameters

P20B SITE 1 CORE 1 SPEC 1 UNITS= SI m M= 6 NR= 2 11:01:19 04-02-1990

SUSC.	DEC	INC	R95	EV	SDEV
MIN	298.22	-1.48	49.0	1.6180E-06	9.483E-09
INT	28.18	2.13	49.0	1.7300E-06	2.156E-08
MAX	62.93	-87.40	1.1	8.8743E-06	5.580E-08

ACMS OUTPUT: Conductivity parameters

P20C SITE 1 CORE 1 SPEC 1 UNITS= SI m M= 6 NR= 2 11:05:58 04-02-1990

SUSC.	DEC	INC	R95	EV	SDEV
MIN	56.03	0.86	26.3	1.4876E-06	7.815E-08
INT	325.99	2.75	26.3	1.9458E-06	1.883E-07
MAX	343.31	-87.11	2.9	8.5854E-06	6.191E-08

ACMS OUTPUT: Conductivity parameters

P20D SITE 1 CORE 1 SPEC 1 UNITS= SI m M= 6 NR= 2 11:10:36 04-02-1990

SUSC.	DEC	INC	R95	EV	SDEV
MIN	271.75	2.74	47.4	1.4973E-06	1.266E-07
INT	358.67	1.72	46.4	1.7006E-06	8.833E-08
MAX	358.61	-88.28	3.0	8.6392E-06	9.877E-08

ACMS OUTPUT: Conductivity parameters

P20E SITE 1 CORE 1 SPEC 1 UNITS= SI m M= 6 NR= 2 11:14:57 04-02-1990

SUSC.	DEC	INC	R95	EV	SDEV
MIN	52.21	4.03	10.2	1.4995E-06	1.041E-07
INT	322.01	2.93	10.1	1.9041E-06	1.498E-07
MAX	16.08	-85.02	1.8	8.9670E-06	9.967E-08

ACMS OUTPUT: Conductivity parameters

P20F SITE 1 CORE 1 SPEC 1 UNITS= SI m M= 6 NR= 2 11:19:33 04-02-1990

SUSC.	DEC	INC	R95	EV	SDEV
MIN	63.11	2.47	4.3	1.3614E-06	1.027E-07
INT	333.00	2.45	4.6	2.0751E-06	9.148E-08
MAX	18.31	-86.52	1.4	8.8564E-06	1.224E-07

ACMS OUTPUT: Conductivity parameters

P20G SITE 1 CORE 1 SPEC 1 UNITS= SI m M= 6 NR= 2 11:24:53 04-02-1990

SUSC.	DEC	INC	R95	EV	SDEV
MIN	339.60	-0.83	70.2	1.4719E-06	1.059E-07
INT	69.28	0.05	70.4	1.5134E-06	7.045E-08
MAX	343.67	89.17	1.8	8.6388E-06	6.539E-08

ACMS OUTPUT: Conductivity parameters

P20H SITE 1 CORE 1 SPEC 1 UNITS= SI m M= 6 NR= 2 11:30:01 04-02-1990

SUSC.	DEC	INC	R95	EV	SDEV
MIN	277.07	-0.76	45.2	1.4799E-06	3.577E-08
INT	7.05	3.08	45.3	1.6752E-06	3.776E-08
MAX	20.89	-86.83	2.7	8.9108E-06	1.348E-07

ACMS OUTPUT: Conductivity parameters

P20I SITE 1 CORE 1 SPEC 1 UNITS= SI m M= 6 NR= 2 11:34:28 04-02-1990

SUSC.	DEC	INC	R95	EV	SDEV
MIN	285.59	0.75	15.5	1.2325E-06	7.152E-08
INT	15.65	4.29	15.5	1.6376E-06	5.526E-08
MAX	5.73	-85.65	1.4	8.7663E-06	2.359E-07

ACMS OUTPUT: Conductivity parameters

P20J SITE 1 CORE 1 SPEC 1 UNITS= SI m M= 6 NR= 2 11:38:57 04-02-1990

SUSC.	DEC	INC	R95	EV	SDEV
MIN	60.86	0.88	35.4	1.4172E-06	6.036E-08
INT	330.86	0.36	35.5	1.6527E-06	9.142E-08
MAX	37.33	-89.05	1.5	8.6679E-06	2.411E-07

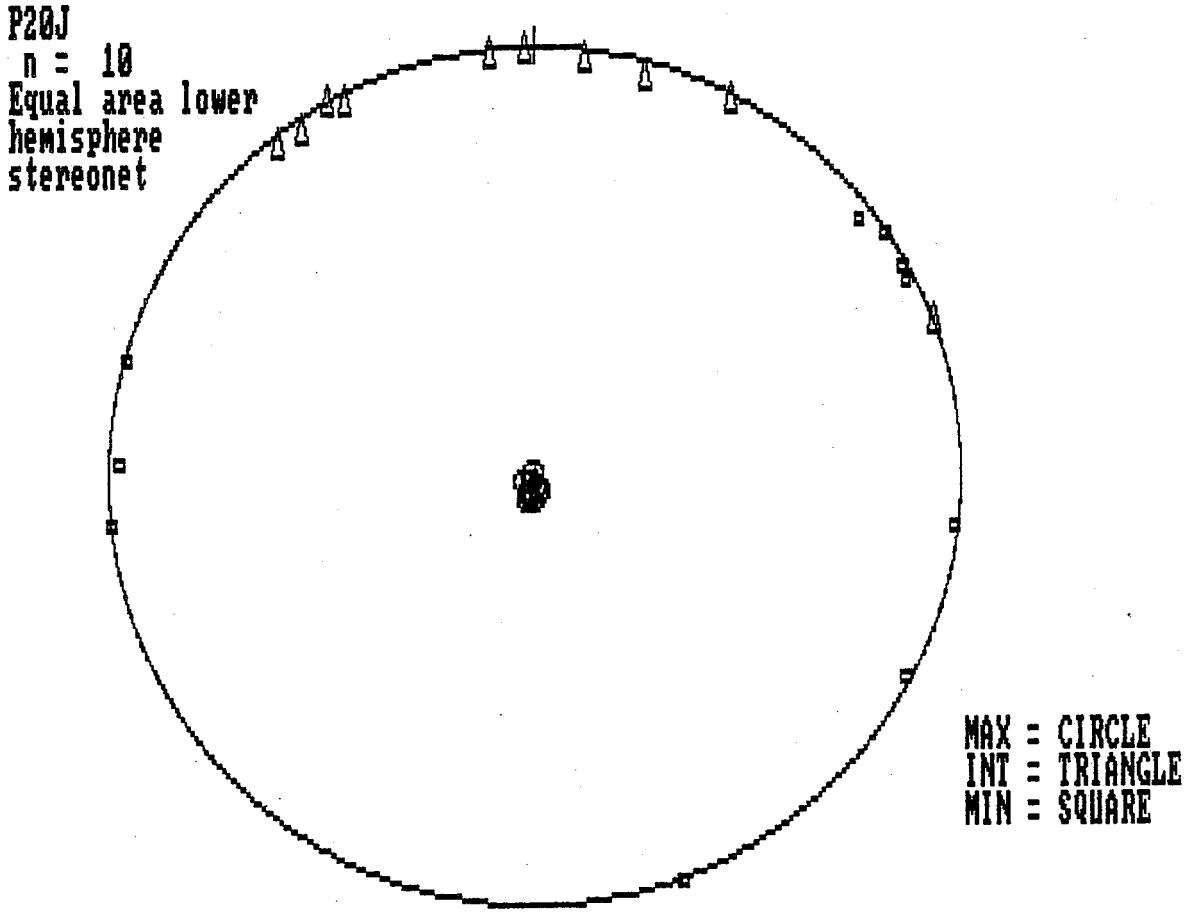

ACMS OUTPUT: Conductivity parameters

P21A SITE 1 CORE 1 SPEC 1 UNITS= SI m M= 6 NR= 2 10:15:58 04-12-1990

SUSC.	DEC	INC	R95	EV	SDEV
MIN	278.44	3.06	9.2	2.1239E-06	9.403E-09
INT	8.27	-3.58	9.5	2.2571E-06	2.195E-08
MAX	48.86	85.29	2.4	6.3164E-06	8.952E-08

ACMS OUTPUT: Conductivity parameters

P21B SITE 1 CORE 1 SPEC 1 UNITS= SI m M= 6 NR= 2 10:20:06 04-12-1990

SUSC.	DEC	INC	R95	EV	SDEV
MIN	290.95	1.04	29.0	1.9768E-06	1.394E-07
INT	20.93	-1.65	29.1	2.2983E-06	4.766E-08
MAX	53.17	88.05	2.7	6.3295E-06	1.294E-07

ACMS OUTPUT: Conductivity parameters

P21C SITE 1 CORE 1 SPEC 1 UNITS= SI m M= 6 NR= 2 10:24:50 04-12-1990

SUSC.	DEC	INC	R95	EV	SDEV
MIN	271.72	3.99	8.9	1.9757E-06	1.458E-07
INT	1.42	-4.73	9.0	2.4150E-06	8.718E-08
MAX	41.66	83.81	1.3	6.0934E-06	1.424E-08

ACMS OUTPUT: Conductivity parameters

P21D SITE 1 CORE 1 SPEC 1 UNITS= SI m M= 6 NR= 2 10:29:21 04-12-1990

SUSC.	DEC	INC	R95	EV	SDEV
MIN	296.77	0.14	39.1	2.1810E-06	8.401E-08
INT	26.78	-0.35	39.1	2.3788E-06	5.969E-08
MAX	41.96	89.62	6.5	6.1981E-06	1.965E-07

ACMS OUTPUT: Conductivity parameters

P21E SITE 1 CORE 1 SPEC 1 UNITS= SI m M= 6 NR= 2 10:34:03 04-12-1990

SUSC.	DEC	INC	R95	EV	SDEV
MIN	52.56	-2.96	35.1	2.1182E-06	6.568E-08
INT	322.51	-1.10	35.2	2.4129E-06	2.131E-07
MAX	31.93	86.84	4.7	6.2524E-06	8.754E-08

ACMS OUTPUT: Conductivity parameters

P21F SITE 1 CORE 1 SPEC 1 UNITS= SI m M= 6 NR= 2 10:39:12 04-12-1990

SUSC.	DEC	INC	R95	EV	SDEV
MIN	78.47	-6.45	13.4	1.9482E-06	6.647E-08
INT	348.27	-1.85	13.7	2.3905E-06	3.181E-08
MAX	62.34	83.28	3.3	6.2423E-06	1.916E-07

ACMS OUTPUT: Conductivity parameters

P21G SITE 1 CORE 1 SPEC 1 UNITS= SI m M= 6 NR= 2 10:46:00 04-12-1990

SUSC.	DEC	INC	R95	EV	SDEV
MIN	74.69	-5.02	19.1	2.0078E-06	1.547E-07
INT	344.73	0.51	18.9	2.5435E-06	1.217E-07
MAX	80.66	84.95	3.3	6.1683E-06	2.642E-08

ACMS OUTPUT: Conductivity parameters

P21H SITE 1 CORE 1 SPEC 1 UNITS= SI m M= 6 NR= 2 10:51:03 04-12-1990

SUSC.	DEC	INC	R95	EV	SDEV
MIN	66.36	-3.70	9.0	2.1285E-06	1.698E-07
INT	336.32	-0.03	7.2	2.7018E-06	6.590E-09
MAX	67.51	86.30	5.4	6.1025E-06	1.342E-07

ACMS OUTPUT: Conductivity parameters

P21I SITE 1 CORE 1 SPEC 1 UNITS= SI m M= 6 NR= 2 10:55:04 04-12-1990

SUSC.	DEC	INC	R95	EV	SDEV
MIN	280.41	3.68	7.3	2.0476E-06	1.039E-07
INT	10.11	-4.63	7.3	2.4152E-06	6.003E-08
MAX	48.72	84.08	1.6	6.1739E-06	1.127E-07

ACMS OUTPUT: Conductivity parameters

P21J SITE 1 CORE 1 SPEC 1 UNITS= SI m M= 6 NR= 2 10:59:07 04-12-1990

SUSC.	DEC	INC	R95	EV	SDEV
MIN	83.15	-6.29	25.9	2.1412E-06	1.087E-07
INT	352.53	-5.55	25.9	2.2849E-06	1.187E-07
MAX	41.41	81.60	3.4	6.1568E-06	1.229E-07

P21J
n = 10
Equal area lower hemisphere stereonet

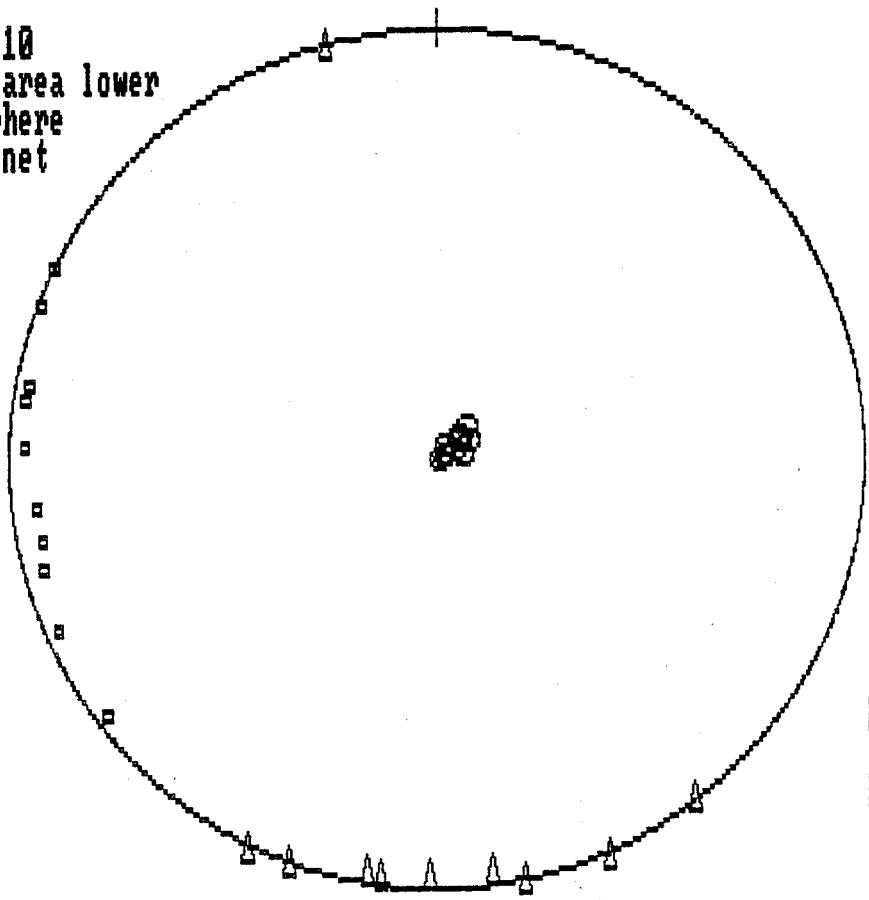

MAX = CIRCLE
INT = TRIANGLE
MIN = SQUARE

ACMS OUTPUT: Conductivity parameters

P22A SITE 1 CORE 1 SPEC 1 UNITS= SI m M= 6 NR= 2 11:11:20 04-10-1990

SUSC.	DEC	INC	R95	EV	SDEV
MIN	313.55	-5.62	6.8	2.2355E-06	2.736E-08
INT	43.66	-1.22	6.8	3.0357E-06	4.685E-08
MAX	325.96	84.24	1.0	1.2925E-05	1.157E-07

ACMS OUTPUT: Conductivity parameters

P22B SITE 1 CORE 1 SPEC 1 UNITS= SI m M= 6 NR= 2 11:15:44 04-10-1990

SUSC.	DEC	INC	R95	EV	SDEV
MIN	321.54	-5.52	14.7	2.4400E-06	7.312E-08
INT	51.38	1.68	14.6	3.0287E-06	1.048E-07
MAX	304.50	84.23	1.0	1.3226E-05	2.133E-08

ACMS OUTPUT: Conductivity parameters

P22C SITE 1 CORE 1 SPEC 1 UNITS= SI m M= 6 NR= 2 11:20:16 04-10-1990

SUSC.	DEC	INC	R95	EV	SDEV
MIN	37.64	-1.57	8.7	2.6766E-06	3.021E-08
INT	307.49	-5.82	8.9	3.0396E-06	1.616E-09
MAX	322.66	83.97	2.0	1.2901E-05	5.264E-09

ACMS OUTPUT: Conductivity parameters

P22D SITE 1 CORE 1 SPEC 1 UNITS= SI m M= 6 NR= 2 11:24:43 04-10-1990

SUSC.	DEC	INC	R95	EV	SDEV
MIN	43.58	-2.00	19.9	2.6099E-06	7.988E-08
INT	313.39	-5.69	19.9	3.0220E-06	4.563E-08
MAX	332.82	83.97	0.7	1.2934E-05	6.367E-08

ACMS OUTPUT: Conductivity parameters

P22E SITE 1 CORE 1 SPEC 1 UNITS= SI m M= 6 NR= 2 11:29:16 04-10-1990

SUSC.	DEC	INC	R95	EV	SDEV
MIN	70.02	1.34	60.0	2.7601E-06	9.738E-08
INT	340.13	-5.43	60.0	2.9725E-06	2.353E-07
MAX	326.24	84.41	0.7	1.2953E-05	8.417E-08

ACMS OUTPUT: Conductivity parameters

P22F SITE 1 CORE 1 SPEC 1 UNITS= SI m M= 6 NR= 2 11:33:37 04-10-1990

SUSC.	DEC	INC	R95	EV	SDEV
MIN	88.56	3.32	54.6	2.6967E-06	1.531E-07
INT	358.23	-4.08	54.8	2.7896E-06	1.946E-07
MAX	319.28	84.76	1.9	1.3159E-05	5.737E-08

ACMS OUTPUT: Conductivity parameters

P22G SITE 1 CORE 1 SPEC 1 UNITS= SI m M= 6 NR= 2 11:38:09 04-10-1990

SUSC.	DEC	INC	R95	EV	SDEV
MIN	47.70	0.62	62.8	2.6055E-06	5.064E-08
INT	317.74	-5.85	62.8	2.9182E-06	2.342E-07
MAX	311.68	84.12	1.3	1.3068E-05	1.529E-07

ACMS OUTPUT: Conductivity parameters

P22H SITE 1 CORE 1 SPEC 1 UNITS= SI m M= 6 NR= 2 11:42:46 04-10-1990

SUSC.	DEC	INC	R95	EV	SDEV
MIN	85.60	3.14	70.0	2.7849E-06	3.032E-08
INT	355.71	-3.68	70.1	2.9010E-06	1.336E-07
MAX	315.24	85.17	1.3	1.2839E-05	8.978E-08

ACMS OUTPUT: Conductivity parameters

P22I SITE 1 CORE 1 SPEC 1 UNITS= SI m M= 6 NR= 2 11:46:53 04-10-1990

SUSC.	DEC	INC	R95	EV	SDEV
MIN	326.87	-5.64	86.6	2.7662E-06	1.824E-07
INT	57.14	0.38	86.9	2.8276E-06	1.203E-07
MAX	323.13	84.35	0.8	1.3109E-05	9.397E-08

ACMS OUTPUT: Conductivity parameters

P22J SITE 1 CORE 1 SPEC 1 UNITS= SI m M= 6 NR= 2 11:50:52 04-10-1990

SUSC.	DEC	INC	R95	EV	SDEV
MIN	80.02	1.72	29.8	2.6813E-06	3.731E-08
INT	350.15	-5.42	29.8	2.8730E-06	4.542E-08
MAX	332.52	84.32	1.6	1.2989E-05	1.199E-07

ACMS OUTPUT: Conductivity parameters

P23A SITE 1 CORE 1 SPEC 1 UNITS= SI m M= 6 NR= 2 10:31:59 04-24-1990

SUSC.	DEC	INC	R95	EV	SDEV
MIN	29.23	1.31	77.2	1.2674E-06	6.066E-08
INT	299.29	-3.09	77.2	1.4838E-06	2.744E-07
MAX	276.31	86.64	1.7	9.6535E-06	1.842E-07

ACMS OUTPUT: Conductivity parameters

P23B SITE 1 CORE 1 SPEC 1 UNITS= SI m M= 6 NR= 2 10:38:18 04-24-1990

SUSC.	DEC	INC	R95	EV	SDEV
MIN	15.37	1.60	26.6	1.4909E-06	2.320E-08
INT	285.46	-3.27	26.6	1.6958E-06	1.076E-07
MAX	79.37	-86.35	1.8	9.5126E-06	6.520E-08

ACMS OUTPUT: Conductivity parameters

P23C SITE 1 CORE 1 SPEC 1 UNITS= SI m M= 6 NR= 2 10:42:54 04-24-1990

SUSC.	DEC	INC	R95	EV	SDEV
MIN	44.48	2.80	0.7	1.3982E-06	2.946E-09
INT	314.52	-0.95	1.1	1.7569E-06	1.012E-08
MAX	63.45	-87.04	0.8	9.5062E-06	3.359E-08

ACMS OUTPUT: Conductivity parameters

P23D SITE 1 CORE 1 SPEC 1 UNITS= SI m M= 6 NR= 2 10:47:20 04-24-1990

SUSC.	DEC	INC	R95	EV	SDEV
MIN	80.31	2.26	56.1	1.5089E-06	4.571E-08
INT	350.22	1.97	56.3	1.6572E-06	6.002E-08
MAX	39.12	-87.00	2.5	9.6488E-06	2.378E-07

ACMS OUTPUT: Conductivity parameters

P23E SITE 1 CORE 1 SPEC 1 UNITS= SI m M= 6 NR= 2 10:51:37 04-24-1990

SUSC.	DEC	INC	R95	EV	SDEV
MIN	26.15	3.02	25.2	1.3775E-06	3.980E-08
INT	296.25	-2.07	25.2	1.4903E-06	9.331E-08
MAX	60.67	-86.34	0.4	9.5694E-06	7.385E-08

ACMS OUTPUT: Conductivity parameters

P23F SITE 1 CORE 1 SPEC 1 UNITS= SI m M= 6 NR= 2 10:56:12 04-24-1990

SUSC.	DEC	INC	R95	EV	SDEV
MIN	62.82	2.69	10.5	1.4162E-06	8.094E-09
INT	332.80	0.68	10.5	1.6857E-06	4.113E-08
MAX	48.31	-87.23	1.2	9.5689E-06	3.852E-08

ACMS OUTPUT: Conductivity parameters

P23G SITE 1 CORE 1 SPEC 1 UNITS= SI m M= 6 NR= 2 11:00:28 04-24-1990

SUSC.	DEC	INC	R95	EV	SDEV
MIN	52.98	3.34	57.2	1.4629E-06	2.949E-08
INT	322.94	-0.77	57.2	1.5128E-06	4.324E-08
MAX	65.98	-86.57	1.7	9.6926E-06	3.003E-08

ACMS OUTPUT: Conductivity parameters

P23H SITE 1 CORE 1 SPEC 1 UNITS= SI m M= 6 NR= 2 11:05:28 04-24-1990

SUSC.	DEC	INC	R95	EV	SDEV
MIN	280.57	-2.28	36.1	1.2478E-06	4.886E-08
INT	10.58	0.51	36.2	1.4277E-06	1.426E-07
MAX	87.57	-87.67	1.2	9.5592E-06	1.193E-07

ACMS OUTPUT: Conductivity parameters

P23I SITE 1 CORE 1 SPEC 1 UNITS= SI m M= 6 NR= 2 11:10:09 04-24-1990

SUSC.	DEC	INC	R95	EV	SDEV
MIN	34.41	1.49	50.9	1.3055E-06	1.046E-09
INT	304.43	-1.42	51.0	1.3843E-06	4.413E-08
MAX	78.14	-87.94	3.2	9.3239E-06	1.532E-08

ACMS OUTPUT: Conductivity parameters

P23J SITE 1 CORE 1 SPEC 1 UNITS= SI m M= 6 NR= 2 11:14:29 04-24-1990

SUSC.	DEC	INC	R95	EV	SDEV
MIN	86.61	1.79	55.9	1.3775E-06	7.880E-08
INT	356.54	0.32	55.9	1.4347E-06	1.146E-07
MAX	75.77	-88.18	1.4	9.4825E-06	6.596E-08

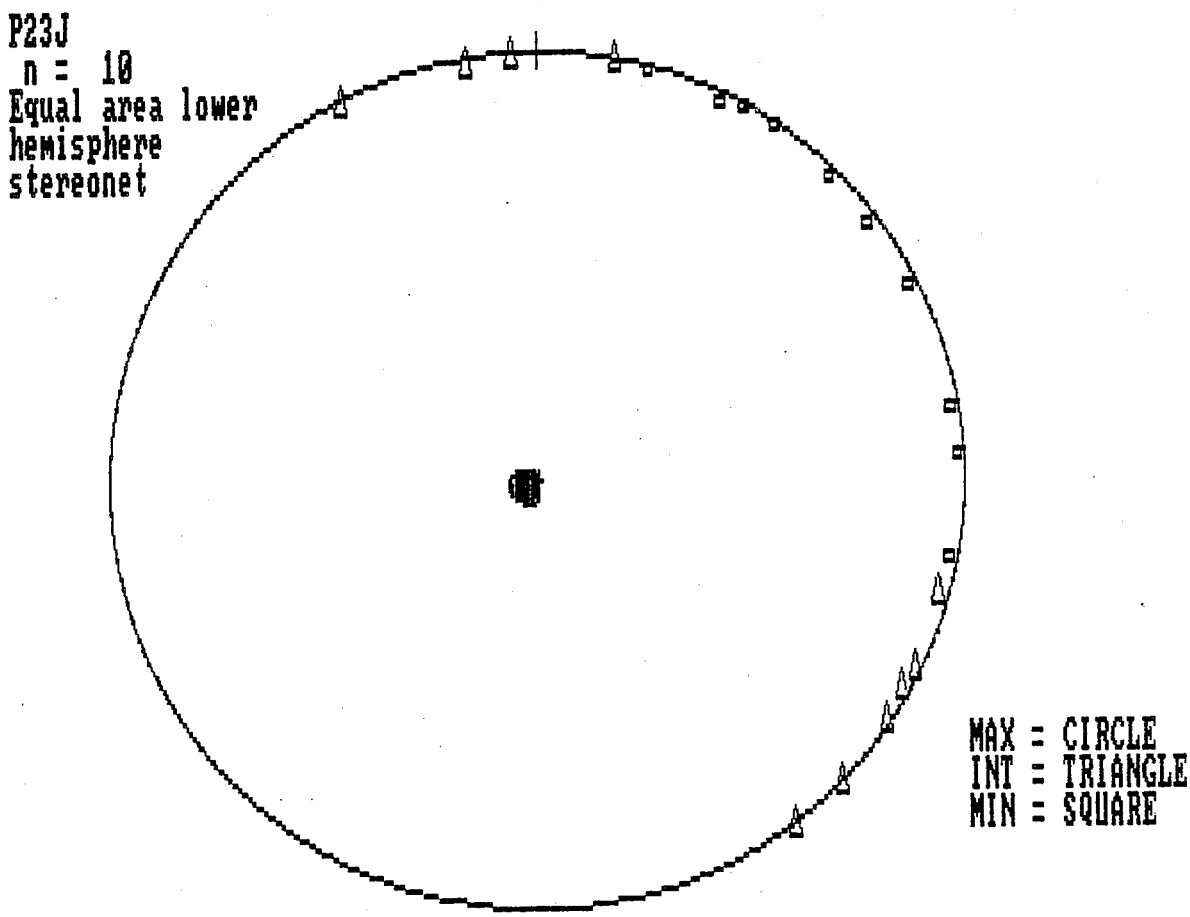

ACMS OUTPUT: Conductivity parameters

P24A SITE 1 CORE 1 SPEC 1 UNITS= SI m M= 6 NR= 2 12:40:44 04-25-1990

SUSC.	DEC	INC	R95	EV	SDEV
MIN	302.54	2.14	60.2	1.5016E-06	2.093E-07
INT	32.67	3.44	58.9	1.7507E-06	2.629E-08
MAX	0.73	-85.95	18.3	2.5003E-06	1.655E-07

ACMS OUTPUT: Conductivity parameters

P24B SITE 1 CORE 1 SPEC 1 UNITS= SI m M= 6 NR= 2 12:45:26 04-25-1990

SUSC.	DEC	INC	R95	EV	SDEV
MIN	315.16	-8.28	51.3	1.4068E-06	2.748E-07
INT	46.27	-7.56	51.5	1.6966E-06	5.257E-08
MAX	358.14	78.76	6.2	2.6336E-06	6.133E-08

ACMS OUTPUT: Conductivity parameters

P24C SITE 1 CORE 1 SPEC 1 UNITS= SI m M= 6 NR= 2 12:49:48 04-25-1990

SUSC.	DEC	INC	R95	EV	SDEV
MIN	17.18	4.80	19.0	1.5453E-06	1.009E-07
INT	287.60	-4.88	18.9	1.7280E-06	5.796E-08
MAX	62.85	-83.14	3.2	2.7146E-06	1.948E-07

ACMS OUTPUT: Conductivity parameters

P24D SITE 1 CORE 1 SPEC 1 UNITS= SI m M= 6 NR= 2 12:54:03 04-25-1990

SUSC.	DEC	INC	R95	EV	SDEV
MIN	336.72	0.76	61.9	1.4754E-06	1.518E-07
INT	66.83	8.79	61.2	1.6278E-06	2.621E-09
MAX	61.85	-81.17	11.8	2.6695E-06	1.108E-08

ACMS OUTPUT: Conductivity parameters

P24E SITE 1 CORE 1 SPEC 1 UNITS= SI m M= 6 NR= 2 12:58:10 04-25-1990

SUSC.	DEC	INC	R95	EV	SDEV
MIN	335.02	-1.76	12.6	1.4344E-06	9.018E-08
INT	65.08	-1.92	15.7	1.6704E-06	2.784E-08
MAX	22.65	87.39	9.5	2.6697E-06	5.592E-08

ACMS OUTPUT: Conductivity parameters

P24F SITE 1 CORE 1 SPEC 1 UNITS= SI m M= 6 NR= 2 13:02:13 04-25-1990

SUSC.	DEC	INC	R95	EV	SDEV
MIN	303.22	3.74	6.0	1.2243E-06	2.237E-07
INT	33.56	5.18	1.2	1.7228E-06	6.244E-08
MAX	357.59	-83.60	5.9	2.7099E-06	1.282E-07

ACMS OUTPUT: Conductivity parameters

P24G SITE 1 CORE 1 SPEC 1 UNITS= SI m M= 6 NR= 2 13:08:16 04-25-1990

SUSC.	DEC	INC	R95	EV	SDEV
MIN	348.98	-12.59	72.7	1.4249E-06	7.876E-08
INT	80.41	-6.38	72.8	1.5754E-06	5.803E-08
MAX	16.71	75.83	3.8	2.4623E-06	8.439E-08

ACMS OUTPUT: Conductivity parameters

P24H SITE 1 CORE 1 SPEC 1 UNITS= SI m M= 6 NR= 2 13:17:29 04-25-1990

SUSC.	DEC	INC	R95	EV	SDEV
MIN	316.93	8.35	33.8	1.4075E-06	2.877E-07
INT	46.22	-4.82	29.7	1.6419E-06	8.054E-08
MAX	286.50	-80.34	16.9	2.6454E-06	1.687E-08

ACMS OUTPUT: Conductivity parameters

P24I SITE 1 CORE 1 SPEC 1 UNITS= SI m M= 6 NR= 2 13:21:53 04-25-1990

SUSC.	DEC	INC	R95	EV	SDEV
MIN	287.80	3.99	43.4	1.4142E-06	1.876E-08
INT	17.61	-2.81	49.0	1.5954E-06	3.253E-08
MAX	72.52	85.12	23.7	2.5051E-06	2.362E-07

ACMS OUTPUT: Conductivity parameters

P24J SITE 1 CORE 1 SPEC 1 UNITS= SI m M= 12 NR= 2 13:29:34 04-25-1990

SUSC.	DEC	INC	R95	EV	SDEV
MIN	313.54	-2.74	25.9	1.3502E-06	1.432E-07
INT	43.74	-4.09	28.7	1.7646E-06	8.948E-08
MAX	9.78	85.07	13.0	2.6165E-06	2.090E-08

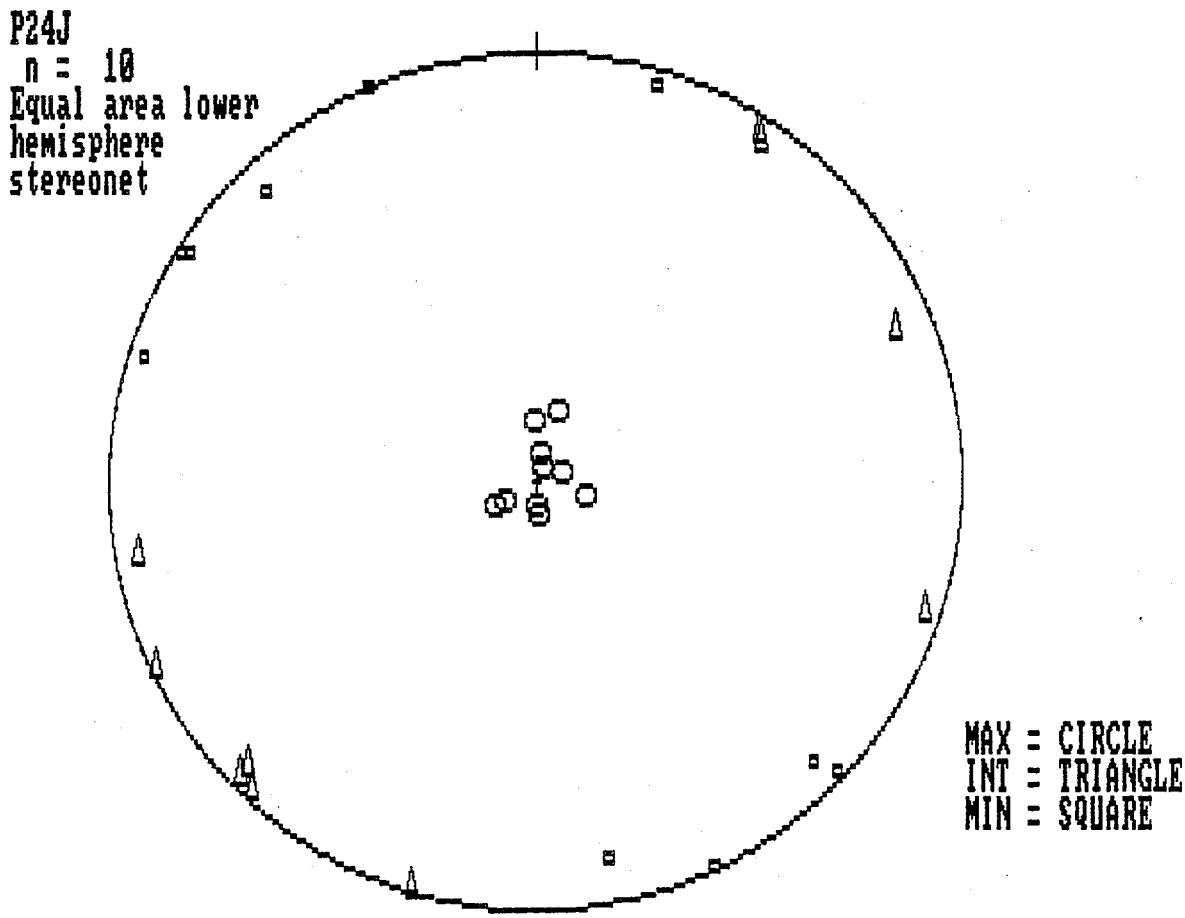

ACMS OUTPUT: Conductivity parameters

P25A SITE 1 CORE 1 SPEC 1 UNITS= SI m M= 6 NR= 2 11:02:42 04-26-1990

SUSC.	DEC	INC	R95	EV	SDEV
MIN	59.22	11.28	60.1	1.4072E-06	3.945E-08
INT	327.55	8.32	61.2	1.4681E-06	4.112E-08
MAX	21.87	-75.92	23.7	2.0527E-06	4.989E-08

ACMS OUTPUT: Conductivity parameters

P25A SITE 1 CORE 1 SPEC 1 UNITS= SI m M= 6 NR= 2 11:07:35 04-26-1990

SUSC.	DEC	INC	R95	EV	SDEV
MIN	38.58	9.06	60.7	1.2176E-06	3.409E-08
INT	312.33	-22.29	62.6	1.6119E-06	3.258E-07
MAX	287.85	65.75	15.6	2.0239E-06	2.284E-09

ACMS OUTPUT: Conductivity parameters

P25B SITE 1 CORE 1 SPEC 1 UNITS= SI m M= 6 NR= 2 11:11:59 04-26-1990

SUSC.	DEC	INC	R95	EV	SDEV
MIN	291.53	28.46	12.7	1.1053E-06	5.941E-08
INT	7.77	-23.70	21.9	1.3909E-06	1.904E-07
MAX	64.37	51.44	18.0	1.9302E-06	4.910E-08

ACMS OUTPUT: Conductivity parameters

P25C SITE 1 CORE 1 SPEC 1 UNITS= SI m M= 6 NR= 2 11:16:12 04-26-1990

SUSC.	DEC	INC	R95	EV	SDEV
MIN	20.03	13.34	54.0	1.2854E-06	5.604E-09
INT	292.98	-12.25	54.0	1.5758E-06	1.920E-07
MAX	64.10	-71.73	9.2	2.0676E-06	7.999E-08

ACMS OUTPUT: Conductivity parameters

P25D SITE 1 CORE 1 SPEC 1 UNITS= SI m M= 6 NR= 2 11:20:58 04-26-1990

SUSC.	DEC	INC	R95	EV	SDEV
MIN	301.06	5.62	79.6	1.2866E-06	1.368E-07
INT	32.70	16.20	81.7	1.5260E-06	3.810E-08
MAX	12.53	-72.81	32.9	2.0327E-06	7.062E-08

ACMS OUTPUT: Conductivity parameters

P25E SITE 1 CORE 1 SPEC 1 UNITS= SI m M= 6 NR= 2 11:25:22 04-26-1990

SUSC.	DEC	INC	R95	EV	SDEV
MIN	313.68	5.71	25.2	1.0111E-06	1.131E-07
INT	43.97	2.94	27.0	1.4655E-06	2.454E-08
MAX	341.13	-83.57	10.4	1.8883E-06	1.017E-08

Very poor data.
Weak deformation and small sample size are factors!

P25E
n = 6
Equal area lower hemisphere stereonet

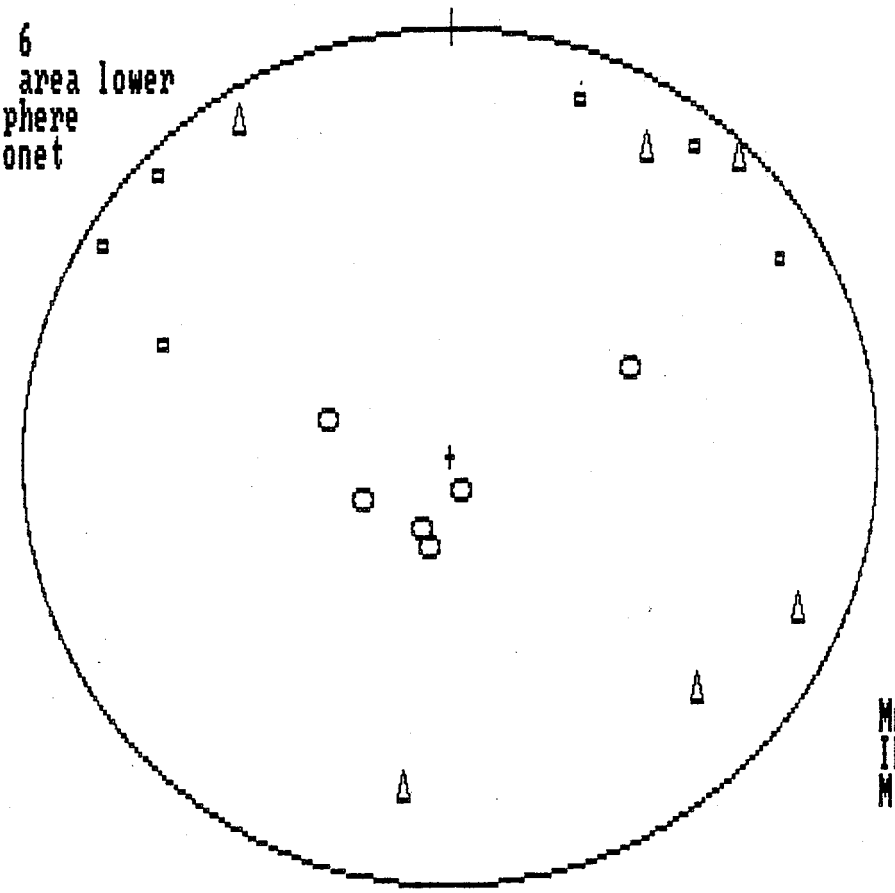

MAX = CIRCLE
INT = TRIANGLE
MIN = SQUARE

ACMS OUTPUT: Conductivity parameters

P026 SITE 1 CORE 1 SPEC 1 UNITS= SI m M= 6 NR= 2 11:49:31 05-01-1990

SUSC.	DEC	INC	R95	EV	SDEV
MIN	278.96	1.81	31.6	8.7307E-07	4.860E-08
INT	8.81	-4.98	31.6	1.0571E-06	2.917E-08
MAX	28.82	84.70	4.8	3.2720E-06	1.081E-08

ACMS OUTPUT: Conductivity parameters

P026 SITE 1 CORE 1 SPEC 2 UNITS= SI m M= 6 NR= 2 11:53:19 05-01-1990

SUSC.	DEC	INC	R95	EV	SDEV
MIN	19.83	1.65	37.4	1.0622E-06	7.309E-08
INT	289.83	0.27	37.5	1.2558E-06	5.707E-09
MAX	9.65	-88.33	3.1	3.2671E-06	7.797E-08

ACMS OUTPUT: Conductivity parameters

P026 SITE 1 CORE 1 SPEC 3 UNITS= SI m M= 6 NR= 2 11:57:08 05-01-1990

SUSC.	DEC	INC	R95	EV	SDEV
MIN	325.36	-5.18	25.5	5.7521E-07	2.013E-07
INT	56.18	-8.96	25.6	9.9984E-07	1.300E-08
MAX	25.68	79.63	2.8	3.3364E-06	7.256E-08

ACMS OUTPUT: Conductivity parameters

P026 SITE 1 CORE 1 SPEC 4 UNITS= SI m M= 6 NR= 2 12:01:23 05-01-1990

SUSC.	DEC	INC	R95	EV	SDEV
MIN	40.68	-13.14	17.5	8.0361E-07	9.956E-09
INT	310.55	-0.66	17.5	1.0902E-06	2.081E-09
MAX	37.67	76.85	0.6	3.1934E-06	5.050E-08

ACMS OUTPUT: Conductivity parameters

P026 SITE 1 CORE 1 SPEC 5 UNITS= SI m M= 6 NR= 2 12:05:53 05-01-1990

SUSC.	DEC	INC	R95	EV	SDEV
MIN	311.17	0.32	37.3	7.4689E-07	1.226E-07
INT	41.15	-4.75	38.7	1.0694E-06	8.142E-08
MAX	44.94	85.24	11.6	3.6114E-06	5.305E-08

ACMS OUTPUT: Conductivity parameters

P026 SITE 1 CORE 1 SPEC 6 UNITS= SI m M= 6 NR= 2 12:10:20 05-01-1990

SUSC.	DEC	INC	R95	EV	SDEV
MIN	3.50	-3.64	53.6	9.8551E-07	1.384E-07
INT	273.38	-2.49	53.5	1.0551E-06	1.478E-07
MAX	329.00	85.59	4.0	3.4411E-06	2.093E-08

ACMS OUTPUT: Conductivity parameters

P026 SITE 1 CORE 1 SPEC 7 UNITS= SI m M= 6 NR= 2 12:14:24 05-01-1990

SUSC.	DEC	INC	R95	EV	SDEV
MIN	49.22	-4.89	16.5	9.2373E-07	7.490E-08
INT	318.83	-4.60	16.5	1.0061E-06	6.257E-08
MAX	5.73	83.28	3.3	3.4596E-06	2.388E-09

ACMS OUTPUT: Conductivity parameters

PO26 SITE 1 CORE 1 SPEC 8 UNITS= SI m M= 6 NR= 2 12:19:30 05-01-1990

SUSC.	DEC	INC	R95	EV	SDEV
MIN	39.47	-5.33	53.7	9.1237E-07	1.465E-08
INT	309.26	-2.31	53.6	1.0264E-06	6.610E-08
MAX	15.91	84.19	2.4	3.5982E-06	4.348E-08

ACMS OUTPUT: Conductivity parameters

PO26 SITE 1 CORE 1 SPEC 9 UNITS= SI m M= 6 NR= 2 12:23:29 05-01-1990

SUSC.	DEC	INC	R95	EV	SDEV
MIN	322.31	-3.33	59.5	7.2456E-07	2.557E-07
INT	52.90	-9.93	59.7	1.0565E-06	5.424E-08
MAX	34.01	79.52	4.8	3.3440E-06	8.084E-08

ACMS OUTPUT: Conductivity parameters

PO26 SITE 1 CORE 1 SPEC 10 UNITS= SI m M= 6 NR= 2 12:27:41 05-01-1990

SUSC.	DEC	INC	R95	EV	SDEV
MIN	295.92	0.12	81.8	7.5019E-07	1.541E-07
INT	25.95	-3.88	81.9	9.8436E-07	7.510E-08
MAX	26.99	86.11	5.9	3.5333E-06	4.549E-08

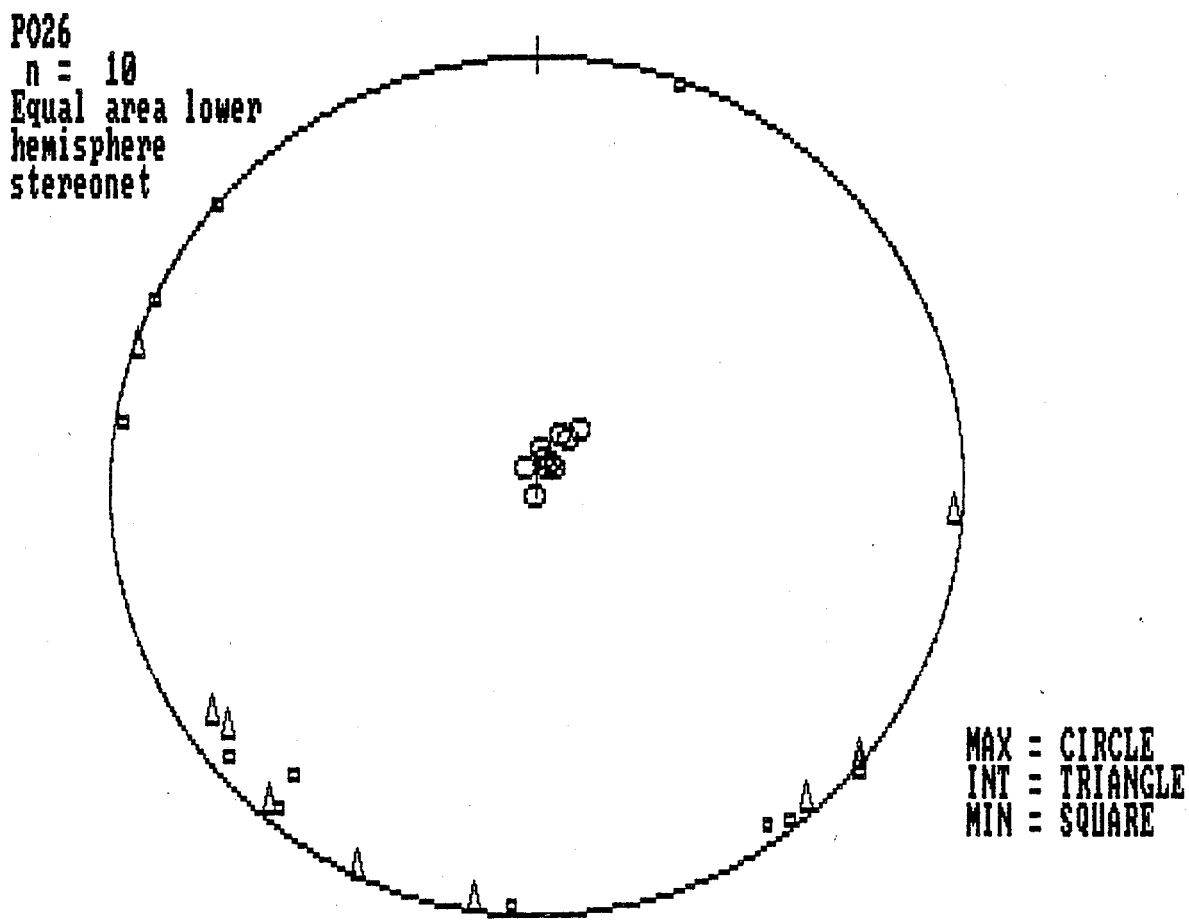

ACMS OUTPUT: Conductivity parameters

P027 SITE 1 CORE 1 SPEC 1 UNITS= SI m M= 6 NR= 2 09:17:42 05-02-1990

SUSC.	DEC	INC	R95	EV	SDEV
MIN	48.45	-6.15	8.8	1.3635E-06	1.382E-07
INT	319.24	7.28	8.6	1.7343E-06	2.916E-08
MAX	278.65	-80.45	1.7	2.7744E-06	1.473E-08

ACMS OUTPUT: Conductivity parameters

P027 SITE 1 CORE 1 SPEC 2 UNITS= SI m M= 6 NR= 2 09:22:04 05-02-1990

SUSC.	DEC	INC	R95	EV	SDEV
MIN	325.87	-7.76	50.1	1.3108E-06	2.273E-07
INT	56.63	-5.55	48.7	1.6599E-06	6.360E-08
MAX	1.87	80.44	13.6	2.7717E-06	1.131E-07

ACMS OUTPUT: Conductivity parameters

P027 SITE 1 CORE 1 SPEC 3 UNITS= SI m M= 6 NR= 2 09:26:59 05-02-1990

SUSC.	DEC	INC	R95	EV	SDEV
MIN	37.15	-6.72	13.3	1.4494E-06	2.841E-08
INT	307.96	6.86	8.3	1.7207E-06	1.128E-07
MAX	83.17	80.38	10.5	2.7044E-06	9.819E-08

ACMS OUTPUT: Conductivity parameters

P027 SITE 1 CORE 1 SPEC 4 UNITS= SI m M= 6 NR= 2 09:32:29 05-02-1990

SUSC.	DEC	INC	R95	EV	SDEV
MIN	342.55	-7.28	7.1	1.2756E-06	1.403E-07
INT	72.93	-2.98	18.3	1.6237E-06	6.902E-08
MAX	5.06	82.13	17.0	2.7107E-06	2.509E-08

ACMS OUTPUT: Conductivity parameters

P027 SITE 1 CORE 1 SPEC 5 UNITS= SI m M= 6 NR= 2 09:37:37 05-02-1990

SUSC.	DEC	INC	R95	EV	SDEV
MIN	52.42	-6.14	86.4	1.4446E-06	5.133E-08
INT	321.58	-7.76	86.4	1.6605E-06	2.760E-07
MAX	0.37	80.08	6.5	2.8111E-06	2.753E-08

ACMS OUTPUT: Conductivity parameters

P027 SITE 1 CORE 1 SPEC 6 UNITS= SI m M= 6 NR= 2 09:42:28 05-02-1990

SUSC.	DEC	INC	R95	EV	SDEV
MIN	42.93	-16.06	70.3	1.3933E-06	1.113E-07
INT	312.96	0.36	70.3	1.4983E-06	1.918E-07
MAX	44.30	73.93	11.9	2.8252E-06	1.047E-07

ACMS OUTPUT: Conductivity parameters

P027 SITE 1 CORE 1 SPEC 7 UNITS= SI m M= 6 NR= 2 09:47:13 05-02-1990

SUSC.	DEC	INC	R95	EV	SDEV
MIN	34.50	-14.18	12.7	1.2881E-06	2.340E-07
INT	304.07	-1.73	9.1	1.6225E-06	4.575E-08
MAX	27.25	75.72	13.5	2.6327E-06	5.217E-08

ACMS OUTPUT: Conductivity parameters

P027 SITE 1 CORE 1 SPEC 8 UNITS= SI m M= 6 NR= 2 09:52:41 05-02-1990

SUSC.	DEC	INC	R95	EV	SDEV
MIN	41.44	0.57	19.7	1.4309E-06	1.307E-07
INT	311.41	3.29	20.8	1.8380E-06	1.777E-07
MAX	321.20	-86.66	6.8	2.7664E-06	1.079E-07

ACMS OUTPUT: Conductivity parameters

P027 SITE 1 CORE 1 SPEC 9 UNITS= SI m M= 6 NR= 2 09:57:32 05-02-1990

SUSC.	DEC	INC	R95	EV	SDEV
MIN	300.27	4.73	14.2	1.2107E-06	2.161E-08
INT	28.71	-18.20	14.1	1.4852E-06	3.208E-08
MAX	44.30	71.16	2.0	2.8202E-06	1.013E-07

ACMS OUTPUT: Conductivity parameters

P027 SITE 1 CORE 1 SPEC 10 UNITS= SI m M= 6 NR= 2 10:02:16 05-02-1990

SUSC.	DEC	INC	R95	EV	SDEV
MIN	301.31	9.61	17.6	1.3113E-06	8.602E-08
INT	30.29	-6.00	16.9	1.5798E-06	2.787E-09
MAX	88.77	78.64	6.8	2.6573E-06	1.230E-08

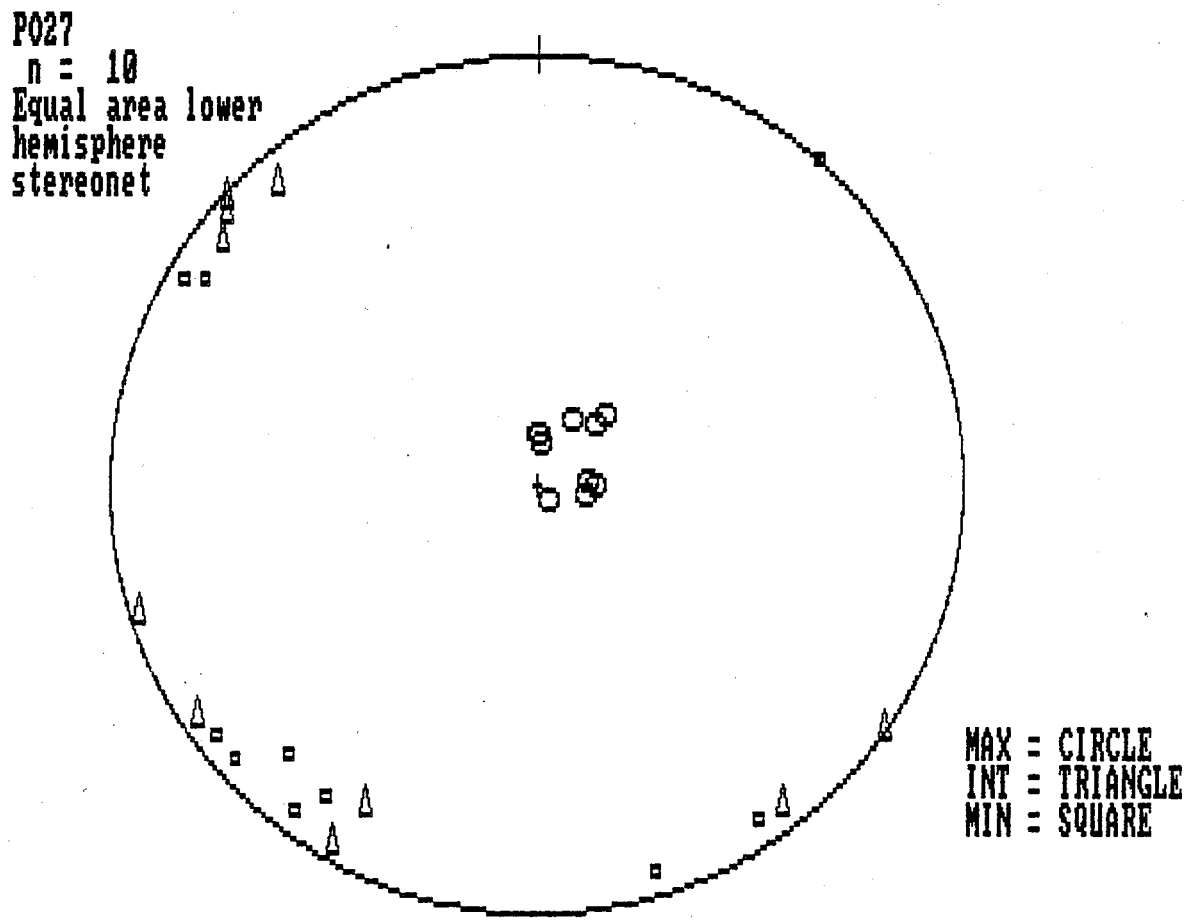

ACMS OUTPUT: Conductivity parameters

P028 SITE 1 CORE 1 SPEC 1 UNITS= SI m M= 6 NR= 2 14:45:45 05-17-1990

SUSC.	DEC	INC	R95	EV	SDEV
MIN	315.45	-5.58	81.0	1.2085E-06	2.737E-08
INT	44.88	5.92	81.0	1.2503E-06	1.418E-08
MAX	88.46	-81.86	3.9	3.0346E-06	6.966E-08

ACMS OUTPUT: Conductivity parameters

P028 SITE 1 CORE 1 SPEC 2 UNITS= SI m M= 6 NR= 2 14:49:37 05-17-1990

SUSC.	DEC	INC	R95	EV	SDEV
MIN	48.44	7.63	81.0	1.1404E-06	5.793E-08
INT	318.03	3.15	81.0	1.2472E-06	3.690E-08
MAX	25.75	-81.74	6.9	2.7641E-06	3.620E-08

ACMS OUTPUT: Conductivity parameters

P028 SITE 1 CORE 1 SPEC 3 UNITS= SI m M= 6 NR= 2 14:54:02 05-17-1990

SUSC.	DEC	INC	R95	EV	SDEV
MIN	60.10	-5.30	59.6	1.1543E-06	2.052E-08
INT	330.45	3.91	59.2	1.2160E-06	4.056E-08
MAX	276.70	-83.41	8.9	2.7299E-06	9.352E-09

ACMS OUTPUT: Conductivity parameters

P028 SITE 1 CORE 1 SPEC 4 UNITS= SI m M= 6 NR= 2 14:58:16 05-17-1990

SUSC.	DEC	INC	R95	EV	SDEV
MIN	271.81	-2.44	58.0	1.1892E-06	1.468E-07
INT	2.09	-5.08	57.9	1.2233E-06	1.448E-07
MAX	336.27	84.36	3.9	2.8539E-06	8.950E-08

ACMS OUTPUT: Conductivity parameters

P028 SITE 1 CORE 1 SPEC 5 UNITS= SI m M= 6 NR= 2 15:02:17 05-17-1990

SUSC.	DEC	INC	R95	EV	SDEV
MIN	69.34	-0.93	52.6	1.2119E-06	2.083E-08
INT	339.40	4.18	53.1	1.3734E-06	9.397E-08
MAX	326.87	-85.72	8.5	2.9148E-06	4.811E-08

ACMS OUTPUT: Conductivity parameters

P028 SITE 1 CORE 1 SPEC 6 UNITS= SI m M= 6 NR= 2 15:06:16 05-17-1990

SUSC.	DEC	INC	R95	EV	SDEV
MIN	301.02	0.44	5.9	1.0809E-06	7.399E-09
INT	30.79	7.85	1.5	1.4160E-06	2.840E-08
MAX	30.73	-82.15	5.7	2.8946E-06	1.994E-08

ACMS OUTPUT: Conductivity parameters

P028 SITE 1 CORE 1 SPEC 7 UNITS= SI m M= 6 NR= 2 15:10:05 05-17-1990

SUSC.	DEC	INC	R95	EV	SDEV
MIN	14.88	0.99	33.9	1.2210E-06	1.699E-08
INT	284.87	0.69	33.8	1.3793E-06	6.044E-08
MAX	339.31	-88.79	14.5	2.7828E-06	2.197E-07

ACMS OUTPUT: Conductivity parameters

P028 SITE 1 CORE 1 SPEC 8 UNITS= SI m M= 6 NR= 2 15:14:54 05-17-1990

SUSC.	DEC	INC	R95	EV	SDEV
MIN	302.58	-2.55	71.3	1.2349E-06	1.005E-07
INT	32.66	-2.00	71.5	1.2759E-06	9.010E-08
MAX	340.74	86.75	10.5	2.6293E-06	4.128E-08

ACMS OUTPUT: Conductivity parameters

P028 SITE 1 CORE 1 SPEC 9 UNITS= SI m M= 6 NR= 2 15:18:56 05-17-1990

SUSC.	DEC	INC	R95	EV	SDEV
MIN	60.76	-0.57	64.5	1.2133E-06	1.781E-08
INT	330.84	8.76	64.8	1.5190E-06	2.542E-07
MAX	327.07	-81.22	7.5	2.7154E-06	2.260E-07

ACMS OUTPUT: Conductivity parameters

P028 SITE 1 CORE 1 SPEC 10 UNITS= SI m M= 6 NR= 2 15:22:49 05-17-1990

SUSC.	DEC	INC	R95	EV	SDEV
MIN	304.43	5.61	4.2	1.0029E-06	3.639E-08
INT	34.64	2.07	1.9	1.3020E-06	5.494E-08
MAX	324.85	-84.02	3.9	2.8016E-06	7.440E-08

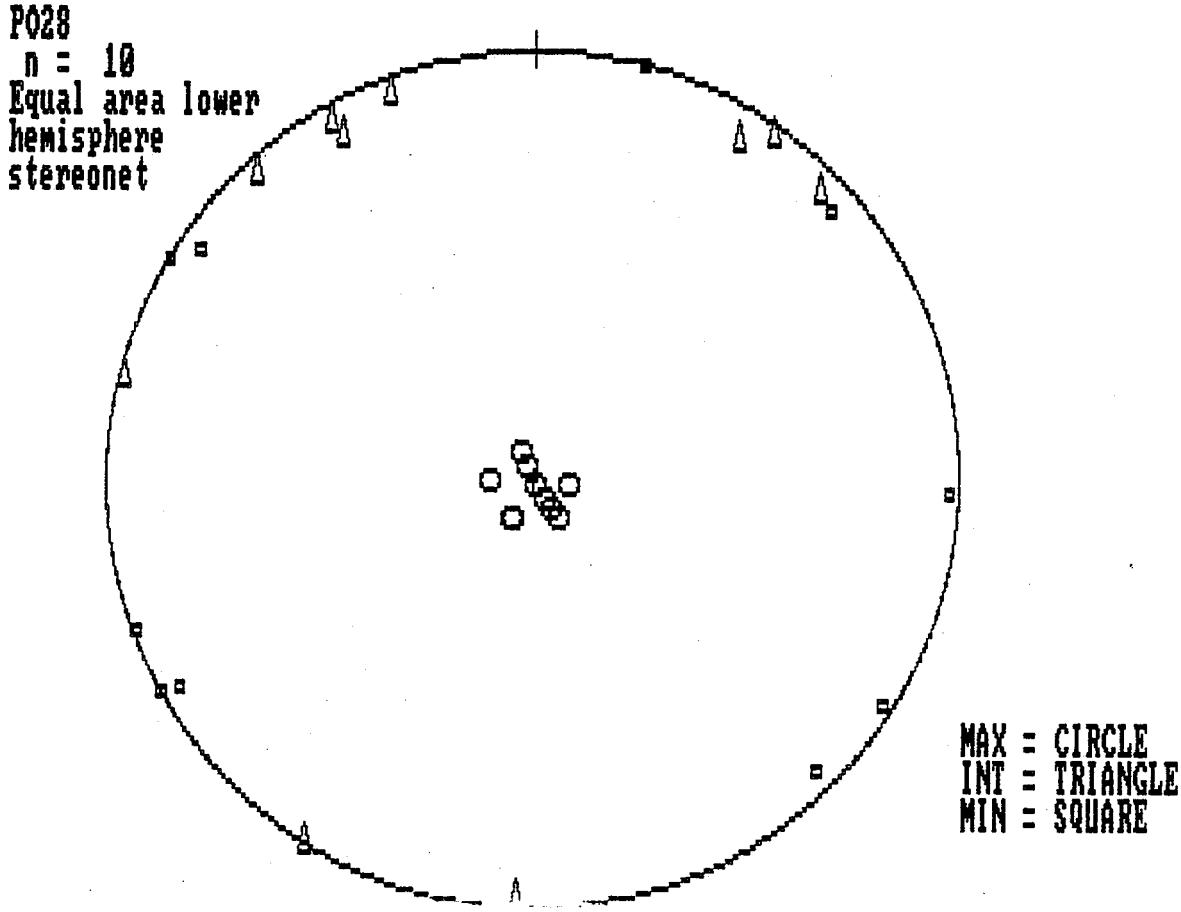

ACMS OUTPUT: Conductivity parameters

TP06 SITE 1 CORE 1 SPEC 1 UNITS= SI m M= 6 NR= 2 15:14:09 06-25-1990

SUSC.	DEC	INC	R95	EV	SDEV
MIN	353.23	3.37	70.3	3.5682E-07	4.032E-08
INT	83.07	-2.68	70.4	3.7381E-07	2.910E-08
MAX	314.66	-85.69	4.4	1.0775E-06	6.105E-08

ACMS OUTPUT: Conductivity parameters

TP06 SITE 1 CORE 1 SPEC 2 UNITS= SI m M= 6 NR= 2 15:17:57 06-25-1990

SUSC.	DEC	INC	R95	EV	SDEV
MIN	7.34	-3.86	34.7	3.2540E-07	3.614E-08
INT	277.43	1.32	35.0	3.9218E-07	9.424E-09
MAX	26.34	85.92	5.5	1.0607E-06	1.354E-08

ACMS OUTPUT: Conductivity parameters

TP06 SITE 1 CORE 1 SPEC 3 UNITS= SI m M= 6 NR= 2 15:21:55 06-25-1990

SUSC.	DEC	INC	R95	EV	SDEV
MIN	49.34	3.04	16.9	2.8007E-07	3.978E-08
INT	319.71	-6.87	17.3	4.0609E-07	2.821E-08
MAX	295.64	82.48	7.2	1.0578E-06	2.346E-08

ACMS OUTPUT: Conductivity parameters

TP06 SITE 1 CORE 1 SPEC 4 UNITS= SI m M= 6 NR= 2 15:25:49 06-25-1990

SUSC.	DEC	INC	R95	EV	SDEV
MIN	25.05	-1.84	4.3	2.6623E-07	5.366E-08
INT	294.91	-4.33	3.4	4.3777E-07	7.726E-09
MAX	317.95	85.30	3.1	1.0150E-06	3.177E-08

ACMS OUTPUT: Conductivity parameters

TP06 SITE 1 CORE 1 SPEC 5 UNITS= SI m M= 6 NR= 2 15:29:30 06-25-1990

SUSC.	DEC	INC	R95	EV	SDEV
MIN	36.87	1.86	8.2	3.1507E-07	1.025E-08
INT	306.86	0.46	5.9	4.3653E-07	6.225E-08
MAX	22.44	-88.08	6.4	1.0831E-06	5.816E-08

ACMS OUTPUT: Conductivity parameters

TP06 SITE 1 CORE 1 SPEC 6 UNITS= SI m M= 6 NR= 2 15:33:07 06-25-1990

SUSC.	DEC	INC	R95	EV	SDEV
MIN	78.37	2.61	63.5	3.2427E-07	4.215E-09
INT	348.37	-1.74	63.8	3.2930E-07	7.592E-09
MAX	292.12	86.86	6.4	1.1008E-06	1.598E-08

ACMS OUTPUT: Conductivity parameters

TP06 SITE 1 CORE 1 SPEC 7 UNITS= SI m M= 6 NR= 2 15:36:46 06-25-1990

SUSC.	DEC	INC	R95	EV	SDEV
MIN	274.08	-5.16	67.1	3.7913E-07	2.094E-08
INT	4.51	-4.34	66.1	3.8699E-07	8.970E-09
MAX	314.41	83.25	13.4	1.1253E-06	6.097E-08

ACMS OUTPUT: Conductivity parameters

TP06 SITE 1 CORE 1 SPEC 8 UNITS= SI m M= 6 NR= 2 15:41:51 06-25-1990

SUSC.	DEC	INC	R95	EV	SDEV
MIN	332.30	-5.52	22.3	2.6090E-07	5.717E-08
INT	62.41	-1.23	23.8	4.0755E-07	3.983E-09
MAX	345.01	84.34	11.1	1.1022E-06	3.446E-08

ACMS OUTPUT: Conductivity parameters

TP06 SITE 1 CORE 1 SPEC 9 UNITS= SI m M= 6 NR= 2 15:46:13 06-25-1990

SUSC.	DEC	INC	R95	EV	SDEV
MIN	32.71	3.09	17.3	3.1351E-07	4.249E-08
INT	302.89	-3.41	18.2	4.6364E-07	6.054E-08
MAX	80.65	-85.39	5.7	1.1058E-06	2.222E-08

ACMS OUTPUT: Conductivity parameters

TP06 SITE 1 CORE 1 SPEC 10 UNITS= SI m M= 6 NR= 2 15:50:05 06-25-1990

SUSC.	DEC	INC	R95	EV	SDEV
MIN	30.46	4.36	0.4	3.1979E-07	2.957E-08
INT	300.45	0.36	1.3	4.1281E-07	1.919E-08
MAX	25.51	-85.62	1.3	1.1499E-06	3.288E-08

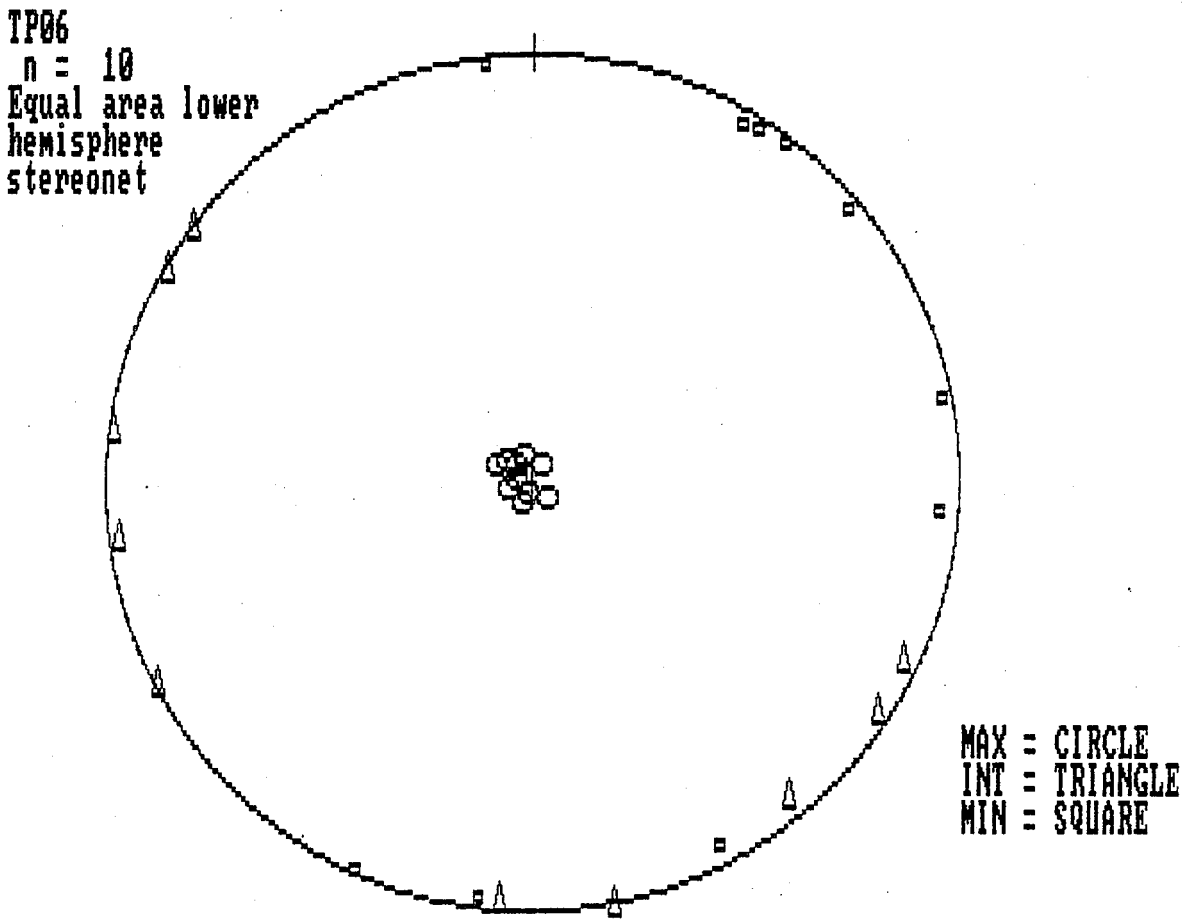

ACMS OUTPUT: Conductivity parameters

TP07 SITE 1 CORE 1 SPEC 1 UNITS= SI m M= 6 NR= 2 13:21:29 07-11-1990

SUSC.	DEC	INC	R95	EV	SDEV
MIN	324.26	-23.04	18.5	9.3922E-07	6.248E-09
INT	59.88	-12.98	34.4	1.1396E-06	2.427E-08
MAX	357.01	63.18	30.0	1.2622E-06	2.750E-08

ACMS OUTPUT: Conductivity parameters

TP07 SITE 1 CORE 1 SPEC 2 UNITS= SI m M= 6 NR= 2 13:25:44 07-11-1990

SUSC.	DEC	INC	R95	EV	SDEV
MIN	21.04	34.14	21.7	1.0945E-06	1.439E-08
INT	297.92	-10.01	62.1	1.2359E-06	4.820E-09
MAX	42.00	-54.02	59.6	1.2665E-06	1.443E-08

ACMS OUTPUT: Conductivity parameters

TP07 SITE 1 CORE 1 SPEC 3 UNITS= SI m M= 6 NR= 2 13:31:39 07-11-1990

SUSC.	DEC	INC	R95	EV	SDEV
MIN	50.05	23.59	81.9	1.0931E-06	1.277E-08
INT	310.84	20.14	93.8	1.1718E-06	3.096E-08
MAX	4.68	-58.14	56.0	1.2281E-06	3.264E-08

ACMS OUTPUT: Conductivity parameters

TP07 SITE 1 CORE 1 SPEC 4 UNITS= SI m M= 6 NR= 2 13:35:34 07-11-1990

SUSC.	DEC	INC	R95	EV	SDEV
MIN	330.25	-6.65	49.4	1.1071E-06	8.509E-08
INT	271.41	77.26	38.5	1.1891E-06	1.442E-09
MAX	58.98	10.77	57.3	1.2221E-06	3.815E-08

ACMS OUTPUT: Conductivity parameters

TP07 SITE 1 CORE 1 SPEC 5 UNITS= SI m M= 6 NR= 2 13:39:10 07-11-1990

SUSC.	DEC	INC	R95	EV	SDEV
MIN	53.82	33.72	53.3	1.0907E-06	5.793E-09
INT	283.68	44.01	71.8	1.1959E-06	3.919E-08
MAX	343.90	-27.21	49.1	1.2473E-06	5.028E-08

TP07
n = 5
Equal area lower hemisphere stereonet

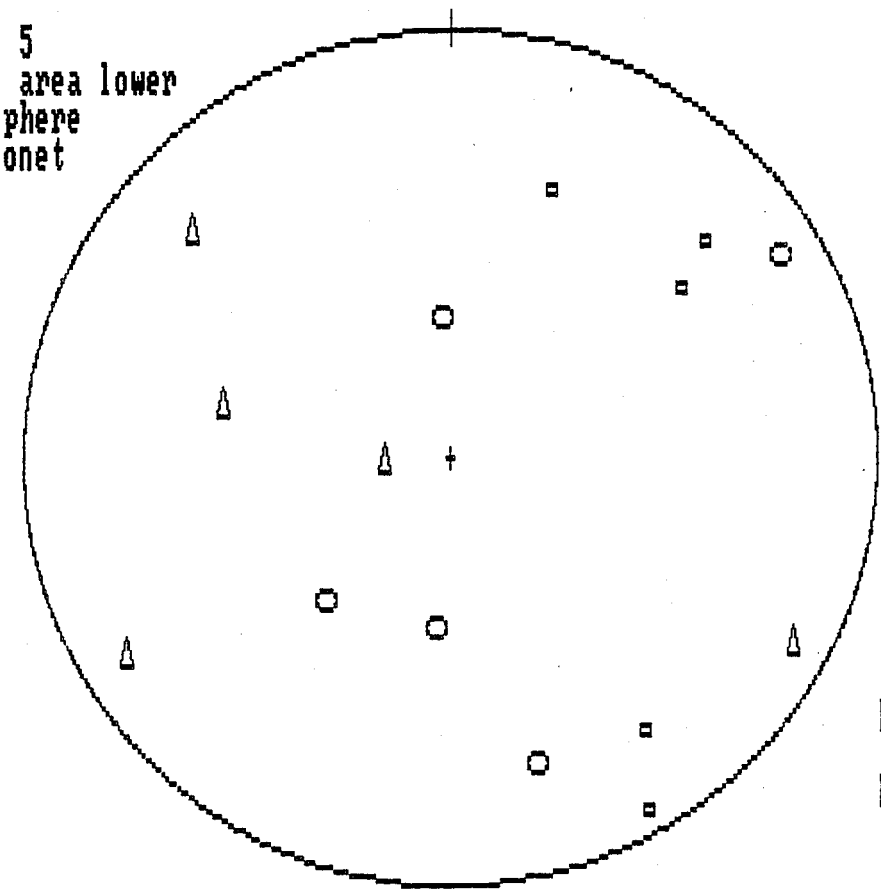

MAX = CIRCLE
INT = TRIANGLE
MIN = SQUARE

ACMS OUTPUT: Conductivity parameters

TP08 SITE 1 CORE 1 SPEC 1 UNITS= SI m M= 6 NR= 2 12:58:15 07-12-1990

SUSC.	DEC	INC	R95	EV	SDEV
MIN	308.13	1.61	9.4	4.1354E-07	6.016E-09
INT	38.25	4.42	10.1	5.3449E-07	1.555E-08
MAX	18.21	-85.29	4.2	1.2498E-06	5.514E-08

ACMS OUTPUT: Conductivity parameters

TP08 SITE 1 CORE 1 SPEC 2 UNITS= SI m M= 6 NR= 2 13:02:01 07-12-1990

SUSC.	DEC	INC	R95	EV	SDEV
MIN	316.34	-7.26	24.6	3.9194E-07	9.880E-09
INT	45.02	10.31	24.2	5.4379E-07	6.299E-09
MAX	80.90	-77.35	4.8	1.2448E-06	2.159E-08

ACMS OUTPUT: Conductivity parameters

TP08 SITE 1 CORE 1 SPEC 3 UNITS= SI m M= 6 NR= 2 13:06:41 07-12-1990

SUSC.	DEC	INC	R95	EV	SDEV
MIN	344.56	1.09	83.3	4.6647E-07	5.863E-08
INT	74.77	11.45	83.2	5.3960E-07	1.240E-08
MAX	69.23	-78.50	5.7	1.2373E-06	4.783E-08

ACMS OUTPUT: Conductivity parameters

TP08 SITE 1 CORE 1 SPEC 4 UNITS= SI m M= 6 NR= 2 13:10:38 07-12-1990

SUSC.	DEC	INC	R95	EV	SDEV
MIN	47.88	6.65	23.6	4.8164E-07	2.162E-08
INT	318.65	-6.64	23.6	5.5410E-07	3.347E-08
MAX	273.24	80.58	4.2	1.2283E-06	1.175E-08

ACMS OUTPUT: Conductivity parameters

TP08 SITE 1 CORE 1 SPEC 5 UNITS= SI m M= 6 NR= 2 13:14:22 07-12-1990

SUSC.	DEC	INC	R95	EV	SDEV
MIN	281.54	-6.54	23.1	4.9383E-07	1.159E-08
INT	10.70	7.33	23.9	6.0304E-07	2.490E-08
MAX	52.87	-80.16	6.4	1.2182E-06	1.281E-08

ACMS OUTPUT: Conductivity parameters

TP08 SITE 1 CORE 1 SPEC 6 UNITS= SI m M= 6 NR= 2 13:17:56 07-12-1990

SUSC.	DEC	INC	R95	EV	SDEV
MIN	39.50	8.28	14.0	4.5909E-07	2.426E-09
INT	309.73	-1.57	14.4	6.3738E-07	1.173E-08
MAX	50.45	-81.56	3.4	1.2351E-06	1.901E-08

ACMS OUTPUT: Conductivity parameters

TP08 SITE 1 CORE 1 SPEC 7 UNITS= SI m M= 6 NR= 2 13:21:32 07-12-1990

SUSC.	DEC	INC	R95	EV	SDEV
MIN	333.32	-3.86	10.5	3.9411E-07	4.985E-08
INT	63.12	2.95	10.6	5.5363E-07	4.327E-08
MAX	295.80	85.14	2.6	1.1556E-06	4.834E-08

ACMS OUTPUT: Conductivity parameters

TP08 SITE 1 CORE 1 SPEC 8 UNITS= SI m M= 6 NR= 2 13:25:32 07-12-1990

SUSC.	DEC	INC	R95	EV	SDEV
MIN	321.42	-0.31	79.7	5.0142E-07	3.217E-08
INT	51.44	7.84	79.9	5.2016E-07	1.461E-08
MAX	53.54	-82.15	5.2	1.1685E-06	1.158E-08

ACMS OUTPUT: Conductivity parameters

TP08 SITE 1 CORE 1 SPEC 9 UNITS= SI m M= 6 NR= 2 13:29:16 07-12-1990

SUSC.	DEC	INC	R95	EV	SDEV
MIN	338.56	-3.70	42.6	5.0296E-07	3.110E-08
INT	68.39	2.62	43.1	5.1353E-07	3.126E-08
MAX	303.13	85.46	6.3	1.1951E-06	2.847E-08

ACMS OUTPUT: Conductivity parameters

TP08 SITE 1 CORE 1 SPEC 10 UNITS= SI m M= 6 NR= 2 13:32:52 07-12-1990

SUSC.	DEC	INC	R95	EV	SDEV
MIN	71.78	12.45	69.7	4.9504E-07	1.293E-08
INT	341.17	2.77	69.6	5.4633E-07	3.564E-08
MAX	58.85	-77.24	4.0	1.2059E-06	7.024E-08

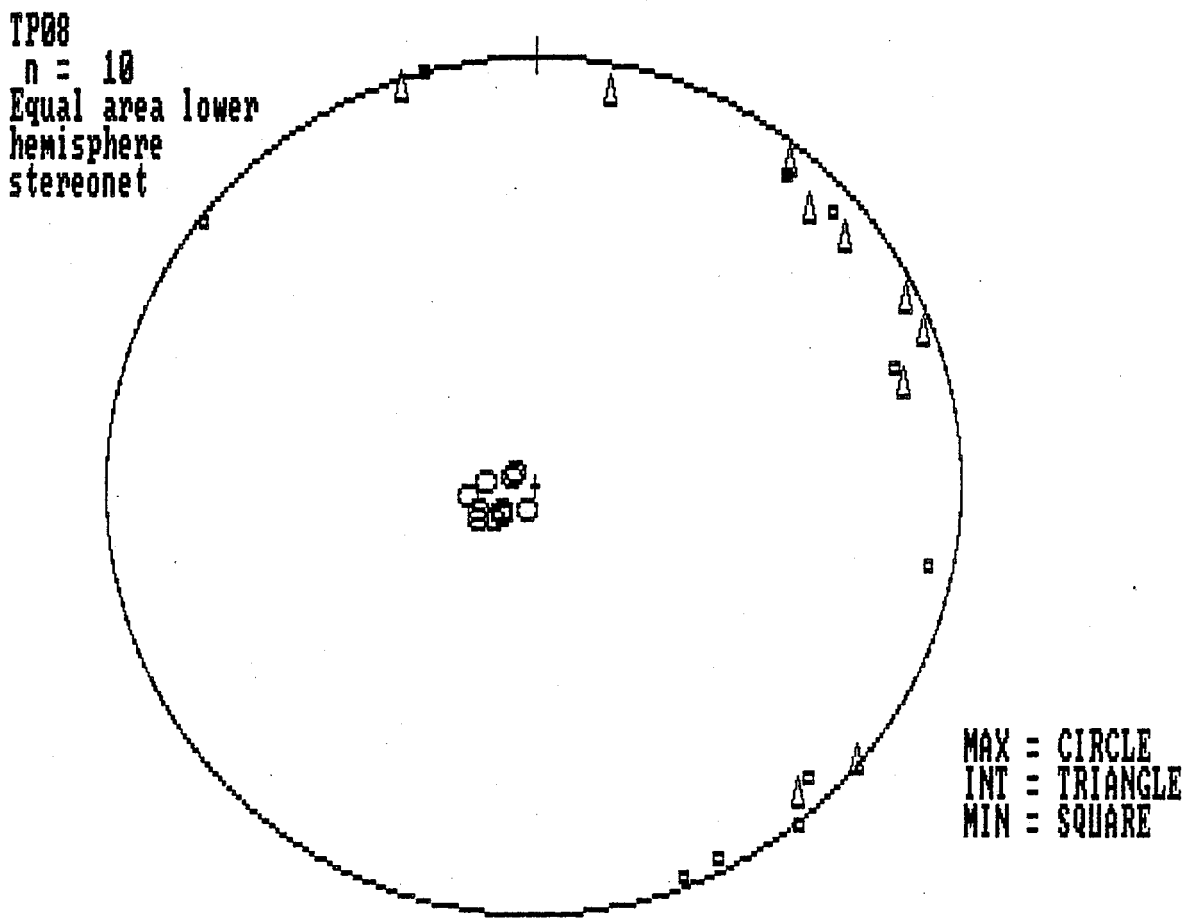

ACMS OUTPUT: Conductivity parameters

TP09 SITE 1 CORE 1 SPEC 1 UNITS= SI m M= 6 NR= 2 11:47:36 07-24-1990

SUSC.	DEC	INC	R95	EV	SDEV
MIN	312.28	3.51	85.3	5.5296E-07	5.910E-09
INT	42.40	2.06	85.3	5.9491E-07	4.776E-08
MAX	342.80	-85.93	0.2	2.4939E-06	4.925E-09

ACMS OUTPUT: Conductivity parameters

TP09 SITE 1 CORE 1 SPEC 2 UNITS= SI m M= 6 NR= 2 11:51:54 07-24-1990

SUSC.	DEC	INC	R95	EV	SDEV
MIN	296.41	3.12	60.3	5.4286E-07	7.867E-08
INT	26.49	1.46	60.3	6.4437E-07	8.442E-09
MAX	321.60	-86.56	0.6	2.4645E-06	1.259E-08

ACMS OUTPUT: Conductivity parameters

TP09 SITE 1 CORE 1 SPEC 3 UNITS= SI m M= 6 NR= 2 11:55:57 07-24-1990

SUSC.	DEC	INC	R95	EV	SDEV
MIN	317.13	2.28	65.6	5.8832E-07	5.896E-08
INT	47.25	3.11	65.6	6.5303E-07	5.426E-10
MAX	11.01	-86.14	1.9	2.4768E-06	6.676E-08

ACMS OUTPUT: Conductivity parameters

TP09 SITE 1 CORE 1 SPEC 4 UNITS= SI m M= 6 NR= 2 12:00:00 07-24-1990

SUSC.	DEC	INC	R95	EV	SDEV
MIN	299.18	3.86	8.9	4.7842E-07	5.427E-08
INT	29.24	1.03	8.9	6.2812E-07	7.622E-09
MAX	314.24	-86.00	3.3	2.5092E-06	7.929E-09

ACMS OUTPUT: Conductivity parameters

TP09 SITE 1 CORE 1 SPEC 5 UNITS= SI m M= 6 NR= 2 12:03:56 07-24-1990

SUSC.	DEC	INC	R95	EV	SDEV
MIN	291.56	3.65	29.4	5.2851E-07	2.978E-08
INT	21.34	-0.06	29.6	5.9796E-07	7.936E-09
MAX	292.41	-86.35	4.2	2.4701E-06	8.398E-08

ACMS OUTPUT: Conductivity parameters

TP09 SITE 1 CORE 1 SPEC 6 UNITS= SI m M= 6 NR= 2 12:07:28 07-24-1990

SUSC.	DEC	INC	R95	EV	SDEV
MIN	294.15	3.98	1.5	5.0314E-07	2.253E-08
INT	24.20	0.84	2.3	6.6830E-07	3.505E-08
MAX	306.27	-85.93	2.5	2.3596E-06	3.296E-08

ACMS OUTPUT: Conductivity parameters

TP09 SITE 1 CORE 1 SPEC 7 UNITS= SI m M= 6 NR= 2 12:11:00 07-24-1990

SUSC.	DEC	INC	R95	EV	SDEV
MIN	306.83	3.63	1.6	4.1111E-07	6.713E-08
INT	36.97	2.23	1.7	6.2004E-07	3.336E-08
MAX	338.52	-85.73	0.8	2.4883E-06	2.559E-08

ACMS OUTPUT: Conductivity parameters

TP09 SITE 1 CORE 1 SPEC 8 UNITS= SI m M= 6 NR= 2 12:14:57 07-24-1990

SUSC.	DEC	INC	R95	EV	SDEV
MIN	319.15	2.01	28.4	4.9454E-07	4.442E-08
INT	49.15	-0.33	28.5	5.9701E-07	3.255E-08
MAX	309.17	-87.96	5.5	2.4740E-06	5.706E-08

ACMS OUTPUT: Conductivity parameters

TP09 SITE 1 CORE 1 SPEC 9 UNITS= SI m M= 6 NR= 2 12:18:39 07-24-1990

SUSC.	DEC	INC	R95	EV	SDEV
MIN	325.46	2.82	57.0	5.0766E-07	2.016E-08
INT	55.35	-2.32	56.9	6.2645E-07	9.573E-08
MAX	285.96	-86.35	2.6	2.4445E-06	3.442E-09

ACMS OUTPUT: Conductivity parameters

TP09 SITE 1 CORE 1 SPEC 10 UNITS= SI m M= 6 NR= 2 12:22:34 07-24-1990

SUSC.	DEC	INC	R95	EV	SDEV
MIN	54.81	1.01	20.9	5.6581E-07	1.803E-08
INT	324.75	3.76	20.9	6.7551E-07	4.639E-08
MAX	339.81	-86.11	1.2	2.4952E-06	1.453E-08

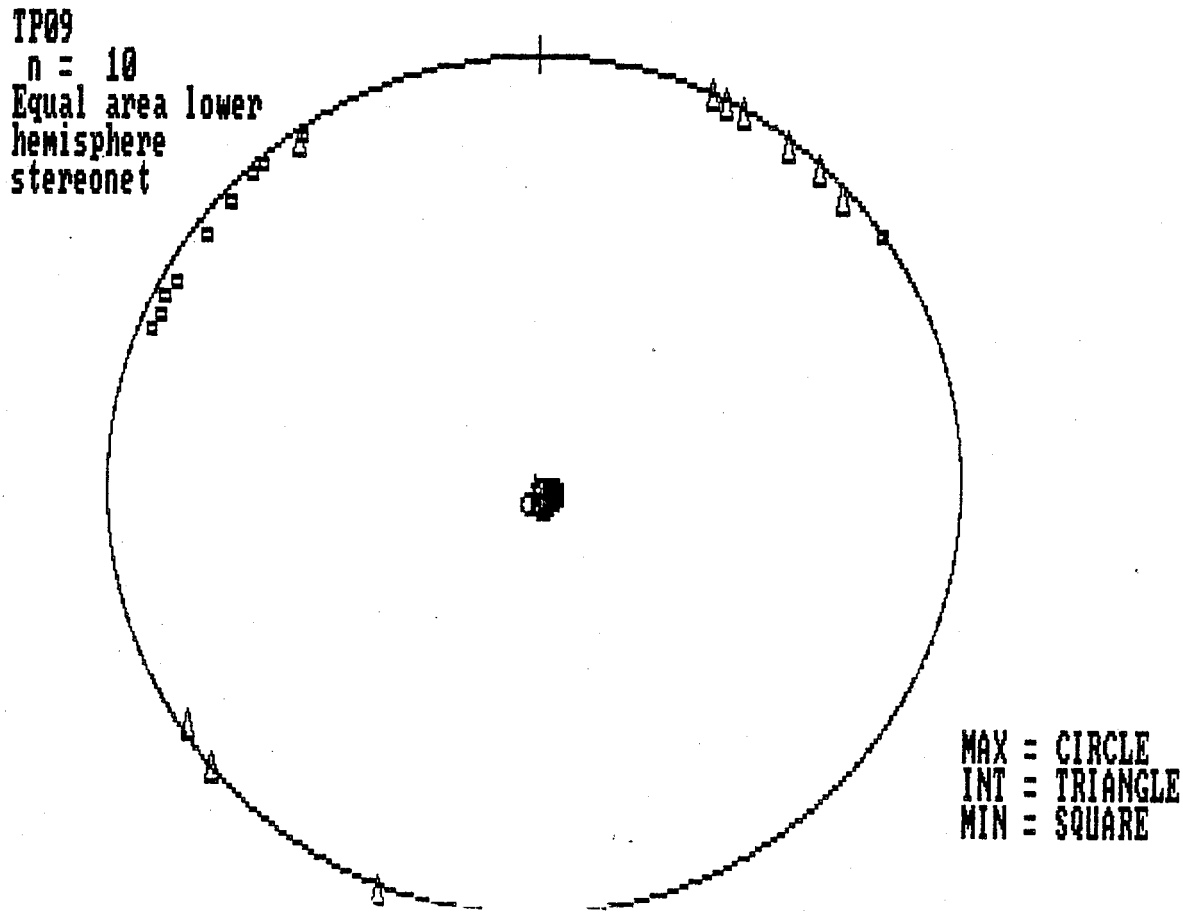

ACMS OUTPUT: Conductivity parameters

TP10 SITE 1 CORE 1 SPEC 1 UNITS= SI m M= 6 NR= 2 14:04:33 07-25-1990

SUSC.	DEC	INC	R95	EV	SDEV
MIN	12.89	1.44	6.0	4.1693E-07	2.401E-08
INT	282.76	5.45	6.5	5.1690E-07	2.860E-08
MAX	297.62	-84.36	3.1	2.1337E-06	4.442E-08

ACMS OUTPUT: Conductivity parameters

TP10 SITE 1 CORE 1 SPEC 2 UNITS= SI m M= 6 NR= 2 14:08:16 07-25-1990

SUSC.	DEC	INC	R95	EV	SDEV
MIN	319.57	4.82	10.6	3.7482E-07	1.961E-08
INT	49.10	-5.53	10.8	4.7836E-07	5.014E-08
MAX	270.39	-82.65	2.0	2.0784E-06	3.007E-09

ACMS OUTPUT: Conductivity parameters

TP10 SITE 1 CORE 1 SPEC 3 UNITS= SI m M= 6 NR= 2 14:11:38 07-25-1990

SUSC.	DEC	INC	R95	EV	SDEV
MIN	357.51	-1.03	53.1	4.4257E-07	1.352E-08
INT	87.57	-6.51	53.0	4.8699E-07	1.817E-08
MAX	78.63	83.41	3.2	2.0159E-06	7.076E-08

ACMS OUTPUT: Conductivity parameters

TP10 SITE 1 CORE 1 SPEC 4 UNITS= SI m M= 6 NR= 2 14:14:44 07-25-1990

SUSC.	DEC	INC	R95	EV	SDEV
MIN	292.98	4.90	31.5	4.0723E-07	1.433E-08
INT	22.95	-0.60	31.5	5.1554E-07	3.414E-08
MAX	285.85	-85.07	1.4	2.1117E-06	2.274E-08

ACMS OUTPUT: Conductivity parameters

TP10 SITE 1 CORE 1 SPEC 5 UNITS= SI m M= 6 NR= 2 14:22:20 07-25-1990

SUSC.	DEC	INC	R95	EV	SDEV
MIN	302.96	6.79	31.7	4.1224E-07	4.046E-08
INT	32.39	-4.82	31.5	4.9260E-07	2.164E-08
MAX	87.29	81.66	4.7	2.0271E-06	1.115E-08

ACMS OUTPUT: Conductivity parameters

TP10 SITE 1 CORE 1 SPEC 6 UNITS= SI m M= 6 NR= 2 14:25:51 07-25-1990

SUSC.	DEC	INC	R95	EV	SDEV
MIN	304.97	7.32	32.1	3.7234E-07	2.655E-09
INT	34.29	-5.30	32.0	4.7907E-07	7.730E-08
MAX	88.65	80.95	2.7	2.0489E-06	7.415E-08

ACMS OUTPUT: Conductivity parameters

TP10 SITE 1 CORE 1 SPEC 7 UNITS= SI m M= 6 NR= 2 14:29:01 07-25-1990

SUSC.	DEC	INC	R95	EV	SDEV
MIN	336.24	0.13	4.5	3.5495E-07	1.394E-08
INT	66.30	-6.50	5.5	5.0642E-07	1.155E-08
MAX	66.88	83.50	3.4	2.0870E-06	3.199E-08

TP10 SITE 1 CORE 1 SPEC 8 UNITS= SI m M= 6 NR= 2   14:32:38 07-25-1990

SUSC.	DEC	INC	R95	EV	SDEV
MIN	284.47	5.41	53.7	4.5775E-07	1.996E-08
INT	14.47	0.61	53.8	4.8285E-07	2.624E-08
MAX	291.05	-84.56	5.6	2.0725E-06	7.279E-08

ACMS OUTPUT: Conductivity parameters

TP10 SITE 1 CORE 1 SPEC 9 UNITS= SI m M= 6 NR= 2   14:35:54 07-25-1990

SUSC.	DEC	INC	R95	EV	SDEV
MIN	51.69	-2.73	6.7	4.3405E-07	2.207E-08
INT	321.99	6.26	7.0	5.6320E-07	2.293E-08
MAX	298.28	-83.17	3.7	2.0153E-06	7.905E-09

ACMS OUTPUT: Conductivity parameters

TP10 SITE 1 CORE 1 SPEC 10 UNITS= SI m M= 6 NR= 2   14:39:12 07-25-1990

SUSC.	DEC	INC	R95	EV	SDEV
MIN	55.66	-7.78	8.3	3.8178E-07	1.011E-08
INT	326.14	3.57	8.3	4.7095E-07	6.956E-08
MAX	80.61	81.44	1.5	2.0678E-06	4.806E-08

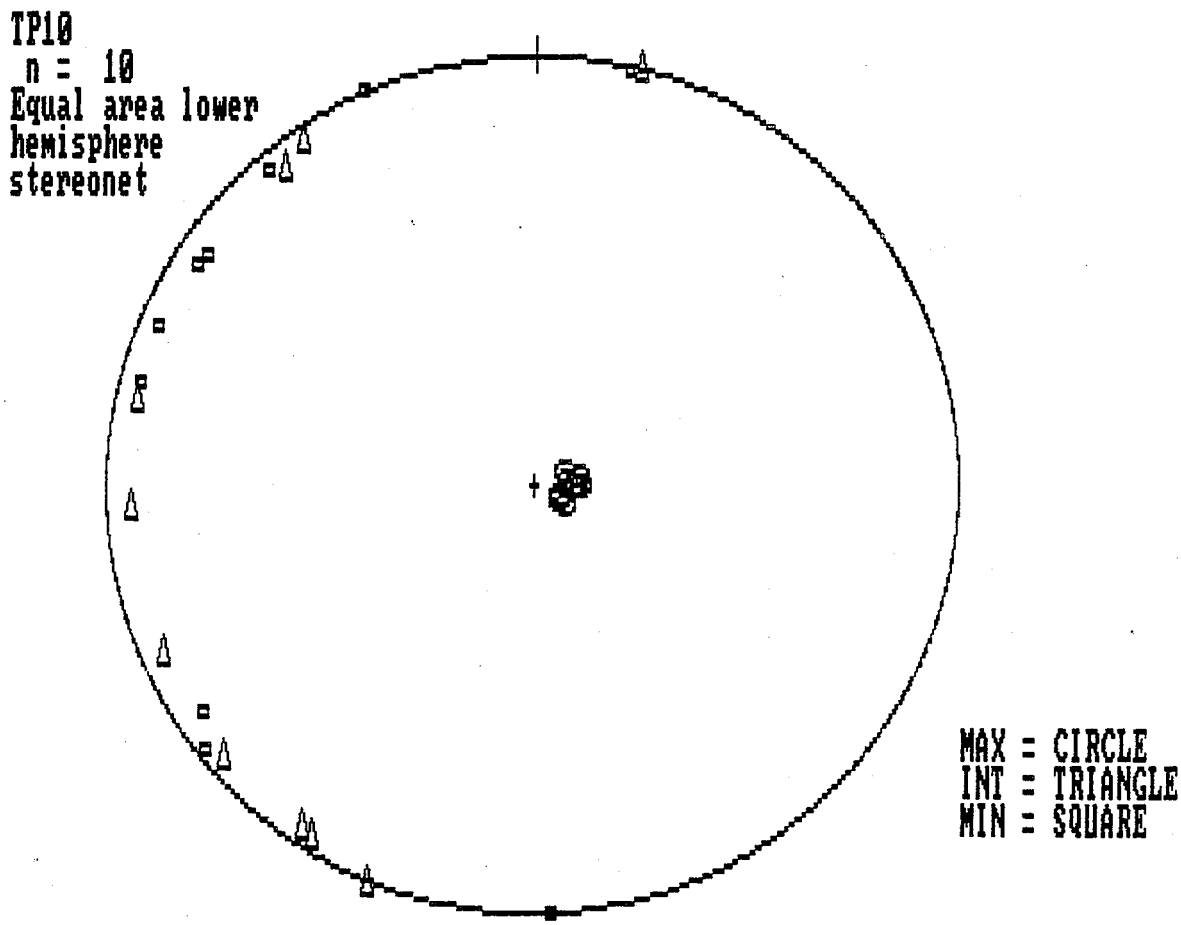

ACMS OUTPUT: Conductivity parameters

TP11 SITE 1 CORE 1 SPEC 1 UNITS= SI m M= 6 NR= 2 10:32:08 09-06-1990

SUSC.	DEC	INC	R95	EV	SDEV
MIN	302.39	0.56	5.7	1.4508E-07	7.668E-08
INT	32.36	-3.37	1.5	2.7594E-07	1.583E-08
MAX	41.79	86.58	5.9	7.1731E-07	1.772E-08

ACMS OUTPUT: Conductivity parameters

TP11 SITE 1 CORE 1 SPEC 2 UNITS= SI m M= 6 NR= 2 10:36:20 09-06-1990

SUSC.	DEC	INC	R95	EV	SDEV
MIN	88.44	0.61	62.3	2.2665E-07	9.205E-09
INT	358.31	6.49	62.3	2.3999E-07	1.754E-08
MAX	3.77	-83.48	1.3	7.4734E-07	5.072E-08

ACMS OUTPUT: Conductivity parameters

TP11 SITE 1 CORE 1 SPEC 3 UNITS= SI m M= 6 NR= 2 10:40:09 09-06-1990

SUSC.	DEC	INC	R95	EV	SDEV
MIN	61.02	11.14	28.3	2.1255E-07	9.817E-09
INT	328.85	10.90	33.0	3.7034E-07	9.292E-08
MAX	15.55	-74.31	17.4	8.1268E-07	9.491E-08

ACMS OUTPUT: Conductivity parameters

TP11 SITE 1 CORE 1 SPEC 4 UNITS= SI m M= 6 NR= 2 10:43:46 09-06-1990

SUSC.	DEC	INC	R95	EV	SDEV
MIN	308.20	-2.00	9.3	2.3465E-07	3.605E-08
INT	38.00	5.65	8.5	3.0655E-07	4.799E-09
MAX	57.57	-84.01	10.4	7.5836E-07	1.442E-08

ACMS OUTPUT: Conductivity parameters

TP11 SITE 1 CORE 1 SPEC 5 UNITS= SI m M= 6 NR= 2 10:50:39 09-06-1990

SUSC.	DEC	INC	R95	EV	SDEV
MIN	306.57	0.53	4.7	1.6776E-07	3.426E-08
INT	36.63	6.19	5.8	2.8846E-07	1.717E-08
MAX	31.74	-83.79	4.1	7.7721E-07	5.707E-08

ACMS OUTPUT: Conductivity parameters

TP11 SITE 1 CORE 1 SPEC 6 UNITS= SI m M= 6 NR= 2 10:54:17 09-06-1990

SUSC.	DEC	INC	R95	EV	SDEV
MIN	50.74	-2.87	87.2	2.4004E-07	5.825E-09
INT	321.29	10.78	87.9	2.9875E-07	7.775E-08
MAX	306.03	-78.84	20.6	7.0994E-07	3.255E-09

ACMS OUTPUT: Conductivity parameters

TP11 SITE 1 CORE 1 SPEC 7 UNITS= SI m M= 6 NR= 2 10:58:05 09-06-1990

SUSC.	DEC	INC	R95	EV	SDEV
MIN	20.98	8.45	50.9	2.6949E-07	4.639E-08
INT	291.13	-1.15	50.9	2.9871E-07	3.941E-08
MAX	28.85	-81.47	1.7	7.6250E-07	3.539E-08

ACMS OUTPUT: Conductivity parameters

TP11 SITE 1 CORE 1 SPEC 8 UNITS= SI m M= 6 NR= 2 11:02:02 09-06-1990

SUSC.	DEC	INC	R95	EV	SDEV
MIN	58.33	0.41	52.0	2.4409E-07	1.896E-08
INT	328.27	13.40	50.9	2.7613E-07	3.660E-08
MAX	330.01	-76.59	13.0	7.6035E-07	8.827E-09

ACMS OUTPUT: Conductivity parameters

TP11 SITE 1 CORE 1 SPEC 9 UNITS= SI m M= 6 NR= 2 11:05:46 09-06-1990

SUSC.	DEC	INC	R95	EV	SDEV
MIN	273.26	5.06	30.4	2.0110E-07	3.981E-08
INT	3.94	7.61	29.4	2.6257E-07	3.800E-09
MAX	329.94	-80.85	10.2	7.1313E-07	1.373E-08

ACMS OUTPUT: Conductivity parameters

TP11 SITE 1 CORE 1 SPEC 10 UNITS= SI m M= 6 NR= 2 11:09:32 09-06-1990

SUSC.	DEC	INC	R95	EV	SDEV
MIN	309.07	-1.84	19.1	1.3630E-07	5.882E-09
INT	39.05	0.76	21.6	2.9168E-07	1.152E-08
MAX	286.24	88.00	10.1	7.5092E-07	3.821E-08

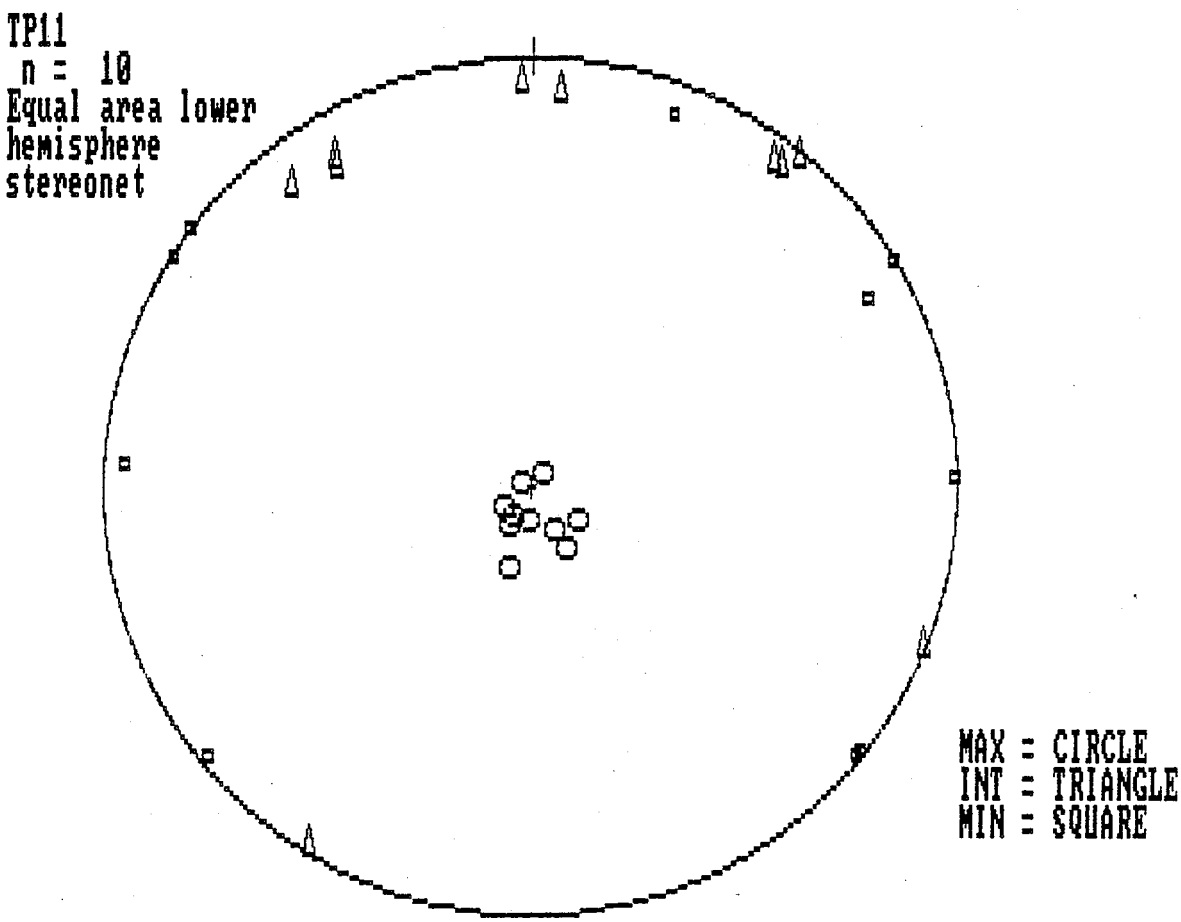

ACMS OUTPUT: Conductivity parameters

TP12 SITE 1 CORE 1 SPEC 1 UNITS= SI m M= 6 NR= 2 12:37:10 09-06-1990

SUSC.	DEC	INC	R95	EV	SDEV
MIN	18.60	4.28	84.4	3.4792E-07	1.632E-08
INT	289.35	-9.97	84.6	3.8151E-07	1.962E-08
MAX	85.67	-79.13	5.7	1.1714E-06	1.516E-08

ACMS OUTPUT: Conductivity parameters

TP12 SITE 1 CORE 1 SPEC 2 UNITS= SI m M= 6 NR= 2 12:40:51 09-06-1990

SUSC.	DEC	INC	R95	EV	SDEV
MIN	38.12	7.48	57.9	3.3632E-07	4.098E-08
INT	307.39	5.50	57.9	3.8953E-07	3.650E-09
MAX	1.41	-80.70	7.0	1.2171E-06	8.757E-08

ACMS OUTPUT: Conductivity parameters

TP12 SITE 1 CORE 1 SPEC 3 UNITS= SI m M= 6 NR= 2 12:44:43 09-06-1990

SUSC.	DEC	INC	R95	EV	SDEV
MIN	7.58	7.35	6.0	3.6555E-07	2.048E-08
INT	278.01	-3.33	6.2	4.4092E-07	2.129E-08
MAX	32.24	-81.92	4.6	1.1581E-06	4.937E-08

ACMS OUTPUT: Conductivity parameters

TP12 SITE 1 CORE 1 SPEC 4 UNITS= SI m M= 6 NR= 2 12:48:13 09-06-1990

SUSC.	DEC	INC	R95	EV	SDEV
MIN	50.28	6.97	21.3	3.1205E-07	4.255E-08
INT	319.72	4.58	19.9	5.0730E-07	5.754E-08
MAX	16.63	-81.64	12.4	1.1137E-06	6.687E-08

ACMS OUTPUT: Conductivity parameters

TP12 SITE 1 CORE 1 SPEC 5 UNITS= SI m M= 6 NR= 2 12:51:44 09-06-1990

SUSC.	DEC	INC	R95	EV	SDEV
MIN	74.39	0.16	6.7	3.1852E-07	4.290E-08
INT	344.45	7.57	9.8	4.8754E-07	5.056E-08
MAX	344.64	-82.43	8.1	1.1616E-06	5.731E-08

ACMS OUTPUT: Conductivity parameters

TP12 SITE 1 CORE 1 SPEC 6 UNITS= SI m M= 6 NR= 2 12:55:22 09-06-1990

SUSC.	DEC	INC	R95	EV	SDEV
MIN	297.71	7.27	15.8	3.4832E-07	1.816E-08
INT	27.27	-3.51	15.8	4.7138E-07	2.133E-09
MAX	271.68	-81.92	2.0	1.0442E-06	2.676E-08

ACMS OUTPUT: Conductivity parameters

TP12 SITE 1 CORE 1 SPEC 7 UNITS= SI m M= 6 NR= 2 12:58:47 09-06-1990

SUSC.	DEC	INC	R95	EV	SDEV
MIN	316.64	2.09	13.4	2.8579E-07	1.944E-08
INT	46.61	-0.96	14.3	4.7384E-07	1.068E-09
MAX	291.67	-87.70	5.0	1.1072E-06	2.819E-08

ACMS OUTPUT: Conductivity parameters

TP12 SITE 1 CORE 1 SPEC 8 UNITS= SI m M= 6 NR= 2 13:02:23 09-06-1990

SUSC.	DEC	INC	R95	EV	SDEV
MIN	309.68	0.89	30.6	3.0445E-07	6.961E-08
INT	39.80	8.23	31.4	4.3242E-07	2.851E-09
MAX	33.57	-81.72	9.5	1.1076E-06	8.694E-09

ACMS OUTPUT: Conductivity parameters

TP12 SITE 1 CORE 1 SPEC 9 UNITS= SI m M= 6 NR= 2 13:05:44 09-06-1990

SUSC.	DEC	INC	R95	EV	SDEV
MIN	9.10	-0.43	13.4	3.2114E-07	2.625E-08
INT	279.06	-5.74	12.0	4.8389E-07	6.253E-09
MAX	283.26	84.24	6.5	1.0131E-06	2.275E-08

ACMS OUTPUT: Conductivity parameters

TP12 SITE 1 CORE 1 SPEC 10 UNITS= SI m M= 6 NR= 2 13:09:11 09-06-1990

SUSC.	DEC	INC	R95	EV	SDEV
MIN	351.38	0.42	47.7	3.5913E-07	3.316E-08
INT	81.41	6.27	47.2	4.2669E-07	3.442E-08
MAX	77.66	-83.72	8.2	1.0589E-06	4.105E-08

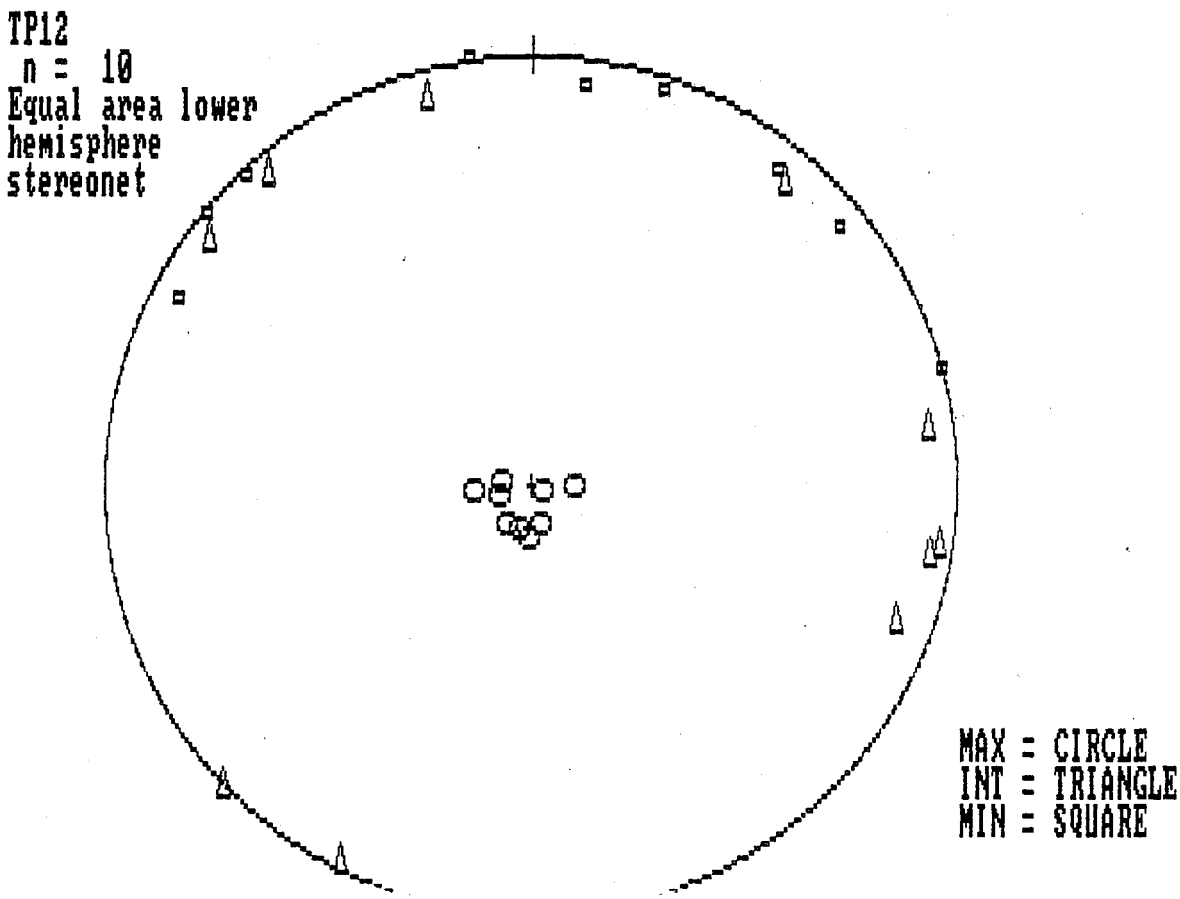

APPENDIX B: AMS Raw Data for Loose Aggregates

The data for AMS measurements on the samples P002 to P028 and TP06 to TP12 are presented in a similar format to the corresponding ACMS data in appendix A. One major difference is that only two AMS measurements were performed on most specimens. This is because the signals were very strong and easily reproducable, with very small errors in the determination of magnitude and direction of the principal magnetic susceptibilities.

P002A SITE 1 CORE 1 SPEC 1 UNITS= SI m M= 12 NR= 2 16:14:04 01-24-1990

SUSC.	DEC	INC	R95	EV	SDEV
MIN	327.79	-83.18	0.3	1.1322E-01	3.213E-05
INT	82.31	-2.84	0.8	1.2457E-01	3.909E-05
MAX	352.61	6.19	0.8	1.2524E-01	4.148E-05

P002B SITE 1 CORE 1 SPEC 1 UNITS= SI m M= 12 NR= 2 16:21:35 01-24-1990

SUSC.	DEC	INC	R95	EV	SDEV
MIN	329.99	-83.12	0.1	1.1327E-01	4.979E-05
INT	83.72	-2.78	2.0	1.2454E-01	2.529E-05
MAX	354.02	6.29	2.0	1.2523E-01	3.959E-05

4-15

P002B
n = 2
Equal area lower hemisphere stereonet

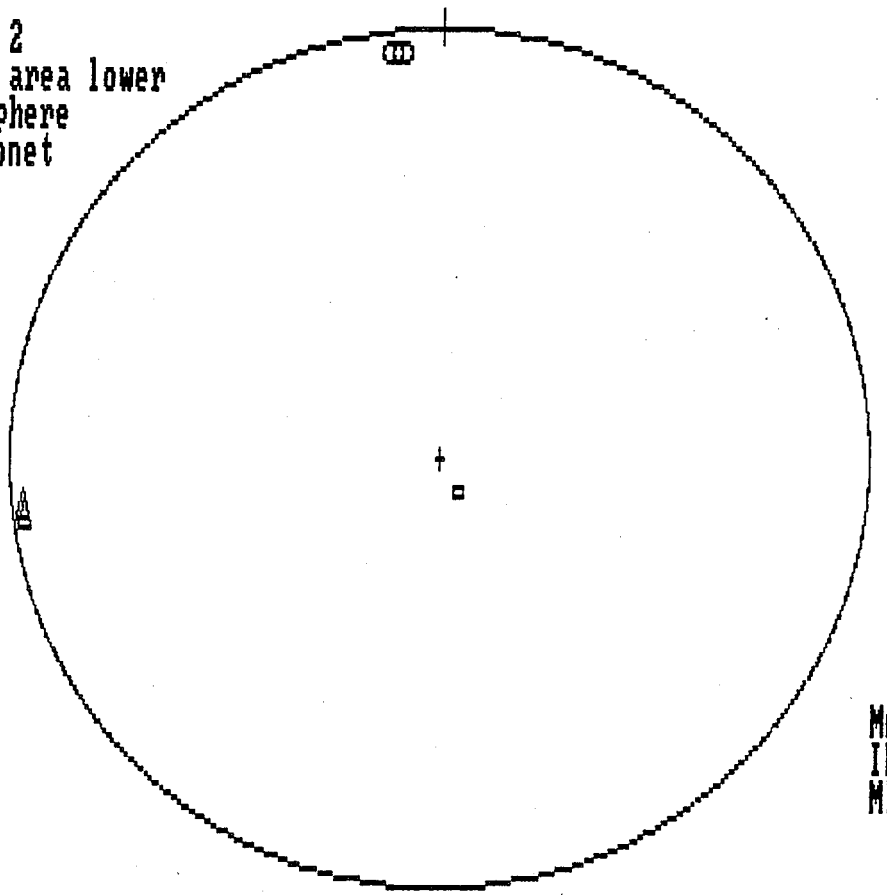

MAX = CIRCLE
INT = TRIANGLE
MIN = SQUARE

AMS

P003A SITE 1 CORE 1 SPEC 1 UNITS= SI m M= 12 NR= 2 14:19:35 01-24-1990

SUSC.	DEC	INC	R95	EV	SDEV
MIN	87.70	-86.54	3.0	1.2239E-01	2.421E-04
INT	76.57	3.39	10.0	1.4462E-01	1.532E-03
MAX	346.61	-0.67	9.7	1.4828E-01	2.568E-04

P003B SITE 1 CORE 1 SPEC 1 UNITS= SI m M= 12 NR= 2 14:28:45 01-24-1990

SUSC.	DEC	INC	R95	EV	SDEV
MIN	86.42	-86.68	0.3	1.2259E-01	4.899E-06
INT	70.35	3.19	1.3	1.4580E-01	7.238E-05
MAX	340.40	-0.92	1.3	1.4843E-01	8.064E-05

AMS

P003B
n = 2
Equal area lower hemisphere stereonet

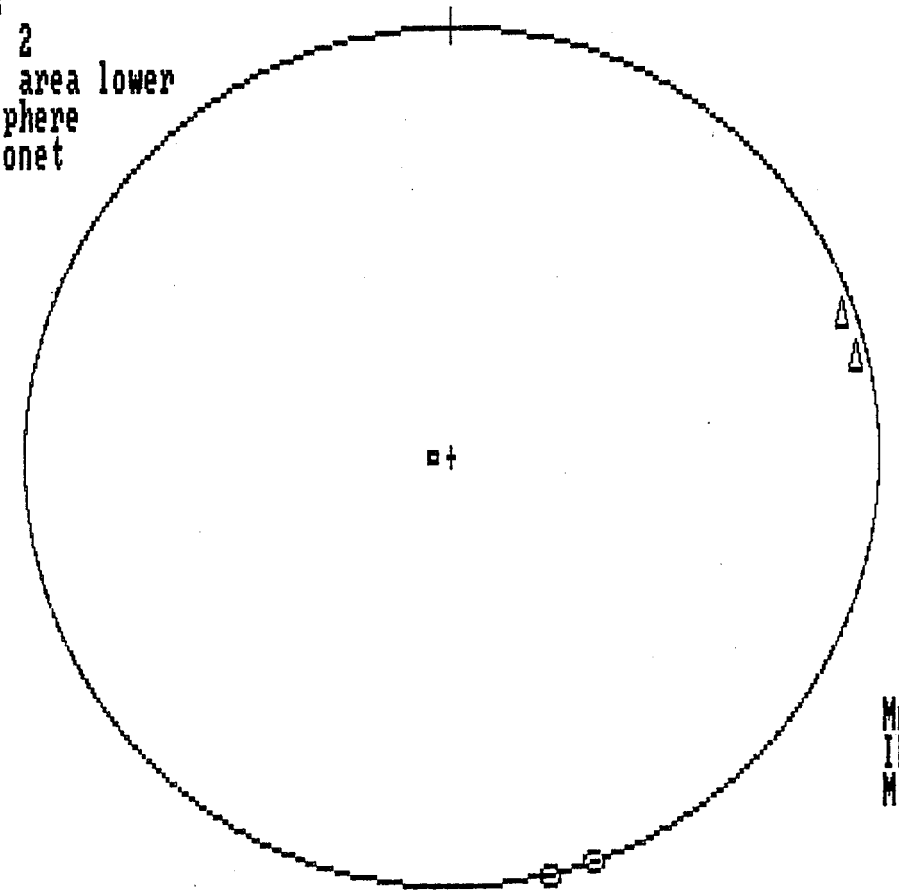

MAX = CIRCLE
INT = TRIANGLE
MIN = SQUARE

P004A SITE 1 CORE 1 SPEC 1 UNITS= SI m M= 12 NR= 2 14:40:00 01-24-1990

SUSC.	DEC	INC	R95	EV	SDEV
MIN	81.59	83.11	0.2	1.0592E-01	2.567E-05
INT	338.30	1.60	3.8	1.3369E-01	5.668E-05
MAX	68.10	-6.71	3.8	1.3538E-01	1.809E-04

P004B SITE 1 CORE 1 SPEC 1 UNITS= SI m M= 12 NR= 2 14:48:23 01-24-1990

SUSC.	DEC	INC	R95	EV	SDEV
MIN	81.52	83.13	0.2	1.0592E-01	5.024E-05
INT	337.99	1.62	4.2	1.3370E-01	4.486E-05
MAX	67.79	-6.68	4.2	1.3539E-01	1.801E-04

AMS

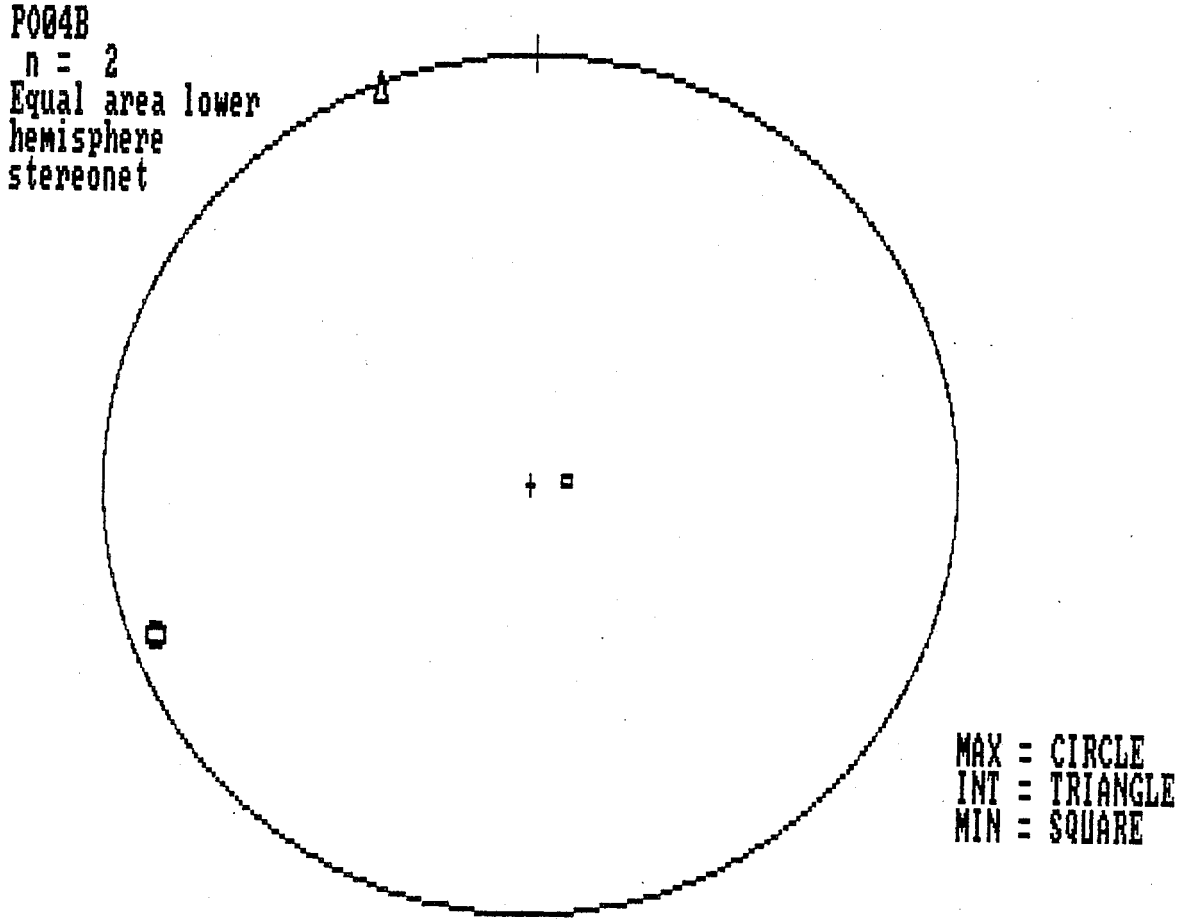

P005A SITE 1 CORE 1 SPEC 1 UNITS= SI m M= 12 NR= 2 15:01:05 01-24-1990

SUSC.	DEC	INC	R95	EV	SDEV
MIN	304.20	-77.40	0.3	1.1680E-01	7.796E-05
INT	322.25	12.00	2.7	1.3176E-01	1.783E-05
MAX	51.44	-3.79	2.7	1.3429E-01	5.869E-05

P005B SITE 1 CORE 1 SPEC 1 UNITS= SI m M= 12 NR= 2 15:09:43 01-24-1990

SUSC.	DEC	INC	R95	EV	SDEV
MIN	304.33	-77.38	0.4	1.1680E-01	7.684E-05
INT	321.74	12.06	1.4	1.3180E-01	2.411E-05
MAX	50.96	-3.67	1.4	1.3415E-01	3.495E-05

AMS

P005B
n = 2
Equal area lower hemisphere stereonet

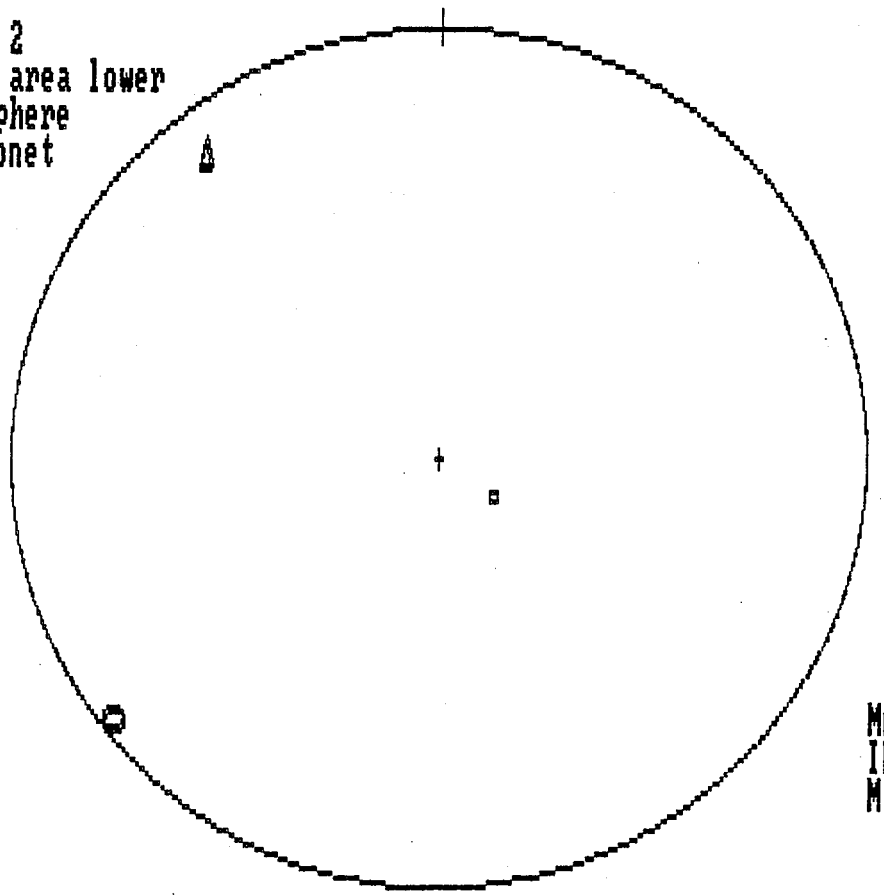

MAX = CIRCLE
INT = TRIANGLE
MIN = SQUARE

P006A SITE 1 CORE 1 SPEC 1 UNITS= SI m M= 12 NR= 2 15:20:39 01-24-1990

SUSC.	DEC	INC	R95	EV	SDEV
MIN	340.80	-83.23	1.1	1.3965E-01	2.368E-05
INT	290.45	4.33	3.0	1.6384E-01	1.285E-05
MAX	20.85	5.19	3.1	1.6560E-01	6.469E-05

P006B SITE 1 CORE 1 SPEC 1 UNITS= SI m M= 12 NR= 2 15:29:43 01-24-1990

SUSC.	DEC	INC	R95	EV	SDEV
MIN	343.91	-82.62	1.0	1.3967E-01	3.483E-05
INT	290.37	4.40	2.8	1.6383E-01	3.545E-05
MAX	20.83	5.91	2.9	1.6558E-01	1.086E-04

AMS

P006B
n = 2
Equal area lower hemisphere stereonet

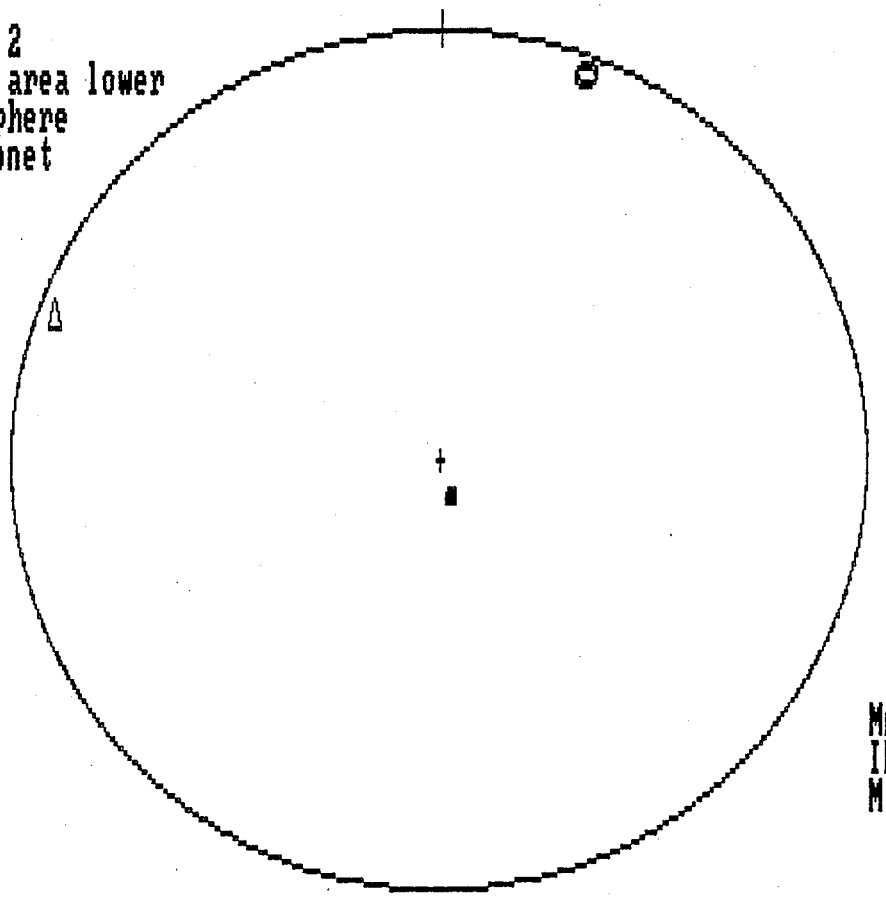

MAX = CIRCLE
INT = TRIANGLE
MIN = SQUARE

rims

P007A SITE 1 CORE 1 SPEC 1 UNITS= SI m M= 12 NR= 2 15:39:05 01-24-1990

SUSC.	DEC	INC	R95	EV	SDEV
MIN	56.36	83.69	0.3	1.1618E-01	2.477E-05
INT	333.80	-0.83	32.6	1.5495E-01	4.341E-06
MAX	63.95	-6.25	32.6	1.5546E-01	1.916E-04

P007B SITE 1 CORE 1 SPEC 1 UNITS= SI m M= 12 NR= 2 15:46:54 01-24-1990

SUSC.	DEC	INC	R95	EV	SDEV
MIN	56.30	83.69	0.3	1.1616E-01	3.878E-05
INT	333.86	-0.84	31.7	1.5494E-01	4.594E-05
MAX	64.01	-6.25	31.8	1.5545E-01	1.899E-04

rims

P007B
n = 2
Equal area lower hemisphere stereonet

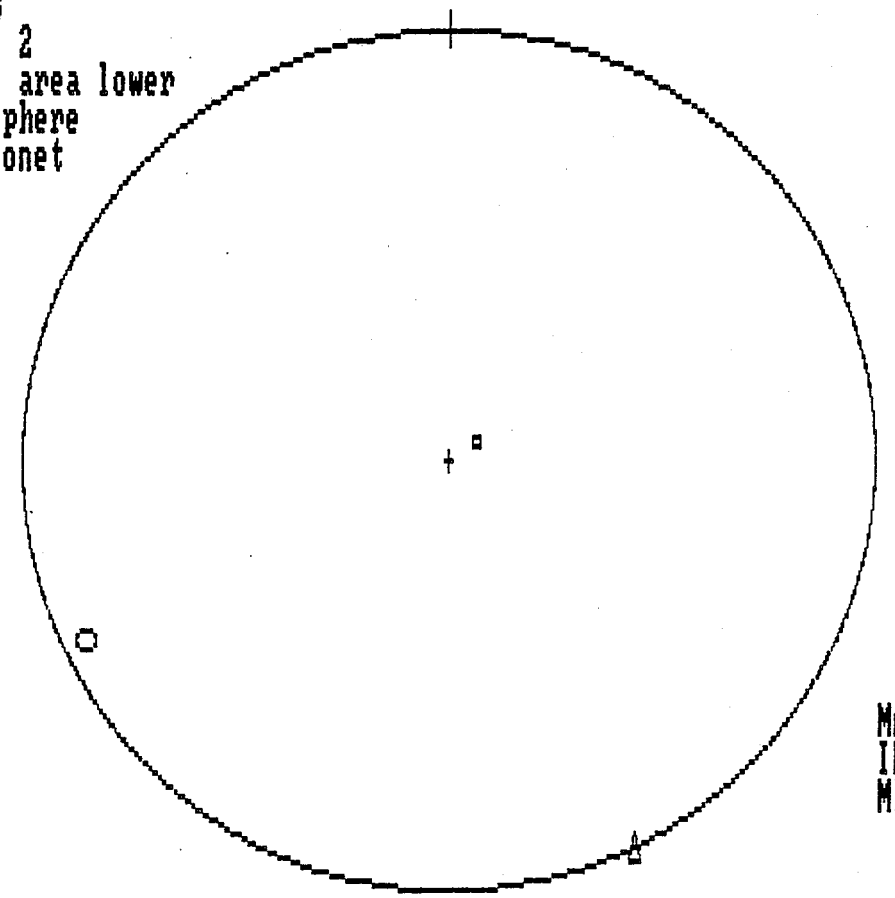

MAX = CIRCLE
INT = TRIANGLE
MIN = SQUARE

P008A SITE 1 CORE 1 SPEC 1 UNITS= SI m M= 12 NR= 2 15:55:23 01-24-1990

SUSC.	DEC	INC	R95	EV	SDEV
MIN	319.62	-81.74	0.6	1.3751E-01	7.191E-05
INT	1.52	6.17	4.2	1.6288E-01	9.644E-05
MAX	271.01	5.49	4.3	1.6402E-01	9.348E-05

P008B SITE 1 CORE 1 SPEC 1 UNITS= SI m M= 12 NR= 2 16:03:00 01-24-1990

SUSC.	DEC	INC	R95	EV	SDEV
MIN	319.23	-81.79	0.6	1.3752E-01	5.347E-05
INT	1.99	6.05	23.5	1.6289E-01	1.430E-04
MAX	271.48	5.54	23.6	1.6377E-01	1.554E-04

P008B
n = 2
Equal area lower hemisphere stereonet

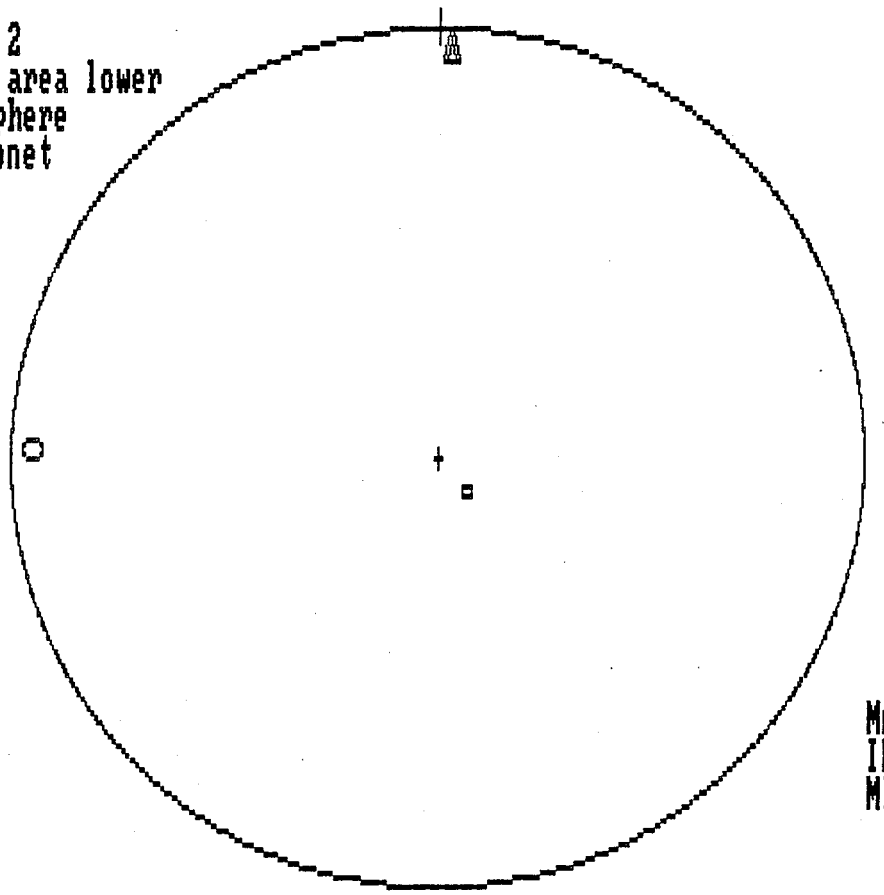

MAX = CIRCLE
INT = TRIANGLE
MIN = SQUARE

AMS

P009A SITE 1 CORE 1 SPEC 1 UNITS= SI m M= 12 NR= 2 15:58:32 03-14-1990

SUSC.	DEC	INC	R95	EV	SDEV
MIN	347.13	79.20	4.1	4.9034E-05	2.468E-08
INT	303.25	-7.83	5.8	5.0365E-05	1.239E-07
MAX	34.27	-7.40	4.8	5.1032E-05	1.997E-07

P009B SITE 1 CORE 1 SPEC 1 UNITS= SI m M= 12 NR= 2 16:07:04 03-14-1990

SUSC.	DEC	INC	R95	EV	SDEV
MIN	341.73	78.75	3.8	4.9010E-05	1.168E-08
INT	307.16	-9.30	2.6	5.0192E-05	1.187E-08
MAX	38.19	-6.27	2.8	5.1192E-05	6.510E-09

AMS

P009B
n = 2
Equal area lower hemisphere stereonet

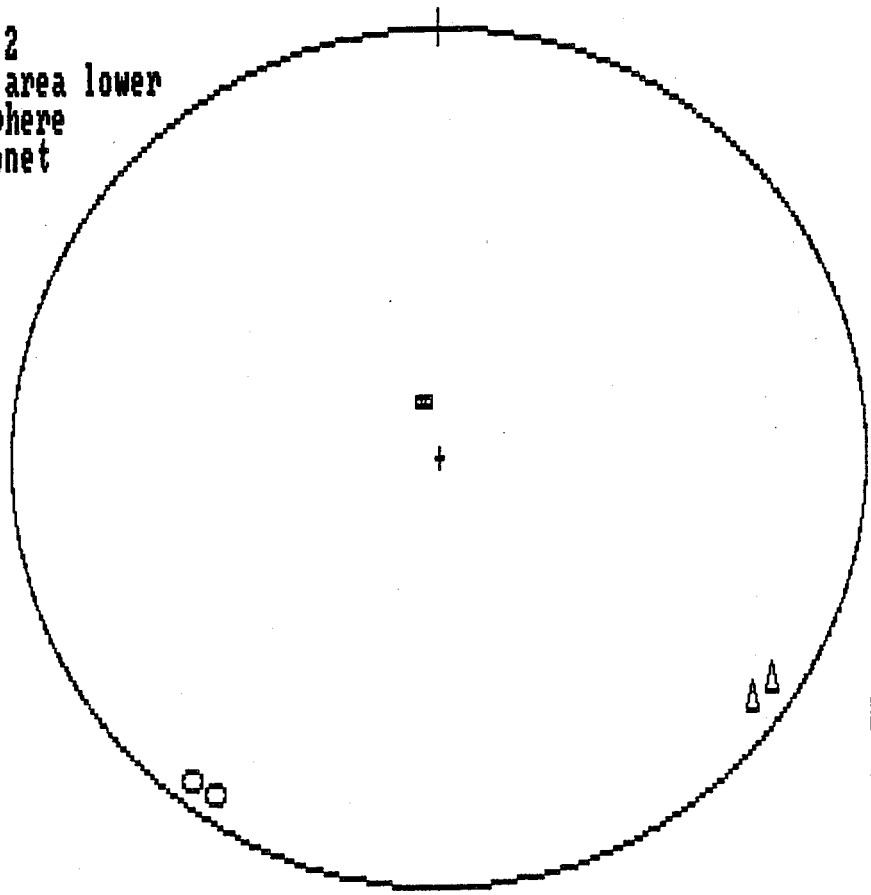

MAX = CIRCLE
INT = TRIANGLE
MIN = SQUARE

AMS

P010A SITE 1 CORE 1 SPEC 1 UNITS= SI m M= 12 NR= 2 16:20:19 03-14-1990

SUSC.	DEC	INC	R95	EV	SDEV
MIN	310.09	63.18	4.4	4.4187E-05	5.476E-08
INT	24.77	-7.61	8.8	4.5271E-05	9.527E-08
MAX	291.11	-25.55	8.1	4.6289E-05	2.961E-08

P010B SITE 1 CORE 1 SPEC 1 UNITS= SI m M= 12 NR= 2 16:32:55 03-14-1990

SUSC.	DEC	INC	R95	EV	SDEV
MIN	308.19	63.57	4.8	4.4180E-05	2.936E-08
INT	24.03	-6.93	7.1	4.5296E-05	4.148E-08
MAX	290.73	-25.37	5.4	4.6270E-05	2.815E-08

AMS

P011A SITE 1 CORE 1 SPEC 1 UNITS= SI m M= 12 NR= 2 16:46:11 03-14-1990

SUSC.	DEC	INC	R95	EV	SDEV
MIN	35.84	-88.12	0.6	2.1070E-05	5.455E-09
INT	73.89	1.48	5.6	2.4336E-05	8.726E-09
MAX	343.85	1.16	5.6	2.4480E-05	1.198E-08

P011B SITE 1 CORE 1 SPEC 1 UNITS= SI m M= 12 NR= 2 16:54:21 03-14-1990

SUSC.	DEC	INC	R95	EV	SDEV
MIN	28.95	-87.78	0.7	2.1071E-05	8.282E-09
INT	74.99	1.55	2.5	2.4339E-05	6.640E-09
MAX	344.93	1.60	2.4	2.4484E-05	6.845E-09

AMS

P012A SITE 1 CORE 1 SPEC 1 UNITS= SI m M= 12 NR= 2 17:07:06 03-14-1990

SUSC.	DEC	INC	R95	EV	SDEV
MIN	83.67	-84.81	0.7	2.3205E-05	6.280E-09
INT	295.62	-4.41	2.7	2.5281E-05	6.036E-09
MAX	25.41	2.73	2.7	2.5585E-05	1.994E-08

P012B SITE 1 CORE 1 SPEC 1 UNITS= SI m M= 12 NR= 2 17:14:34 03-14-1990

SUSC.	DEC	INC	R95	EV	SDEV
MIN	82.46	-84.88	1.2	2.3208E-05	4.358E-09
INT	295.30	-4.31	1.6	2.5287E-05	5.258E-09
MAX	25.09	2.77	2.0	2.5594E-05	1.443E-08

AMS

P012B
n = 2
Equal area lower hemisphere stereonet

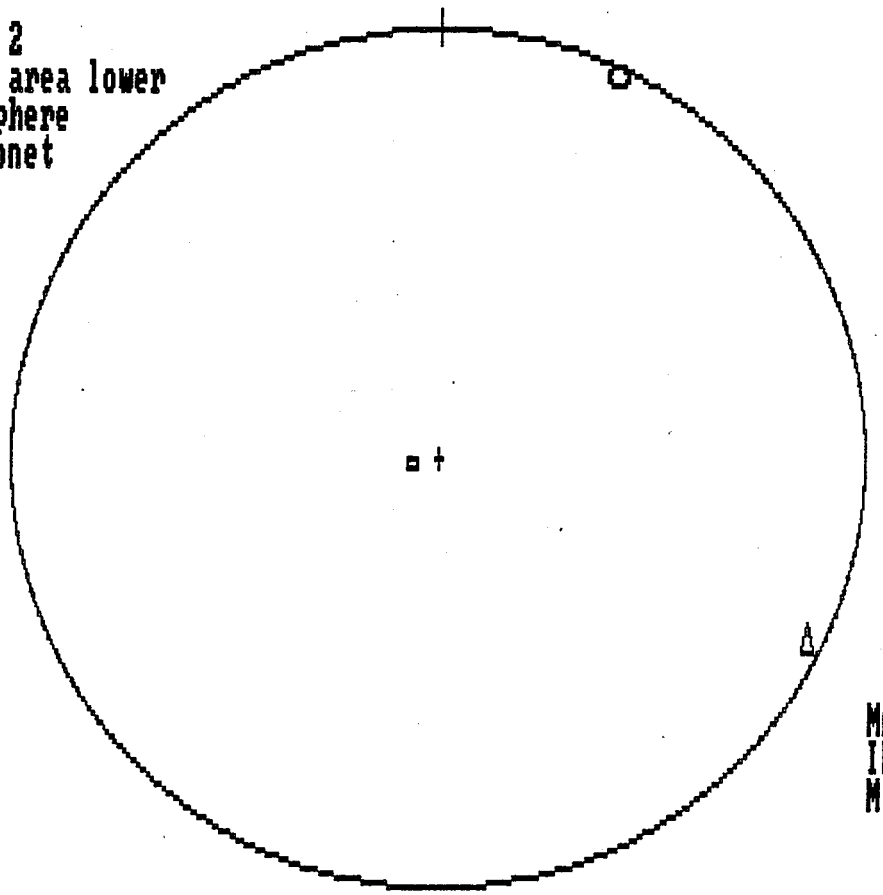

MAX = CIRCLE
INT = TRIANGLE
MIN = SQUARE

HMS DATA P013

P013A SITE 1 CORE 1 SPEC 1 UNITS= SI m M= 12 NR= 2 11:28:54 03-13-1990

SUSC.	DEC	INC	R95	EV	SDEV
MIN	73.08	85.44	1.1	2.1814E-05	8.998E-09
INT	4.62	-1.68	17.4	2.3813E-05	2.104E-08
MAX	274.76	4.24	17.4	2.3973E-05	3.298E-08

P013B SITE 1 CORE 1 SPEC 1 UNITS= SI m M= 12 NR= 2 11:37:49 03-13-1990

SUSC.	DEC	INC	R95	EV	SDEV
MIN	73.82	85.42	0.9	2.1863E-05	8.299E-09
INT	0.97	-1.36	9.2	2.3882E-05	1.163E-08
MAX	270.00	4.39	8.1	2.4030E-05	1.382E-08

P014A SITE 1 CORE 1 SPEC 1 UNITS= SI m M= 12 NR= 2 10:13:56 03-14-1990

SUSC.	DEC	INC	R95	EV	SDEV
MIN	64.59	85.53	1.2	2.3170E-05	4.801E-09
INT	326.68	0.63	1.8	2.4609E-05	1.794E-08
MAX	56.63	-4.43	2.1	2.5338E-05	5.717E-08

P014B SITE 1 CORE 1 SPEC 1 UNITS= SI m M= 12 NR= 2 10:33:32 03-14-1990

SUSC.	DEC	INC	R95	EV	SDEV
MIN	63.03	85.53	1.2	2.3214E-05	8.788E-09
INT	326.33	0.54	0.9	2.4661E-05	2.539E-09
MAX	56.28	-4.44	1.5	2.5397E-05	3.156E-08

AMS

P014B
n = 2
Equal area lower hemisphere stereonet

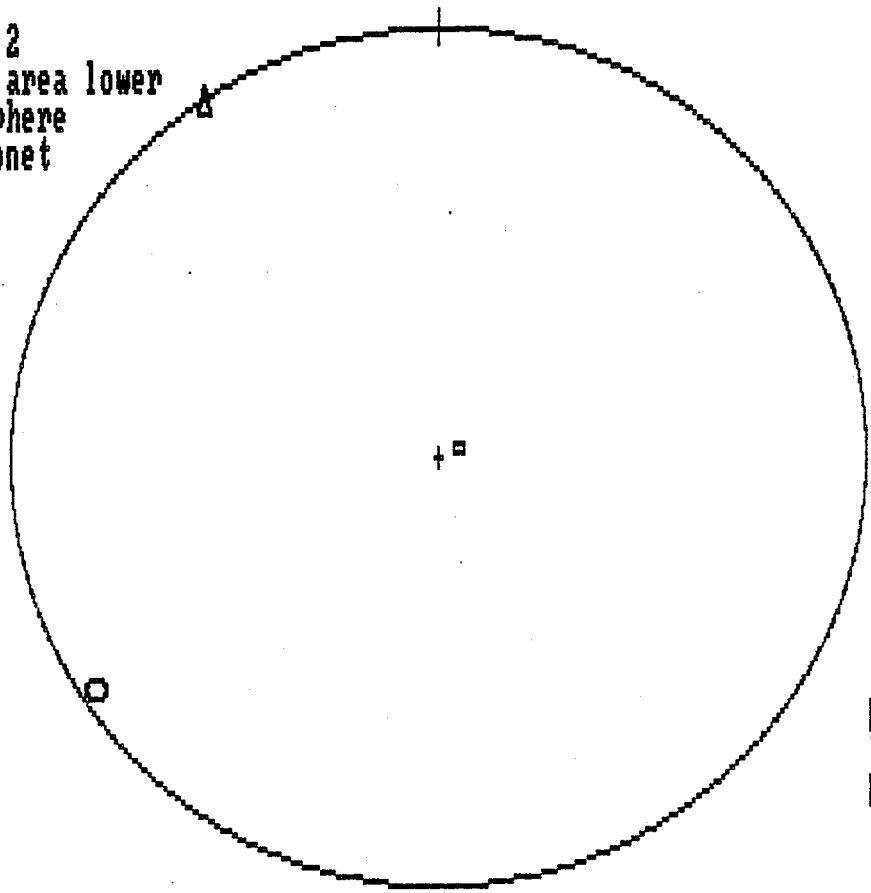

MAX = CIRCLE
INT = TRIANGLE
MIN = SQUARE

AMS DATA

P015A SITE 1 CORE 1 SPEC 1 UNITS= SI m M= 12 NR= 2 11:55:18 03-14-1990

SUSC.	DEC	INC	R95	EV	SDEV
MIN	358.64	88.72	0.8	2.1560E-05	1.211E-08
INT	344.69	-1.24	1.9	2.4481E-05	5.564E-09
MAX	74.69	-0.32	2.0	2.4631E-05	3.487E-09

P015B SITE 1 CORE 1 SPEC 1 UNITS= SI m M= 12 NR= 2 12:05:16 03-14-1990

SUSC.	DEC	INC	R95	EV	SDEV
MIN	2.78	88.72	0.8	2.1526E-05	1.414E-08
INT	348.39	-1.25	4.0	2.4424E-05	7.930E-09
MAX	78.39	-0.31	4.1	2.4575E-05	3.465E-09

A-5

P015B
n = 2
Equal area lower hemisphere stereonet

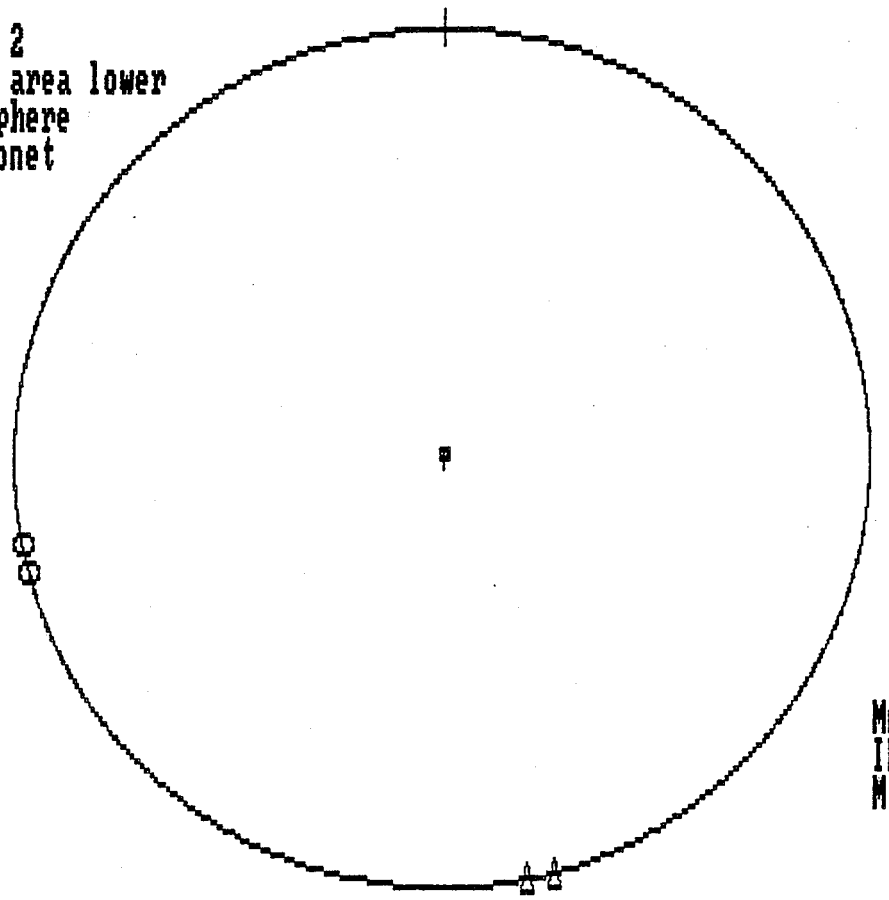

MAX = CIRCLE
INT = TRIANGLE
MIN = SQUARE

AMS

P016A SITE 1 CORE 1 SPEC 1 UNITS= SI m M= 12 NR= 2 15:06:42 03-14-1990

SUSC.	DEC	INC	R95	EV	SDEV
MIN	18.44	83.69	0.7	2.2972E-05	3.815E-09
INT	84.44	-2.58	2.0	2.5554E-05	5.320E-09
MAX	354.17	-5.75	1.9	2.5881E-05	9.373E-09

P016B SITE 1 CORE 1 SPEC 1 UNITS= SI m M= 12 NR= 2 15:14:57 03-14-1990

SUSC.	DEC	INC	R95	EV	SDEV
MIN	26.11	83.52	2.1	2.2985E-05	2.053E-09
INT	85.17	-3.35	3.2	2.5568E-05	1.001E-08
MAX	354.83	-5.55	2.5	2.5903E-05	8.887E-09

AMS

P016B
n = 2
Equal area lower hemisphere stereonet

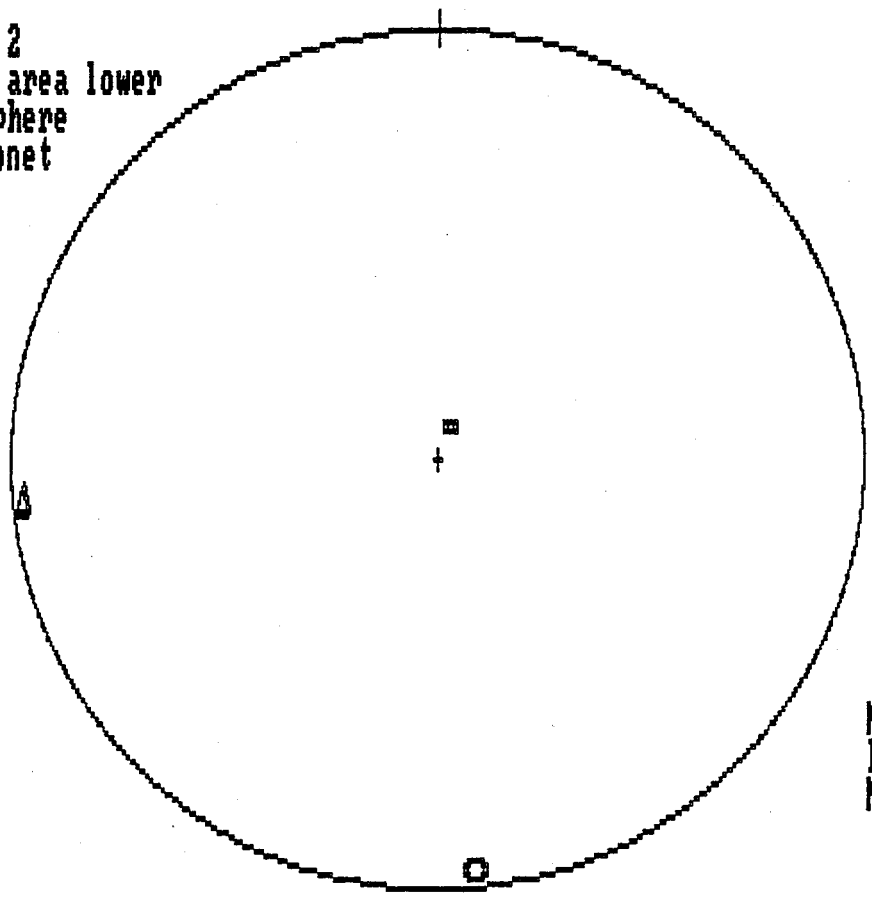

MAX = CIRCLE
INT = TRIANGLE
MIN = SQUARE

AMS

P018A SITE 1 CORE 1 SPEC 1 UNITS= SI m M= 12 NR= 2 11:06:32 03-15-1990

SUSC.	DEC	INC	R95	EV	SDEV
MIN	332.30	84.17	1.1	2.1914E-05	7.303E-09
INT	23.88	-3.63	1.3	2.5242E-05	6.719E-09
MAX	293.59	-4.56	1.0	2.5683E-05	4.599E-09

P018B SITE 1 CORE 1 SPEC 1 UNITS= SI m M= 12 NR= 2 11:15:08 03-15-1990

SUSC.	DEC	INC	R95	EV	SDEV
MIN	331.99	84.17	1.4	2.1912E-05	5.717E-09
INT	24.18	-3.59	1.2	2.5245E-05	4.898E-09
MAX	293.89	-4.60	0.6	2.5685E-05	9.537E-09

AMS

P018B
n = 2
Equal area lower hemisphere stereonet

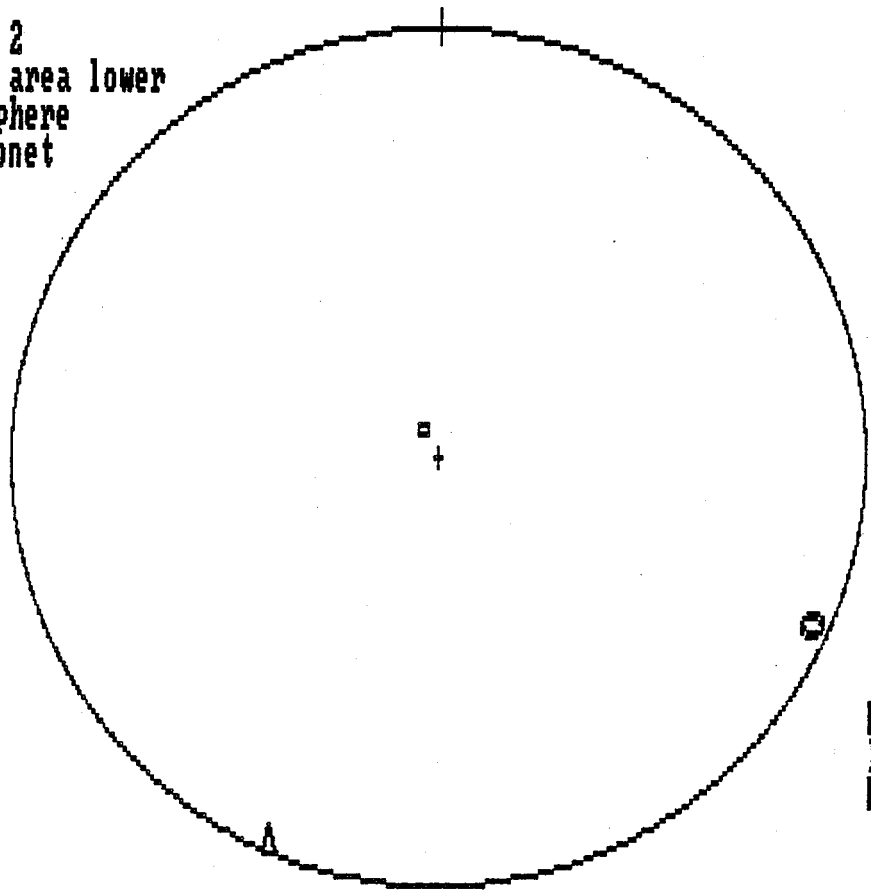

MAX = CIRCLE
INT = TRIANGLE
MIN = SQUARE

AMS

P019A SITE 1 CORE 1 SPEC 1 UNITS= SI m M= 12 NR= 2 15:30:35 03-27-1990

SUSC.	DEC	INC	R95	EV	SDEV
MIN	348.43	-87.77	0.8	1.8720E-05	4.041E-09
INT	325.47	2.06	3.8	2.3935E-05	3.008E-08
MAX	55.50	0.87	3.9	2.4253E-05	5.861E-08

P019B SITE 1 CORE 1 SPEC 1 UNITS= SI m M= 12 NR= 2 15:40:50 03-27-1990

SUSC.	DEC	INC	R95	EV	SDEV
MIN	348.86	-87.49	0.9	1.8705E-05	7.029E-09
INT	324.26	2.28	3.4	2.3979E-05	9.287E-09
MAX	54.31	1.04	3.5	2.4296E-05	3.803E-08

AMS

P019B
n = 2
Equal area lower hemisphere stereonet

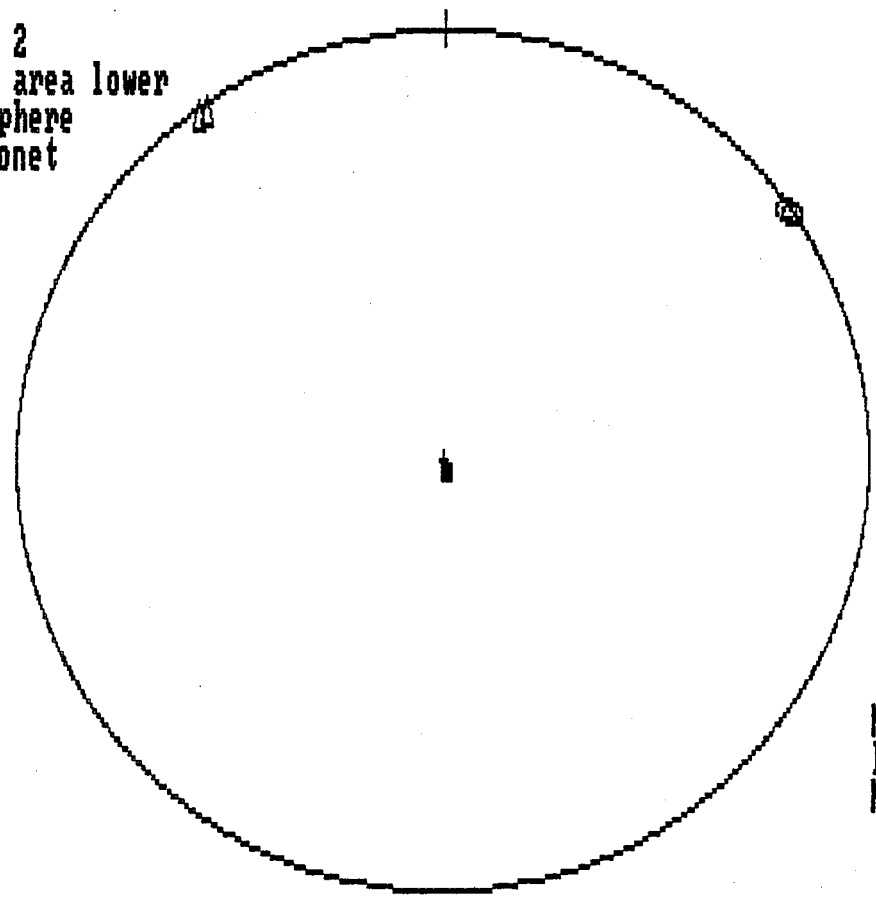

MAX = CIRCLE
INT = TRIANGLE
MIN = SQUARE

AMS

```
P020A SITE 1   CORE 1 SPEC 1 UNITS= SI m M= 12  NR= 2   16:32:59  03-30-1990
SUSC.     DEC     INC    R95     EV           SDEV
MIN      18.37 -88.36    1.6  2.0714E-05  8.104E-08
INT      76.33   0.88   11.8  2.4127E-05  3.126E-08
MAX     346.29   1.39   11.7  2.4236E-05  6.202E-09

P020B SITE 1   CORE 1 SPEC 1 UNITS= SI m M= 12  NR= 2   16:41:10  03-30-1990
SUSC.     DEC     INC    R95     EV           SDEV
MIN      14.22 -88.13    1.0  2.0753E-05  1.037E-08
INT      75.43   0.91    6.5  2.4082E-05  1.421E-08
MAX     345.38   1.64    6.5  2.4185E-05  9.521E-09
P020B FSN= 1  LSN= 1  D SN= 0  NT= 1  NA= 2  16:42:26  03-30-1990
```

AMS

P020B
n = 2
Equal area lower hemisphere stereonet

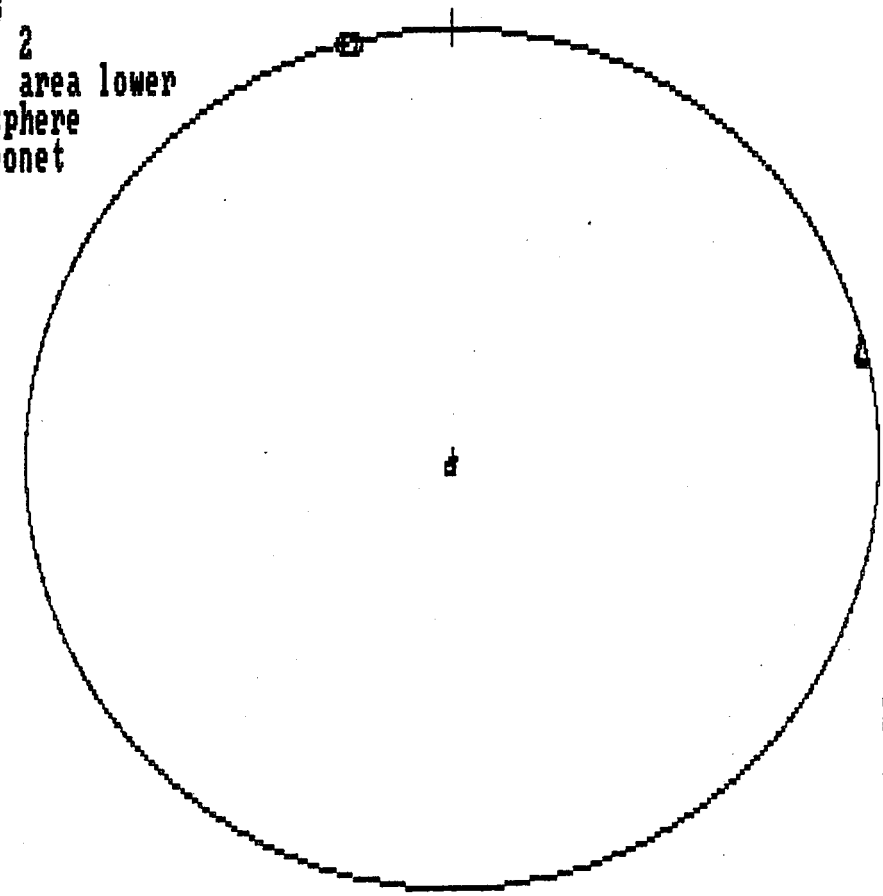

MAX = CIRCLE
INT = TRIANGLE
MIN = SQUARE

AMS

P021A SITE 1 CORE 1 SPEC 1 UNITS= SI m M= 12 NR= 2 11:16:55 04-12-1990

SUSC.	DEC	INC	R95	EV	SDEV
MIN	20.16	88.63	0.5	1.8296E-05	6.224E-09
INT	4.60	-1.33	1.1	2.0695E-05	9.396E-09
MAX	274.61	0.37	1.1	2.1271E-05	1.662E-09

P021B SITE 1 CORE 1 SPEC 1 UNITS= SI m M= 12 NR= 2 11:25:37 04-12-1990

SUSC.	DEC	INC	R95	EV	SDEV
MIN	23.54	88.62	0.9	1.8304E-05	3.417E-09
INT	4.39	-1.31	1.0	2.0703E-05	4.202E-09
MAX	274.41	0.45	0.9	2.1273E-05	5.541E-09

AMS

P021B
n = 2
Equal area lower hemisphere stereonet

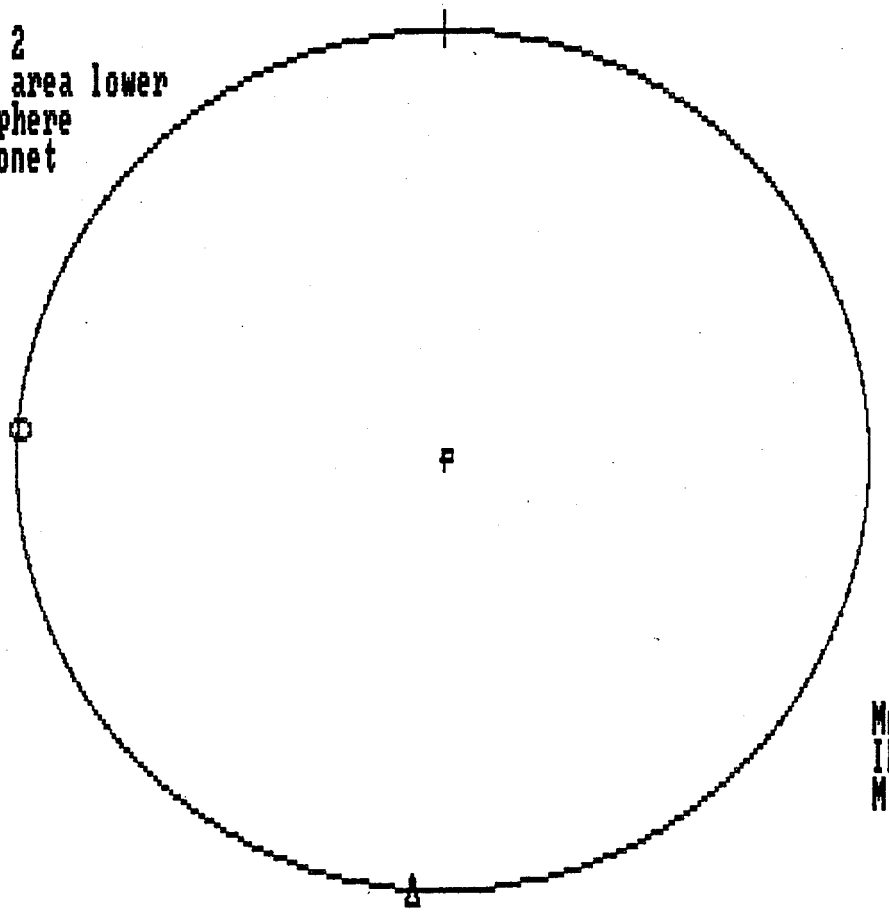

MAX = CIRCLE
INT = TRIANGLE
MIN = SQUARE

A115

P022A SITE 1 CORE 1 SPEC 1 UNITS= SI m M= 12 NR= 2 14:15:49 04-10-1990

SUSC.	DEC	INC	R95	EV	SDEV
MIN	322.28	84.95	0.5	2.0046E-05	4.731E-09
INT	64.88	1.11	2.1	2.3967E-05	9.690E-09
MAX	334.99	-4.93	2.1	2.4162E-05	6.470E-09

P022B SITE 1 CORE 1 SPEC 1 UNITS= SI m M= 12 NR= 2 14:24:25 04-10-1990

SUSC.	DEC	INC	R95	EV	SDEV
MIN	321.29	84.80	0.6	2.0058E-05	6.809E-09
INT	66.20	1.35	1.7	2.3995E-05	6.946E-09
MAX	336.32	-5.03	1.5	2.4186E-05	4.213E-09

AMS

P023A SITE 1 CORE 1 SPEC 1 UNITS= SI m M= 12 NR= 2 11:49:38 04-24-1990

SUSC.	DEC	INC	R95	EV	SDEV
MIN	47.66	87.84	0.2	2.0361E-05	1.469E-08
INT	65.15	-2.06	2.7	2.3751E-05	7.771E-09
MAX	335.12	-0.65	2.7	2.3898E-05	8.481E-09

P023B SITE 1 CORE 1 SPEC 1 UNITS= SI m M= 12 NR= 2 11:58:07 04-24-1990

SUSC.	DEC	INC	R95	EV	SDEV
MIN	64.34	87.41	0.7	2.0391E-05	4.557E-09
INT	65.16	-2.59	0.9	2.3752E-05	8.560E-09
MAX	335.13	-0.02	0.6	2.3911E-05	6.844E-09

AMS

P023B
n = 2
Equal area lower hemisphere stereonet

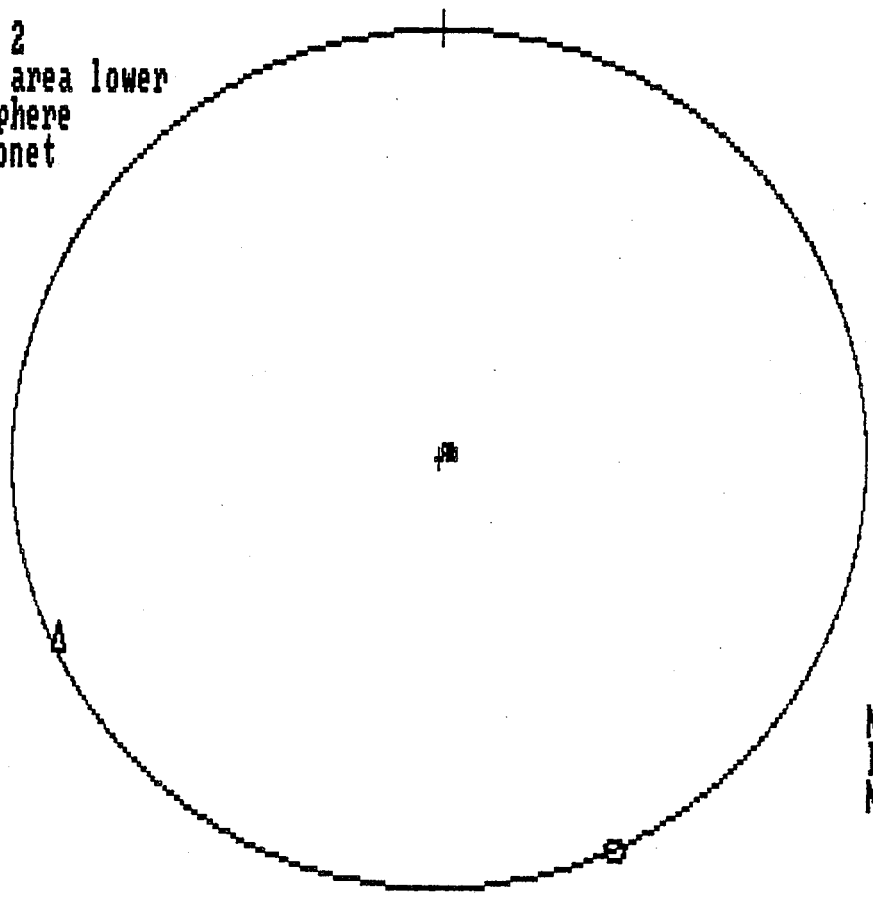

MAX = CIRCLE
INT = TRIANGLE
MIN = SQUARE

AMS

P024A SITE 1 CORE 1 SPEC 1 UNITS= SI m M= 12 NR= 2 11:36:06 04-25-1990

SUSC.	DEC	INC	R95	EV	SDEV
MIN	308.80	-81.84	5.3	3.1047E-05	3.444E-08
INT	283.48	7.39	10.8	3.1988E-05	5.599E-08
MAX	13.93	3.45	11.3	3.2367E-05	8.830E-08

P024B SITE 1 CORE 1 SPEC 1 UNITS= SI m M= 12 NR= 2 11:45:17 04-25-1990

SUSC.	DEC	INC	R95	EV	SDEV
MIN	306.96	-82.26	3.1	3.1136E-05	6.407E-09
INT	283.30	7.09	2.8	3.2076E-05	3.879E-09
MAX	13.69	3.07	3.9	3.2528E-05	3.249E-08

P024C SITE 1 CORE 1 SPEC 1 UNITS= SI m M= 12 NR= 2 11:57:29 04-25-1990

SUSC.	DEC	INC	R95	EV	SDEV
MIN	307.49	-82.10	3.4	3.1150E-05	6.298E-09
INT	282.10	7.15	2.6	3.2087E-05	3.650E-09
MAX	12.52	3.35	3.6	3.2543E-05	2.481E-08

P024C
n = 3
Equal area lower hemisphere stereonet

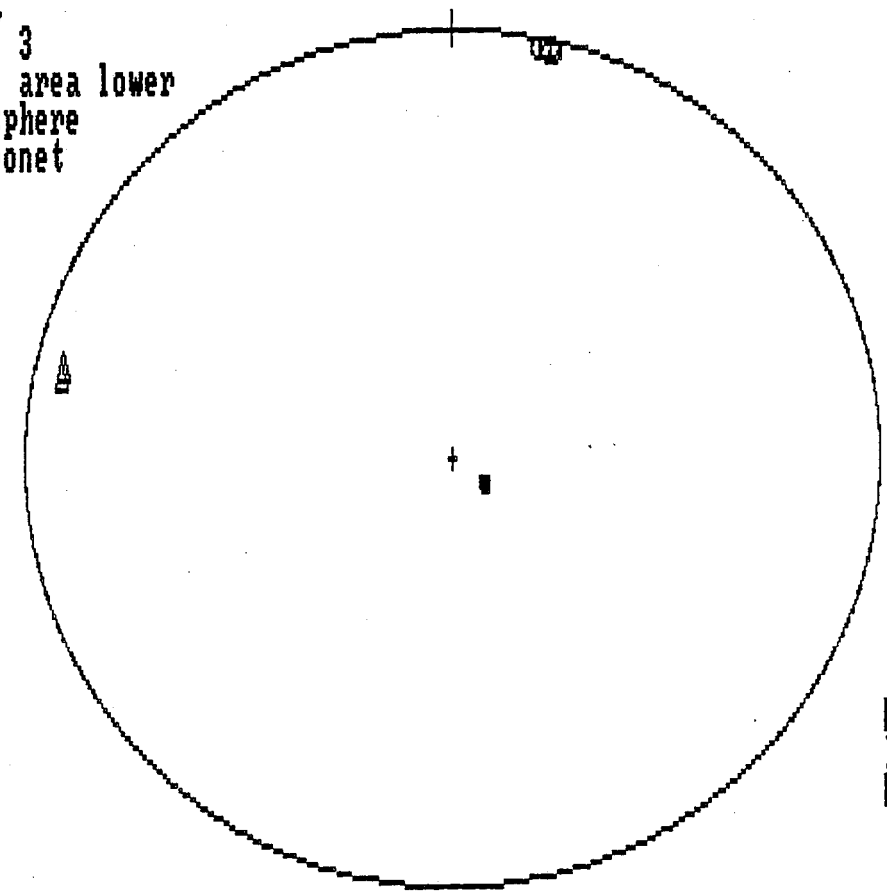

MAX = CIRCLE
INT = TRIANGLE
MIN = SQUARE

AMS

P025A SITE 1 CORE 1 SPEC 1 UNITS= SI m M= 12 NR= 2 11:41:40 04-26-1990

SUSC.	DEC	INC	R95	EV	SDEV
MIN	41.85	69.05	2.4	3.0850E-05	2.443E-08
INT	306.98	1.87	4.2	3.1781E-05	1.838E-08
MAX	36.25	-20.85	4.7	3.1844E-05	1.846E-08

P025A SITE 1 CORE 1 SPEC 2 UNITS= SI m M= 12 NR= 2 11:49:56 04-26-1990

SUSC.	DEC	INC	R95	EV	SDEV
MIN	42.33	69.43	3.0	3.0895E-05	3.598E-08
INT	306.28	2.27	10.1	3.1808E-05	5.266E-09
MAX	35.42	-20.44	10.5	3.1890E-05	4.245E-08

AMS

P025A
n = 2
Equal area lower hemisphere stereonet

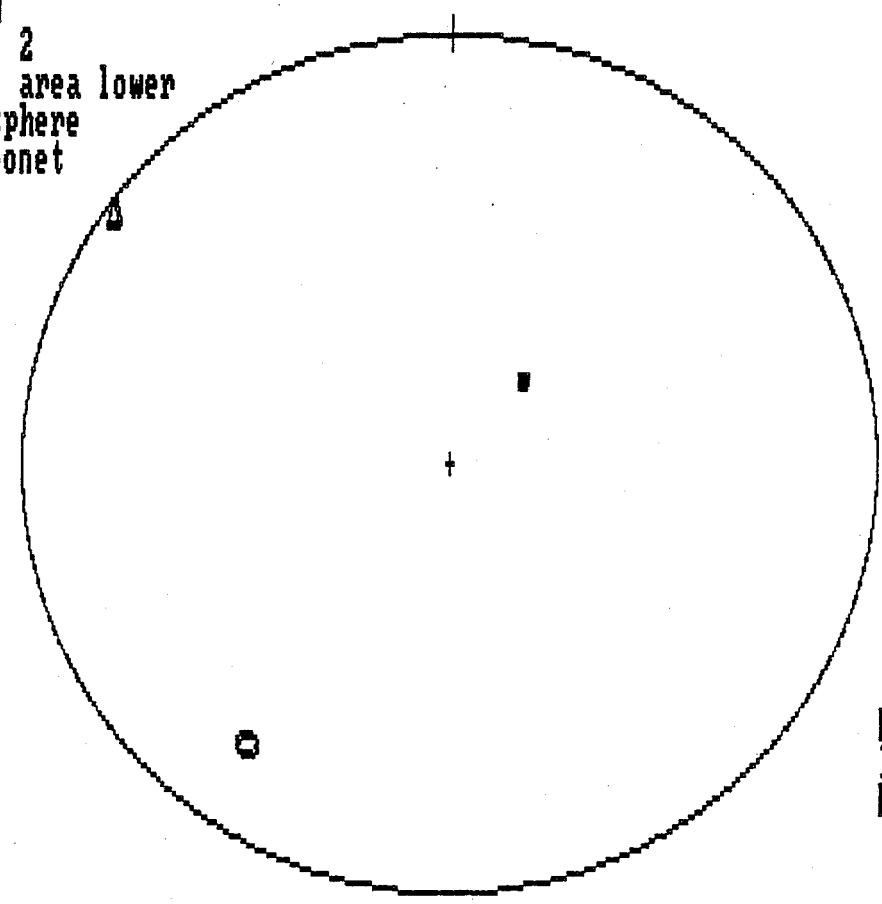

MAX = CIRCLE
INT = TRIANGLE
MIN = SQUARE

AMS

P026A SITE 1 CORE 1 SPEC 1 UNITS= SI m M= 12 NR= 2 11:22:57 05-01-1990

SUSC.	DEC	INC	R95	EV	SDEV
MIN	292.97	-88.84	1.4	2.4080E-05	4.034E-08
INT	14.03	0.22	6.5	2.6890E-05	2.862E-08
MAX	284.02	1.15	6.4	2.7112E-05	8.539E-09

P026A SITE 1 CORE 1 SPEC 2 UNITS= SI m M= 12 NR= 2 11:31:20 05-01-1990

SUSC.	DEC	INC	R95	EV	SDEV
MIN	296.75	-88.92	2.2	2.4112E-05	1.453E-08
INT	6.05	0.40	5.9	2.6940E-05	1.453E-08
MAX	276.05	1.01	5.7	2.7115E-05	1.180E-08

AMS

P026A
n = 2
Equal area lower hemisphere stereonet

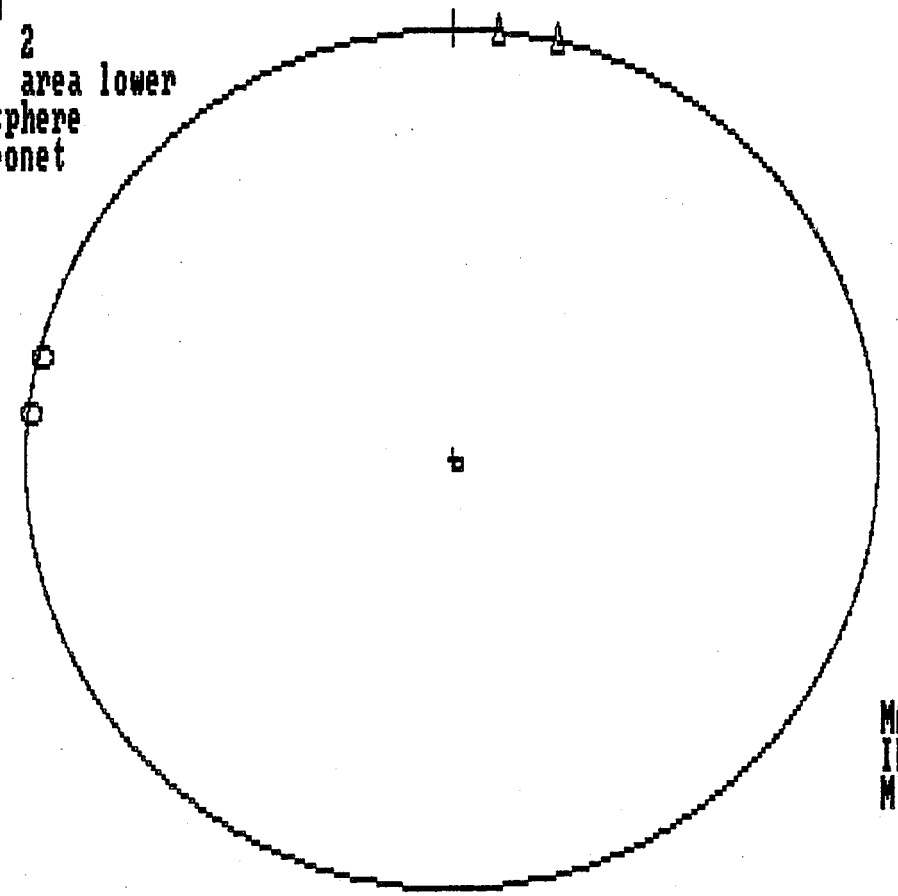

MAX = CIRCLE
INT = TRIANGLE
MIN = SQUARE

AMS

P027A SITE 1 CORE 1 SPEC 1 UNITS= SI m M= 12 NR= 2 10:19:55 05-02-1990

SUSC.	DEC	INC	R95	EV	SDEV
MIN	48.17	84.62	1.3	2.6977E-05	1.735E-09
INT	48.51	-5.38	1.2	2.8050E-05	3.238E-08
MAX	318.50	-0.01	1.0	2.8361E-05	1.175E-08

P027A SITE 1 CORE 1 SPEC 2 UNITS= SI m M= 12 NR= 2 10:28:53 05-02-1990

SUSC.	DEC	INC	R95	EV	SDEV
MIN	47.57	84.57	2.5	2.6992E-05	7.201E-09
INT	50.65	-5.42	2.8	2.8060E-05	1.658E-08
MAX	320.62	-0.29	1.3	2.8375E-05	3.950E-09

AMS

P027A
n = 2
Equal area lower hemisphere stereonet

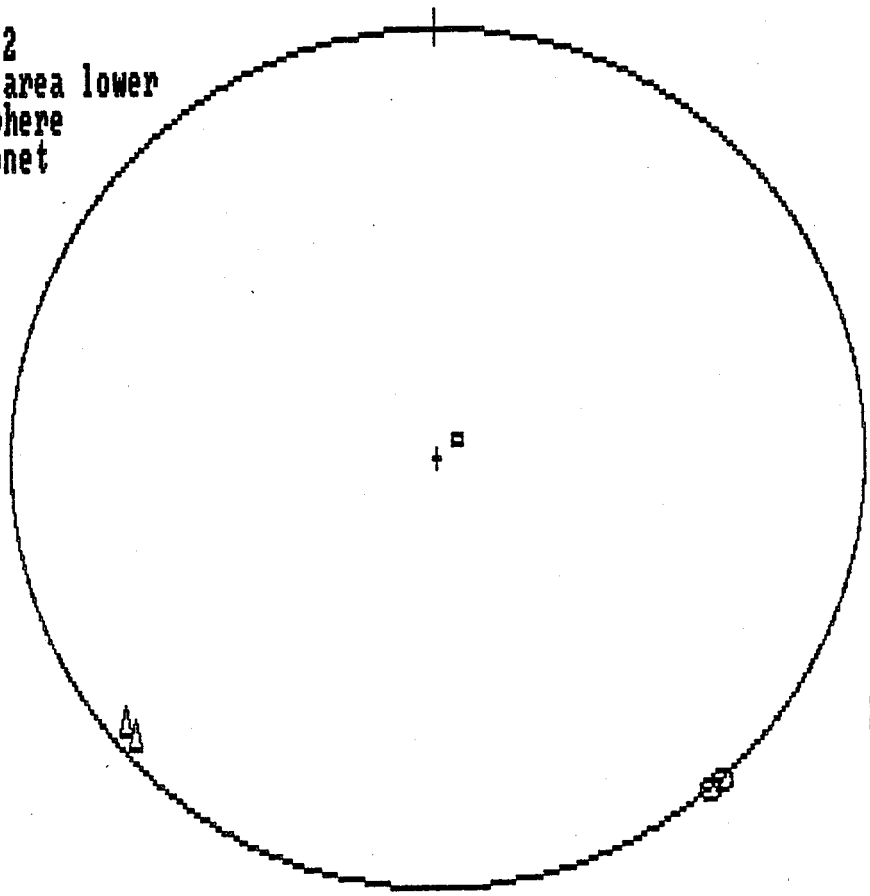

MAX = CIRCLE
INT = TRIANGLE
MIN = SQUARE

A:15

P028A SITE 1 CORE 1 SPEC 1 UNITS= SI m M= 12 NR= 2 15:37:54 05-17-1990

SUSC.	DEC	INC	R95	EV	SDEV
MIN	63.03	82.46	7.6	2.7976E-05	1.193E-07
INT	308.72	3.12	14.7	2.9773E-05	1.317E-07
MAX	38.34	-6.86	15.4	3.0075E-05	2.068E-08

P028A SITE 1 CORE 1 SPEC 2 UNITS= SI m M= 12 NR= 2 15:46:15 05-17-1990

SUSC.	DEC	INC	R95	EV	SDEV
MIN	62.27	82.69	8.4	2.7930E-05	8.764E-08
INT	325.56	0.87	11.8	2.9906E-05	5.297E-09
MAX	55.44	-7.25	14.4	3.0121E-05	2.444E-08

P028A FSN= 0 LSN= 0 D SN=-1 NT= 2 NA= 2 15:47:30 05-17-1990

AMS

P028A
n = 2
Equal area lower hemisphere stereonet

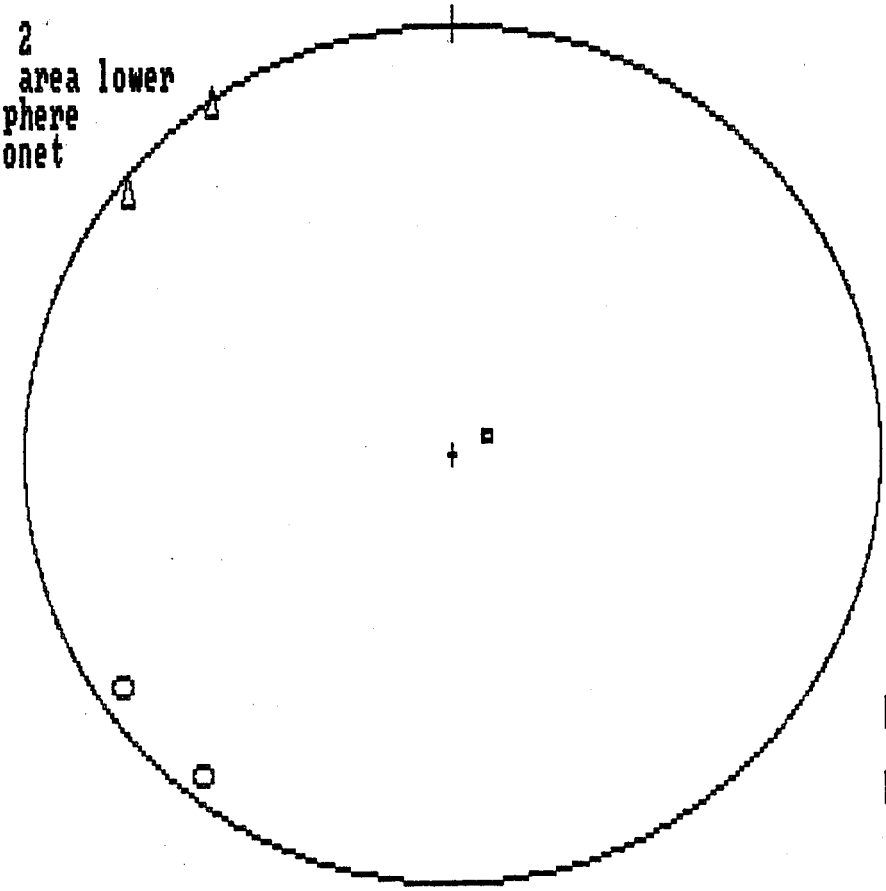

MAX = CIRCLE
INT = TRIANGLE
MIN = SQUARE

AMS

TP06A SITE 1 CORE 1 SPEC 1 UNITS= SI m M= 12 NR= 2 16:07:43 06-25-1990

SUSC.	DEC	INC	R95	EV	SDEV
MIN	0.14	84.96	1.0	2.3488E-05	5.973E-09
INT	12.80	-4.92	45.0	2.5111E-05	1.221E-08
MAX	282.72	-1.11	45.1	2.5139E-05	3.179E-08

TP06A SITE 1 CORE 1 SPEC 2 UNITS= SI m M= 12 NR= 2 16:15:58 06-25-1990

SUSC.	DEC	INC	R95	EV	SDEV
MIN	357.35	85.04	1.2	2.3509E-05	8.000E-09
INT	6.32	-4.90	57.9	2.5144E-05	5.129E-09
MAX	276.37	-0.78	57.9	2.5156E-05	8.839E-09

AMS

TP06A
n = 2
Equal area lower hemisphere stereonet

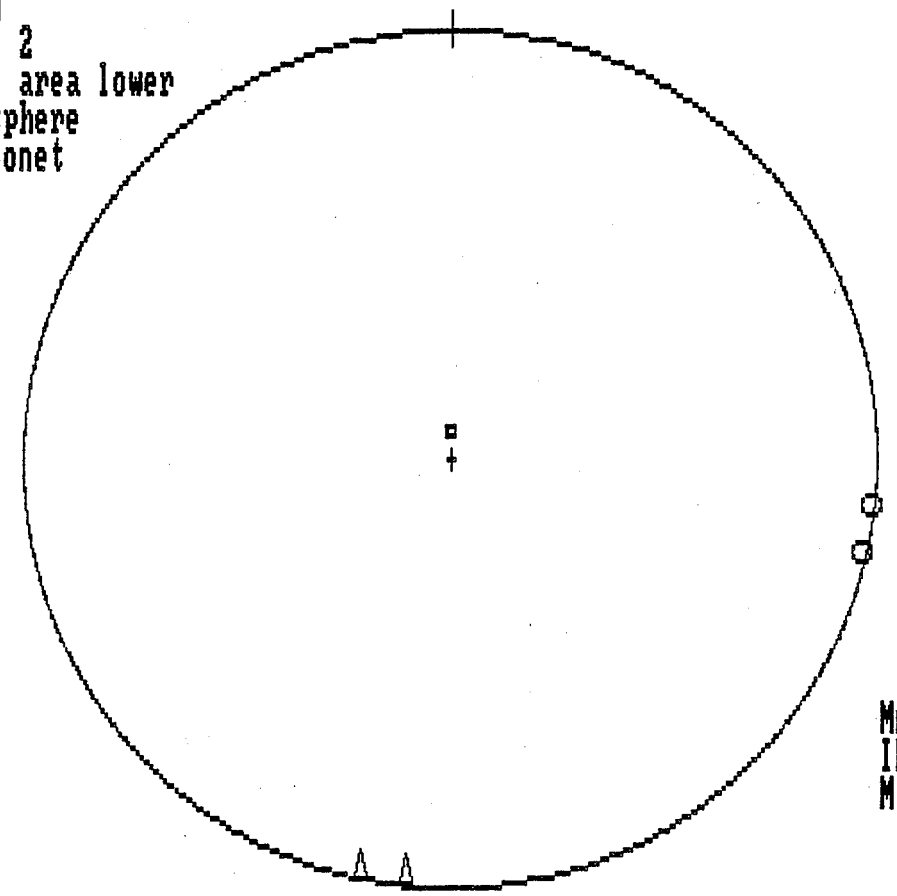

MAX = CIRCLE
INT = TRIANGLE
MIN = SQUARE

AMS

TP07A SITE 1 CORE 1 SPEC 1 UNITS= SI m M= 12 NR= 2 14:16:14 07-11-1990

SUSC.	DEC	INC	R95	EV	SDEV
MIN	14.21	-77.71	2.1	4.4467E-05	3.839E-08
INT	298.64	3.11	5.8	4.6150E-05	6.225E-08
MAX	29.30	11.88	6.1	4.6459E-05	5.135E-08

TP07A SITE 1 CORE 1 SPEC 2 UNITS= SI m M= 12 NR= 2 14:23:32 07-11-1990

SUSC.	DEC	INC	R95	EV	SDEV
MIN	15.00	-77.81	2.9	4.4530E-05	2.061E-08
INT	294.88	2.13	2.6	4.6208E-05	1.004E-08
MAX	25.34	12.00	3.7	4.6534E-05	2.420E-08

AMS

TP07A
n = 2
Equal area lower hemisphere stereonet

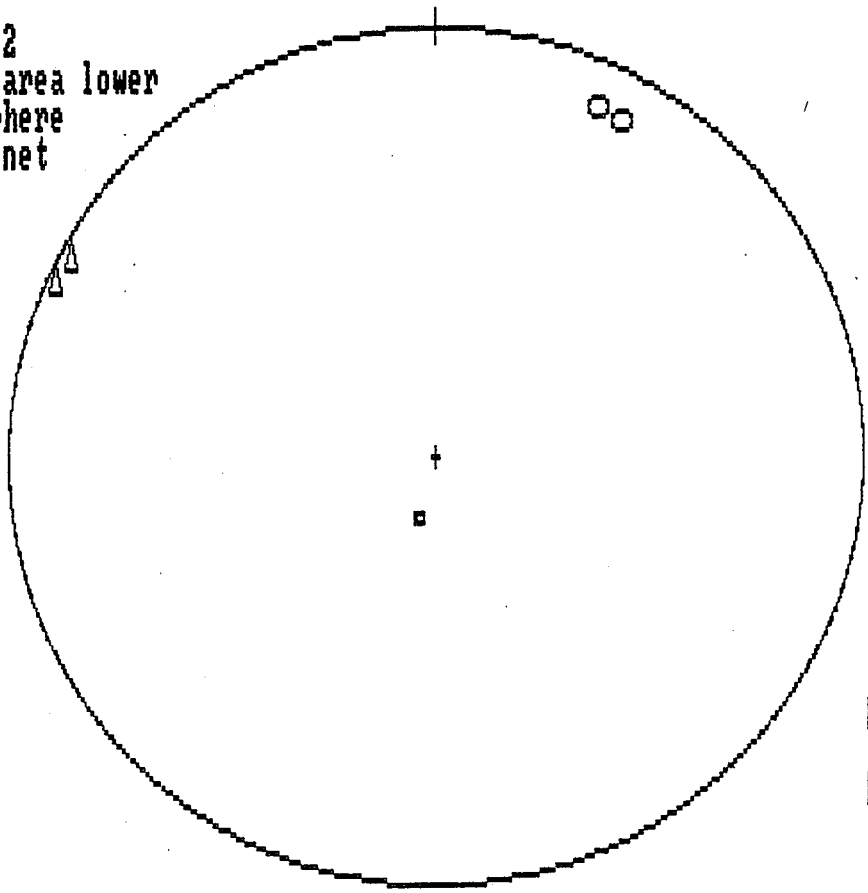

MAX = CIRCLE
INT = TRIANGLE
MIN = SQUARE

AMS

TP08A SITE 1 CORE 1 SPEC 1 UNITS= SI m M= 12 NR= 2 12:38:06 07-12-1990

SUSC.	DEC	INC	R95	EV	SDEV
MIN	270.61	77.10	2.8	2.4753E-05	2.647E-08
INT	82.83	12.79	71.1	2.5950E-05	2.878E-08
MAX	353.18	-1.70	71.1	2.5977E-05	7.261E-08

TP08A SITE 1 CORE 1 SPEC 2 UNITS= SI m M= 12 NR= 2 12:46:11 07-12-1990

SUSC.	DEC	INC	R95	EV	SDEV
MIN	270.69	77.10	2.1	2.4803E-05	8.229E-09
INT	277.85	-12.80	23.6	2.6001E-05	1.682E-08
MAX	7.51	1.56	23.7	2.6059E-05	2.315E-08

AMS

TP08A
n = 2
Equal area lower hemisphere stereonet

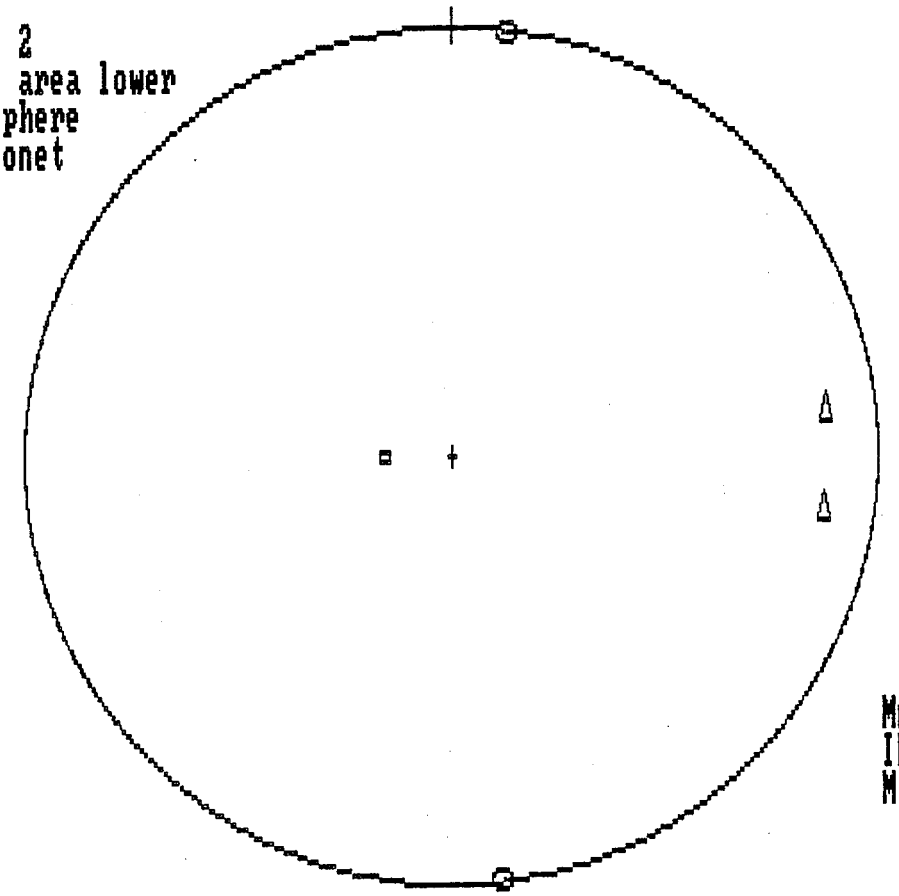

MAX = CIRCLE
INT = TRIANGLE
MIN = SQUARE

TP09A SITE 1 CORE 1 SPEC 1 UNITS= SI m M= 12 NR= 2 12:37:40 07-24-1990

SUSC.	DEC	INC	R95	EV	SDEV
MIN	332.18	-86.30	0.6	2.0959E-05	6.386E-09
INT	338.50	3.68	3.3	2.3214E-05	1.392E-08
MAX	68.47	-0.40	3.3	2.3456E-05	1.302E-08

TP09A SITE 1 CORE 1 SPEC 2 UNITS= SI m M= 12 NR= 2 12:44:47 07-24-1990

SUSC.	DEC	INC	R95	EV	SDEV
MIN	332.83	-86.26	0.7	2.0973E-05	2.280E-09
INT	337.61	3.73	2.1	2.3229E-05	5.288E-09
MAX	67.59	-0.31	2.1	2.3471E-05	1.227E-08

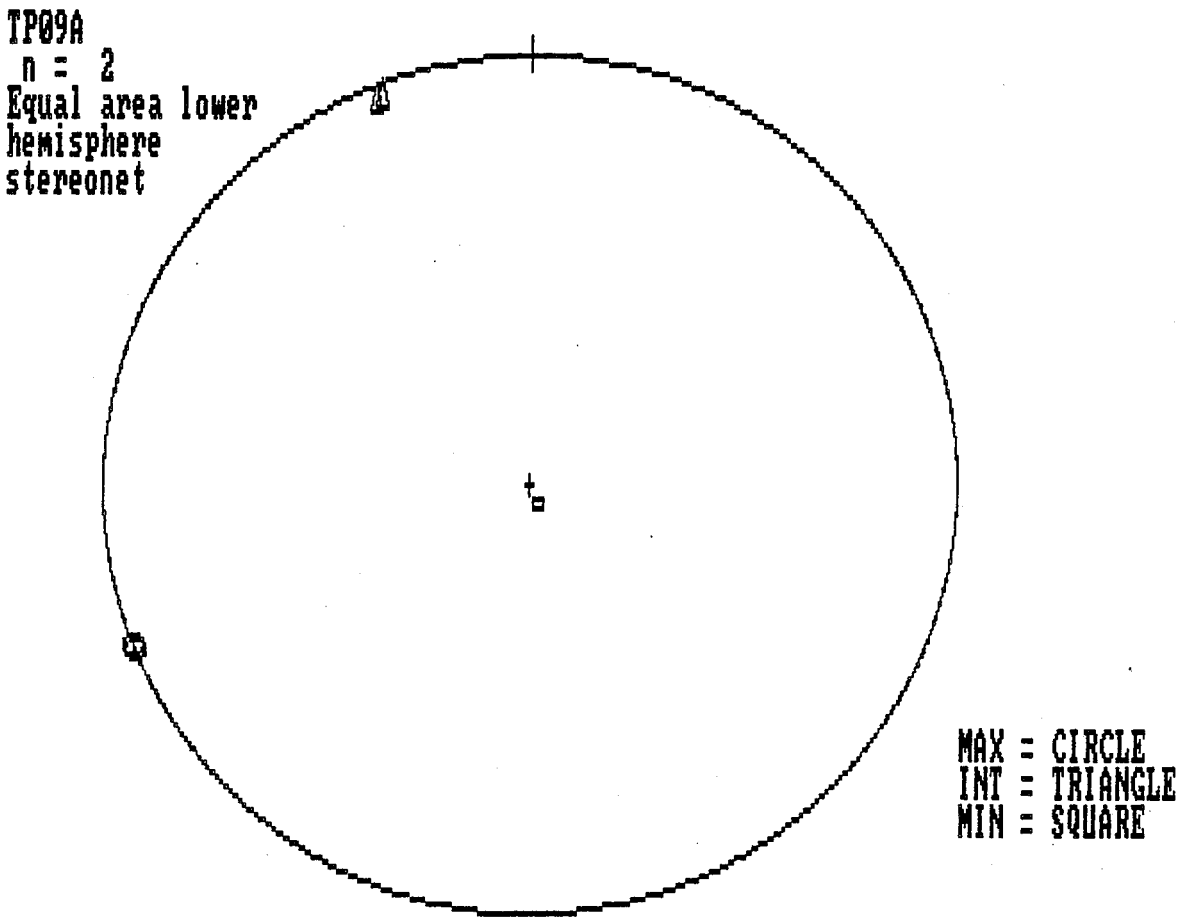

TP10A SITE 1 CORE 1 SPEC 1 UNITS= SI m M= 12 NR= 2 14:53:28 07-25-1990

SUSC.	DEC	INC	R95	EV	SDEV
MIN	87.50	83.75	0.7	2.1775E-05	8.747E-09
INT	317.47	4.03	1.0	2.3674E-05	6.085E-09
MAX	47.13	-4.77	1.2	2.3839E-05	6.867E-09

TP10A SITE 1 CORE 1 SPEC 2 UNITS= SI m M= 12 NR= 2 14:59:29 07-25-1990

SUSC.	DEC	INC	R95	EV	SDEV
MIN	88.16	83.80	1.2	2.1787E-05	7.862E-09
INT	317.95	4.01	1.2	2.3683E-05	7.691E-09
MAX	47.62	-4.72	1.7	2.3845E-05	3.487E-09

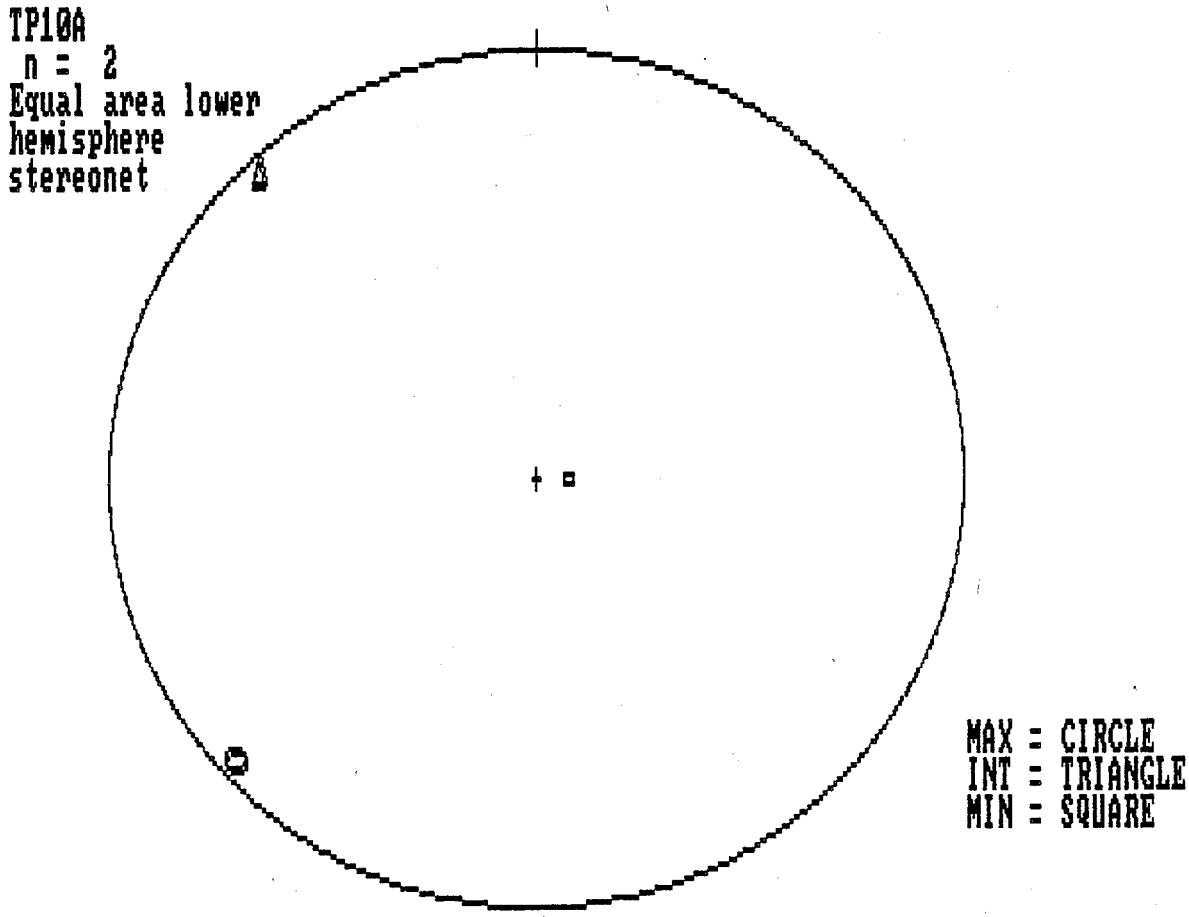

AMS

TP11A SITE 1 CORE 1 SPEC 1 UNITS= SI m M= 12 NR= 2 11:26:56 09-06-1990

SUSC.	DEC	INC	R95	EV	SDEV
MIN	77.61	86.64	1.1	2.1286E-05	8.333E-09
INT	25.96	-2.09	32.4	2.3186E-05	5.412E-08
MAX	296.06	2.63	32.4	2.3331E-05	2.509E-08

TP11A SITE 1 CORE 1 SPEC 2 UNITS= SI m M= 12 NR= 2 11:34:56 09-06-1990

SUSC.	DEC	INC	R95	EV	SDEV
MIN	72.91	86.78	0.8	2.1308E-05	6.536E-09
INT	28.92	-2.32	19.6	2.3223E-05	3.495E-08
MAX	299.01	2.24	19.5	2.3351E-05	8.821E-09

AMS

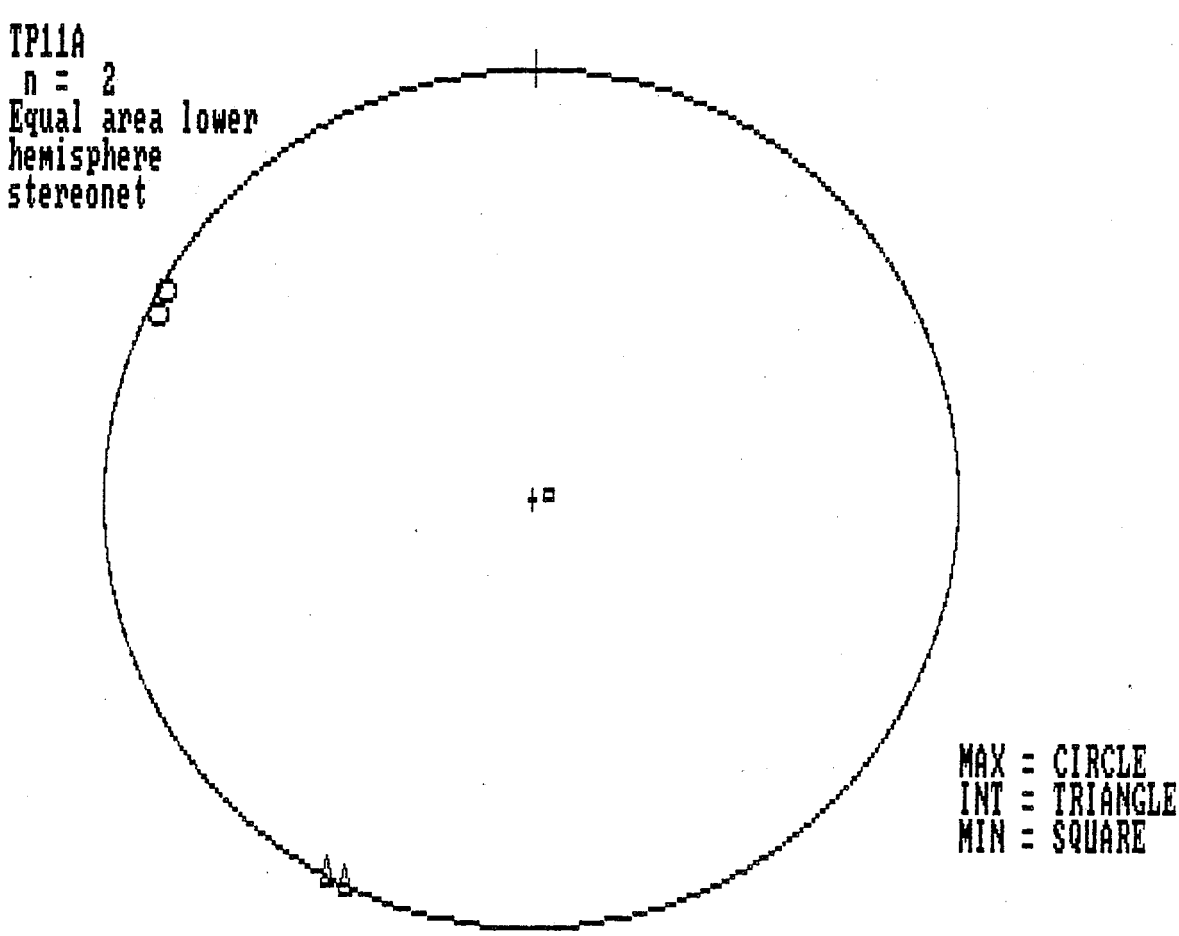

AMS

TP12A SITE 1 CORE 1 SPEC 1 UNITS= SI m M= 12 NR= 2 13:22:31 09-06-1990

SUSC.	DEC	INC	R95	EV	SDEV
MIN	333.18	-82.85	3.6	2.2989E-05	2.527E-08
INT	0.54	6.36	49.3	2.4421E-05	5.986E-08
MAX	270.33	3.28	49.5	2.4490E-05	8.445E-08

TP12A SITE 1 CORE 1 SPEC 2 UNITS= SI m M= 12 NR= 2 13:29:41 09-06-1990

SUSC.	DEC	INC	R95	EV	SDEV
MIN	333.54	-83.01	2.8	2.3026E-05	2.318E-09
INT	357.84	6.37	41.8	2.4512E-05	1.731E-08
MAX	87.38	-2.83	41.7	2.4540E-05	4.908E-08

AMS

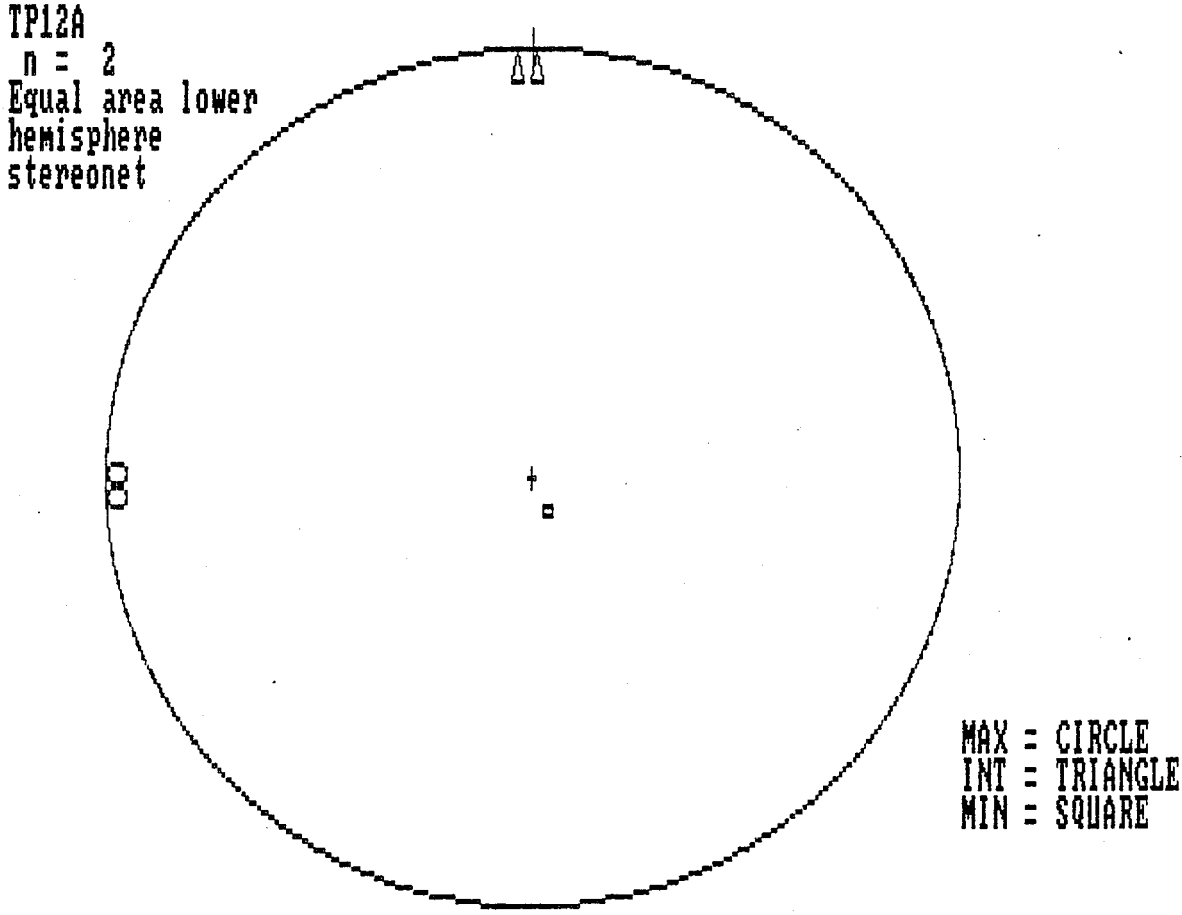

APPENDIX C: Rf versus Ø Plots

Rf versus Ø plots for each of the digitized pyrrhotite aggregates follow. The variable Ø is plotted on the X-axis in degrees and is denoted by the symbol ANGLE AX. Rf is plotted on the Y-axis where Rf = the grain shape ratio X/Y. Each point on the graphs represents a single digitized grain. The specimen number can be found in the six-digit number below ID. NR.. For example, 000002 represents P002 and 000028 represents P028.

SELECTED DATABROUP
ID.NR. TR SA EXT.1
000002 00 01 222221
CHANNELGROUP -1
4.000
3.000
2.000
1.000
0.000
100.0
200.0
ANGLE AX

SELECTED DATAGROUP

ID.NR. TR SA EXT.1
000003 00 01 ??????

CHANNELGROUP -1

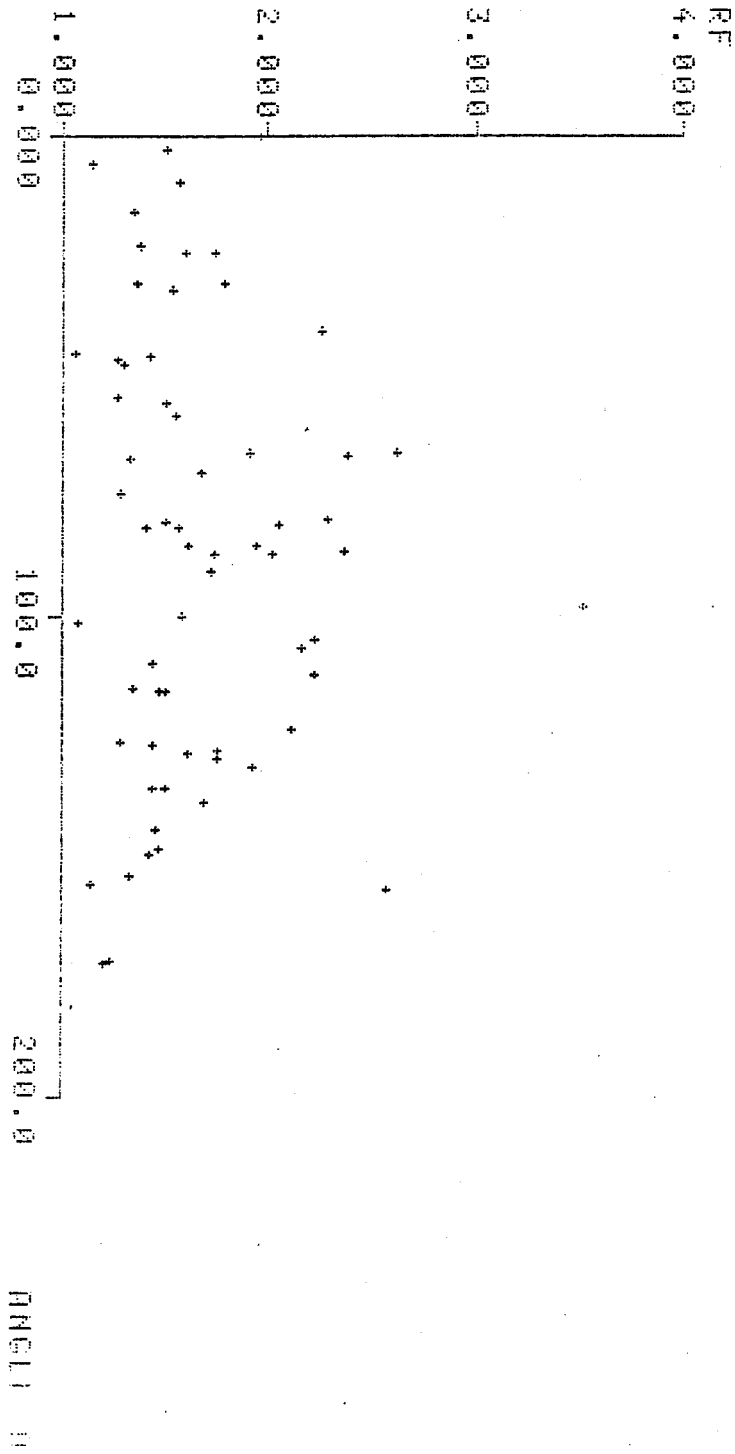

SELECTED DATAGROUP

ID.NR. TR SA EXT.1
000004 00 01 999999

CHANNELGROUP -1

SELECTED DATAGROUP

ID.NR. TR SA EXT.1
000005 00 01 ??????

CHANNELGROUP -1

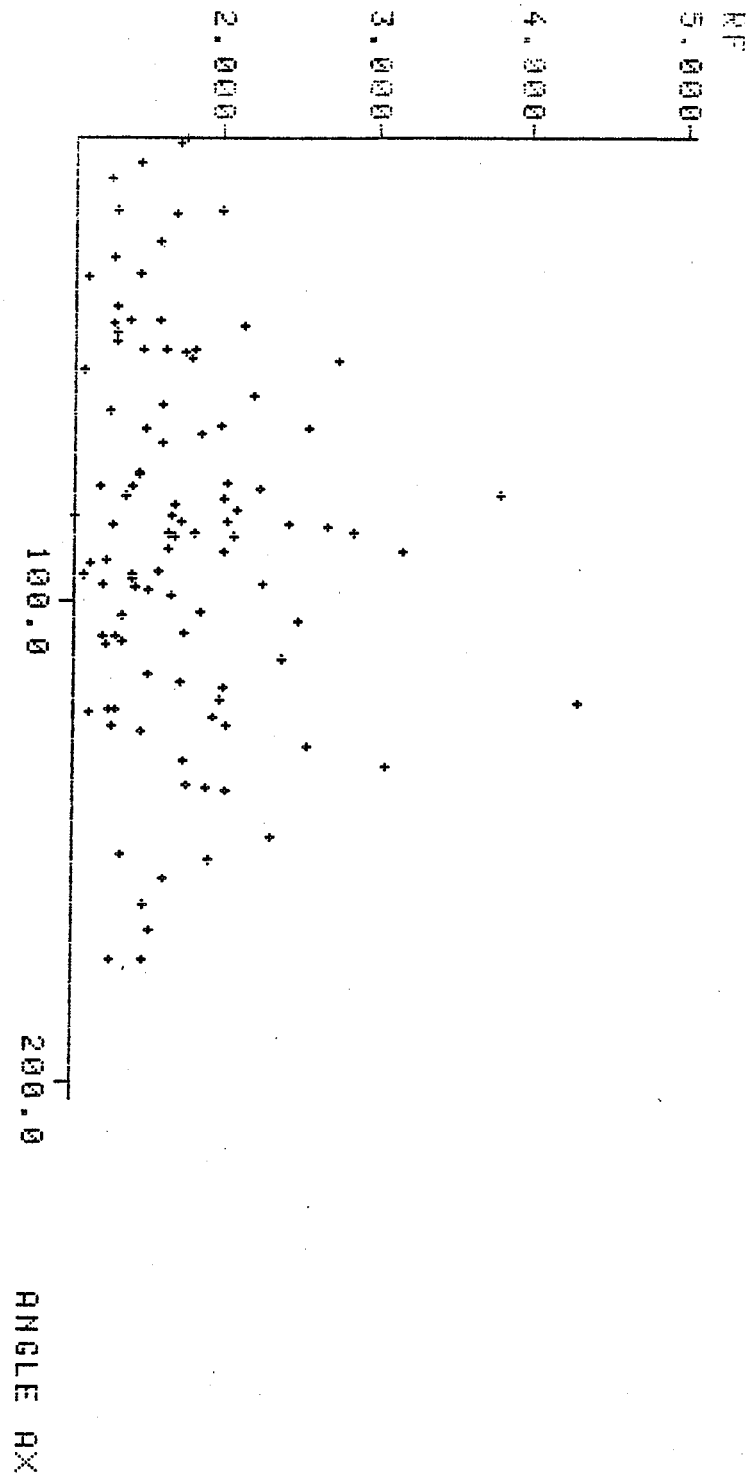

SELECTED DATAGROUP

ID.NR. TR SA EXT.1
000006 00 01 ??????

CHANNELGROUP -1

SELECTED DATAGROUP
ID.NR. TR SA EXT.1
000007 00 01 ??????
CHANNELGROUP -1
RF
4.000
3.000
2.000
100.0
200.0
ANGLE AX

SELECTED DATAGROUP

ID.NR. TR SA EXT.1
000008 00 01 ??????

CHANNELGROUP -1

SELECTED DATAGROUP
ID.NR. TR SA EXT.1
000009 00 01 ??????
CHANNELGROUP -1
RF
5.000
4.000
3.000
2.000
100.0
200.0
ANGLE AX

SELECTED DATAGROUP

ID.NR. TR SA EXT.1
000010 00 01 777777

CHANNELGROUP -1

SELECTED DATAGROUP

ID.NR. TR SA EXT.1
000011 00 01 ??????

CHANNELGROUP -1

SELECTED DATAGROUP

ID.NR. TR SA EXT.1
000012 00 01 ??????

CHANNELGROUP -1

SELECTED DATAGROUP
ID.NR. TR SA EXT.1
000014 00 01 ??????
CHANNELGROUP -1
RF
4.000
3.000
2.000
100.0
200.0
ANGLE AX

SELECTED DATAGROUP
ID.NR. TR SA EXT.1
000015 00 01 ??????
CHANNELGROUP -1
RF
4.000
3.000
2.000
100.0
200.0
ANGLE AX

SELECTED DATAGROUP

ID.NR. TR SA EXT.1
000016 00 01 ??????

CHANNELGROUP -1

SELECTED DATAGROUP

ID.NR. TR SA EXT.1
000018 00 01 ??????

CHANNELGROUP -1

SELECTED DATAGROUP

ID.NR. TR SA EXT.1
000019 00 01 ??????

CHANNELGROUP -1

SELECTED DATAGROUP

ID.NR. TR SA EXT.1
000020 00 01 ??????

CHANNELGROUP -1

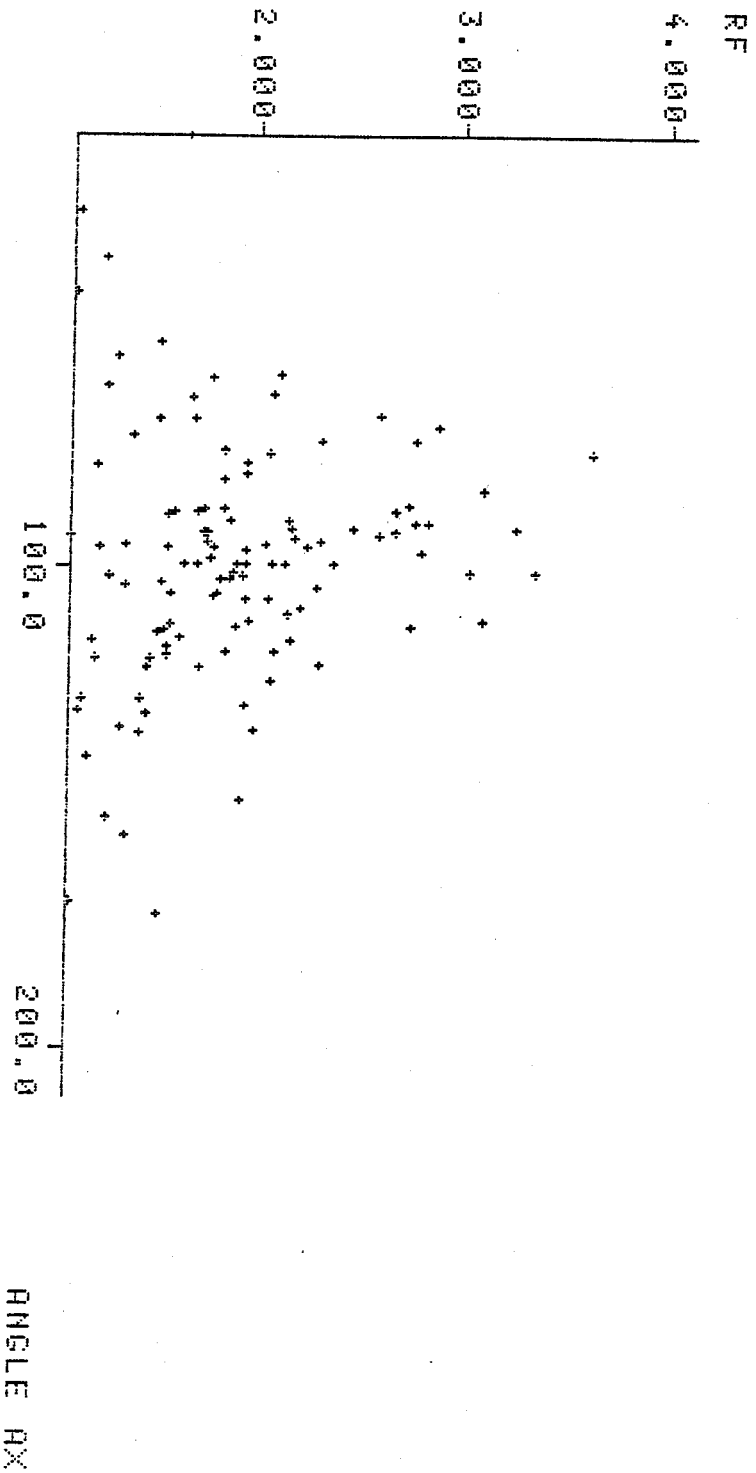

SELECTED DATAGROUP

ID.NR. TR SA EXT.1
000025 00 01 ??????

CHANNELGROUP -1

SELECTED DATAGROUP

ID.NR. TR SA EXT.1
000023 00 01 ??????

CHANNELGROUP -1

SELECTED DATAGROUP

ID.NR. TR SA EXT.1
000024 00 01 ??????

CHANNELGROUP -1

SELECTED DATAGROUP

ID.NR. TR SA EXT.1
000025 00 01 ??????

CHANNELGROUP -1

SELECTED DATAGROUP

ID.NR. TR SA EXT.1
000026 00 01 ??????

CHANNELGROUP -1

SELECTED DATAGROUP

ID.NR. TR SA EXT.1
000027 00 01 ??????

CHANNELGROUP -1

SELECTED DATAGROUP

ID,NR, TR SA EXT,1
000028 00 01 777777

CHANNELGROUP -1

APPENDIX D: Massive Specimen Data

The raw ACMS and AMS data for the Shebandowan massive sulphide specimens are listed below. The format is essentially the same as for the loose aggregates in appendices A and B. Data for each sample is found on a single page with conductive ACMS data, including P' and T followed by the corresponding AMS data.

Note the extremely low P' (ACMS) values. Also, most conductive fabrics are oblate (positive T), meaning that resistive fabrics are prolate (negative T). AMS fabrics all have oblate anisotropy (positive T). This is a much different relationship than existed between ACMS and AMS fabrics in the loose pyrrhotite aggregates.

ACMS OUTPUT: Conductivity parameters

SB01 SITE 1 CORE 1 SPEC 1 UNITS= SI v M= 6 NR= 2 15:36:18 10-04-1990

SUSC.	DEC	INC	R95	EV	SDEV
MIN	309.16	-74.27	0.2	6.1341E-01	5.731E-05
INT	38.37	0.25	1.4	6.5748E-01	5.755E-05
MAX	308.23	15.72	1.3	6.6328E-01	2.299E-04

ACMS OUTPUT: Conductivity parameters

SB01 SITE 1 CORE 1 SPEC 2 UNITS= SI v M= 6 NR= 2 15:41:12 10-04-1990

SUSC.	DEC	INC	R95	EV	SDEV
MIN	310.55	-74.46	0.3	6.1322E-01	4.357E-05
INT	39.00	0.45	1.2	6.5745E-01	3.616E-04
MAX	308.84	15.53	1.2	6.6297E-01	4.182E-04

SB01 FSN= 0 LSN= 0 D SN=-1 NT= 2 NA= 2 15:42:22 10-04-1990

CN	SN	K1/K2	K2/K3	ln(A)	ln(B)	P'	T
1	1	1.0088	1.0718	0.0088	0.0694	1.0894	0.7753
1	2	1.0084	1.0721	0.0084	0.0696	1.0894	0.7857
mean		1.0086	1.0720	0.0086	0.0695	1.0894	0.7805
sdev		0.0003	0.0000	0.0002	0.0001	0.0000	0.0052

Normalised-principal and bulk susceptibilities follow

CN	SN	Kmax	Kint	Kmin	K(bulk)g	K(bulk)a
1	1	1.0294	1.0204	0.9520	6.4433E-01	6.4472E-01
1	2	1.0292	1.0206	0.9520	6.4416E-01	6.4454E-01

SB001 SITE 1 CORE 1 SPEC 1 UNITS= SI v M= 12 NR= 2 15:55:48 10-04-1990

SUSC.	DEC	INC	R95	EV	SDEV
MIN	295.21	-67.57	0.8	5.3124E-02	1.690E-03
INT	18.23	2.87	7.0	2.7424E-01	5.239E-05
MAX	287.05	22.23	7.0	3.0910E-01	5.017E-04

SB001 FSN= 0 LSN= 0 D SN=-1 NT= 1 NA= 1 15:56:58 10-04-1990

CN	SN	K1/K2	K2/K3	ln(A)	ln(B)	P'	T
1	1	1.1271	5.1623	0.1197	1.6414	7.1566	0.8641
mean		1.1271	5.1623	0.1197	1.6414	7.1566	0.8641
sdev		0.0000	0.0000	0.0000	0.0000	0.0000	0.0000

Normalised-principal and bulk susceptibilities follow

ACMS OUTPUT: Conductivity parameters

SB02 SITE 1 CORE 1 SPEC 1 UNITS= SI v M= 6 NR= 2 09:59:31 10-05-1990

SUSC.	DEC	INC	R95	EV	SDEV
MIN	288.75	68.59	0.0	5.8855E-01	9.628E-05
INT	349.94	-10.70	0.0	6.3966E-01	1.210E-04
MAX	76.35	18.31	0.0	6.9856E-01	1.633E-04

SB02 FSN= 0 LSN= 0 D SN=-1 NT= 1 NA= 1 10:00:47 10-05-1990

CN	SN	K1/K2	K2/K3	ln(A)	ln(B)	P'	T
1	1	1.0921	1.0868	0.0881	0.0833	1.1869	-0.0280
mean		1.0921	1.0868	0.0881	0.0833	1.1869	-0.0280
sdev		0.0000	0.0000	0.0000	0.0000	0.0000	0.0000

Normalised-principal and bulk susceptibilities follow

CN	SN	Kmax	Kint	Kmin	K(bulk)g	K(bulk)a
1	1	1.0903	0.9984	0.9186	6.4069E-01	6.4226E-01

SB002 SITE 1 CORE 1 SPEC 1 UNITS= SI v M= 12 NR= 2 09:48:04 10-05-1990

SUSC.	DEC	INC	R95	EV	SDEV
MIN	50.69	81.23	1.1	9.8753E-02	6.413E-04
INT	27.70	-8.08	1.5	2.7333E-01	1.102E-03
MAX	298.18	3.38	1.2	2.9637E-01	2.973E-05

SB002 FSN= 0 LSN= 0 D SN=-1 NT= 1 NA= 1 09:49:04 10-05-1990

CN	SN	K1/K2	K2/K3	ln(A)	ln(B)	P'	T
1	1	1.0843	2.7678	0.0809	1.0181	3.4040	0.8527
mean		1.0843	2.7678	0.0809	1.0181	3.4040	0.8527
sdev		0.0000	0.0000	0.0000	0.0000	0.0000	0.0000

Normalised-principal and bulk susceptibilities follow

CN	SN	Kmax	Kint	Kmin	K(bulk)g	K(bulk)a
1	1	1.4819	1.3667	0.4938	2.0000E-01	2.2282E-01

ACMS OUTPUT: Conductivity parameters

SB03 SITE 1 CORE 1 SPEC 1 UNITS= SI v M= 6 NR= 2 10:10:58 10-05-1990

SUSC.	DEC	INC	R95	EV	SDEV
MIN	276.96	18.93	0.2	5.9630E-01	2.503E-04
INT	2.86	-11.79	0.5	6.4439E-01	2.196E-04
MAX	62.67	67.46	0.5	6.6695E-01	1.502E-04

SB03 FSN= 0 LSN= 0 D SN=-1 NT= 1 NA= 1 10:12:11 10-05-1990

CN	SN	K1/K2	K2/K3	ln(A)	ln(B)	P'	T
1	1	1.0350	1.0806	0.0344	0.0775	1.1215	0.3852
mean		1.0350	1.0806	0.0344	0.0775	1.1215	0.3852
sdev		0.0000	0.0000	0.0000	0.0000	0.0000	0.0000

Normalised-principal and bulk susceptibilities follow

CN	SN	Kmax	Kint	Kmin	K(bulk)g	K(bulk)a
1	1	1.0500	1.0145	0.9388	6.3519E-01	6.3588E-01

SB003 SITE 1 CORE 1 SPEC 1 UNITS= SI v M= 12 NR= 2 10:24:44 10-05-1990

SUSC.	DEC	INC	R95	EV	SDEV
MIN	300.80	37.16	1.0	8.8947E-02	1.122E-03
INT	67.91	38.52	2.9	2.5003E-01	7.348E-04
MAX	5.05	-29.82	2.7	2.7589E-01	1.387E-04

SB003 FSN= 0 LSN= 0 D SN=-1 NT= 1 NA= 1 10:26:12 10-05-1990

CN	SN	K1/K2	K2/K3	ln(A)	ln(B)	P'	T
1	1	1.1034	2.8110	0.0984	1.0335	3.5047	0.8261
mean		1.1034	2.8110	0.0984	1.0335	3.5047	0.8261
sdev		0.0000	0.0000	0.0000	0.0000	0.0000	0.0000

Normalised-principal and bulk susceptibilities follow

CN	SN	Kmax	Kint	Kmin	K(bulk)g	K(bulk)a
1	1	1.5070	1.3657	0.4859	1.8307E-01	2.0495E-01

ACMS OUTPUT: Conductivity parameters

SB04 SITE 1 CORE 1 SPEC 1 UNITS= SI v M= 6 NR= 2 10:53:55 10-05-1990

SUSC.	DEC	INC	R95	EV	SDEV
MIN	278.96	34.50	0.3	6.6451E-01	1.184E-04
INT	7.02	-2.83	0.9	6.9396E-01	2.397E-04
MAX	272.91	-55.35	0.9	7.0416E-01	1.878E-04

SB04 FSN= 0 LSN= 0 D SN=-1 NT= 1 NA= 1 10:57:45 10-05-1990

CN	SN	K1/K2	K2/K3	ln(A)	ln(B)	P'	T
1	1	1.0147	1.0443	0.0146	0.0434	1.0622	0.4964
mean		1.0147	1.0443	0.0146	0.0434	1.0622	0.4964
sdev		0.0000	0.0000	0.0000	0.0000	0.0000	0.0000

Normalised-principal and bulk susceptibilities follow

CN	SN	Kmax	Kint	Kmin	K(bulk)g	K(bulk)a
1	1	1.0245	1.0096	0.9668	6.8734E-01	6.8754E-01

SB004 SITE 1 CORE 1 SPEC 1 UNITS= SI v M= 12 NR= 2 10:41:08 10-05-1990

SUSC.	DEC	INC	R95	EV	SDEV
MIN	309.95	63.24	0.9	2.1106E-01	1.788E-03
INT	69.82	14.10	0.9	3.7883E-01	1.536E-03
MAX	345.72	-22.25	0.7	4.4300E-01	1.809E-03

SB004 FSN= 0 LSN= 0 D SN=-1 NT= 1 NA= 1 10:42:06 10-05-1990

CN	SN	K1/K2	K2/K3	ln(A)	ln(B)	P'	T
1	1	1.1694	1.7949	0.1565	0.5849	2.1850	0.5779
mean		1.1694	1.7949	0.1565	0.5849	2.1850	0.5779
sdev		0.0000	0.0000	0.0000	0.0000	0.0000	0.0000

Normalised-principal and bulk susceptibilities follow

CN	SN	Kmax	Kint	Kmin	K(bulk)g	K(bulk)a
1	1	1.3489	1.1535	0.6427	3.2841E-01	3.4429E-01

ACMS OUTPUT: Conductivity parameters

SB05 SITE 1 CORE 1 SPEC 1 UNITS= SI v M= 6 NR= 2 13:36:56 10-05-1990

SUSC.	DEC	INC	R95	EV	SDEV
MIN	40.66	-24.22	0.1	6.3772E-01	1.733E-04
INT	323.74	26.71	0.2	7.1294E-01	2.321E-04
MAX	274.75	-52.52	0.2	7.4355E-01	1.795E-04

SB05 FSN= 0 LSN= 0 D SN=-1 NT= 1 NA= 1 13:37:54 10-05-1990

CN	SN	K1/K2	K2/K3	ln(A)	ln(B)	P'	T
1	1	1.0429	1.1180	0.0420	0.1115	1.1720	0.4525
mean		1.0429	1.1180	0.0420	0.1115	1.1720	0.4525
sdev		0.0000	0.0000	0.0000	0.0000	0.0000	0.0000

Normalised-principal and bulk susceptibilities follow

CN	SN	Kmax	Kint	Kmin	K(bulk)g	K(bulk)a
1	1	1.0674	1.0234	0.9154	6.9663E-01	6.9807E-01

SB005 SITE 1 CORE 1 SPEC 1 UNITS= SI v M= 12 NR= 2 13:48:49 10-05-1990

SUSC.	DEC	INC	R95	EV	SDEV
MIN	55.64	-51.71	0.6	1.5985E-01	2.199E-03
INT	1.76	24.95	7.7	3.3325E-01	8.440E-05
MAX	285.50	-26.97	7.8	3.5422E-01	1.677E-03

SB005 FSN= 0 LSN= 0 D SN=-1 NT= 1 NA= 1 13:49:28 10-05-1990

CN	SN	K1/K2	K2/K3	ln(A)	ln(B)	P'	T
1	1	1.0629	2.0847	0.0610	0.7346	2.4245	0.8466
mean		1.0629	2.0847	0.0610	0.7346	2.4245	0.8466
sdev		0.0000	0.0000	0.0000	0.0000	0.0000	0.0000

Normalised-principal and bulk susceptibilities follow

CN	SN	Kmax	Kint	Kmin	K(bulk)g	K(bulk)a
1	1	1.3305	1.2517	0.6004	2.6623E-01	2.8244E-01

ACMS OUTPUT: Conductivity parameters

SB09 SITE 1 CORE 1 SPEC 1 UNITS= SI v M= 6 NR= 2 14:08:44 10-05-1990

SUSC.	DEC	INC	R95	EV	SDEV
MIN	295.40	-70.55	0.0	6.1839E-01	4.484E-04
INT	69.71	-13.86	1.9	7.6185E-01	8.450E-04
MAX	343.07	13.38	1.9	8.1944E-01	1.081E-03

SB09 FSN= 0 LSN= 0 D SN=-1 NT= 1 NA= 1 14:09:42 10-05-1990

CN	SN	K1/K2	K2/K3	ln(A)	ln(B)	P'	T
1	1	1.0756	1.2320	0.0729	0.2086	1.3394	0.4823
mean		1.0756	1.2320	0.0729	0.2086	1.3394	0.4823
sdev		0.0000	0.0000	0.0000	0.0000	0.0000	0.0000

Normalised-principal and bulk susceptibilities follow

CN	SN	Kmax	Kint	Kmin	K(bulk)g	K(bulk)a
1	1	1.1254	1.0463	0.8493	7.2814E-01	7.3323E-01

SB009 SITE 1 CORE 1 SPEC 1 UNITS= SI v M= 12 NR= 2 14:00:30 10-05-1990

SUSC.	DEC	INC	R95	EV	SDEV
MIN	320.08	-71.29	0.6	9.9405E-02	9.005E-04
INT	64.64	-4.87	11.5	2.5509E-01	8.539E-04
MAX	336.23	18.02	11.5	2.6091E-01	1.317E-03

SB009 FSN= 0 LSN= 0 D SN=-1 NT= 1 NA= 1 14:01:19 10-05-1990

CN	SN	K1/K2	K2/K3	ln(A)	ln(B)	P'	T
1	1	1.0228	2.5662	0.0226	0.9424	3.0085	0.9533
mean		1.0228	2.5662	0.0226	0.9424	3.0085	0.9533
sdev		0.0000	0.0000	0.0000	0.0000	0.0000	0.0000

Normalised-principal and bulk susceptibilities follow

CN	SN	Kmax	Kint	Kmin	K(bulk)g	K(bulk)a
1	1	1.3898	1.3588	0.5295	1.8773E-01	2.0513E-01